SHEAR STRESSES IN TURBULENT FLOW THROUGH CONCENTRIC ANNULI

BY

A.L. KENNEDY

A thesis submitted in complete fulfilment
of the requirements for the degree
Master of Science in Engineering

Department of Civil Engineering,
UNIVERSITY OF CAPE TOWN

December 1976.

DECLARATION OF CANDIDATE

I, A.L. Kennedy, hereby declare that this thesis is my own work and that it has not been submitted for a degree at another University.

Signed by candidate

TABLE OF CONTENTS

		Page No
Title		
Table of contents		1
List of plates		4
Synopsis		5
Acknowledgements		6
List of symbols		8
SECTION 1	Introduction	12
SECTION 2	Velocity and Shear Stress Measuring Devices	14
2.1	The Pitot Tube	14
2.2	The Double Pitot Tube	20
2.3	The Preston Tube	21
2.4	The Hot Wire Anemometer	26
SECTION 3	Previous Shear Stress Measurements in Annular Flow	37
3.1	Indirect Shear Stress Measurement	37
3.1.1	Owen	37
3.1.2	Brighton and Jones	39
3.1.3	Olson and Sparrow	42
3.1.4	Turbulence Models	42
3.1.5	Lawn and Elliot	46
3.1.6	Rehme	48
3.2	Direct Wall Shear Stress Measurement	50
3.2.1	Rothfus	51
3.2.2	Quarmby	52
3.2.3	Smith, Lawn and Hamlin	55

		Page No
SECTION 4	The Floating Sleeve Method of Direct Shear Stress Measurement	59
4.1	Description of the Test Apparatus	59
4.2	The Bottom Leakage Gap and the Top Annular Meniscus	73
4.3	Roller Bearing Friction	74
4.4	Weight Measurements	74
4.5	Pressure Measurements	76
4.6	End Corrections	78
SECTION 5	Roughness	84
5.1	Nikuradse's Investigation into Rough Pipes	84
5.2	Roughness Materials for the Floating Sleeve	88
5.3	Method Used to Roughen the Floating Sleeve	90
5.4	Pressure Tappings and End Corrections for the Floating Sleeve	91
SECTION 6	Theoretical Analysis	95
6.1	Derivation of the Conservation Equations for Mass and Linear Momentum	95
6.1.1	Conservation of Mass	96
6.1.2	Conservation of Linear Momentum	97
6.1.3	The Insolubility of the Navier Stokes Equations	101
6.2	The Mean Flow Equations and their Application to Circular Pipes and Annuli	102
6.2.1	The Expansion of the Mean Flow Equations in Cylindrical Coordinates	103
6.2.2	Simplifications for Pipe and Annular Flow	104
6.2.3	Results for Pipe Flow	106
6.2.4	Results for Annular Flow	108

		Page No
SECTION 7	Analysis of Results	113
7.1	The Sensitivity of the Floating Sleeve	113
7.1.1	Density of Flotation Liquid	113
7.1.2	Changes in Float Size	114
7.1.3	Roller Bearing Friction	114
7.1.4	Pressure Tapping Gradient	115
7.1.5	Prolonged Flow through the Leakage Gap	117
7.2	Calibration of the Floating Sleeve for the Bottom Leakage Gap Effects	117
7.2.1	Static Head Methods	118
7.2.2	Theoretical Method	122
7.3	Smooth Annular Tests	124
7.3.1	Equations for the Evaluation of Data	123
7.3.2	Discussion	126
7.4	Rough Annular Tests	146
7.4.1	Determination of Rough Sleeve Diameters	146
7.4.2	Equations for the Evaluation of Data	148
7.4.3	Discussion	148
SECTION 8	Conclusion	159
Bibliography		161
Appendix A:	Data	165
Appendix B:	Derivation of Mean Flow Equations in Cylindrical Coordinates	188

LIST OF PLATES

		Page No
PLATE 1	Part of the floating sleeve	7
PLATE 2	Floating sleeve inlet details	62
PLATE 3	The complete floating sleeve	63
PLATE 4	Floating sleeve outlet details	71

SYNOPSIS

A novel experimental approach to the direct measurement of wall shear stresses in fully developed turbulent flow in concentric annuli is presented. By means of a specially constructed 6 m test rig known as the 'floating sleeve', results of individual wall shear stresses, friction factors and shear stress distributions were obtained for Reynolds numbers from 25 000 to 220 000 with radius ratios from 0,091 to 0,376. Tests were conducted using both smooth and rough annuli.

A summary of previous investigations and an examination of the measuring devices most commonly used in annular flow are also presented.

ACKNOWLEDGEMENTS

I would like to thank the following who helped in the production of this thesis.

Professor F.A. Kilner who was always ready with help, guidance and encouragement throughout the thesis; and more particularly for his valuable and thorough reviews of this document.

Mr G. Bertuzzi for his helpful suggestions and skilful aid in machining and constructing the test apparatus.

Mrs L. Behm for her patience and expertise in producing an excellently typed manuscript at short notice.

Charlie Basson for printing and binding the final product.

Research for this thesis was carried out with the aid of a grant from the C.S.I.R.

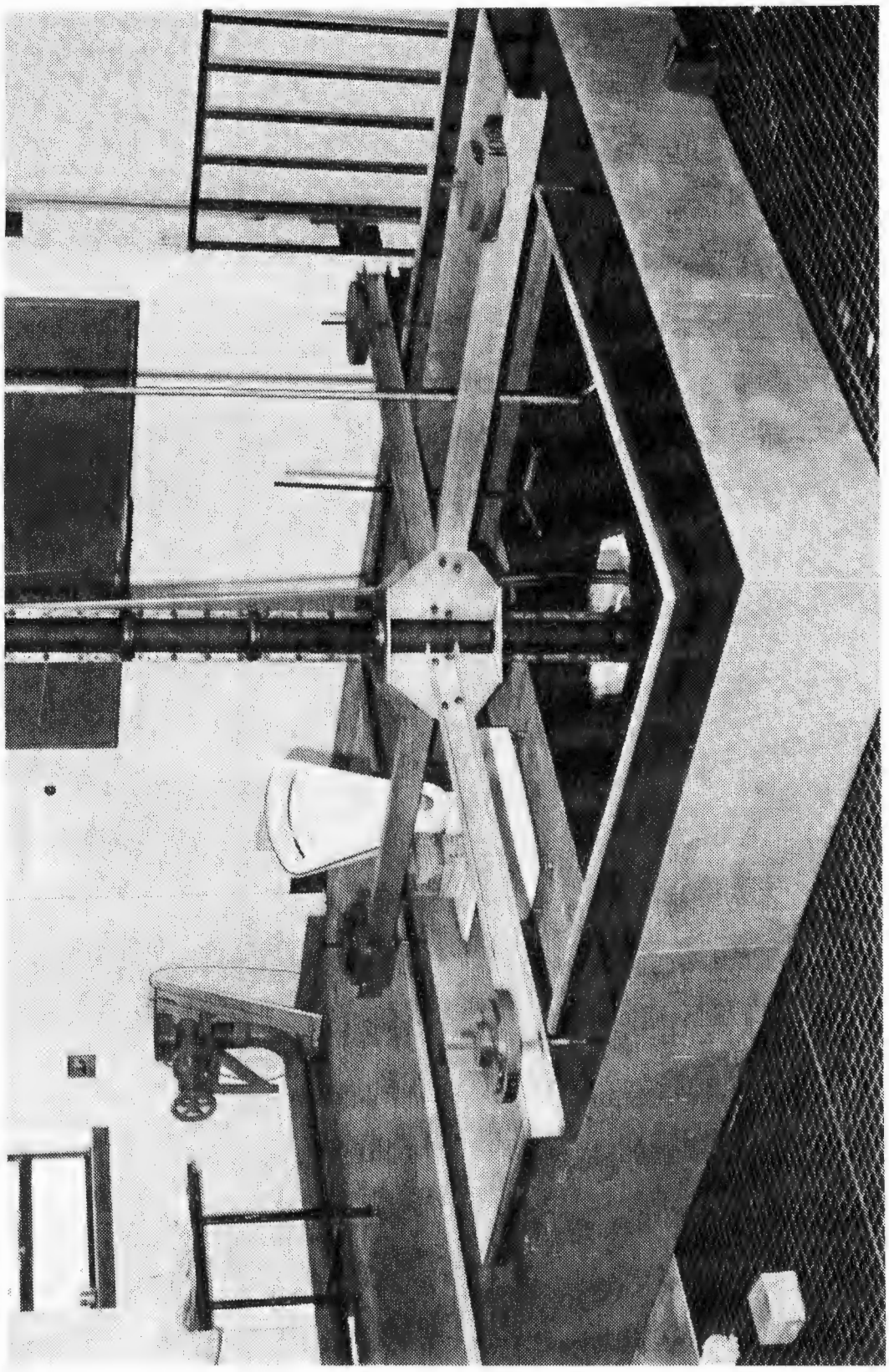

PLATE 1: PART OF THE FLOATING SLEEVE

LIST OF SYMBOLS

			Units
A	=	area	L^2
D_e	=	equivalent diameter for annulus = $2(r_2 - r_1)$	L
D_w	=	equivalent 'water volume' diameter for rough sleeve	L
f	=	friction factor = $\dfrac{\tau}{\frac{1}{2}\rho\hat{U}_x^2}$	
F	=	force	ML/T^2
P_s	=	time average static pressure	M/LT^2
P_v	=	time average dynamic pressure = $\frac{1}{2}\rho U^2$	M/LT^2
P_t	=	time average total pressure = $(P_s + P_v)$	M/LT^2
p	=	instantaneous total pressure	M/LT^2
Q	=	discharge	L^3/T
Re	=	Reynolds number = $\dfrac{\hat{U}_x D_e}{\nu}$	
r	=	radius from central axis	L
r_1	=	outside radius of core	L
r_2	=	inside radius of sleeve or pipe	L
r_m	=	radius of maximum velocity	L
r_0	=	radius of zero shear stress	L
s^*	=	$(\beta - \alpha)/(1 - \beta)$	
t	=	time	T
T	=	fixed time value	T
U	=	time average velocity $= \lim_{T\to\infty} \frac{1}{T} \int_0^T u\,dt$	L/T
U_x	=	time average velocity in x-direction	L/T
U_r	=	time average velocity in r-direction	L/T
U_θ	=	time average velocity in θ-direction	L/T
$\hat{U}_x$	=	spatial average velocity $= \dfrac{2}{r_2^2 - r_1^2} \int_{r_1}^{r_2} U_x r\,dr$	L/T

			Units
U_{τ_1}	=	friction velocity at inner wall	L/T
	=	$\sqrt{\tau_1/\rho}$	L/T
U_{τ_2}	=	friction velocity at outer wall	L/T
	=	$\sqrt{\tau_2/\rho}$	
U^+	=	dimensionless velocity = U/U_τ	
u	=	instantaneous velocity	L/T
u'_x	=	instantaneous velocity fluctuation in x-direction	L/T
u'_y	=	instantaneous velocity fluctuation in y-direction	L/T
u'_r	=	instantaneous velocity fluctuation in r-direction	L/T
u'_θ	=	instantaneous velocity fluctuation in θ-direction	L/T
$\overline{\rho u'_x u'_r}$	=	Reynolds shear stress	M/LT^2
	=	$\lim_{T\to\infty} \frac{1}{T} \rho \int_0^T u'_x u'_r dt$	
$\overline{\rho u'_x u'_\theta}$	=	Reynolds shear stress	M/LT^2
	=	$\lim_{T\to\infty} \frac{1}{T} \rho \int_0^T u'_x u'_\theta dt$	
x	=	coordinate in longtitudinal direction	L
y	=	distance from wall	L
y^+	=	dimensionless coordinate = yU_τ/ν	
α	=	ratio of radius of core to radius of sleeve	
	=	r_1/r_2	
β	=	ratio of radius of zero shear to radius of sleeve	
	=	r_0/r_2	
ε	=	kinematic eddy viscosity	L^2/T
μ	=	dynamic viscosity	M/LT
ν	=	kinematic viscosity	L^2/T

			Units
ξ	=	value of $\overline{u'_x u'_r}$ at r_m	L^2/T^2
ρ	=	mass density	M/L^3
τ	=	shear stress	M/LT^2
σ_{ij}	=	Cartesian stress tensor	M/LT^2

Subscripts

1	inner (e.g. τ_1	= shear stress on inner or core wall)
2	outer (e.g. F_2	= shear force on outer or sleeve wall)
T	total (e.g. f_T	= total friction factor for inner and outer walls or F_T = sum of shear forces on the inner and outer walls)

ℓ = laminar (e.g. $r_{0\ell}$ means the radius of zero shear stress for laminar flow).

t = turbulent (e.g. r_{mt} means the radius of maximum velocity for turbulent flow).

$\underline{\ }$ = vector

Superscripts

$\overline{\ \ }$ = time average

$\hat{\ }$ = spatial average

A note on units: SI units have been used throughout the text, the exception being the limited use of grams force (abbreviated gf and equal to 9,81 mN), when referring to certain scale readings and weights.

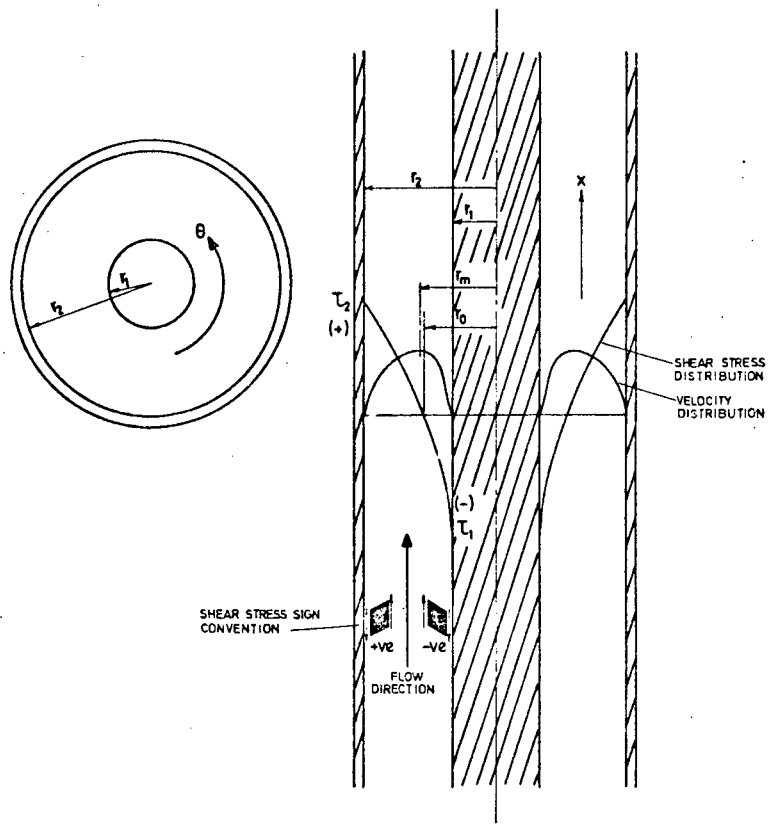

Fig. (i) Definition sketch for annuli

S E C T I O N 1

INTRODUCTION

Steady, fully developed flow of a Newtonian fluid in the annular duct between two coaxial cylindrical pipes, has been the subject of many investigations attempting to augment the well-known work of Nikuradse and others on the plain pipe and the parallel plate channel. In this document, concentric coaxial pipes of this nature will be referred to as annuli; the inner pipe will be known as the core and the outer pipe will be known as the sleeve.

The governing equations for incompressible flow are the Navier Stokes equations, derived separately by Navier and Stokes in 1827 and 1845 respectively. These are partial non-linear equations and are therefore insoluble by any analytical method known today. Only for simplified cases, such as laminar flow, does the advective term in the Navier-Stokes equation become zero, thus reducing the equations to a linear form and permitting a solution. Generally therefore, flow variables such as head loss, velocity profiles and heat transfer must be determined in the laboratory.

Fully developed annular flow is of interest to the engineer because of its direct engineering applications ranging from oil refineries, in which pipes of this type are in common use, to nuclear power plants, where heat transfer from core rods needs to be analysed. For the fluid mechanician, turbulent annular flow can provide insight into the problem of developing a complete theory of turbulence. This is because the annulus is the most general case of circular duct flow. Simpler flows such as those in cylindrical pipes and parallel plates (the parallel plate is a limiting case of annular flow) have previously been studied in detail; the velocity distributions heat transfer and friction factors can be predicted both from experimental data and with the use of semi-empirical 'universal' velocity distributions.

However, research into the problem of annular flow has produced no unified theory. Instead, the results to date are examples of disparity and contradiction. Yet it is worth noting what Bradshaw [3], an authority on turbulence, has to say of the circular pipe. "The circular pipe is a more difficult case than the duct of high aspect ratio . . . the flow looks innocuous but is in reality diabolically complicated". If the flow is so complicated in the relatively simple circular pipe with a radially symmetric velocity and shear stress profile, it is perhaps not surprising that the flow characteristics of the more complicated annulus with its radially asymmetric velocity and shear stress profiles have not been determined conclusively.

The purpose of this thesis was threefold:

(i) To determine the extent and results of past research into the flow in annular pipes

(ii) To construct an apparatus to measure directly the shear force on one of the walls of an annulus, as well as the axial pressure gradient; thus enabling the shear force on both walls to be calculated

(iii) To carry out tests on various annular geometries, thus yielding new information on the shear stress distributions within annuli

Because the differing method of velocity and shear stress measurement in annular flow are the source of contradictions in the results to date, Section 2 examines these methods in outline. Section 3 details previous research in this field and comments on the methods used and results achieved. Section 4 describes in detail the apparatus, known as the floating sleeve, which was constructed to measure the outer wall shear force directly. Section 5 deals with the choice and application of roughness, with special reference to the constructed apparatus. In Section 6, the governing equations are derived in vector notation and some results and insights yielded by the equations are studied. The floating sleeve results for flows in the Reynolds number range 25 000 to 220 000 for smooth and rough pipes, and smooth and rough annuli with radius ratios from 0,091 to 0,376 are presented and discussed in Section 7.

SECTION 2

VELOCITY AND SHEAR STRESS MEASURING DEVICES

All experimental work involves the measurement of the physical quantities concerned. The required degree of accuracy of the measurements dictates the experimental requirements and depends upon the nature of the information needed.

A knowledge of the instruments used in these measurements is essential if one is to be aware of their accuracy and of the principles upon which they operate. Only if this knowledge is present can constructive criticism about the validity of their results be produced. The large inconsistencies and contradictions of past research into turbulent concentric annular flow have resulted mainly from the limitations of the measuring devices.

The main requirement of this thesis was to determine the wall shear stresses in an annulus. An examination of the previous instruments used for directly or indirectly measuring these stresses is not only informative but also serves to show why, because of the difficulties encountered, these methods were rejected in favour of the 'floating sleeve method' of determining the wall shear stresses, as described in Section 4.

2.1 The Pitot Tube

The total pressure at a point in a moving fluid can be measured as the stagnation pressure at the front of a suitable body. The body used should cause as little disturbance to the velocity streamlines as possible and a suitable choice of shape was first made by Henri Pitot in 1732. The so-called Pitot tube is in constant use today and consists simply of a thin tube, (in very small sizes these may be made from hypodermic needles) aligned along the flow direction. However, the use of the Pitot tube for the accurate determination of velocity profiles is not as straightforward as is frequently thought. Bradshaw [2] gives the accuracy of the pressure recorded by the tube

The dynamic pressure at a distance y_0 from the solid boundary is given by:

$$(P_v)_{y_0} = \frac{\rho U^2}{2} \qquad \text{(Eq. 1)}$$

where P_v = difference between static pressure of the stream and total pressure at the stagnation point

y_0 = distance from the solid boundary to the geometric centre of the Pitot tube

Now if the shear flow consists of turbulent velocity stream in which the velocity distribution is approximated by a one seventh power law then

$$(P_v)_{y_0} = \frac{k^2 y_0^{\frac{2}{7}} \rho}{2}$$

The spatial average dynamic pressure $\hat{P}_v$ over the whole tube opening is therefore

$$\hat{P}_v = \int_{y_0 - \frac{1}{2}d}^{y_0 + \frac{1}{2}d} \frac{(k^2 y^{\frac{2}{7}} \rho)\, dy}{2d}$$

$$= \frac{7k^2\rho}{18d} \{(y_0 + \tfrac{1}{2}d)^{\frac{9}{7}} - (y_0 - \tfrac{1}{2}d)^{\frac{9}{7}}\} \qquad \text{(Eq. 2)}$$

where d = width of Pitot tube opening

y = distance from solid boundary to an arbitrary individual point within the tube opening

If the centre of the Pitot tube is say one to two tube diameters from the solid boundary then $(P_v)_{y_0}$ approximates $\hat{P}_v$ to within one per cent. This is certainly more accurate than is the case for the same tube placed in a viscous boundary layer as also shown in Fig. 1. In this situation the velocity gradient is approximated by a linear relationship.

Thus:

$$(P_v)_{y_0} = \frac{k^2 y_0^2 \rho}{2}$$

and

$$\hat{P}_v = \int_{y_0 - \frac{1}{2}d}^{y_0 + \frac{1}{2}d} \frac{(k^2 y^2 \rho)\, dy}{2d}$$

$$= \frac{k^2 \rho}{6d} \{(y_0 + \tfrac{1}{2}d)^3 - (y_0 - \tfrac{1}{2}d)^3\} \qquad \text{(Eq. 3)}$$

If the centre of the Pitot tube in this case is say half a tube diameter away from the solid boundary, than $\hat{P}_v$ is about 30% greater than $(P_v)_{y_0}$.

Thus when Pitot tubes are used in shear flows a correction is needed to find the effective position of the tube which is non-coincident with the actual position. The magnitude of this correction is largely governed by the magnitude of the velocity gradient in which the tube is placed.

In order to circumvent this correction use is often made of a flattened Pitot tube such as that shown in Fig. 2.

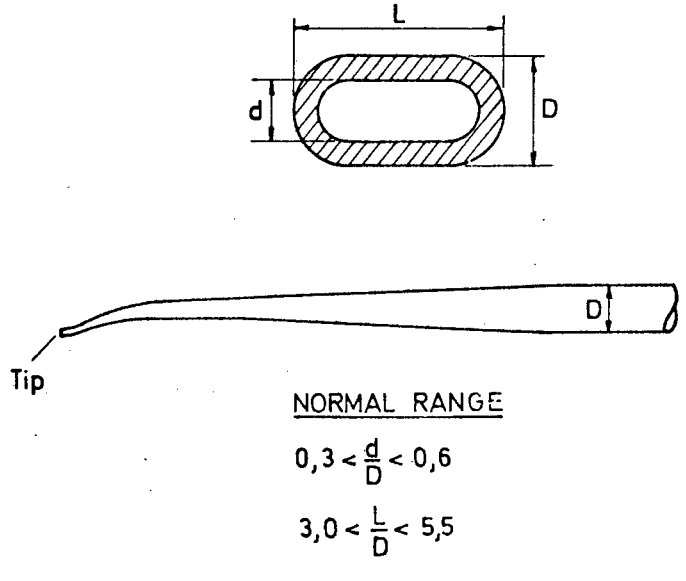

Fig. 2 Typical flattened Pitot tube

For these flattened Pitot tubes, the corrections for displacement are often ignored as being of a smaller order of magnitude than the accuracy necessary for the positioning of the tube.

Another error which may be present in the viscous layer, occurs when there is such a large pressure change across the tube opening that secondary circulation in this region causes a further displacement of the centre of pressure of the tube in the direction of the increasing velocity gradient.

(ii) Correction for displaced centre due to surface proximity:

It has been found experimentally that Pitot tube calibrations made in streams remote from solid boundaries yield incorrect results when used for measurements close to a boundary. This is partly due to the change in velocity profile as noted above and partly due to the mutual interference of the tube and the boundary. Bradshaw [2] noted that "The correction of Pitot tube readings for proximity to a solid surface is less straightforward than the correction for transverse velocity gradient because the error depends on the whole of the velocity profile between the tube position and the wall". But it appears that little information on the details of this correction are available and no empirical results could be found.

(iii) Correction for turbulence:

For turbulent flow, the Pitot tube reading is increased by an amount of the order of $\frac{1}{2}\rho(\overline{u_x'^2} + \overline{u_y'^2} + \overline{u_z'^2})$ assuming that the mean square fluctuations are all approximately equal. The value of the error in total head as measured by the Pitot tube is difficult to determine, however limited experiments have shown that for small tubes the mean total pressure may be measured with acceptable accuracy.

(iv) Corrections for flow disturbance:

Because any object placed in a velocity stream affects the static pressure upstream, care must be taken when using a Pitot-static tube

or a Pitot tube in conjunction with a wall piezometer to correct for these distrubances. The magnitude of the correction is dependent on the individual characteristics of the tube.

(v) Correction for inclination:

There is general experimental agreement that the correction to the reading for circular tubes with plane ends, with regard to the yaw of the tube in the stream, is negligible for angles of incidence less than 10 degrees.

(vi) Correction for burrs:

Microscopic burrs and irregularities often affect the tube readings of small tubes. It has been found easier to calibrate for the pressure coefficient P_{coef}:

$$P_{coef} = (P'_t - P_s)/(P_t - P_s) \qquad \text{(Eq. 4)}$$

where P_t = actual total pressure

P'_t = measured total pressure

P_s = actual static pressure

which takes into account all physical characteristics of the tube, rather than to exercise special care in their manufacture.

For many practical purposes the above limitations and corrections for Pitot tube use are trivial. Yet for the precise measurement of total pressure in annular flow two difficulties arise. In regions of steep velocity gradient the total pressure measured by the Pitot tube requires large corrections determined mainly by the magnitude of the velocity gradient and the proximity to a surface. In regions of flat velocity gradients the Pitot tube is too inaccurate to measure (at least in detail sufficient for the determination of the exact position of maximum velocity), the small differences in total pressure between different points on the flat profile. As will be seen later, attempts

to measure accurately the position of maximum velocity in annular turbulent flow, have for these reasons been unsuccessful.

2.2 The Double Pitot Tube

Attempts to measure precisely the flat portions of a velocity profile, such as those found in the central zone of turbulent channel or annular flow, by means of a single Pitot tube have proved unsatisfactory. A good overall profile can be obtained but the results for the precise determination of the position of maximum velocity have been too variable and inconsistent to be conclusive.

In order to try and determine the position of maximum velocity precisely, the double Pitot tube was introduced by Brighton and Jones [4]. Since the accurate determination of this position of maximum velocity is usually of no importance, it is perhaps not surprising that there is very little literature available on the double Pitot tube. As will be seen later for some experiments in annular flow, the determination of this position was fundamental to the determination of the wall shear stresses and wall friction factors.

The double Pitot tube such as that shown in Fig. 3, consists merely of two ordinary Pitot tubes mounted very close together and connected via a differential manometer. Some idea of the size of tubes can be gained from previous research.

Brighton and Jones [4] used two hypodermic needles having external diameters of 0,64 mm and internal diameters of 0,32 mm spaced 5 mm apart.

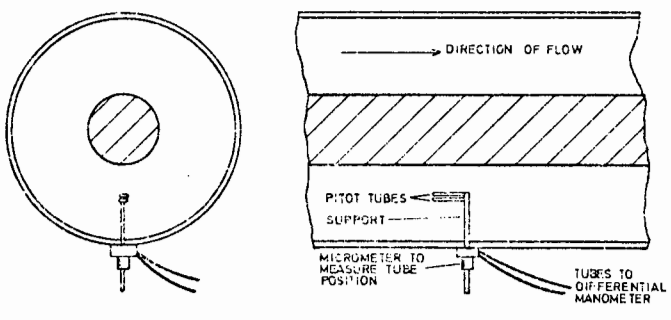

Fig. 3 Double Pitot tube in an annulus

Quarmby [32] used needles flattened to 0,25 mm with an effective spacing of 1,27 mm.

It would appear that the double Pitot tube would present an accurate method of determining the position of maximum velocity - at least more accurate than the standard single Pitot tube. One of the only theoretical criticisms would be that the null differential manometer reading, indicating the position of maximum velocity, would not necessarily correspond to the point midway between the two tubes. This error would be minimised by reducing the separation between tubes.

Yet Quarmby [32] has shown experimentally that the double Pitot tube is no more accurate than the single Pitot tube, especially at low Reynolds numbers. His results showed that the positions of maximum velocity obtained with a double Pitot tube were too variable to be conclusive.

Experiments have shown that little faith can be placed in the determination of the position of maximum velocity by single or double Pitot tubes with the accuracy required for annular flow calculations.

2.3 The Preston Tube

More than 20 years ago Preston [30] published a method of measuring wall shear stresses, based on the use of a modified Pitot tube resting on the wall-surface, the so called Preston tube, together with an extension of the Stanton tube outside the laminar sublayer. The Stanton tube consisted of a very small flattened Pitot tube placed in the viscous sublayer of a shear flow. In theory the tube could be used to measure the wall shear stress for both a laminar and a turbulent main flow, however in practice it was found difficult to construct a tube small and robust enough to lie entirely within the viscous sublayer. The Preston tube is a much larger circular Pitot tube that extends right into the turbulent portion of the nominally constant stress layer. Preston's original tubes ranged in external diameter from 0,74 mm to 3,08 mm and all had a constant ratio of internal to external tube diameter of close to 0,6. They were mounted on the wall surface as shown in Fig. 4. The placement of Preston tubes in annuli is shown in Fig. 5.

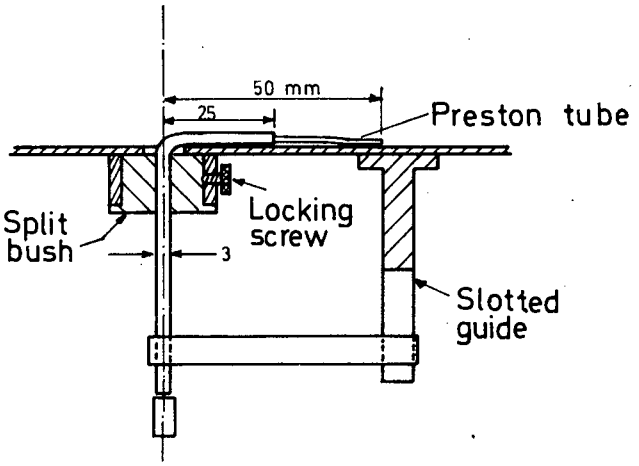

Fig. 4 Preston's original Pitot tube mounting

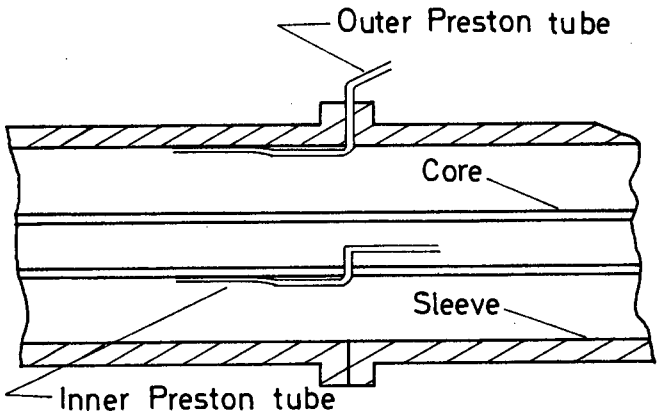

Fig. 5 Preston tubes in an annulus

The concept of measuring wall shear stresses with a Preston tube rests on the assumption that close to the wall surface in turbulent shear flow there exists a region in which the flow is determined by the wall shear stress and the relevant properties of the fluid only, i.e. independent of the nature of the outer turbulent flow. Past experiments had indicated, and the mixing length had predicted, the validity of this assumption which can be expressed mathematically as

$$\frac{U}{U_\tau} = fn_1\left(\frac{yU_\tau}{\nu}\right) \qquad \text{(Eq. 5)}$$

where U = time mean velocity at a distance y from the wall

U_τ = friction velocity $(\tau_w/\rho)^{\frac{1}{2}}$

τ_w = wall shear stress

Empirically Eq. 5 has been shown to apply to a region close to the wall of the order of 1/10 of the flat plate boundary layer thickness. This region is therefore far larger than the viscous sublayer which it incorporates. Close to the wall in the viscous sublayer Eq. 5 assumes the form

$$\frac{U}{U_\tau} = \frac{yU_\tau}{\nu}, \qquad \text{(Eq. 6)}$$

and this is the basis of the Stanton tube method.

If Eq. 5 is valid then it appears as if the only independent variables in this region are ρ, ν, τ_w and a suitable length. For a Preston tube mounted on a wall surface the difference between the total pressure read by the tube and the related undisturbed static pressure at the wall would be the dependent variable depending only on ρ, ν, τ_w and d the internal diameter of the tube. Selecting d for geometric similarity, ρ for dynamic similarity and ν for kinematic similarity the Buckingham-π method of dimensional analysis yields the equation used by Preston:

$$\frac{\hat{P}_v d^2}{\rho\nu^2} = fn_2\left(\frac{\tau_w d^2}{\rho\nu^2}\right) \qquad \text{(Eq. 7)}$$

Providing Eq. 7 is valid, the form of fn_2 can be established in a horizontal circular pipe where the wall shear stress can be obtained from the axial pressure gradient. For this situation

$$\tau_w = \frac{\Delta P_s D}{4L} \qquad \text{(Eq. 8)}$$

where ΔP_s = value of axial static pressure drop over a length L

D = internal diameter of pipe

Now if the results of a range of geometrically similar Preston tubes are plotted in the form of Eq. 7 for varying ΔP_s, and are found to lie on a well defined curve, then the curve represents fn_2 and the existence of a region of local dynamical similarity has been established. Fig. 6 shows the positioning of a Preston tube in relation to the mean velocity variation in a pipe. Fig. 7 shows Preston's result for the value of fn_2.

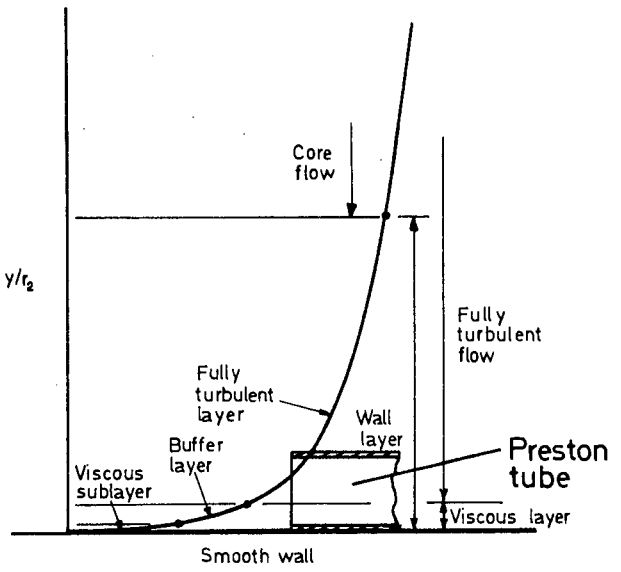

Fig. 6 Preston tube in wall layer

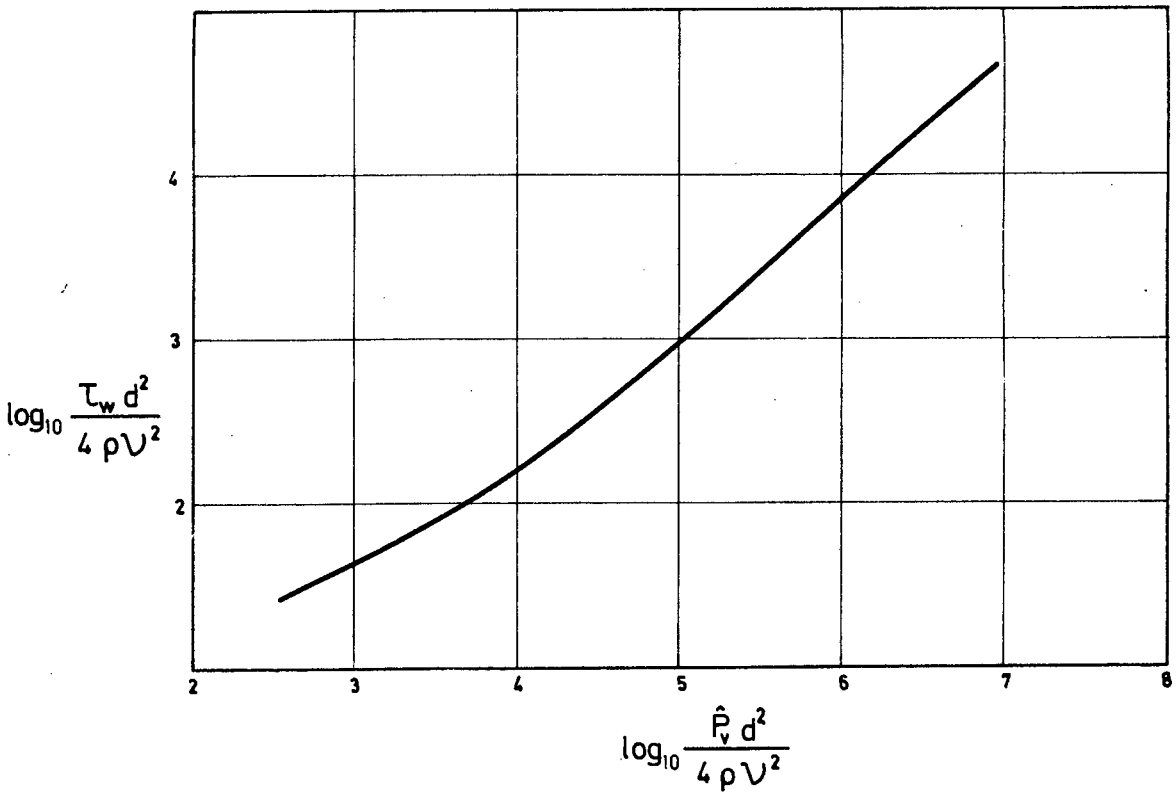

Fig. 7 Preston's result for the value of fn_2

Having established the form and value of fn_2, the Preston tube may be used to determine the wall shear stresses (in any situation where this calibration is valid) by means of Eq. 7. It can be shown that the experimental calibration curve described in Fig. 7 is compatible with that derived from the universal logarithmic law of the wall for flow in a circular pipe provided the relevant corrections for Pitot tubes, discussed in 2.1, are applied.

Although Preston's experimental results substantiated the validity of the method, considerable doubt was cast upon the universality of his findings by independent researchers in England and America. It was left to Head and Rechenberg [10] to provide convincing evidence that the function fn_2 defining the law of the wall was universal for fully developed turbulent flow in pipes and channels, and that it applied also in the wall region of a turbulent boundary layer; thus substantiating the Preston tube method. Their

experiments consisted of demonstrating that a Preston tube gave the same readings in pipe and flat plate boundary layer flows for the same values of wall shear stress. However, whilst their results established the validity of the Preston tube method, Patel [29] established that although Preston's concept had been correct, his calibration had in fact been in error. Today the Preston tube is usually used in conjunction with Patel's calibration.

Yet it is necessary to realise that the validity of the Preston tube method is dependent on three conditions:

(i) The Preston tube representative length dimension must be small compared with the pipe diameter

(ii) The Preston tube must lie within the region for which Eq. 5 holds

(iii) The Preston tube may only be used in flows where the universal logarithmic velocity profile is the same for which the tube has been calibrated

Thus it appears to date that the Preston tube is a good and accurate means of determining skin friction for flow situations similar to those for which it has been calibrated. This last stipulation is important as will be seen later on when dealing with annular flows.

2.4 The Hot Wire Anemometer

For steady laminar flow, instruments such as the Pitot tube are suitable for measuring velocities in all regions except those close to solid boundaries. When turbulent flow is present, only the temporal mean velocities can be measured by the Pitot tube. Although modern day developments include sophisticated methods such as laser-Doppler techniques, the most satisfactory method at present of measuring turbulent fluctuations is the hot wire anemometer.

In essence, the hot wire anemometer is a resistance thermometer with a high excitation current. The instrument consists of a thin

wire ($d < 0{,}025$ mm) usually not more than 5 mm long, supported at the ends between two inert probes (for diagram see Fig. 8). The wire is usually made of platinum, a platinum alloy or tungsten, the disadvantage of tungsten being that it cannot be soft soldered. The wire is heated by passing an electric current through it and noting the heat loss from the wire caused by the velocity stream. This heat loss (neglecting secondary effects), equals the heat generated through the wire by virtue of its electrical resistance. The wire may either be operated at constant current by using a large series resistor in conjunction with the power supply or at constant temperature as one arm of a Wheatstone bridge.

The rate of heat transfer (per unit length) Θ/L from a long fine wire, the axis of which is normal to a uniform gas flow of velocity U, depends upon:

d = the wire diameter

λ = the mean free path of gas molecules

T_w = the absolute temperature of the wire

T_f = the absolute temperature of the free stream velocity

k = fluid thermal conductivity

ν = diffusivity of momentum

κ = diffusivity of heat at free stream temperature

Using dimensional analysis one obtains:

$$Nu = fn\,(Re, Pr, T_w/T_f, Kn) \qquad \text{(Eq. 9)}$$

where $$Nu = \frac{\text{rate of heat transfer}}{k(\text{temperature gradient})\ \text{area of wire}}$$

$$= \frac{\Theta d}{\pi\, d\, L\, k\, (T_w - T_f)} \qquad \text{(Eq. 10)}$$

$$= \frac{\Theta/L}{k(T_w - T_f)}$$ and is known as the Nusselt number

$Re = ud/\nu$ and is known as the Reynolds number

$Pr = \nu/\kappa$ and is known as the Prandtl number

$Kn = \lambda/d$ and is known as the Knudsen number

Most of the parameters in the above law can be neglected. For example Pr is reasonably constant for any one gas in the normal operating range and Kn is negligible for gases where Kn is less than 0,015 and this is usually the case. Empirical results (from Hinze [11]) shows that

$$Nu = 0{,}42\ Pr^{0,2} + 0{,}57\ Pr^{0,33}\ Re^{0,5} \qquad \text{(Eq. 11)}$$

which can be written in the form

$$Nu = A + B\sqrt{u/\nu} \text{ where A and B are constant} \qquad \text{(Eq. 12)}$$

Now the energy dissipation per unit time from the wire must be equal to the heat generated per unit time by virtue of the electrical current passing through its resistance.

$$\therefore \quad \Theta = I^2R_w = VI \qquad \text{(Eq. 13)}$$

where I = instantaneous value of current through the wire

R_w = instantaneous value of the wire resistance

V = instantaneous voltage across probe tips

Replacing Θ in Eq. 10 gives

$$Nu = \frac{I^2R_w}{k(T_w - T_f)L} \qquad \text{(Eq. 14)}$$

The temperature differential in the Nusselt number may be equated to a resistance differential due to the temperature dependence of the wire resistance. Thus

$$R_w = R_f\,(1 + \alpha(T_w - T_f)) \qquad \text{(Eq. 15)}$$

where R_f = resistance of wire at fluid mean stream temperature

α = temperature coefficient of resistance

Eq. 15 has assumed the ambient fluid temperature as a reference and that α is the average value between T_f and T_w. A reference temperature of say 0° C could equally well have been chosen. Sometimes, small variations of k and α occur with temperature, and corrections, which will not be dealt with here, are necessary. Usually isothermal conditions are assumed and thus variation in k and α are neglected. Substituting Eq. 15 into Eq. 14 gives

$$Nu = \frac{I^2 R_w R_f \alpha}{\pi L k (R_w - R_f)}$$

$$I^2 R_w = \frac{\pi k L}{\alpha} \frac{R_w - R_f}{R_f} (0{,}42\ Pr^{0,2} + 0{,}57\ Pr^{0,33}\ Re^{0,5}) \qquad \text{(Eq. 16)}$$

Assuming constant temperature conditions, this can be written as

$$\frac{I^2 R_w}{R_w - R_f} = C + D\sqrt{u} \qquad \text{(Eq. 17)}$$

In practice, the constants C and D are not calculated but are determined experimentally. This is quite easily done. The determination of Nu as a function of Re and Pr can be simplified as shown to finding the variation with

$\sqrt{u}$ of $R_w/(R_w - R_f)$ for constant current,

or the variation with

$\sqrt{u}$ of I^2 for constant temperature probes.

The relationship between I^2 and $\sqrt{u}$ is linear as shown by Eq. 17 and calibration of the hot wire is usually done with a Pitot-static tube in a smooth gas flow whose turbulent fluctuation intensity is as low as possible. The simplification is possible because the constants omitted from Re and Nu are ~~constant~~ fixed for a given wire probe.

The validity of the above calibration will now be established for low turbulence intensities. Consider a hot wire probe placed normal to the mean velocity stream U_x (see Fig. 8). It is important and yet not obvious that the cylindrical hot wire is sensitive only to the u'_x fluctuations:

Assume that the wire is exposed to fluctuating air flow of a low relative intensity of turbulence such that

$$u'_x/U_x << 1$$

where u'_x = fluctuating component of the x-direction velocity

U_x = temporal mean component of the x-direction velocity

Assume also that the mean flow is unidirectional and equal to U_x and suppose that the wire is unaffected by fluctuations parallel to its axis. Then

$$u_x >> u_y \sim u_z$$

where u_x, u_y and u_z are the instantaneous velocities in the x, y and z directions respectively.

$$\therefore \quad (U_x + u'_x) >> (U_y + u'_y) \sim (U_z + u'_z)$$

$$\therefore \quad (U_x + u'_x) >> u'_y \sim u'_z$$

But $u'_x \sim u'_y \sim u'_z$ because at the axis of a conduit turbulence is isotropic. Therefore the sensitivity to the u'_x fluctuations must be concerned with U_x. The magnitude of any fluctuation in the plane normal to the wire axis causes the response of the wire and

$$u_{res} = \sqrt{(U_x + u'_x)^2 + u'^2_y} \qquad \text{(Eq. 18)}$$

$$= U_x \left(1 + u'_x/U_x + u'^2_y/2U^2_x - u'_x u'^2_y/2U^3_x + \ldots\right) \qquad \text{(Eq. 19)}$$

The fluctuating part of which is approximately equal to

$$u'_x + \frac{u'_y}{2U_x} .$$

Thus if $u'_x \sim u'_y << U_x$, the hot wire can be assumed to measure the u'_x fluctuations and the linearised calibration established earlier is valid. This is because the relative magnitude of the u'_y fluctuations is small

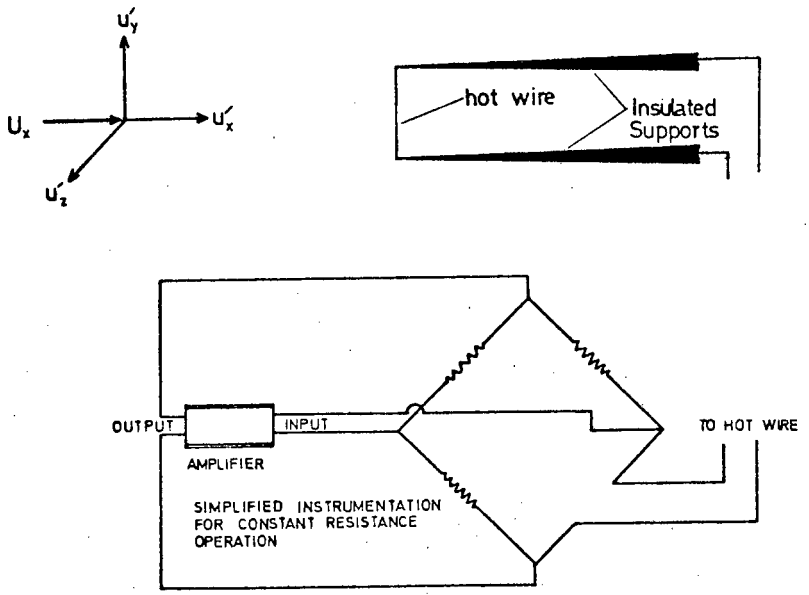

Fig. 8 Hot wire anemometer in a unidirectional turbulent flow

However, it is very important to consider the effect of large scale turbulence fluctuations on the hot wire response. The previous linear calibration of $Nu = C + D\sqrt{u}$ is no longer valid due to the now significant effect of the u'_y component. From Eq. 18

$$\sqrt{u_{res}} = \sqrt[4]{(U_x + u'_x)^2 + u'^2_y}$$

$$= \sqrt{U_x}(1 + u'_x/2U_x - u'^2_x/8U^2_x + u'^2_y/4U^2_x + u'^3_x/$$

$$16U^3_x - 3u'_x u'^2_y/8U^3_x + \ldots)$$

Now if $u'_x/U_x \ll 1$ is no longer valid then the cooling of the wire is affected by the u'_x and u'_y components and the expression needed for calibration is therefore:

$$Nu = C + D\sqrt{U_x}(1 + u'_x/2U_x - u'^2_x/8U^2_x + u'^2_y/4U^2_x + \ldots)$$

(Eq. 20)

Thus it can be seen that a non-linear calibration is required. Furthermore, the calibration requires at least a prior knowledge of the nature of the intensities to be measured. Sometimes the effect of high turbulence intensities is investigated by vibrating the hot wire in a flow of low intensity, thus approximating an undirectional high intensity, but this cannot be deemed entirely satisfactory. It seems that the correct measurement of turbulence of high intensity is extremely difficult.

Until now, the supposition has been made that the fluctuating velocity component parallel to the wire axis does not affect the heat loss. Unless the u'_z component is very large this supposition is correct. This can be proved for an infinitely long wire and in practice has been found true for hot wire probes. Empirical and dimensional results have shown that when there is a flow with a velocity component parallel to the wire axis:

$$u_{eff} = u_{res} \cos \alpha$$

where α = angle between the plane normal to the wire axis and u_{res}

u_{res} = resultant velocity at probe

The use of the slant probe and crosswire probe are based on the cosine law. For a slant probe Eq. 12 becomes

$$Nu = C + D \sqrt{u_{res} \cos \alpha}$$

The measurement of the turbulent intensity involves the determination of the fluctuating velocities.

(i) To measure the $\sqrt{\overline{u_x'^2}}$ component of turbulent intensity:

A single hot wire as shown in Fig. 8 is inserted perpendicular to the direction of mean flow U_x. The hot wire is sensitive to u_x' fluctuations only, for the reasons outlined above. After suitable electronic correction, the instantaneous amplifier output is proportional to u_x' and an oscillograph record such as that shown in Fig. 10 is obtained. The meter shown in Fig. 11 would yield a reading proportional to $\sqrt{\overline{u_x'^2}}$

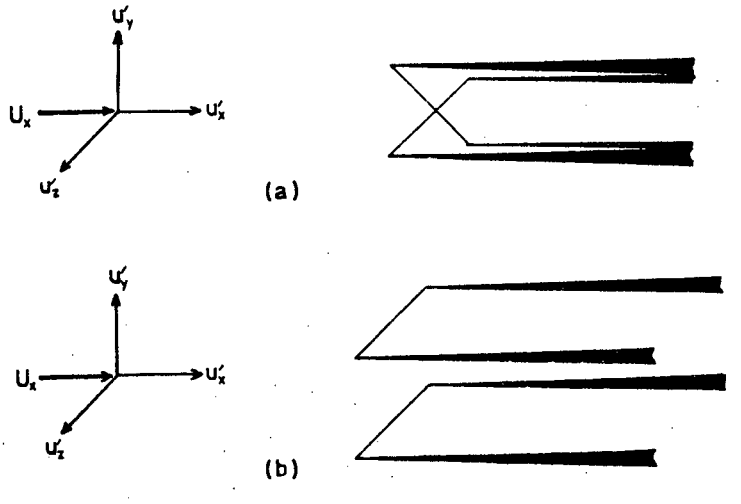

Fig. 9 Various types of hot wire probes

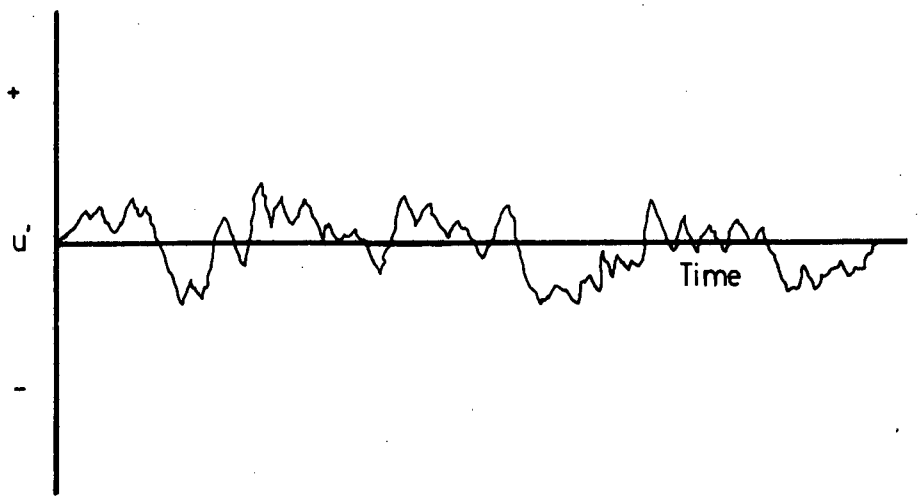

Fig. 10 Oscillograph record of velocity fluctuations

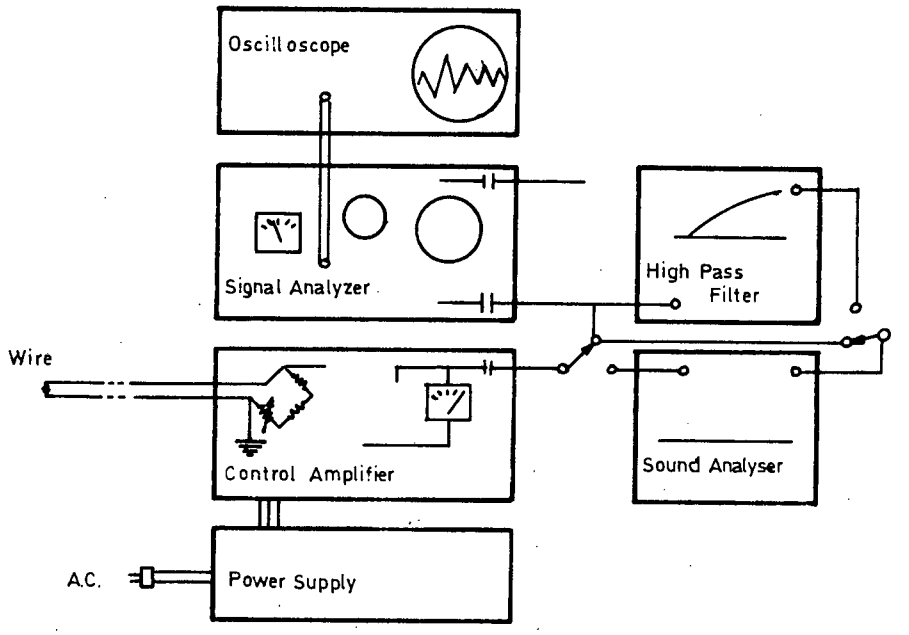

Fig. 11 Typical hot wire instrumentation

(ii) To measure $\sqrt{\overline{u_x'^2}}$ and $\sqrt{\overline{u_y'^2}}$ components of turbulent intensity:

A cross wire anemometer (Fig. 9a) or a slant probe is used to measure the x and y components of the turbulent intensity. The cross wire anemometer is in common use today and consists of two identical wires, one placed at a positive, and the other at a negative angle to the mean velocity stream, with the plane of the wires in the direction of the stream. Now if v_1 and v_2 are the instantaneous voltages across wires 1 and 2 respectively, the following relationship has been given by Knudsen and Katz [12]:

$$\sqrt{\overline{u_y'^2}} \propto \sqrt{\overline{(v_1 - v_2)^2}} \text{ and}$$

$$\sqrt{\overline{u_x'^2}} \propto \sqrt{\overline{(v_1 + v_2)^2}}$$

of course $\sqrt{\overline{u_x'^2}}$ could be obtained by rotating the probe in the x-z plane.

(iii) To measure $\overline{u_x'u_y'}$ and $\overline{u_x'u_z'}$ components of turbulent shear:

The turbulent shear components can also be measured using a x-wire probe. If the probe is orientated in the x-y plane (as shown in Fig. 9a)

$$\overline{u_x'u_y'} \propto \overline{v_1^2} - \overline{v_2^2}$$

and if in the x-z plane

$$\overline{u_x'u_z'} \propto \overline{v_1^2} - \overline{v_2^2}$$

In the foregoing analysis it has been assumed that there is no thermal inertia of the probe wire. In other words, that voltage fluctuations would give a true picture of velocity fluctuations with time on an oscillograph. In reality, thermal inertia causes a noticeable time lag. This and many other problems such as probe support conduction, wire contamination and thermal wire sag necessitate complicated corrections and calibrations of the wire.

Many of these corrections are now compensated for by suitable electronic equipment, the details of which belong in the field of electrical engineering.

The main advantage of the constant temperature over the constant current hot wire is that the compensation circuit to maintain the constant temperature does not need manual adjustment. Thus the operating conditions can be varied greatly without adjustment or fear of the wire burning out if the flow stops. The constant temperature amplifier is however more complicated than its counterpart.

Thus although the hot wire anemometer is a valuable tool for the determination of fluctuating velocity components, it is as well to realise that it is an expensive and sophisticated instrument which requires a large amount of knowledge and experience for its satisfactory operation.

SECTION 3

PREVIOUS SHEAR STRESS MEASUREMENTS IN ANNULAR FLOW

Attempts to measure wall shear stresses in annular flow can be divided into two main categories, that is to say indirect and direct methods of measurement.

3.1 Indirect Shear Stress Measurement

Indirect methods are concerned with calculating the wall shear stresses from indirect measurements such as the velocity profiles. Most indirect methods rely on the accurate determination of the position of some unique feature of the flow, such as the position of maximum velocity or that of zero shear stress. In annular flow both these positions lie closer to the core wall than to the sleeve wall. Of all the indirect methods used, those involving the hot wire anemometer have proved the most reliable.

Disadvantages of the indirect methods stem from the fact that the accurate and precise determination of the relevant maxima or zero value is extremely difficult or expensive. Hot wire anemometers, it has been noted, are complex and costly pieces of equipment. The use of simpler instruments such as Pitot tubes have proved misleading. An advantage of indirect methods is the extra information that they provide such as mean velocity distributions and shear stress intensities. This extra information is not immediately available from direct wall shear stress measurements.

Some of the most notable investigations using indirect methods of wall shear stress determination will now be examined:

3.1.1 Owen [28]

In 1951 Owen attempted to measure some of the variables in annular flow. He seems not to have considered the desirability of

measuring the stresses on the individual walls of the annulus and his results are therefore concerned with the wall shear stress of the system as a whole. In addition to the total friction factor versus Reynolds number (f_T vs Re) curve, Owen also presented velocity distribution curves for different annular geometries with a Reynolds number range of 4 000 to 700 000.

Owen's apparatus consisted of two basically similar rigs; one with a 152 mm sleeve and 30,5 m length, the other with a 51 mm sleeve and a 11,0 m length. Cores were located by means of metal spiders placed well downstream from the Pitot or static pressure measuring devices, in order to minimise disturbances. Both rigs were horizontal and Owen estimated that the maximum core deflections which occurred for the 51 mm sleeve were 3% of the distance between core and sleeve wall. No details of the core sag for the 152 mm sleeve were given. The axial pressure gradient was determined simply from wall piezometers connected to a head loss manometer. The velocity distributions were obtained from Pitot-static probes. Water was supplied to the rig by a constant head tank.

Owen's results consisted of a presentation of the f_T vs Re curve and velocity distributions. From the velocity traverse results, it can be seen that the profile is asymmetric across the annular gap and that the position of the point of maximum velocity remains constant, within the limits of experimental accuracy, for a given annular pipe. This position was found to lie approximately 0,4 of the distance between the core and sleeve walls, from the core. However, the author was not concerned with the calculation of separate wall shear stresses from this position and repeated attempts at the determination of the location of the maximum velocity would probably have yielded scattered results not shown on Owen's graphs. Owen further determined the existence of a logarithmic law of the wall relationship for both sleeve and core walls and further found that the exponent n in the relationship $U_x = ay^n$ is always less at the core than at the sleeve wall.

Owen's research serves to illustrate the rather basic approach to the problems of annular flow before the 1960's. Very little attempt was made to determine the far more complex features of annular flow such as the position of zero shear stress. Indeed the first really significant effort to measure all the flow variables was made by Brighton and Jones in 1964.

3.1.2 Brighton and Jones [4]

The Brighton and Jones paper constitutes the first authoritative approach into all facets of turbulent annular flow. It presented data for friction factors, velocity profiles, positions of maximum velocity, as well as turbulence distributions for a Reynolds number range of 46 000 to 327 000.

Their test rig consisted of two concentric aluminium pipes 8,8 m long. The sleeve had a diameter of 203 mm. Four different cores were used to give radius ratios of 0,0625; 0,125; 0,375 and 0,562. The authors attempted to aid the development of an artificially thickened boundary layer of air by placing a screen of concentric circular wire rings together with a 0,9 m length of sand roughened pipe at the test rig inlet. They appear to be the first investigators to use the double Pitot tube for measuring the position of maximum velocity, as well as the first to use the hot wire anemometer for the measurement of turbulence intensities in annuli. Mean velocity profiles were measured with Pitot tubes made from hypodermic needles. For the purpose of determining friction factors at low Reynolds number, a water flow apparatus was used. Apart from the fact that this apparatus consisted of a clear plastic sleeve of 15,9 mm diameter 1,8 m long, with core wires of 1,9 mm and 3,2 mm diameter, no information about this rig is given. It can only be assumed that it yielded information about the overall friction factor only.

Unfortunately most of the data presented in the Brighton and Jones paper appears to be condensed from the work done by Brighton in 1963 for his Ph.D. thesis. Many comments voiced by later researchers

refer to the more comprehensive results found only in the thesis. Because this thesis was not available at U.C.T., some evaluations on Brighton's results must come from second hand sources. The most important of these comes from Quarmby [32] who found that Brighton's method of determining velocity profiles would not be very accurate for low Reynolds number and that the use of the double Pitot tube for maximum velocity position determination cannot reduce the unacceptably large scatter of past results for this position. Furthermore, Rehme [35] found that Brighton's results for the position of zero shear stress, as determined by hot wire anemometry showed so much scatter as to be inconclusive. Thus an examination of the Brighton and Jones paper, in the absence of the Brighton thesis, can be deceptive since little information on the scatter of the results is shown.

Integrating the following equation:

$$\frac{1}{\rho}\frac{\partial P}{\partial x} = -\frac{1}{r}\frac{\partial}{\partial r}\left(r\overline{u'_x u'_r}\right) + \frac{\nu}{r}\frac{\partial}{\partial r}\left(r\frac{\partial U_x}{\partial r}\right)$$

and applying the boundary conditions $\frac{\partial U_x}{\partial r} = 0$ and $\overline{u'_x u'_r} = \xi$ at r_{mt}, the authors obtained

$$\overline{u'_x u'_r} = -\frac{1}{2\rho}\frac{\partial P}{\partial x}\left(\frac{r^2 - r_{mt}^2}{r}\right) + \nu\frac{\partial U_x}{\partial r} + \frac{r_{mt}}{r}\xi \qquad \text{(Eq. 22)}$$

If it was assumed that $\xi = 0$ then Eq. 22 simplifies to

$$\overline{u'_x u'_r} = -\frac{1}{2\rho}\frac{\partial P}{\partial x}\left(\frac{r^2 - r_{mt}^2}{r}\right) \qquad \text{(Eq. 23)}$$

for the turbulent region. This would enable the calculation of the Reynolds stress distribution.

Measurements performed by the authors suggested to them that ξ was in fact zero at r_{mt}. As will be seen in the theoretical section there is no analytical basis for this assumption.

The authors then calculated their shear stress distributions from r_{mt} and $\partial P/\partial x$, and checked these with the values obtained from hot wire anemometry. It can be seen that the determination of r_{mt} is critical, since even with the assumption that $\xi = 0$ the shear stress profile and the Reynolds stress profile depends upon r_{mt}^2, and as Quarmby has pointed out, Brighton's method of determining r_{mt} resulted in scatter.

Despite inaccuracies in the extremely difficult measurement of certain variables, Brighton and Jones laid an excellent and commendable foundation upon which others could build. Indeed most future research using indirect methods has been concerned with refining and reproducing Brighton and Jones' methods and results. The most important results which the authors presented were:

(i) The friction factors for flow in annuli with smooth walls were slightly higher (1% to 10%) than friction factors for pipe flow at corresponding Reynolds numbers

(ii) The friction factors depend only on the Reynolds number and are independent of radius ratio α, at least for $\alpha > 0{,}0625$

(iii) Within the accuracy of the experimental results, the zero Reynolds stress and maximum velocity occur at the same point, the position of which ranges from 0,2 to 0,45 of the distance between the core and sleeve walls from the core; and depends only upon the radius ratio.

(iv) The Prandtl mixing length is very large in the region of maximum velocity

(v) The location of the point of maximum velocity is nearer the inner wall than for laminar flow. Consequently the ratio of the shear stress at the inner wall to the shear stress at the outer wall is less than for laminar flow. That is

$$(\tau_1/\tau_2)_{turbulent} < (\tau_1/\tau_2)_{laminar}$$

3.1.3 Olson and Sparrow [27]

Any fluid entering a duct from some exterior source is subjected to a development of its velocity profile caused by the viscous forces acting within it. This development continues in the entrance region of the duct until the viscous forces balance the pressure forces causing the flow. Once this has occurred the mean velocity profile is essentially fully developed and constant.

If fully developed turbulent duct flow is to be studied experimentally, some development region known as the hydrodynamic entrance length must be incorporated into the test rig before any measurement station. Olson and Sparrow present few worthwhile details of wall shear stresses in their paper, yet their work has great value in having produced results on the entrance length necessary for fully developed flow in annuli.

For turbulent flow in circular pipes the hydrodynamic entrance length is equal to approximately 20 equivalent diameters. Olson and Sparrow's fundamental and most important results was that the hydrodynamic entrance length for annuli, necessary for the pressure gradient to approach to within 5% of the fully developed pressure gradient, was 20 to 25 equivalent diameters. This result is roughly an order of magnitude less than the only other information concerning this problem, namely that obtained by Rothfus and co-workers [37] using their suspended core system. As will be seen later, little faith can be placed in the accuracy of the suspended core system or its results.

The work of Olson and Sparrow was valuable in determining the entrance length necessary for the floating sleeve rig.

3.1.4 Turbulence Models

Using the important experimental results of Brighton and Jones as comparison, many attempts were made at producing a mathematical model of turbulent flow in annuli. The most important of these are listed below:

(i)

Macagno and McDougal [18] based their model on the assumption that for fully developed turbulent flow the logarithmic velocity distribution is applicable to the inner and outer layers, separated by the cylindrical surface of maximum velocity, and without interaction on each other. The authors made no assumption as to the position of this isovel or the ratio of the shear stresses, and realised that there were no grounds for transferring some of the characteristics of laminar flow to turbulent flow. They did, however, assume that $r_{0t} = r_{mt}$ (although no reasons were presented for this assumption); as well as the notion that not only were the constants in both logarithmic layers identical, but also that they were equal to those ascertained in the Prandtl-von Karman approach to circular pipes. These are indeed wide ranging assumptions and ones that have not been validated by recent research.

The above assumptions enabled the authors to compute individual friction factors, positions of zero shear stress and velocity profiles. Through a simple process of manipulation based on

$$\frac{U_j}{\sqrt{\tau_j/\rho}} = A \log\left[\frac{\sqrt{\tau_j/\rho}}{\nu} y_j\right] + B \qquad \text{for } j = 1,2$$

and the usual force balance for annular cylinders, the authors obtained

$$\left[\frac{\beta^2 - \alpha^2}{\alpha(1-\beta^2)}\right]^{\frac{1}{2}} = \frac{\log\left[\frac{C}{4\sqrt{2}}\left(\frac{1-\beta^2}{1-\alpha}\right)^{\frac{1}{2}}\left(\frac{1-\beta}{1-\alpha}\right) Re\sqrt{f}\right]}{\log\left[\frac{C}{4\sqrt{2}}\left(\frac{\beta^2-\alpha^2}{\alpha-\alpha^2}\right)^{\frac{1}{2}}\left(\frac{\beta-\alpha}{1-\alpha}\right) Re\sqrt{f}\right]} \qquad \text{(Eq. 24)}$$

where $\alpha = r_1/r_2$

$\beta = r_0/r_2$

C = a combined constant

Eq. 24 enables the position of zero shear stress to be calculated for input value of $Re\sqrt{f}$. The mean velocity was then calculated by intergrating the velocity distribution curves thus yielding the total flow and dividing this by the flow area. The well-known expression

$$f = \frac{2\tau}{\rho \hat{U}_x^2}$$

is then used to compute the friction factor. A similar procedure is applied for the individual wall friction factors.

The deviations of the predictions of the above analysis from experimental data is a result of the authors faith in an unsubstantiated 'universal velocity profile' applicable to pipes and annuli. Whilst realising correctly that no assumptions could be made regarding the ratio of wall shear stresses in annuli and the deduction therefrom of velocity profiles, the authors erroneously made an assumption concerning the shape of velocity profiles and thus deduced the wall shear stresses.

(ii)

Clump and Kwasnoski [7] used a diffusivity model to predict velocity distributions. In analysing the related equations the authors also assumed that $r_{mt} = r_{0t}$ and since the model requires the input of r_{0t} this was obtained firstly by assuming that $r_{0t} = r_{mt} = r_{m\ell}$ and secondly by using Brighton and Jones' experimental results for the position of r_{mt}. Brighton and Jones have already shown experimentally that $r_{mt} \neq r_{m\ell}$, thus invalidating the first assumption.

This model is concerned with the prediction of velocity profiles based on a diffusivity model and not with the prediction of shear stresses which is the main topic of this thesis. The idea of using a diffusivity model is a good one and the authors have had some success in predicting velocity profiles. However it could be argued that this success is largely due to the model being based upon the very results it is supposed to predict. Should the assumption that $r_{0t} = r_{mt}$ be proved false, then the model is not a true eddy diffusivity model since it attempts to predict velocity profiles based upon the shear stress profile as determined by a position of maximum velocity and not by a position of zero shear stress. It would be profitable to repeat the analysis without the assumption that $r_{0t} = r_{mt}$ and input more reliable results for r_{0t}.

(iii)

Levy [15] succeeded in producing a model which produced results that coincided well with the available experimental results for the position of zero shear. Levy disregarded all assumptions as to the nature of the velocity profiles, or the translation of features of laminar flow to turbulent flow in annuli.

However, in order to produce a mathematical simulation of turbulence in annuli, use must be made either of a fundamental assumption concerning flow conditions (such as the form of the velocity profile) or some relevant experimental data (such as the value of the mixing length constant).

Levy's assumptions concerned the form of the eddy diffusivity of momentum, the value of the mixing length constant near the outer wall and the hypothesis that $r_{0t} = r_{mt}$. Using the standard method of separating the turbulent core region from the viscous wall region, Levy derived expressions for the position of zero shear and friction factors.

Reichardt's expression for the eddy diffusivity of momentum in a circular pipe is:

$$\frac{\varepsilon}{\nu} = \frac{kR^+}{6}\left[1 - (r/r_2)^2\right]\left[1 + 2(r/r_2)^2\right] \qquad \text{(Eq. 25)}$$

where k is the mixing length constant = 0,4

and $R^+ = r_2\sqrt{\tau_2\rho}/\nu$

Levy's fundamental postulate was that this expression was valid in an annulus for the flow regions on both sides of the line of zero shear. Thus Eq. 25 becomes

$$\frac{\varepsilon}{\nu} = \frac{k_j}{6}\left|(r_j - r_m)\right|\frac{\sqrt{\tau_j/\rho}}{\nu}\left[1 - \left(\frac{r - r_m}{r_j - r_m}\right)^2\right]$$

$$\times\left[1 + 2\left(\frac{r - r_m}{r_j - r_m}\right)^2\right] \qquad \text{(Eq. 26)}$$

where $j = 1,2$

That Levy's model was more accurate (in the sense of predicting experimental results) than Macagno and McDougal's, must be due to the difference in fundamental assumptions made by the respective authors. Indeed it seems more plausible and fundamental to assume that an expression for eddy diffusivity derived for pipe flow could be related to annular flow, than to assume that an expression for the velocity profile in pipe flow would be applicable to annular flow.

A point of interest to be noted in Levy's and indeed in any eddy diffusivity model to date has been the assumption that $r_{0t} = r_{mt}$. Should this assumption be incorrect it means that between the location of $\partial U_x/\partial r = 0$ and $\tau_{xr} = 0$ the eddy diffusivity is negative. If this is the case, can the eddy diffusivity method be applied to the transfer of momentum in annuli ? Answers to such questions have not been considered by those using the eddy diffusivity model. What might happen in a case such as this, is that the usual energy transfer mechanism is reversed, energy being transferred in this narrow region from the eddies to the main flow.

On the whole, models of turbulence in annular flow have been able to predict fairly satisfactorily the results obtained empirically. It is impossible to give figures comparing accuracy, yet it is fair to say that the standards reached by the Prandtl-von Karman approaches to the far simpler circular pipe have not yet been achieved for annuli. Two of the main desirable attributes of turbulence models are accuracy and universality. For annular flow, only the second has been satisfactorily achieved.

3.1.5 Lawn and Elliot [13]

The above authors used a vertical test duct which was supplied with air slightly above atmospheric pressure by an airscrew fan for a Reynolds number range of 30 000 to 240 000. The outer sleeve diameter was 144,3 mm and the inner sleeve diameters of 12,7 mm, 25,4 mm and

57,1 mm were held in position by wires (of size 26 s.w.g.) at several axial positions. These geometries provided radius ratios of 0,088; 0,176 and 0,396.

Essentially this research was a repeat of the Brighton & Jones work. The authors used hot wire anemometers to measure the zero shear stress position and Pitot tubes and static taps to measure velocity profiles and pressure gradients. As a check on the metered flow (no details given) the velocity profiles were determined with a double Pitot and compared with results obtained by graphically differentiating some of the profiles and interpolating to the point of zero velocity on the velocity gradient plot. These results agreed within the limit of 0,25 mm.

The authors' main interest seems to have centred on velocity profiles, however, they did establish the non-coincidence of the positions of zero shear stress and maximum velocity. Lawn and Elliots' main results are summarised below:

(i) The friction factor of a smooth annulus based on the equivalent diameter is between 5 and 8,5 per cent greater than that of a pipe

(ii) The hot wire anemometer is capable of locating the position of zero shear to within 0,2 mm

(iii) The positions of zero shear and maximum velocity are non-coincident, the former being closer to the core wall. The position of zero shear is independent of Reynolds number. The ratio of shear stresses shown in Table 1 are thus independent of Reynolds number.

r_1/r_2	f_1/f_2	f_1/f_T	f_2/f_T
0,088	1,61	1,532 ± 1,8%	0,952 ± 1,1%
0,176	1,42	1,336 ± 1,0%	0,940 ± 0,5%
0,396	1,96	1,108 ± 0,8%	0,958 ± 0,6%

Table 1

(iv) Considerable deviations from the universal law of the wall occur in the velocity profiles associated with the core wall. (This tends to invalidate the Macagno/McDougal model and casts doubt upon the applicability of the Preston tube method to annuli).

Lawn and Elliot appear to be the first authors to establish experimentally that $r_{0t} \neq r_{mt}$ for smooth annuli. This is an extremely important result since it casts doubt upon the findings of all previous experimental results, and invalidates the basic assumption made in the theoretical models of turbulence in annular flow, namely that these positions are coincident.

3.1.6 Rehme [35]

The author used an air rig consisting of an outer brass tube 100 mm in diameter and 7,5 m long, together with cores of stainless steel (9,98 mm in diameter) and aluminium wires (3,96 mm and 1,98 mm in diameter) thus giving three radius ratios of α = 0,04; 0,02 and 0,1. The influence of spacers (used by most previous researchers) was investigated. Turbulence measurements were made with a DISA hot wire anemometer whilst velocity distributions were measured with 0,6 mm outer diameter Pitot tubes. The mass flow was measured using an orifice plate. As a basis for comparison Rehme also measured wall shear stresses with Preston tubes using Patels calibration. As was the case with Lawn and Elliot, Rehme's approach is basically similar to, and a repetition of, Brighton and Jones' fundamental work.

Rehme's most important results were:

(i) The friction factors for annuli increase slightly with increasing radius ratio; for α = 0,04 they are about 1,1% higher whilst for α = 0,1 they are about 4% higher than for a plain pipe. It should be noted here that Rehme's radius ratios are considerably lower than those used by other experimenters, there is no reason to assume that this trend of increasing friction factor with increasing radius ratios should continue for larger radius ratios.

(ii) The radius to the point of zero shear stress was determined with an accuracy of ± 0,05 mm; indeed a remarkable result which is 400% more accurate than that claimed by Lawn and Elliot.

(iii) The accuracy of the location of the radius of maximum velocity as determined by double Pitot tubes was very bad for $Re < 10^5$. Reasons for this inaccuracy have been discussed in Section 2. No estimate of the accuracy of the double Pitot tube is given.

(iv) The positions of zero shear stress and maximum velocity are clearly non-coincident. For example for $\alpha = 0,1$ there is a discrepancy in position of about 8% in radius. This confirms Lawn and Elliot's results.

(v) The position of zero shear stress as calculated from the Preston tube method are in excellent agreement with those obtained by hot wire anemometry. This is perhaps a surprising result and one that is in contradiction with Smith et al's [40] conclusion that the Preston tube method is in error when calibrated for pipe flow.

(vi) The dependency of the position of zero shear stress upon Reynolds number increases with decreasing radius ratio. For $\alpha = 0,1$ there is only a slight dependence which increases markedly for $\alpha = 0,02$.

(vii) Experimental results have shown that velocity and turbulence distributions are greatly disturbed by the inclusion of core spacers or, in the case of a horizontal rig, by the sag of cores and wires. In particular, these disturbances affect the positions of zero shear stress and maximum velocity, which are the most important positions for the determination of flow parameters.

Summarising the results achieved by indirect methods of wall shear stress determination, three points become clear:

(i) Since about 1972 the general consensus of opinion has been that $r_{0t} \neq r_{mt}$. Whilst more faith can be placed in this result than in earlier results, due to the development of more sophisticated measuring devices, it is well to note that the general consensus can and has been wrong in the past. It was wrong before in assuming $r_{0t} = r_{mt}$ and earlier still, in assuming that $r_{0t} = r_{0\ell}$. The accuracy in the method of determining r_{mt} leaves much to be desired, at least for $Re < 10^5$.

(ii) There still remain discrepancies and contradictions in results obtained essentially by similar methods. The dependence of r_{0t} upon α and Re for example has still to be established conclusively, as does the nature of the individual wall stresses and friction factors. Results such as those concerning the validity of the Preston tube method remain to be checked.

(iii) More experiments are necessary to determine conclusively the flow parameters. In this respect the development of a different experimental approach from the common one employing hot wires and Pitot tube might prove valuable.

3.2 Direct Wall Shear Stress Measurement

The desirability of a direct measurement of wall shear stress, has been emphasised by the discrepancies encountered in the results of researchers using indirect methods. Obviously if an accurate method of direct measurements could be found, this would avoid errors inherent in indirect methods, such as the precise determination of critical positions.

Direct methods are concerned only with wall shear stress measurements and do not yield any values of velocity or Reynolds stress

profiles, as would be gained from velocity or hot wire traverses. The direct method is therefore also independent of any valid or invalid assumptions that the position of zero shear stress and zero velocity gradients coincide. It has been seen in Section 3.2 that assumptions about this coincidence have in the past led to difficulties.

It was at first thought that the direct measurement of wall shear stresses was a novel idea until a literature search (carried out after the U.C.T. test rig had been built) showed that there had in fact been 3 previous attempts at direct measurement, none of which ~~were~~ was very successful.

3.2.1 Rothfus et al [37]

In 1955 Rothfus attempted to measure the drag on an annulus core by suspending the core from a spring balance (see Fig. 12). The rig varied in length from 1,22 m to 3,66 m in 1,22 m long sections, and was constructed from 28,6 mm diameter plexiglass tubing which surrounded copper tubing cores of 15,88 mm or 9,53 mm diameter. The working fluid was water, which was passed downward through the annular gap and the resultant drag observed, using a cathetometer to measure the elongation of the calibrated spring. The flow was measured volumetrically and the experiments covered a Reynolds number range of 900 to 45 000.

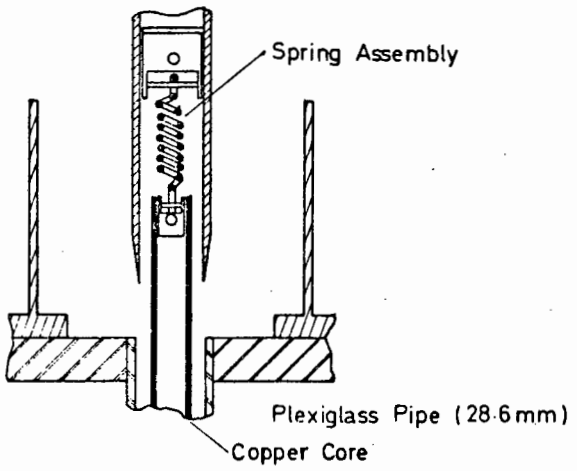

Fig. 12 Rothfus' suspended core system

Instead of using pressure tappings to measure the axial pressure gradient in conjunction with the core drag readings, thus enabling a force balance equation to determine τ_1 and τ_2, Rothfus curiously made the assumption that $r_{mt} = r_{m\ell}$. Since $r_{m\ell}$ (and hence according to Rothfus r_{mt}) can be calculated from the geometric properties of the annulus, $\tau_{2\ell}$ (and hence τ_{2t}) could be solved analytically. This assumption defeats one of the main purposes of a direct method of wall shear stress measurement; namely that the value of the individual wall shear stresses may be obtained independently of any prior knowledge about the position of zero shear stress.

It is perhaps not surprising that Rothfus' results contained many gross inaccuracies, when one considers carefully the details of his experiments. In fact, errors may have occurred for any of 4 possible reasons:

(i) The false assumption that $r_{0t} = r_{m\ell}$ and hence $\tau_{2t} = \tau_{2\ell}$.

(ii) The neglect of the considerable end effects which are inherent in any attempt to measure directly the drag on a suspended core.

(iii) The lack of any core tensioning facility (the core must of necessity be completely free).

(iv) The absence of any entrance length sufficient for the flow to become fully developed before entering the measuring section.

The results of Rothfus are probably no better than those obtained using indirect methods.

3.2.2 Quarmby [32]

In 1966 Quarmby attempted to measure the individual wall shear stresses, using semi-direct measurements from Preston tubes. Quarmby conducted a thorough investigation, using both a horizontal and a vertical 6,096 m long rig, with radius ratios of 2,88, 5,62 and 9,37, in a Reynolds number range of 6 000 to 90 000. The working fluid was air.

In this horizontal rig, the annulus was supported by aerofoil shaped struts 2,4 mm thick, which were adjustable and allowed centering of the core. The vertical rig was constructed in order to avoid the interference caused by struts. Cores were of stainless steel and could be tensioned. Velocity profiles were determined using traversing Pitot tubes and micromanometers. In both rigs, mass flows were determined by traversing a plain tube upstream of the annular section with a Pitot tube. Pressure tappings were situated at 76 mm intervals along the pipe. Quarmby placed Preston tubes on both inner and outer walls (see Fig. 5), in order to measure the shear stresses, and checked these results with the pressure gradient obtained from the pressure taps.

In another paper 'On the use of the Preston Tube in Concentric Annuli', Quarmby [31] himself raises some of the objections which could be lodged against the use of the Preston tube in annuli:

> 'The validity of the original proposal by Preston [30] for measuring turbulent skin friction depends on the existence of a law of the wall common to both boundary layers and fully developed pipe flow. Patel [29] has confirmed the validity of the original concept. It is clear that the calibration of a Preston tube in pipe flow could be checked in another fully developed axisymmetric duct flow, in which the skin friction would be available from the static pressure drop. The parallel plate and the concentric annulus suggest themselves. The objections which might be made to the annulus are: firstly, that the velocity profile close to the core tube is formed on a convex surface whose curvature could be quite sharp and the concept of flow similarity might not be valid; and secondly, that there is presumably some lower limit to the size of the core which could be used with a Preston tube of given size. It would be doubtful whether acceptable results would be obtained if, for example, they were equal in diameter'.

Quarmby goes on to say that if τ_1 and τ_2 were found by Preston tube measurements and if these results checked with those obtained from static taps through the force balance on an elemental length dx of the fluid, which is given by the following equation

$$\frac{dP}{dx} = \frac{2(\tau_1 r_1 + \tau_2 r_2)}{r_2^2 - r_1^2}, \qquad \text{(Eq. 27)}$$

then this would establish, at least in part, the validity of Preston's concept when extended to convex surfaces, and the correctness of the calibration employed.

Although Quarmby obtained good correlation between his prediction of the axial pressure gradient obtained from Preston tubes and that obtained from static taps, his conclusion that the Preston tubes are giving the correct values of the wall shear stresses is invalid. It has been seen in Section 2 that Preston tubes can only give correct values if the dimensionless velocity in the wall region is the same as the universal velocity profile for which the tube was calibrated. Quarmby used Patel's [29] calibration, as Lyall [17] pointed out, of

$$U^+ = 5{,}5 \log_{10} y^+ + 5{,}45$$

together with Macmillan's [7] Pitot tube correction. However, in looking at Quarmby's profiles it is evident that there are significant differences from the universal profile. Thus it was incorrect to use this universal profile as a Preston tube calibration for annuli. These differences appear to depend on radius ratio and Reynolds number; it is conceivable therefore, that the correct axial pressure gradient could be obtained from Preston tubes whilst still yielding incorrect values of individual wall shear stress. Quarmby's contention as to the validity of the use of Preston tubes in annuli must therefore remain suspect.

From a more practical point of view, the Preston tube has serious drawbacks, One being the limitation on the size of the core that can be used with a Preston tube; an other being the lack of evidence to show that it could be used satisfactorily in roughened surface situation.

Having established the difficulty in measuring velocity profiles for high Reynolds numbers using Pitot or double Pitot tubes, Quarmby considered he had discovered a new and more accurate way of determining the radius of maximum velocity (r_{mt}) by using the results of the Preston tubes. Notwithstanding the possible inaccuracy of τ_1 and τ_2 obtained in this manner, Quarmby goes on to state that

$$r_{mt}^2 = \left(\frac{\tau_1 r_2 + \tau_2 r_1}{\tau_1 r_1 + \tau_2 r_2}\right) r_1 r_2 \qquad \text{(Eq. 28)}$$

This of course is incorrect, and what he is presuming to find is the radius of zero shear stress.

Thus it appears that further investigation is necessary before the Preston tube method of determining wall shear stresses can be applied to annuli with any large degree of confidence.

3.2.3 Smith, Lawn and Hamlin [40]

In 1968 Smith attempted to measure directly the shear stress on a small part of an inner core. The test rig (see Fig. 13), consisted of a 3,96 m long vertical mild steel outer duct of 144,3 mm diameter. The core tube was of mild steel 12,7 mm in diameter and air was blown through the annulus by a Rootes type blower. Pressure tappings, spaced at 305 mm intervals, enabled the axial pressure gradient to be determined. Four equally spaced four legged spiders, made from 26 s.w.g. tension wire, connected to the outer duct, held the core in the correct position. These wires must have caused some disruption to the flow but no correction was made for this effect.

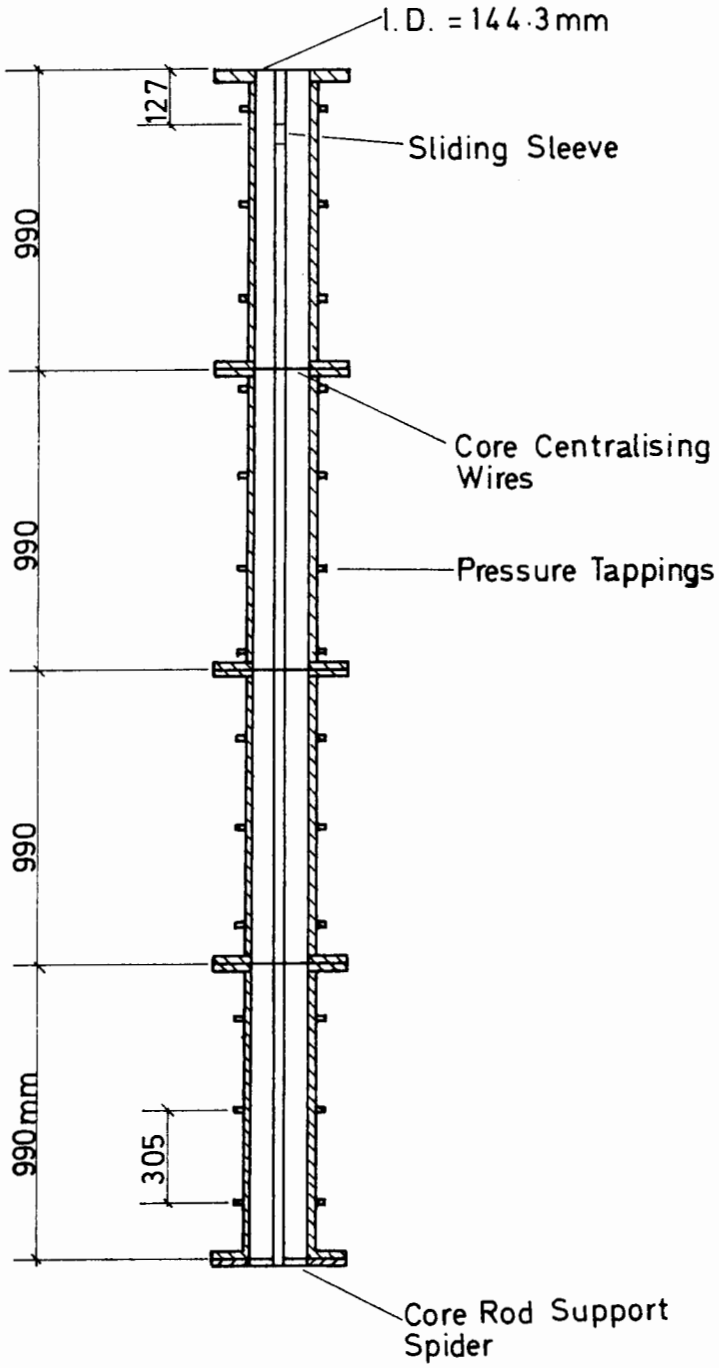

Fig. 13 The 'sliding sleeve' test rig

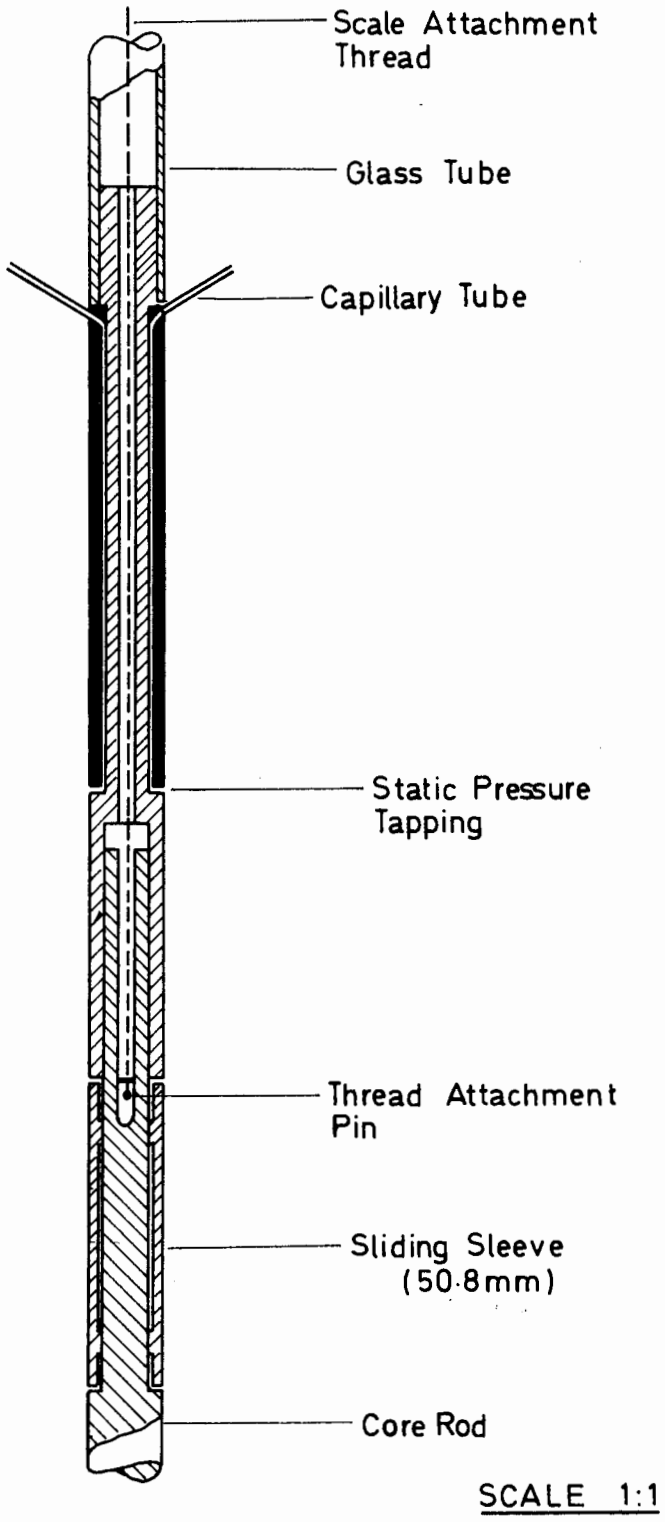

Fig. 14 The 'sliding sleeve' details

The part of the core used for direct shear stress measurement, known as the sliding sleeve (see Fig. 14), consisted of a small section of the core tube that was free to slide; the change in the apparent weight of the sliding section leading to the direct measurement of the wall shear stress. In principle, the apparatus was similar to that used by Rothfus, although on a much smaller scale. However, unlike Rothfus, Smith recognised the existence of end effects and attempted to correct for them by using different lengths of sliding sleeve (50,8 mm, 38, 1 mm or 25,4 mm). In their paper dealing exclusively with this method of direct measurement, Smith incorrectly deducted constant values for the gap effect caused by the sliding sleeve, Thus the uncertainty in their values of $\tau_1/\frac{1}{2}\rho\hat{U}_x^2$ was greater than estimated. In attempting to overcome this problem, Smith introduced pressure tappings at the base of the sliding sleeve. However, although the results now appeared more consistent, certain physical phenomena of the apparatus and results remain inexplicable.

It is probable that the small size of the sliding sleeve might have contributed to some of the error in Smith's results. Indeed Smith found that the gap effect force correction was equivalent to the wall shear force acting over 8 mm of the sleeve. Since one of the sleeve lengths was 25,4 mm, one sees that the order of magnitude of the correction was one third that of the results. This would surely have led to considerable inaccuracies.

Although Smith's results for direct shear stress measurement are inconclusive, another part of his results merits attention: Smith used Pitot tubes to determine the velocity profile in the annulus and concluded that the wall velocity profile is not of the universal form proposed by Patel, thus casting serious doubt on Quarmby's results.

This conclusion emphasises the uncertainty to date of all methods of determining wall shear stresses in annuli, including those of direct measurement. Up until now, the hot wire anemometer, despite its complications, appears to be the most reliable method of determining stress distributions.

SECTION 4

THE FLOATING SLEEVE METHOD OF DIRECT SHEAR STRESS MEASUREMENT

In view of the conflicting information on annular wall shear stresses available from past investigations, it was decided to construct a novel apparatus to measure the stress on one annular wall directly, as well as the axial pressure drop along the duct. These two measurements would enable the individual wall stresses to be calculated. The apparatus constructed for these measurements is called the 'floating sleeve'.

The principle behind the floating sleeve method is simple. The apparent loss in weight of a vertically suspended pipe, caused by a fluid passing vertically upwards through it, is a measure of the wall shear force on the pipe. If this apparent loss in weight could be measured accurately - on a weigh scale, for instance - then a method of direct measurement has been determined.

This was the method used for the determination of wall shear stresses in: a smooth pipe, smooth annuli, rough pipes and rough annuli. A detailed description of the test rig and the methods of measurement now follow:

4.1 Description of the Test Apparatus

In this description the bracketed lower case letters reference parts of the apparatus on the accompanying diagrams, the letters being common to all diagrams. Fig. 15 shows an overall view of the test rig. As can be seen, the floating sleeve was mounted vertically in a three storied hydraulics tower and passed through holes cut in the steel grating floors.

A 15 m high constant head tank (a) of 100 m^3 capacity supplied the water for the tests. The tank was part of the existing facilities of the Hydraulics Department of the University of Cape Town, water being pumped to it via a recirculating channel and pipe system.

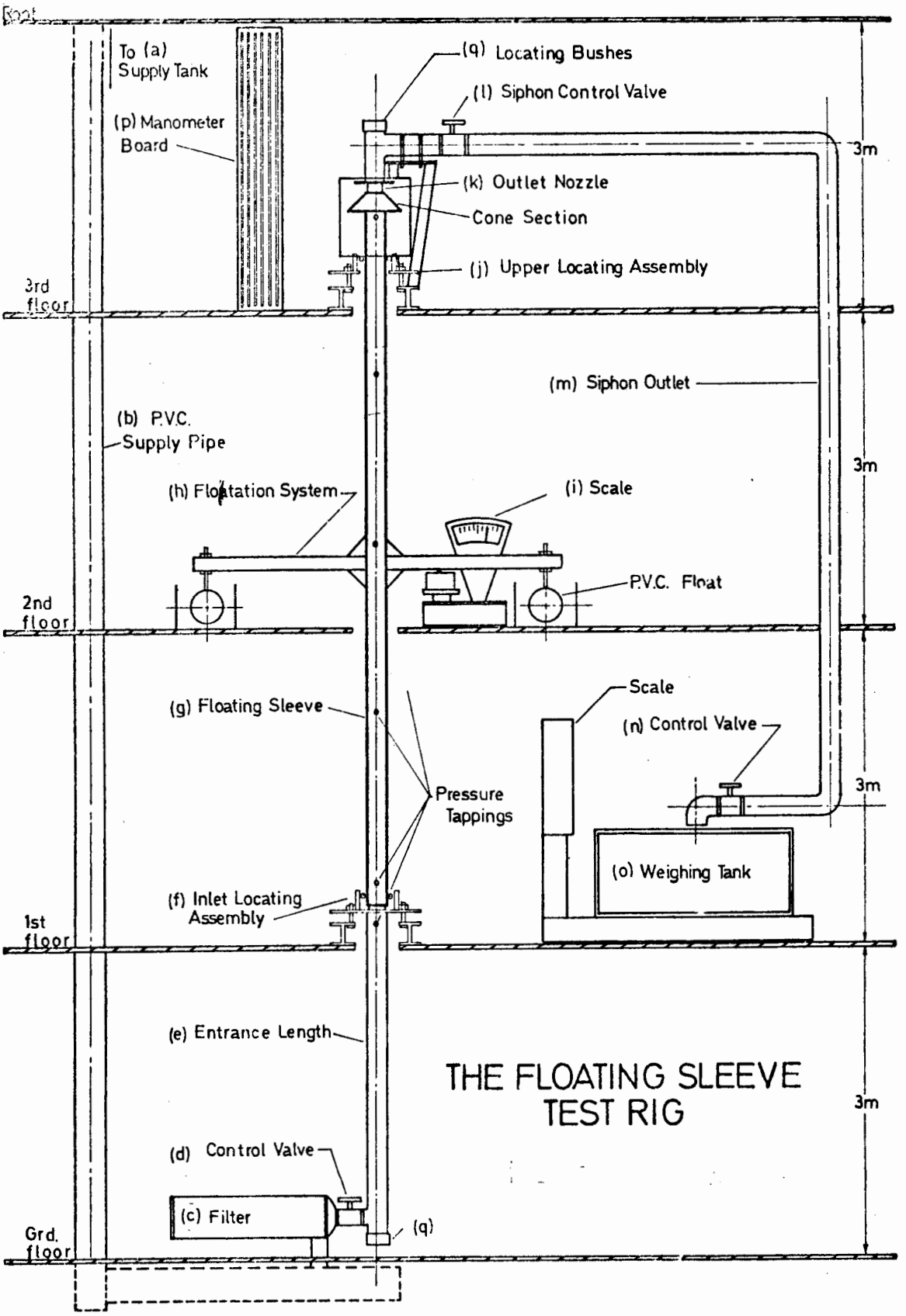

Fig. 15 Overall view of apparatus. See also Plate 3.

A 150 mm diameter P.V.C. pipe (b), carried the water from the tank to the filter (c). Before entering the filter the diameter was reduced to 75 mm. The filter, enlarged in Fig. 16, was of an agricultural type being approximately 200 mm in diameter and 1 m long. Inside the filter was a fine mesh bag of similar dimensions through which the water passed, leaving the sediment behind. The hole size of the mesh was approximately 200 μm. It was found very necessary to incorporate a filter in the system as will be seen later. Two prime requirements in the choice of a filter were: that it must prevent particles from passing through the system, and, that it should not cause excessive head loss through the system. With a bag mesh size 200 μm both these requirements were well met. The water flow through the filter was regulated by a 75 mm control valve (d). A remote control device enabled the valve to be adjusted from any floor level.

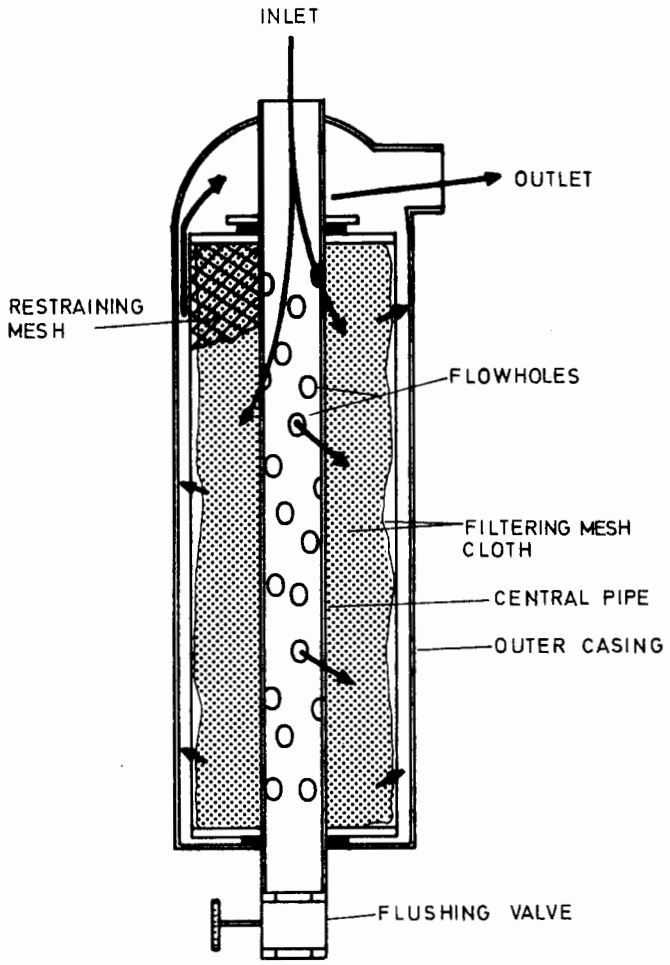

Fig. 16 Section through filter (c)

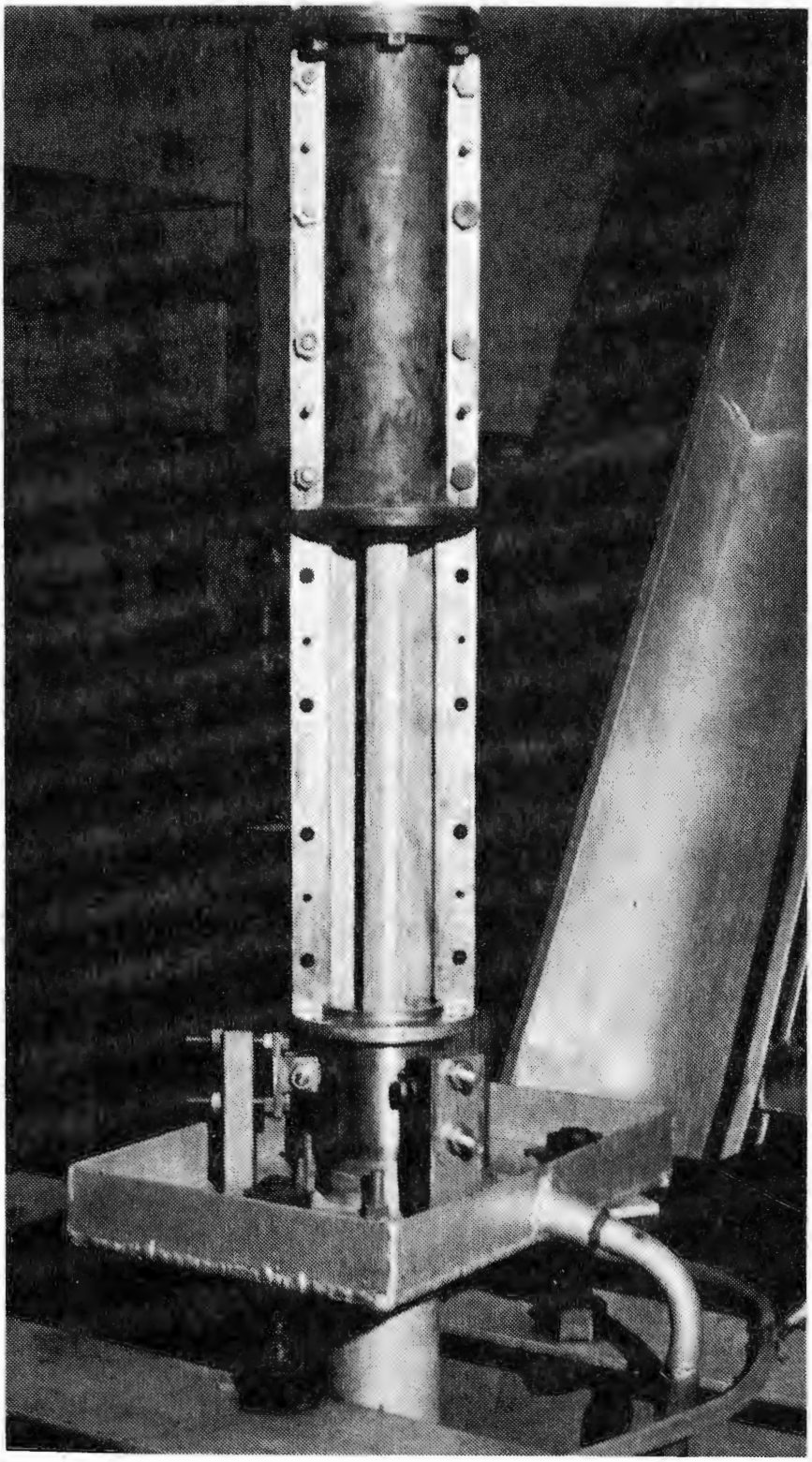

PLATE 2: FLOATING SLEEVE INLET DETAILS WITH ONE SECTION REMOVED TO SHOW CORE AND MESH ROUGHNESS

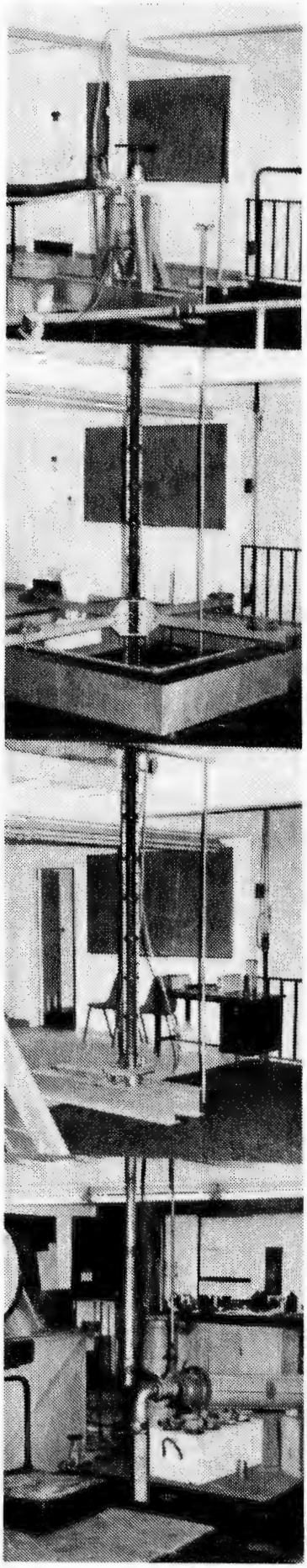

PLATE 3: THE COMPLETE FLOATING SLEEVE TEST RIG

From the control valve the water passed through a 2,5 m long 65 mm diameter galvanised steel pipe, which served as an entrance length (e) to the test rig. Owing to the irregularities in commercial pipes, the pipe was run in a lathe, heated and bent to a true straight before being assembled. The entrance length was machined to fit flush with the inlet locating assembly (f). This assembly (detailed in Fig. 17) was mounted via three adjustable 25 mm steel bolts to two I-beams which had been securely attached to the floor. The entrance assembly consisted of a machined brass inlet nozzle accurately located and soldered to the steel base plate, and three collar sub-assemblies which were bolted firmly to the base plate at 120° around the inlet nozzle. These sub-assemblies consisted of a roller-bearing mounted in a horizontally adjustable bracket, and enabled the inlet sleeve to be accurately adjusted and positioned about the inlet nozzle.

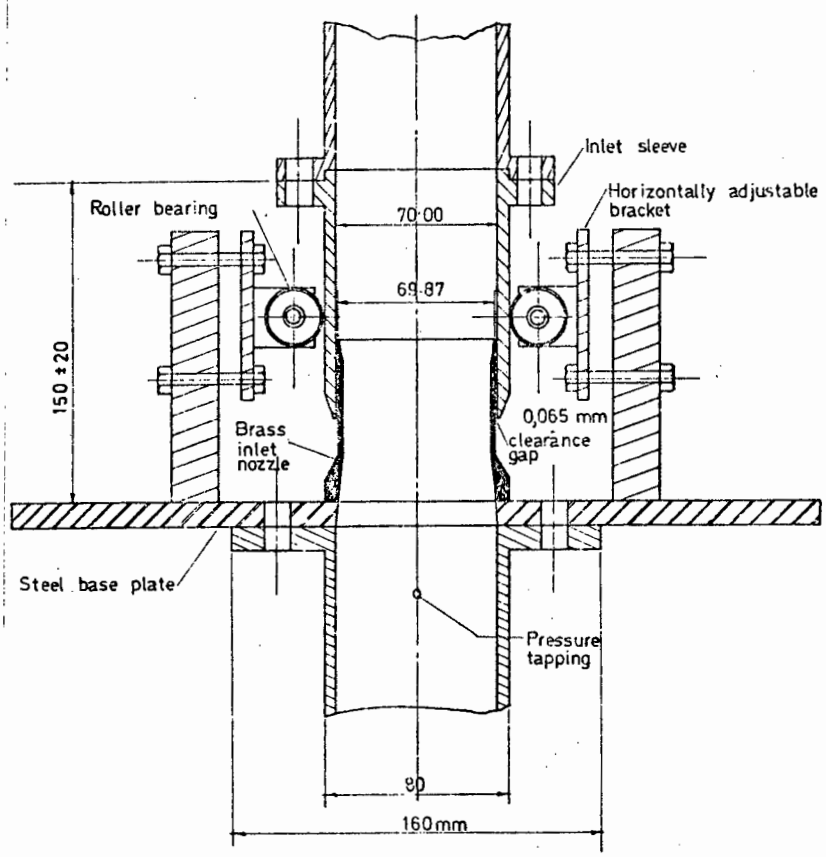

Fig. 17 Details of the inlet locating assembly (f). See also Plate 2.

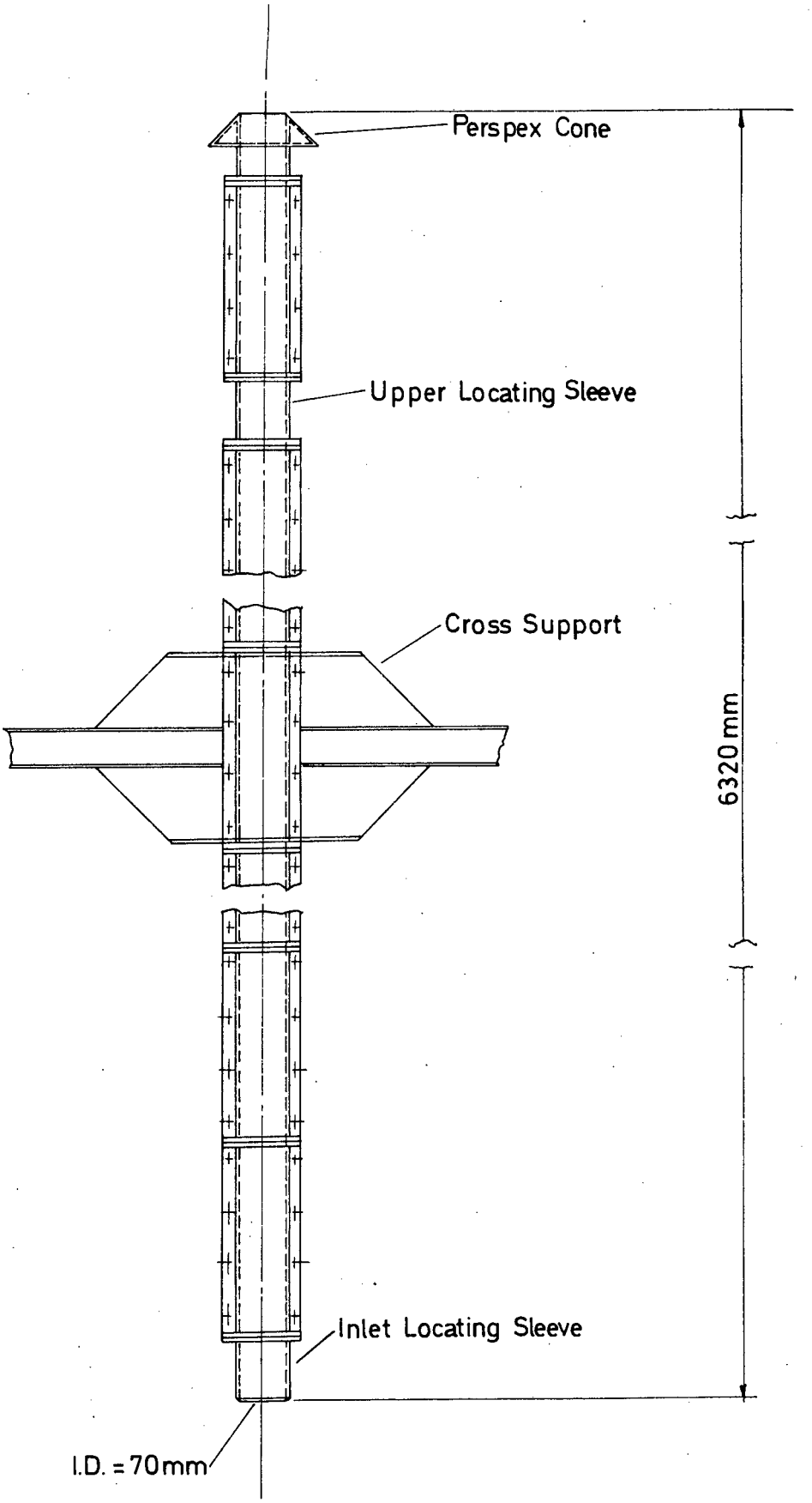

Fig. 18 Parts of the floating sleeve (g)

The inlet sleeve formed the first section of the complete 'floating sleeve' and was thus machined to the same internal diameter as the rest of the floating sleeve. The inlet nozzle had been carefully machined to slide inside the inlet sleeve, with an all round clearance of 0,065 mm on radius. The outside of the inlet sleeve was also machined so as to provide a smooth surface for the roller bearings to slide or roll against. The positioning of the inlet sleeve was adjustable and located by the roller bearings. Both the inlet nozzle and sleeve were machined from solid brass sections. The complete floating sleeve (g), consisted of the inlet sleeve, twenty pipe sections each 300 mm long (shown in Fig. 19), an upper locating sleeve (shown in Fig. 20) and a perspex cone section (shown in Fig. 21), all of the same 70 mm internal diameter. The 300 mm long pipe sections were cast of phosphor-bronze. Each section could be split longitudinally to enable a uniform roughness coating to be applied to the inside. The inside diameter was accurately machined to a 70 mm bore with a smooth but not polished surface. A test of the sleeve roughness made on a sophisticated stylus type testing machine showed the relative roughness to be 0,000114 ($= k/2r_2$).

The two half sections of pipe were located with taper pins for easy reassembly and bolted together longitudinally. Each complete section had a male and female end and all sections bolted together to form the main part of the floating sleeve. A fine layer of pipe-sealer was applied to the joints before assembly to prevent any leakage. The upper locating sleeve (shown in Fig. 20) held the upper portion of the floating sleeve in the correct position and enabled alignment with the outlet nozzle (k) (shown in Fig. 23). The outlet portion of the floating sleeve consisted of a perspex cone (see Fig. 21), which formed the transition between the floating sleeve and outlet nozzle. There was a clearance of 0,3 mm on radius between the perspex sleeve and the outlet nozzle.

The complete floating sleeve was supported halfway along its length by the flotation system (h). The float itself consisted of P.V.C. tubing 200 mm in diameter with a wall thickness of 9 mm. Four equally sized lengths of tubing were corner welded together using a

P.V.C. welding technique thus making a float, square in plan, which surrounded the floating sleeve (g). This is shown in Fig. 22. The float having been sealed, the welded corners were fibre-glassed to provide extra strength and prevention against leaks. The P.V.C. float was completely immersed in water in a specially constructed square trough. The floating sleeve was joined to the P.V.C. float by a horizontal steel cross made from 50 × 20 mm channel sections. At each outer arm of the cross a short piece of vertically adjustable screw rod connected the cross support to the P.V.C. float. Almost all the weight of the floating sleeve was thus taken by the flotation system (h). For the purpose of measurement, the floating sleeve was thus almost weightless.

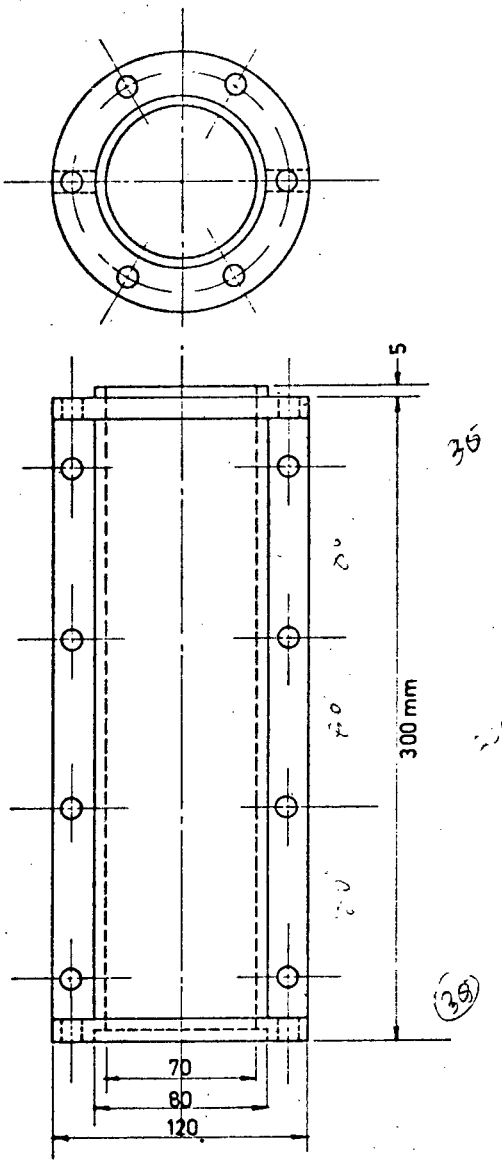

Fig. 19 Typical pipe section in the floating sleeve

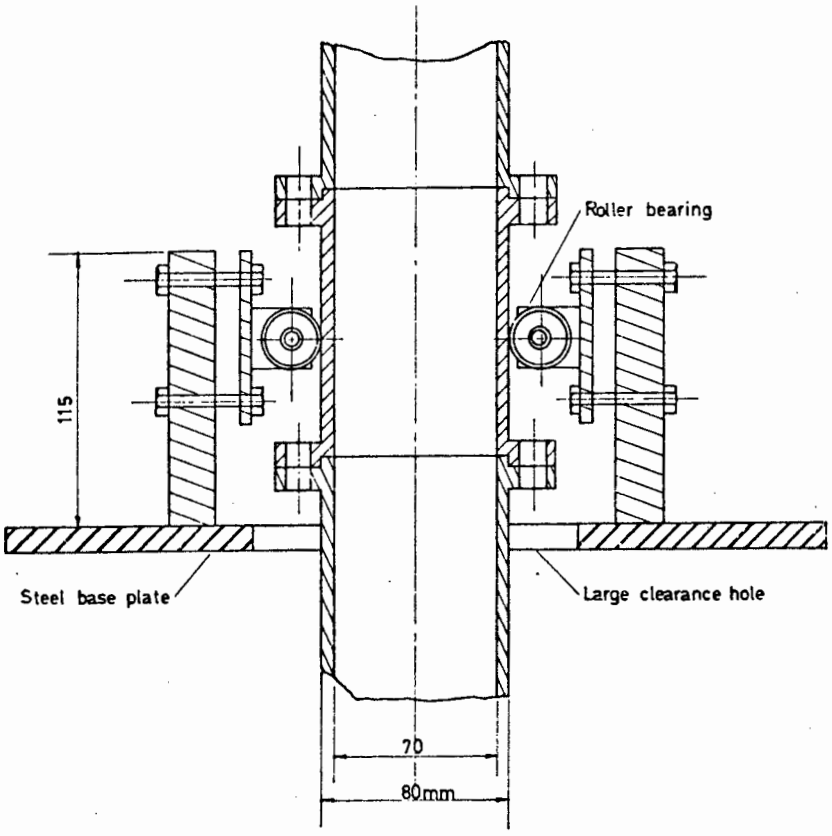

Fig. 20 Upper locating assembly (j)

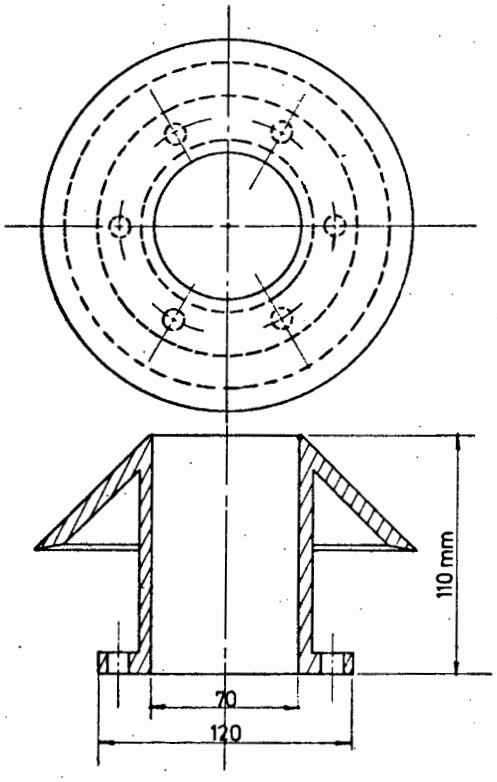

Fig. 21 Floating sleeve cone section

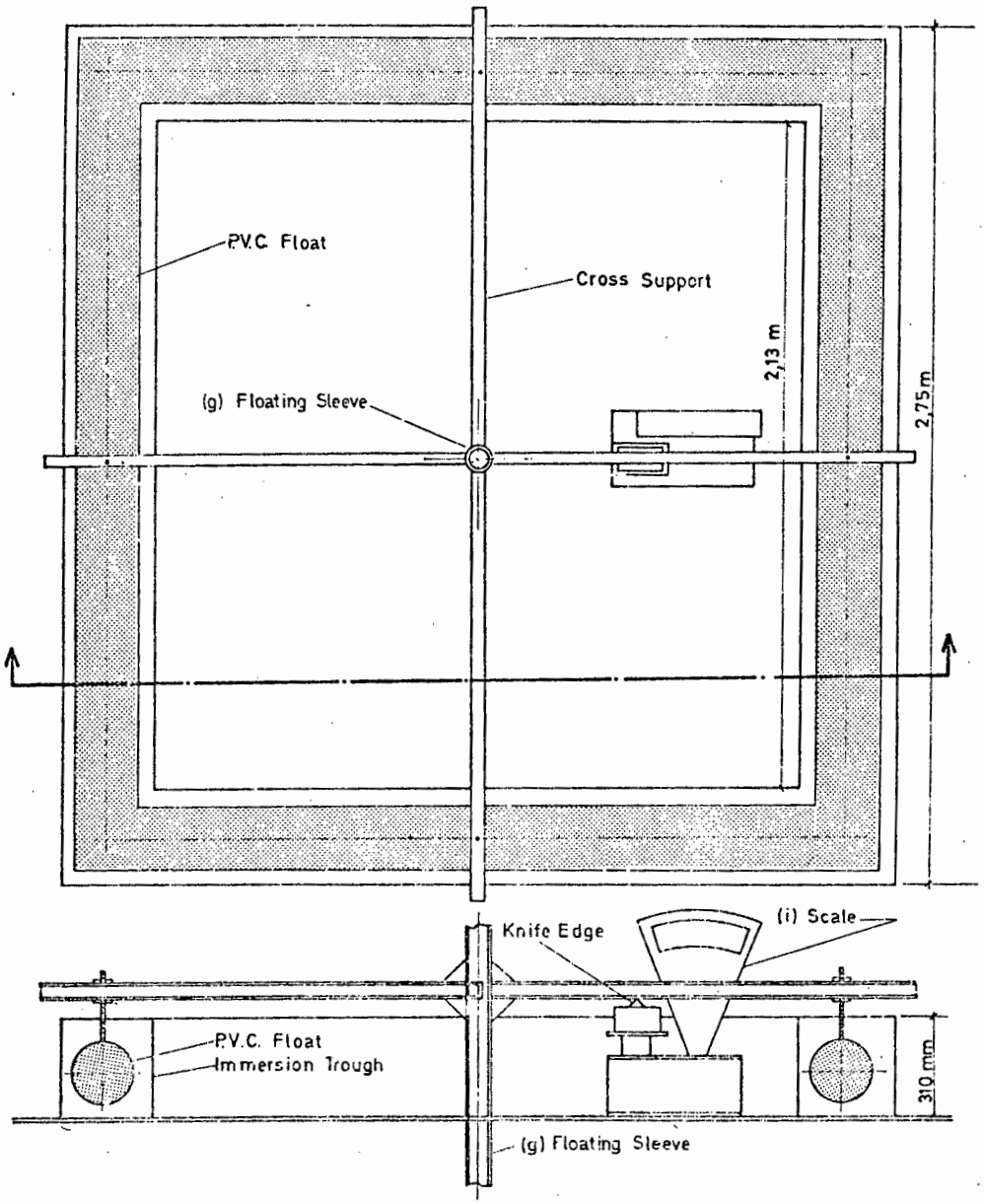

Fig. 22 Details of the flotation system (h).
See also Plate 1.

One of the cross arm supports of the flotation system rested lightly on a platform scale (i), with a total reading capacity of 500 g in 5 g divisions and a total displacement of 16 mm. The capacity of the scale could be extended to 15 kg, by the addition of suitable weights. This scale registered the very small surplus weight of the floating sleeve which was not taken by the flotation system; and was used, in conjunction with scale weights, to determine directly the upthrust on the floating sleeve wall when water was passed upwards through the duct.

The upper locating assembly (j) (shown in Fig. 20) was similar in construction to the inlet locating assembly (f) already described, except for a large clearance hole in the base plate, this allowed the floating sleeve to pass through, and the upper locating sleeve to be positioned by the roller sub-assemblies.

After the water from the supply tank (a) had passed up the floating sleeve, it was diverted by a siphon system to a weighing tank (o). The outlet nozzle (k) (shown in Fig. 23) formed the first part of the siphon outlet (m). The outlet nozzle was machined from a solid brass section. A clearance gap of about 0,3 mm on radius existed between the outlet nozzle on the perspex cone of the floating sleeve (g).

A hand valve (l) enabled the siphon flow to be regulated. The beginning of the 75 mm diameter siphon outlet (m) was supported by a solidly welded steel bracket, necessary in order to hold the outlet nozzle vertical and rigid. A further hand valve (n) was used to throttle down the siphon for low flows.

The outflow was measured in a weighing tank on a direct reading Avery platform scale, using time and mass measurements. The full scale capacity of 1 000 kg was utilised. The water temperature was measured at this point for viscosity estimation.

A manometer board (p) situated at the outlet nozzle was used to measure the axial pressure gradient as registered by the static pressure tappings. The board consisted of six glass tubes 2 m high.

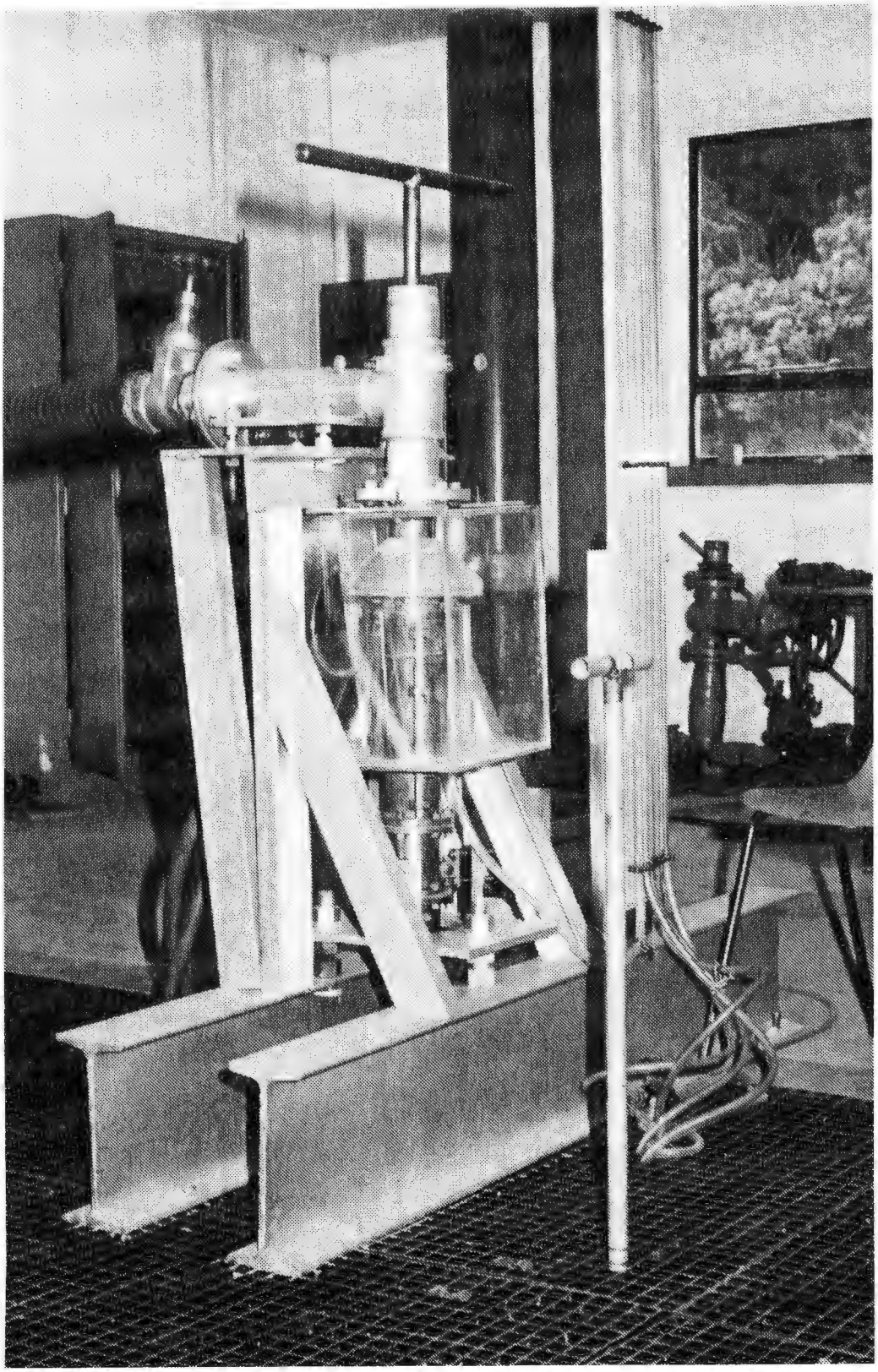

PLATE 4: FLOATING SLEEVE OUTLET DETAILS

Water was the manometric fluid. The tops of the tubes were normally open to the atmosphere but facilities existed for extending the manometer range by pressurising the tubes. The manometer registered the static heads of five pressure tappings, equally spaced about 1,5 m apart, in the wall of the floating sleeve. The sixth pressure tapping was situated at the top of the entrance length (e) as shown in Fig. 17 and enabled the static pressure just below the leakage gap to be determined. In order to support the fixed core rods, locating bushes (q) were soldered to the bottom of the entrance length (h) and top of the outlet nozzle. Specially machined locating cylinders rested against the bushes and held the core concentric. The bushes also provided flanges against which the cores were tightened.

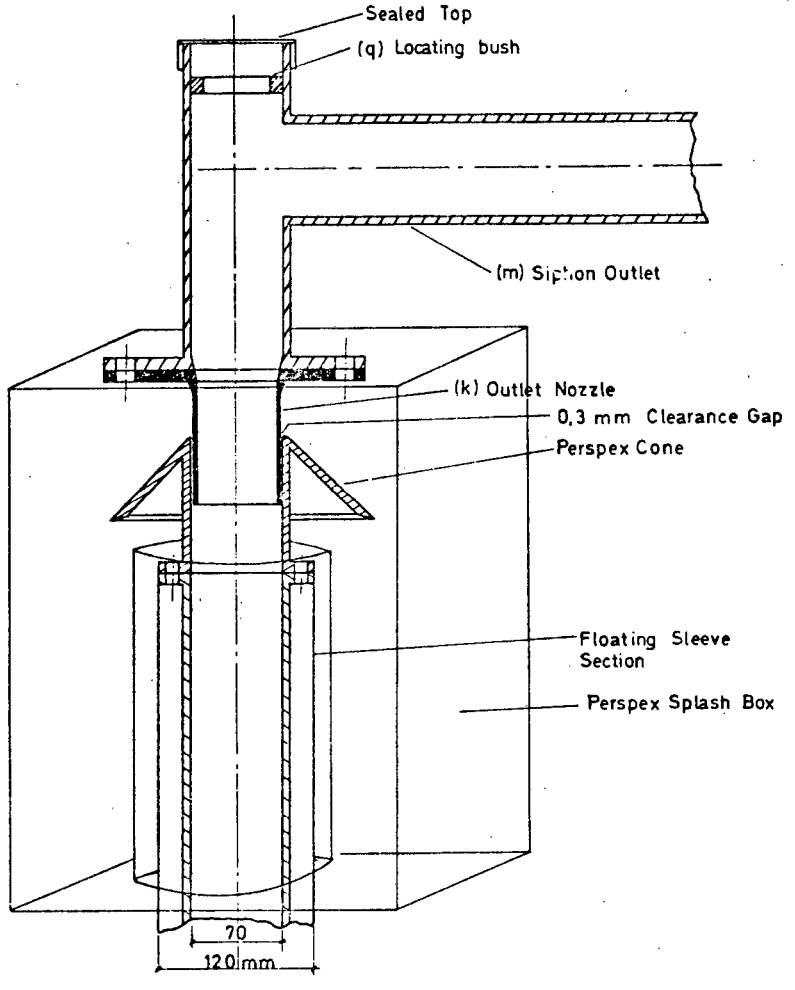

Fig. 23 Details of the outlet nozzle (k). See also Plate 4.

Three different cores were used to give radius ratios of 0,091; 0,226 and 0,363. The two largest cores were made from solid brass rod. These cores consisted of 1,2 m sections which were screwed together to form a smooth joint. The smallest core consisted of one long length of aluminium rod. The cores were lowered into the floating sleeve from the top. A roughness test showed the cores to be nominally smooth.

4.2 The Bottom Leakage Gap and the Top Annular Meniscus

As has been described the floating sleeve is in essence a length of pipe which is free to move vertically up or down. It cannot therefore be attached to anything which is solidly fixed and unable to move. For this reason there exists a clearance gap of 0,065 mm on radius between the inlet sleeve and inlet nozzle; as well as a clearance gap of about 0,3 mm on radius between the perspex cone section and the outlet nozzle.

When water flows upwards through the floating sleeve a small part of this flow (less than 2%) will leak out through the clearance gap (known as the leakage gap) between the inlet nozzle and inlet sleeve. This minor flow through the leakage gap will cause a downward shear force on the floating sleeve. Now the scale (i) will only register the resultant of this downward shear force and the upward shear force of the main flow through the floating sleeve. Since the upward shear force is the required result, some correction to the scale reading will be necessary to yield this upward shear force. Methods of determining this correction will be discussed later. It can be appreciated that because of the extremely small size of the leakage gap, any solid matter sticking in the gap would render the floating sleeve inoperable. This was the reason for installing the filter in the supply line. Before installation of the filter, clogging of the leakage gap had in fact occurred. The leakage gap was made as small as possible to minimize the downward leakage shear force and the disturbances to the main flow caused by the leakage.

When the main flow, passing up the floating sleeve, reached the outlet nozzle it was siphoned away to the weighing tank. The suction pressure in the siphon could be altered by means of the siphon control valve (1). If this control valve was throttled down too far, water would flow out through the clearance gap between the perspex cone section and the outlet nozzle (k). If the control valve was opened too far, air would be sucked in through the clearance gap. Since both these situations are undesirable (water outflow or air inflow) the valve was always adjusted between the above extremes, so that an annular meniscus of 'stationary' water existed in the clearance gap. In fact this meniscus was not quite stationary but fluctuated up and down because of the turbulent flow. For ease of manufacture and future adjustment, the top clearance gap was made considerably larger than the bottom leakage gap.

4.3 Roller Bearing Friction

It was realised that it was essential to constrain the floating sleeve in a horizontal plane, leaving it free to move vertically. This alone enabled the very small clearance gap at the bottom inlet nozzle to be used. However, whilst in theory a horizontal restraining force need not have any component in the vertical direction, in practice due to friction this is not so. It was hoped to minimise this frictional force by using roller bearings as the constraining mechanism. Since the minimum number of bearings needed for constraint and adjustment in the horizontal plane is three, only two sets of three bearings (top of bottom), were used to constrain the floating sleeve. Measurement showed that the total frictional resistance of all assemblies whilst the rig was in operation, was 4 to 10 grams weight. The actual value depended on cleanliness and lubrication.

4.4. Weight Measurements

Weight measurements are concerned with the direct determination of the wall shear stresses on the floating sleeve wall, caused by the flow of water upward through the sleeve.

The dead weight of the floating sleeve was about 200 kg. To achieve a reasonable accuracy of stress measurement on the sleeve wall, a weight measurement sensitive to the order of a few grams weight was required. Because scales with the capacity to support the whole dead weight of the sleeve with the desired sensitivity are not available, the possibility of weighing the whole sleeve, in order to determine the apparent loss in weight caused by water flowing upwards through it, was precluded. For this reason almost all the weight of the sleeve was permanently supported by the flotation system. Only the small residual dead weight (of the order of 200 grams weight) was supported by the scale. Changes in this residual weight were measures of the shear forces acting on the floating sleeve. Of course the value of this residual weight could easily be altered by the addition of suitable weights to the floating sleeve.

The advantage of floating the sleeve is that the dimensions of the sleeve are not dictated by the scale characteristics.

Now when water is passed upwards through the sleeve, the scale registers the resultant force of: the residual dead weight of the sleeve, the upward shear force of the main flow and the downward shear force of the leakage flow.

$$\therefore \quad F_2 = F_i - F_f + F_L \qquad \text{(Eq. 29)}$$

where F_2 = upward shear force on the sleeve caused by the main flow

F_i = initial scale reading for the dry sleeve

F_f = final scale reading showing the resultant force on the scale

F_L = downward shear force on the sleeve caused by the leakage flow (methods of determining F_L remain to be discussed)

Now

$$\tau_2 = F_2/A_2 \qquad \text{(Eq. 30)}$$

where τ_2 = upward shear stress on the sleeve wall

A_2 = surface area of the sleeve upon which F_2 acts

and providing F_L can be determined, a method of determining directly the outer wall shear stress of an annulus has been achieved.

4.5 Pressure Measurements

Pressure measurements are concerned with measuring the axial static pressure gradient along the floating sleeve, and the approximate static pressure at the leakage gap. For this purpose six pressure tappings (five in the floating sleeve wall and one at the base of the inlet nozzle) were connected to the manometer board (p) shown in Fig. 15.

Two methods of measuring the axial pressure gradient suggested themselves:

(i) The manometer board and tubes could be attached to the floating sleeve, thereby enabling pressure measurements to be made at the same time as weight readings for a particular velocity.

(ii) The manometer board and tubes could be separate from the floating sleeve. Thus weight tests would have to be performed for varying flows with the pressure tubes disconnected from the floating sleeve, followed by pressure tests for varying flows, with the sleeve clamped in position.

The first method has the advantage that a direct subtraction of sleeve shear force (obtained from weight readings), from the total shear force on the system (obtained from the pressure gradient), would yield the core shear force. This direct approach is possible because both sets of readings would have been taken for the same velocity and temperature and hence at the same Reynolds number. However, since in this method the manometer board and tubes would have been attached to the floating sleeve, a change in sleeve weight caused by the varying weight of water in the manometer tubes would have to have been allowed for.

For this reason, the second method was adopted. It is important to note that as the two sets of readings were taken at different

temperatures, the subtraction of the resultant shear forces could not be done directly. This was because significant temperature changes in the interim period between tests, altered the Reynolds number for a particular velocity. For this reason, the core shear force was obtained by an indirect method involving the subtraction of values on the f vs Re curves. Fig. 24 shows the sleeve shear force vs velocity for weight and pressure measurements.

Now using the axial pressure drop along the duct (as obtained from pressure measurements) and the shear stress on the sleeve wall (as obtained from weight measurements) the basis of the method used to calculate the individual wall shear stresses for an annulus with a concentric core becomes evident. A simple force balance gives:

$$2\pi r_1 \tau_1 = \frac{dP}{dx} \pi (r_0^2 - r_1^2) \qquad \text{(Eq. 31)}$$

$$2\pi r_2 \tau_2 = \frac{dP}{dx} \pi (r_2^2 - r_0^2) \qquad \text{(Eq. 32)}$$

$$\therefore \quad \tau_1 = \frac{dP}{dx} \left(\frac{r_0^2 - r_1^2}{2r_1} \right) \qquad \text{(Eq. 33)}$$

$$\tau_2 = \frac{dP}{dx} \left(\frac{r_2^2 - r_0^2}{2r_2} \right) \qquad \text{(Eq. 34)}$$

Adding Eq. 33 and Eq. 34 yields

$$\tau_1 = \frac{1}{2r_1} \left[\frac{dP}{dx} (r_2^2 - r_1^2) - 2r_2 \tau_2 \right] \qquad \text{(Eq. 35)}$$

and τ_2 can be obtained directly from $\tau_2 = F_2/A_2$. Division of Eq. 33 by Eq. 34 yields a method of determining the position of zero shear stress. Thus

$$r_0 = \sqrt{r_1 r_2 \left[\frac{\tau_1 r_2 + \tau_2 r_1}{\tau_{2\,2} + \tau_{1\,1}} \right]} \qquad \text{(Eq. 36)}$$

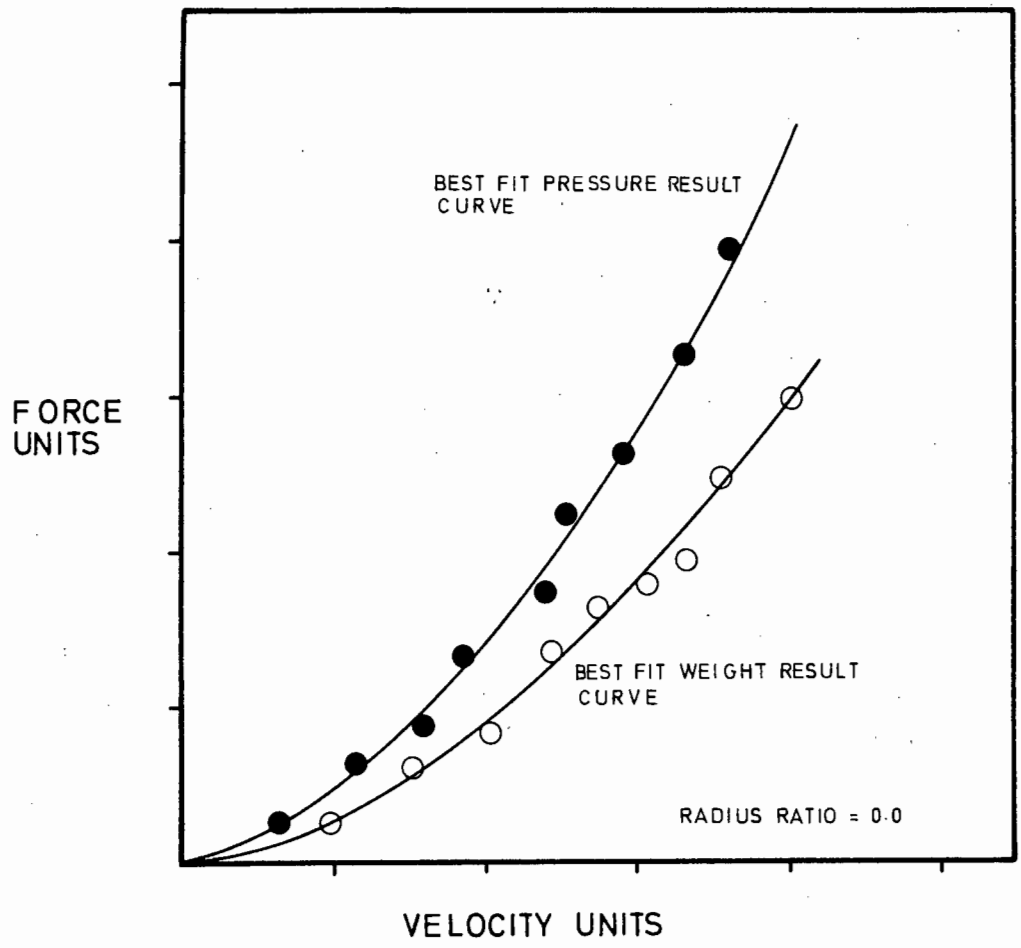

Fig. 24 Typical shear force vs velocity curves for $\alpha = 0$.
Non coincidence is due to viscosity effects
(i.e. the two curves were obtained at different temperatures)

4.6 End Corrections

One of the main difficulties encountered so far in methods of direct measurement (excluding semi-direct Preston tube methods) has been the correction or elimination of secondary end effects. In the floating sleeve, for example, a correction is necessary to account for the downward leakage shear force. Whatever the method of direct measurement used, corrections for end effects have been necessary. Also the nature of the correction has so far always been

pressure dependent. For the case of a suspended core element [Smith et al (40)], the position was complicated by the fact that the pressure gradient produced two components of the necessary force correction on the ends of the suspended element. One was due to the axial pressure gradient reaction, the other to the dynamic gap effect caused by the moving velocity stream. The axial pressure gradient reaction force proved relatively easy to correct for, but as expected, a suitable method of correction for the dynamic gap effect was difficult to achieve.

As well as reducing the number of end effects from two to one, the floating sleeve method successfully eliminated any correction for dynamic end effects. This was because all boundaries of the floating sleeve in contact with the velocity stream were parallel to the mean stream direction. The end effect was limited to the leakage gap between the inlet nozzle and sleeve. No end effect was present at the outlet because of the siphon outflow. Of course, if air were to be used as the working fluid, instead of water, the siphon would be unnecessary and the end effect would still be limited to the bottom leakage shear force.

If the floating sleeve was filled with static water and no upward flow existed, the pressure head caused a flow through the leakage gap, and hence a downward shear force on the floating sleeve. When a flow existed through the duct only the magnitude of the leakage shear force was changed, due to the increased head on the gap. This suggested a method of determining the correction for the leakage force:

For a particular overlap distance (Fig. 25), the downward leakage shear force is a function of the pressure difference across the leakage gap. If the floating sleeve was filled with different static water heads, measured on the inlet nozzle pressure tapping, then the resultant downward leakage force could be measured on the scale. With a velocity flow upward through the floating sleeve, the pressure head on the leakage gap would be increased. The assumption that the

extrapolation of the static pressure head versus the downward leakage force graph, would yield correct results for flow conditions was made. The justification for this assumption was that the nature of the correction was not altered by flow conditions. Fig. 26 shows such a graph of static head versus leakage force.

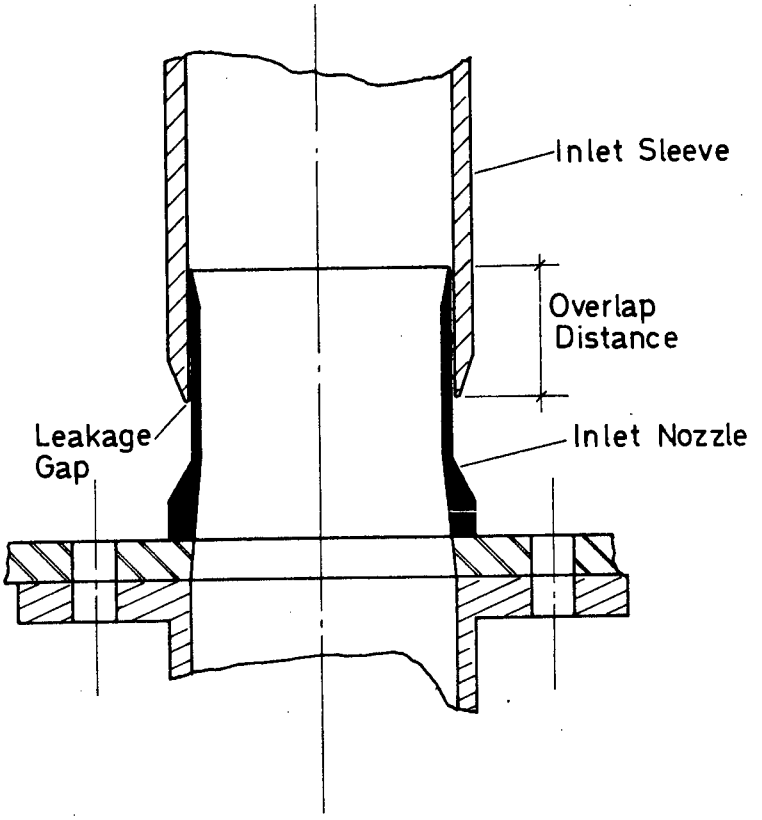

Fig. 25 The leakage gap

The normal method of using the graph to determine the leakage force, was to define F_i as the initial scale reading for the residual dead weight of the dry sleeve *. When flow existed through the duct the head on the leakage gap could be determined from the inlet sleeve pressure tapping (this was the only purpose of this pressure tapping). Using the graph the leakage force could be found.

* It will be seen later that the definition of F_i had to be altered if the floating sleeve was roughened.

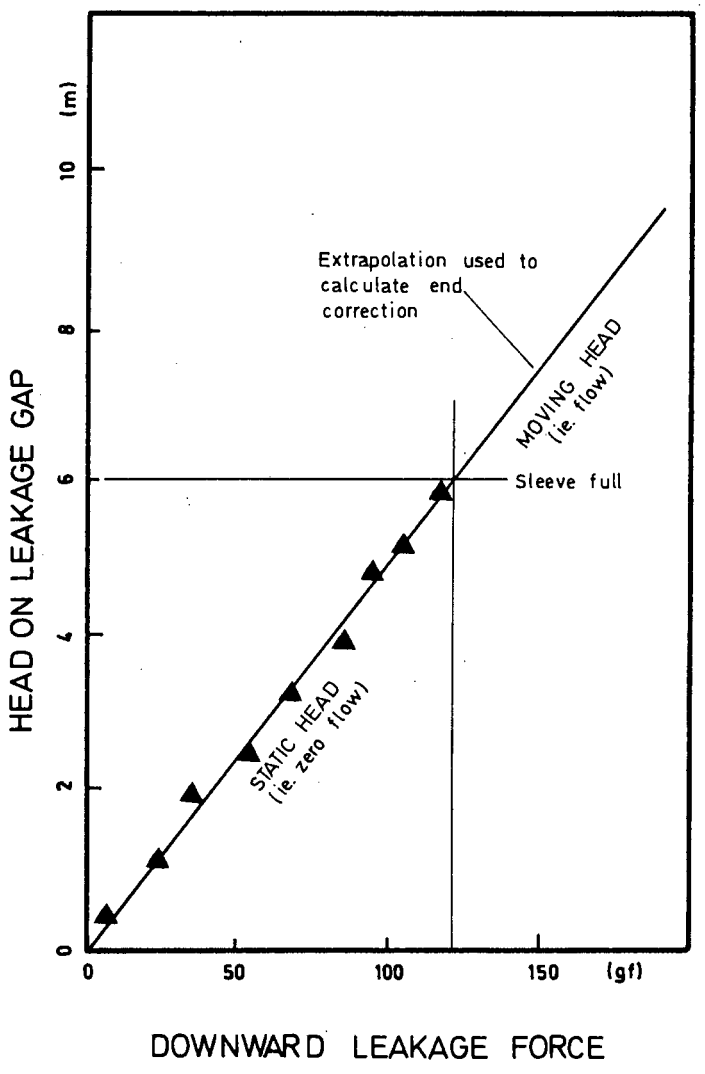

Fig. 26 Graph of head on leakage gap versus downward leakage force

The correction force for leakage shear was found to be

$$F_L = k_1 (z + h)$$

where F_L = leakage force in grams weight

z = length of sleeve (top of inlet nozzle to bottom of outlet nozzle)

h = head of water above the bottom of the outlet nozzle

$(z + h)$ = head of water on leakage gap

k_1 = slope factor from graph of static pressure head versus leakage force

Another advantage of the floating sleeve method becomes apparent when assessing the accuracy of the end corrections. The advantage is that the corrected floating sleeve results for the wall shear stress obtained from weight measurements with no core inserted (that is, as a plain pipe), can be compared with the well documented results for turbulent pipe flow as well as with the results of the sleeve pressure measurements, (for which no end corrections are necessary). One thus has a method of checking the accuracy of the end correction. By its very nature this is impossible in a suspended core system.

A further crude estimation of the leakage force correction for the floating sleeve, can also be made using the formula for laminar flow through the annular leakage gap. This check can only be expected to indicate the correct order of magnitude of the correction. Thus

$$F_L = 4\mu A_L \hat{U}_L \left[\frac{r_2^2 - r_m^2}{r_2(r_2^2 + r_1^2 - 2r_m^2)} \right]$$

where in this case

A_L = surface area of sleeve upon which F_L acts

$\hat{U}_L$ = average spatial velocity through the annular leakage gap (this would have to be measured)

r_2 = radius of inlet sleeve

r_1 = outer radius of inlet nozzle

r_m = position of maximum velocity. As the difference between r_1 and r_2 is so small and in view of the approximation* of this method it is acceptable to take $r_m = \frac{1}{2}(r_1 + r_2)$

Thus a method of determining the one end effect which occurs in the floating sleeve has been determined. The accuracy of this method can be checked by comparing the corrected results for pipe flow with those obtained from pressure measurements and by comparison (albeit crude) with a theoretical laminar flow prediction.

* For example it is unlikely that the inlet sleeve is exactly concentrically placed about the inlet nozzle

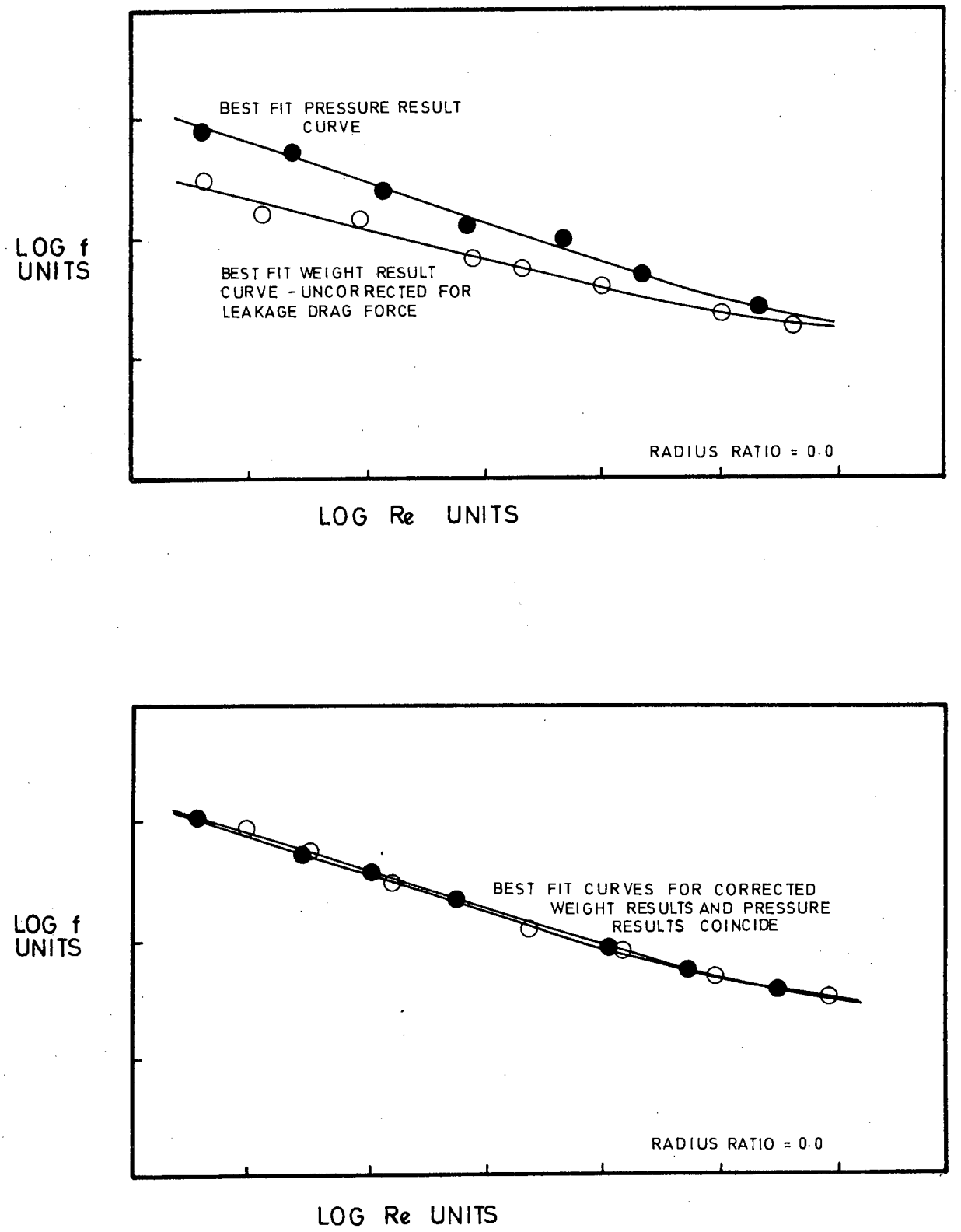

Fig. 27 The influence of the correction for the bottom leakage drag force on the f_2 vs Re diagram

SECTION 5

ROUGHNESS

Many investigations into turbulent flow in annuli have been made. These investigations have greatly increased the knowledge of annular flow and the turbulence mechanism, although this knowledge is still incomplete. As was the case in 1933, when Nikuradse extended his investigations of smooth pipes to those of artificially roughened pipes, the logical development in annular flow would be the study of the laws governing turbulent flow in annuli with roughened surfaces. Indeed, the study of rough annuli is probably of more practical significance than that of smooth annuli, in view of its industrial application.

5.1 Nikuradse's Investigation into Rough Pipes

The first systematic and authoritative investigation into artificially roughened pipes, was carried out by Nikuradse in 1933 under the supervision of Prandtl. The Nikuradse paper forms the very basis of all subsequent work into pipe roughness, so much so, that present day commercial pipes are still specified by the equivalent sand grain relative roughness as determined by Nikuradse. It is therefore essential to know something of Nikuradse's work.

Dimensional analysis had indicated that similitude required geometrically similar pipes and similar wall surfaces. In order to obtain a variety of similar wall surfaces Nikuradse made use of ordinary building sand which was graded to a 0,04 mm tolerance by sieving. The test pipe was coated using the rather laborious method of filling the pipe with a thin Japanese lacquer, draining it, refilling it with graded sand, draining it again, refilling it with lacquer and draining it yet again. The process was not only laborious but also time consuming. The reason for this was that carefully controlled drying periods (up to 3 weeks), were necessary after the sand had been applied to the pipe and again after the final lacquer coating

had been applied. The whole process of applying one roughness coating would therefore take about $1\frac{1}{2}$ months. Furthermore a considerable amount of time must have been spent on originating and developing a workable technique for roughening the pipe.

One of Nikuradse's* main results was the production of an f versus Re chart for varying relative roughness k/d, where k is defined as the average height of the in-situ roughness projection, and d as the diameter of the pipe. Although Nikuradse's chart has helped standardise the determination and effect of wall roughness, it must be open to two serious objections: both of these objections centre around the definition of the parameter characterising roughness. Dimensional analysis, it is true, has shown that

$$f = fn(Re, k/d) \qquad \text{(Eq. 37)}$$

*A point of some interest came to light whilst researching Nikuradse's work. It is well known that von Karman used Nikuradse's smooth pipe velocity distribution results, to obtain the numerical constants for the equation of velocity distribution in the transition region between viscous and fully developed turbulent flow. It appears that shortly after the last world war a research group in America (see Miller [21]) noticed an unaccountable discrepancy between Nikuradse's smooth pipe data and results. It was decided to write to Professor Prandtl, who had been Nikuradse's immediate supervisor at the Kaiser Wilhelm Institute, in an endeavour to find some explanation for what has now euphemistically come to be known as Nikuradse's 'shifted velocity profile'. At the time the request arrived Nikuradse was in fact revisiting the Institute, and Prandtl was able to enlist an explanation for the discrepancy. It appears that Nikuradse arbitrarily shifted his data so that it coincided with Prandtl's laminar film hypothesis. There was absolutely no basis for this shift, or for the magnitude of the shift. This shift (actually equal to 7 units of the dimensionless distance from the wall yU_τ/ν) was simply a distortion of the data to make it seem to agree with an hypothesis.

Robertson et al [36] working 16 years later came across certain 'strange if not contradictory' features in Nikuradse's presentation of his rough pipe results. Suffice to say here that it appears from Robertson's investigation that Nikuradse again modified certain of his results, this time in order to agree with values predicted by the universal logarithmic law relation for von Karman's parameter of k = 0,4.

where k is some roughness characteristic. Nikuradse has taken k to be the average projection of the roughness. However, k could just as easily have been taken to represent the average spacing of the sand grains, since this is also a roughness characteristic. It is quite possible that the spacing of the roughness elements is of more importance than the grain size and therefore Nikuradse's curve could be taken to show the dependence of the function factor f on λ/d where λ is the spacing of the wall roughness elements in the direction of flow.

In fact it seems logical to stipulate roughness in terms of 3 variables: k, λ and s the clear peripheral spacing between elements. Thus Eq. 37 would become:

$$f = fn(Re, k/d, \lambda/d, s/d) \qquad \text{(Eq. 38)}$$

and if more terms were required to define the effects of roughness these would be incorporated in Eq. 38 . Morris [23] for example produced convincing reasons for assuming the spacing λ as the fundamental parameter influencing the rate of energy dissipation and took λ as the significant correlating length in place of k. He describes, in terms of λ, the three different types of flow phenomena that may occur near the wall:

(i) If the wall roughness elements are far apart, the individual elements will act as isolated bodies on which drag forces are exerted by the fluid flow. The vortices generated are dissipated before the next roughness element is encountered. The friction loss would therefore depend upon the form drag of the isolated roughness and the skin drag of the wall surface between elements. Thus λ/k could be expected to be the significant correlating parameter.

(ii) If the wall roughness elements are sufficiently close, so that the vortex generations are not completely dissipated before the next element is encountered, a zone of intense and complex vorticity and turbulence can be expected to occur near the wall. The wall skin drag is now absent. Hence the spacing

λ is of major importance and the size of the pipe will partially control the radial extent of this wall region of intense turbulence. Therefore, Morris suggests that the important correlating parameter will be λ/d.

(iii) If the roughness elements are so close together that the flow essentially skims the crests of the elements, Morris postulates that there will be regions of dead water containing stable vortices between roughness elements. Most of the energy dissipation will be caused by the maintenance of these 'groove vortices'. Thus λ/k or λ/j, where j is the groove width, would be expected to be the correlating parameter.

The other lesser objection that can be raised is the notion of k as the average grain size projection. Nikuradse automatically imposed certain limits on the grain size by means of close tolerance sieving and the grain projection was found to be equal to the grain size. It is suggested here, that k should be defined between certain limits.

Another source of trouble often occurs when computing the relative roughness of a sand coated surface. This centres around the fact that the ratio of in-situ surface projections to grain size diameter is very rarely unity. As can be seen from Table 2*, this ratio varies from 1,00 to 1,64 and it is quite understandable that $k > d_{sand}$ occurs frequently. Indeed it says much for Nikuradse and Schlichting's methods that they were able to keep their ratios at unity. It can be seen that sand grain diameter is not a sufficiently accurate measure of k. Thus the use of an ordinary sieve analysis as a measure of k may deviate by more than 60 per cent from the true value.

*

Table from Robertson et al (36)

Experimentor	Apparatus-fluid	Source and size (d_{sand})	$\frac{k}{d_{sand}}$
Schlichting (1936) Goettingen	40 mm rectangular channel-air	Hamburg sand 1,35 mm	1,64
Colebrook & White (1937)	57 mm pipe-air	Aylesford sand 0,35 mm	1,36
University of Illinois Burkhart (1962) Martin (1963)	76 mm pipe-air	Ottawa sand 0,89 & 1,07 mm	1,35 1,13
Schlichting (1936)	40 mm rectangular channel-air	Goettingen sand	1,00
Nikuradse (1933) Goettingen	24 to 100 mm pipes-water	Goettingen building sand 0,1 to 1,6 mm	1,00

Table 2

5.2 Roughness Materials for the Floating Sleeve

Various methods of roughening surfaces were investigated in order to determine a method suitable for the floating sleeve and cores. Four conditions were imposed upon the choice of roughness material:

(i) The roughness must be uniform in two directions

(ii) Various degrees of roughness for the same material must be available

(iii) The roughness must be easily removable and must not damage the basically smooth surfaces of the sleeve and cores

(iv) The roughness must be non-corrodible

Materials for roughness can generally be divided into two categories: granular roughness and fabric roughness. As will be seen, fabric roughness was most suited to the floating sleeve. Some of the roughness materials considered are: Granular roughness, this is roughness consisting of individual particles.

(i) Sand: This was the cheapest and most easily available material. Large variations in roughness grades and tolerances may easily be achieved through sieving. The use of a mixture of glue and thinning agent made the application of the sand to the surface relatively simple.

(ii) Small balls (as used in ballbearings), or lead shot: Both these materials would provide uniform roughness but their cost made them prohibitive.

(iii) Plastic or glass beads: Investigation showed that plastic beads of 1 to 2 mm diameter could be obtained but that these were more cylindrical than spherical and were not entirely uniform in shape. Glass beads were unobtainable commercially at sizes less than 5 mm.

(iv) Emery cloth or waterpaper: Although sold in sheets these materials consist of granular particles. Emery cloth was readily available and was thought to be quite suitable until it was found that water dissolved the resin bonding the grains to the cloth. Apparently a silicon based water proofing agent (DC 2002) is available and this would make the cloth suitable for use in water. However, since no sample of this was readily available, it was decided to forego this method. The waterpaper, whilst resisting deterioration in water for longer periods than emery cloth, was not available in sizes of sufficient roughness projection. It was not certain whether those available would produce hydraulic roughness within the range of operation of the floating sleeve.

Fabric roughness, this is roughness consisting of sheets of some material devoid of any granular particles.

(i) Water resistant fabrics: Fabrics such as canvas have been used in the past as roughness agents. Canvas would be easy to apply and remove. However, it was not available either in sufficient roughness height nor sufficient roughness grades. The uniformity of roughness was also suspect.

(ii) Rubber matting: Various samples of commercially available rubber matting were obtained. Although one or two samples satisfied most of the criteria, those that did were not available in sufficiently varied grades.

(iii) Stainless steel mesh: This mesh was available in various roughness grades, was uniform in both directions and manufactured to very high tolerances of accuracy. If it were to be used, a suitable method of adhesion would have to be found.

5.3 Methods used to Roughen the Floating Sleeve

It was eventually decided to use sand as the roughening agent because of its suitable qualities, although it was realised at the time that a certain risk was involved in the use of any granular material. Should any one of the multitude of granular particles become lodged in either the bottom or top leakage gaps, the floating sleeve would 'stick' and become inoperable until cleaned. Cleaning involved the removal of the relevant sleeve sections, and removal necessitated readjustment upon assembly. This would prove a time consuming operation.

As has been described in Section 4, the sleeve could be split axially and radially into sections to enable access to the interior surface for the purpose of applying a roughening material. The sleeve was split radially into four long sections and these sections split axially as a whole. The sand was applied to these sections.

Ordinary Pattex glue was used as the adhesion material. If was found necessary to dilute the glue with Pattex thinners, before applying it to the surface. Sand was then applied to the surface and the glue allowed to dry. The excess loose sand was removed and the sleeve was reassembled.

It soon became evident that small particles were indeed becoming lodged in both the clearance gaps. Frequent cleaning was necessary. It became difficult to tell whether a reading had become invalidated because of 'sticking' in the leakage gap. In spite of these difficulties a series of weight and pressure readings was eventually obtained.

In view of the time wasted in attempting to clean the leakage gaps and of the uncertainty of the weight results, it was decided to use a different roughening material.

The materials considered have already been listed. In the light of the problems involved in using sand as the roughening material, it was decided not to use any roughening material of a granular nature. The next choice of material fell upon the stainless steel mesh.

The main problem encountered with the mesh was that of fastening it satisfactorily to the sleeve and core walls. It was decided to use a soft soldering method. Before soft solder can be applied to stainless steel, the steel must be brushed with a mixture of nitric and hydrochloric acid, otherwise the solder will not bond. In order to apply the mesh to the sleeve, two methods were tried:

(i) The sleeve was split axially and the mesh spot soldered in 1 meter long strips onto the half circular sections

(ii) A cylindrical mesh shell was soldered together on a wooden mandril and slid into a complete sleeve section - the tight fit holding the mesh in place

Both methods proved time consuming although the second proved slightly easier. This method also had the advantage of easy removal. The results warranted the effort, for a good uniform corrosion free roughness had been achieved. The short inlet locating sleeve and outlet cone sections were not roughened and therefore did not interfere with either of the nozzle sections. The rough sleeve and two geometries of rough annuli were investigated.

5.4 Pressure Tappings and End Corrections for the Rough Sleeve

As was the case with the smooth sleeve, tests were first conducted with the rough sleeve only, that is, with no core inserted. This was used as a check to ensure that both pressure and weight readings were producing similar results.

Some doubts had been expressed by Nikuradse about the use of wall piezometers for measuring the static pressure gradient with a rough wall surface. According to Nikuradse, marked errors occur when this method is used. He reasons that vortices which result from flow around projections, produce pressure or suction depending on the position of the aperture and the nature of the projection. For these reasons, Nikuradse rejected the piezometer in favour of the hooked tube for use in his rough pipe investigations.

Although the reasons offered by Nikuradse appear plausible, tests carried out on the roughened floating sleeve showed that the piezometers were in fact giving consistent results, of the type obtained under smooth conditions, in spite of the roughness projections. Pressure tests showed that the axial pressure gradient was still a straight line and that the coefficient of determination was the same as that for the smooth walled sleeve. It was decided to continue using the wall tappings as a method for obtaining reliable measurements of the pressure gradient.

Recalling the series of events obtained by filling the smooth empty sleeve with water, it was noted that:

(i) When the empty sleeve was filled with various static heads of water, the scale registered a downward force over and above the empty sleeve reading, due to the leakage force.

(ii) Once a significant flow occurred through the sleeve the scale would register a decrease in weight, related to the flow velocity, caused by the upward force of the water on the sleeve wall.

Now when a roughness coating was applied to the sleeve walls, a different series of events was observed:

(i) When the empty rough sleeve was filled with various static heads of water, the scale registered an upward force (in relation to the empty sleeve reading) which was in proportion to the head of water on the leakage gap.

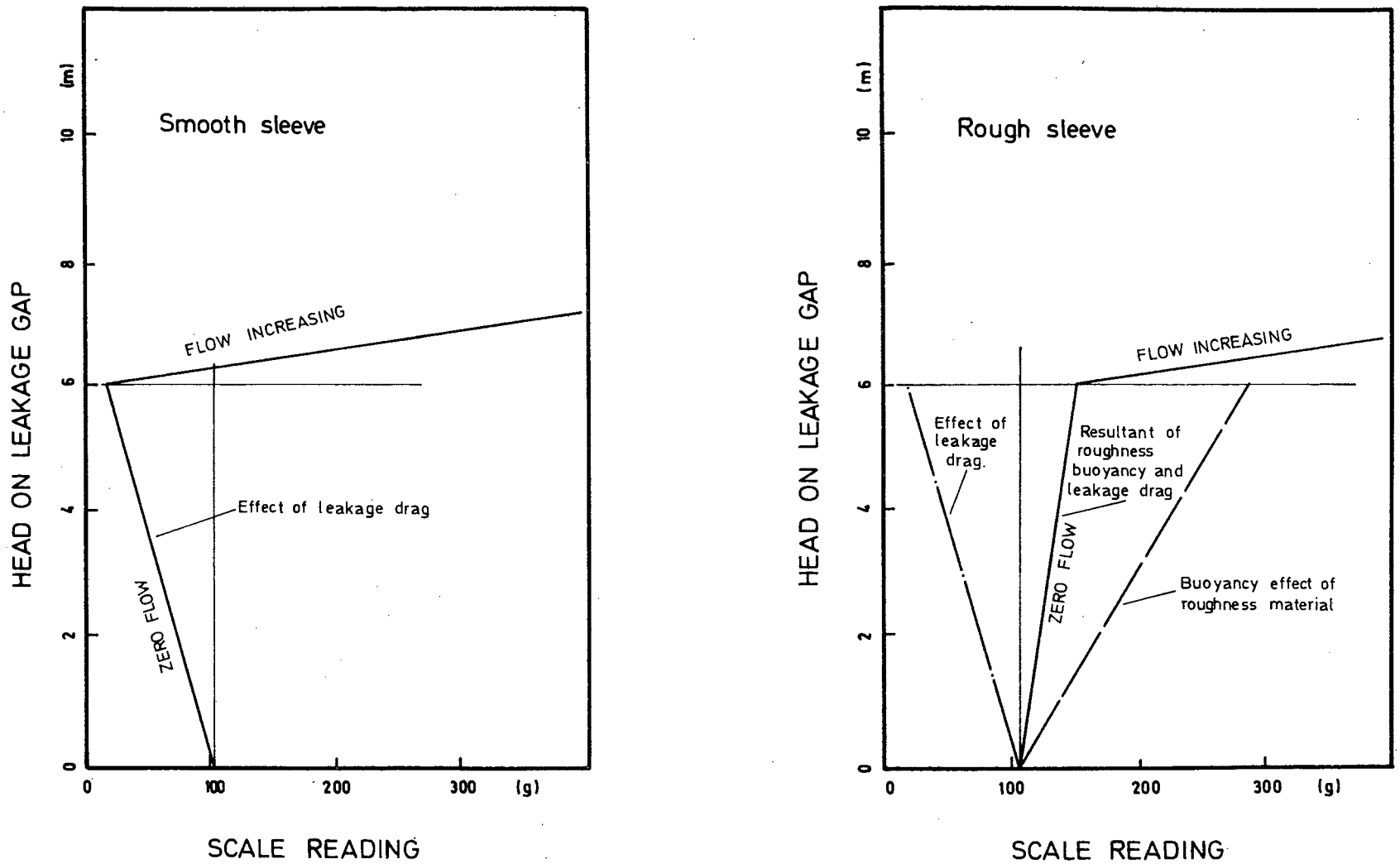

Fig. 28 The effect of roughness on the floating sleeve weight measurements

(ii) Once a flow occurred through the sleeve the scale would again register a further upward shear force related to the flow velocity.

Fig. 28 shows what is happening: the downward leakage shear force is being overshadowed by the upward buoyancy of the roughness material, which occurs in terms of Archimedes' Principle. The sleeve thus suffers a net upthrust which increases with increasing static heads.

Now in order to obtain the true upthrust on the floating sleeve a correction for the downward leakage force and for the roughness buoyancy must be applied. However, if the initial zero flow scale reading is taken to occur when the sleeve is just full, with a static head on the leakage gap (instead of zero head) then the only correction necessary will be for the increased leakage shear stress that will occur when there is a flow velocity through the sleeve; the buoyancy effect will have automatically been taken into account. Checks proved that for smooth annuli two methods of correcting for the downward leakage shear gave consistent results, viz. considering the empty sleeve weight as the initial condition, or considering the sleeve weight when filled with static water as the initial condition. Whilst both methods could be (and were) applied to the smooth sleeve, only the second could be used for the rough sleeve. Thus the problem of ascertaining the magnitude of the buoyancy was circumvented.

SECTION 6

THEORETICAL ANALYSIS

The basic equations governing fluid flow are the Navier Stokes equations. These are partial non-linear differential equations and are thus generally insoluble. Various simplifying assumptions or boundary conditions can sometimes be imposed to yield solutions for laminar flows, as well as providing welcome information about turbulence and turbulent flows. In Section 6.1 the equations for the conservation of mass and linear momentum will be derived in outline.* In Section 6.2 the mean flow equations will be derived in cylindrical coordinates and some results of these equations for pipe and annular flow will be examined.

6.1 Derivation of the Conservation Equations for Mass and Linear Momentum

The three basic Newtonian laws of mechanics are the conservation of mass, momentum and energy. Unfortunately, these laws have been formulated in a Lagrangian rather than Eulerian description of motion. That is, they describe the trajectories of individual particles rather than describing what happens at each fixed point in space as a function of time. In fluid mechanics the vector velocity of the fluid is usually of fundamental importance rather than say the particle displacements. For this reason, the Eulerian description is less cumbersome than the Lagrangian and will be used here.

Before the basic equations can be applied to fluid mechanics, the assumption of a continuum must be made. In essence this means that for the purpose of performing mathematical operations, such as taking derivations, the fluid can be divided up into smaller elements without limit and still remain a continuum. This assumption is valid for almost all fluids since the dimensions of the problem under consideration are very large when compared with the molecular dimensions.

* Detailed discussions (for example that dealing with the representation of surface forces by the stress tensor) will not be dealt with here.

6.1·1 Conservation of Mass

Consider a fixed region in space containing a volume V of fluid bounded by a closed surface of area S, which has δV as an element of the enclosed volume V and δS (with a unit outward normal $\underline{n}$) as an element of the bounding surface S. From the law of conservation of mass it follows that the rate of change of mass contained in the region must equal the mass flux into the region. This can be expressed mathematically as

$$\frac{d}{dt}\int_V \rho(\underline{x},t)\, dV = -\int_S \rho(\underline{x},t)\, \underline{u}\cdot\underline{n}\, dS, \qquad \text{(Eq. 39)}$$

where ρ is the mass density of the fluid at position $\underline{x}$ at time t. The surface integral can be tranformed into a volume integral using Gauss' divergence theorem:

$$\therefore \quad \frac{d}{dt}\int_V \rho dV = -\int_V \nabla\cdot(\rho\underline{u})\, dV$$

and because V is fixed in space,

$$\int_V \left[\frac{\partial\rho}{\partial t} + \nabla\cdot(\rho\underline{u})\right] dV = 0,$$

which is the global expression for the conservation of mass. This global equation is zero for any choice of fixed volume V and therefore the integral is zero because the integrand is zero.

$$\therefore \quad \frac{\partial\rho}{\partial t} + \nabla\cdot(\rho\underline{u}) = 0 \qquad \text{(Eq. 40)}$$

which is the local form of the conservation of mass. This is equivalent to

$$\frac{\partial\rho}{\partial t} + \rho(\nabla\cdot\underline{u}) + \underline{u}\cdot\nabla\rho = 0,$$

which can be expressed using the material derivative as

$$\frac{D\rho}{Dt} + \rho(\nabla\cdot\underline{u}) = 0. \qquad \text{(Eq. 41)}$$

This form of the equation is important for the consideration of incompressible flow. A stringent definition of incompressible flow necessitates a knowledge of thermodynamics. For fluid mechanics, a definition equivalent in most respects is usually taken as: a fluid whose density does not vary with time as one follows the fluid.

$$\therefore \quad \frac{D\rho}{Dt} = 0$$

and a consequence of this is that $\nabla \cdot \underline{u} = 0$ for an incompressible fluid.

6.1.2 Conservation of Linear Momentum

The conservation of linear momentum will be derived for a constant viscosity incompressible fluid, since this is the form most widely used in hydraulics. The linear momentum at time t possesed by the fluid which occupies a region of volume V(t) (which moves with the fluid) is

$$\int_{V(t)} \underline{u}\, \rho \, dV,$$

and the rate of change of this linear momentum is given by

$$\frac{d}{dt} \int_{V(t)} \underline{u}\, \rho \, dV$$

which can be equated by means of the Reynolds transport theorem* to

$$\int_{V(t)} \rho \frac{D\underline{u}}{Dt} \, dV. \qquad \text{(Eq. 42)}$$

Disregarding surface tension, the forces which may act on V(t) can be divided into two groups, namely body forces and surface forces.

Body forces are forces which act at each point in V(t). If $\underline{f}\,(\underline{x},t)$ is the vector resultant of the body forces, per unit mass, then the total body force acting on V(t) is

$$\int_{V(t)} \rho\, \underline{f} \, dV. \qquad \text{(Eq. 43)}$$

* See Batchelor (1)

Surface forces are forces which act at the surface of an element and are caused by direct mechanical contact between interacting elements. The value of the surface forces acting on an element is thus dependent upon the surface area of the element; furthermore, these forces are considered to act on a plane surface element and are specified as the total force exerted on one side of the fluid element by the fluid on the other side. Consider a point $\underline{x}$ (with a unit outward normal $\underline{n}$) at time t on the boundary S(t) of V(t), then $\underline{\Sigma}(\underline{x},\underline{n},t)$ is the force per unit area or local stress exerted at $\underline{x}$ by the material outside V(t) on the material inside V(t). $\underline{\Sigma}(\underline{x},\underline{n},t)$, which may be written as $\Sigma_i(\underline{x},\underline{n},t)$, may be represented by a Cartesian tensor thus:

$$\Sigma_i(\underline{x},\underline{n},t) = \sigma_{ij}(\underline{x},t)n_j$$

where σ_{ij} is now independent of $\underline{n}$. The total surface force exerted on V(t) by the material outside V(t) is therefore

$$\int_{S(t)} \sigma_{ij} n_j dS = \int_{V(t)} \frac{\partial \sigma_{ij}}{\partial x_j} dV, \qquad \text{(Eq. 44)}$$

the right hand side again being obtained from the divergence theorem. A global balance of linear momentum for the selected region of fluid V(t), in Cartesian coordinates gives:

$$\int_{V(t)} \rho \frac{Du_i}{Dt} dV = \int_{V(t)} \rho f_i \, dV + \int_{V(t)} \frac{\partial \sigma_{ij}}{\partial x_j} dV.$$

This relationship holds for any choice of material volume V(t) and thus

$$\rho \frac{Du_i}{Dt} = \rho f_i + \frac{\partial \sigma_{ij}}{\partial x_j} \qquad \text{(Eq. 45)}$$

From the definition of a fluid, the shearing stresses must be zero when the fluid is at rest. Thus if P is the hydrostatic pressure, then the stress tensor for a fluid at rest becomes

$$\sigma_{ij} = -P\,\delta_{ij}$$

where δ_{ij} is the Kronecker delta. In a moving fluid P is defined as $-\frac{1}{3}\sigma_{ii}$.

It can be seen by examining, for example, a cubical element of fluid that the nine components of the stress tensor are not all independent. Considering an element such as that shown in Fig. 29 the sum of the moments about the z-axis through the centre of the element is

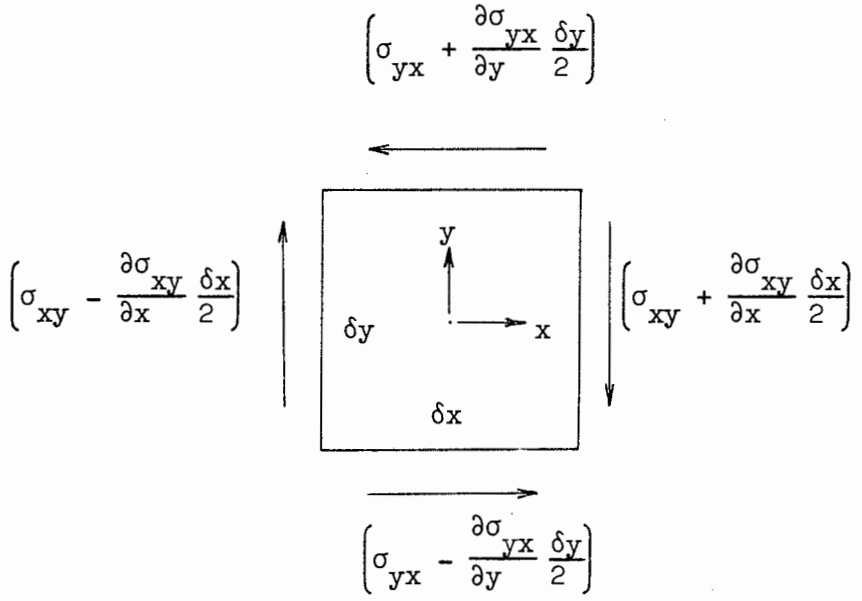

Fig. 29 Stresses giving moments about the z-axis

$$\left(\sigma_{yx} + \frac{\partial \sigma_{yx}}{\partial y}\frac{\delta y}{2} + \sigma_{yx} - \frac{\partial \sigma_{yx}}{\partial y}\frac{\delta y}{2}\right)\frac{\delta y}{2}\,\delta x\delta z$$

$$- \left(\sigma_{xy} + \frac{\partial \sigma_{xy}}{\partial x}\frac{\delta x}{2} + \sigma_{xy} - \frac{\partial \sigma_{xy}}{\partial x}\frac{\delta x}{2}\right)\frac{\delta x}{2}\,\delta y\delta z.$$

According to Newton's law this net moment must be equal to the moment of inertia of the element times its angular acceleration $\ddot{\theta}$ about the z axis

$$\therefore \quad (\sigma_{yx} - \sigma_{xy})\delta x\delta y\delta z = \rho\delta x\delta y\delta z\left[\frac{(\delta x)^2 + (\delta y)^2}{12}\right]\ddot{\theta},$$

as the dimensions of the element approach zero, the moment of inertia approaches zero as the square of the dimensions and thus $\sigma_{xy} = \sigma_{yx}$. In general therefore $\sigma_{ij} = \sigma_{ji}$ and the stress tensor is symmetric. The stress tensor may now be written as

$$\sigma_{ij} = - P \delta_{ij} + d_{ij}$$

where $P \delta_{ij}$ is the isotropic part having the same form as the stress tensor in a fluid at rest, and where d_{ij} is the non-isotropic part and is due entirely to the motion of the fluid. It remains to express the deviatoric stress tensor d_{ij} in terms of the rate of strain tensor e_{ij} which is defined as being $e_{ij} = \frac{1}{2}(\partial u_i/\partial x_j + \partial u_j/\partial x_i)$. There is no way of deducing the dependence of d_{ij} upon $\partial u_i/\partial x_j$ for fluids, and so the assumption is made that this relationship is typical of transport phenomena; viz., that the flux density of the transported quantity varies linearly with the spatial gradient of the quantity normal to the surface element. Thus for a pure shear flow this relationship can be expressed as

$$d_{ij} = \mu \frac{\partial u_i}{\partial x_j},$$

in which the 'driving force' for the momentum transport is the velocity gradient. Symmetry is retained if we write this relationship as $d_{ij} = 2 \mu e_{ij}$.

$$\therefore \quad \sigma_{ij} = - P \delta_{ij} + 2 \mu e_{ij}$$

and substituting this into Eq. 45 gives

$$\rho \frac{Du_i}{Dt} = \rho f_i + \frac{\partial}{\partial x_j} (-P \delta_{ij} + 2 \mu e_{ij})$$

$$= \rho f_i - \frac{\partial P}{\partial x_i} + \mu \frac{\partial}{\partial x_j} \left(\frac{\partial u_i}{\partial x_j} + \frac{\partial u_j}{\partial x_i} \right)$$

$$= - \frac{\partial p}{\partial x_i} + \mu \frac{\partial^2 u_i}{\partial x_j \partial x_j}$$

or

$$\rho \frac{D\underline{u}}{Dt} = - \nabla p + \mu \nabla^2 \underline{u} \qquad \text{(Eq. 46)}$$

where p is the modified pressure which takes into account the body forces (which are usually only gravitational).

6.1.3 The Insolubility of the Navier Stokes Equations

The Navier Stokes equations are non-linear partial differential equations and are thus generally insoluble by any known method. It is usually the non-linear advective term which prevents solution. If this advective term is made zero by applying certain conditions to the equations, then the solution sometimes becomes easier. However, the solutions obtained then apply to the limited flow regimes determined by the conditions imposed. Exact solutions of laminar pipe and Couette flow for example, are obtained by these means.

What is required for the solution of turbulent flow is the mathematical prediction of turbulence. This prediction should be forthcoming since it is generally agreed that turbulent flow fully satisfies the Navier Stokes equations. However, Emmons [8] suggests that attempting any sort of mathematical prediction of turbulence would be futile. Examining the problem of turbulent pipe flow he shows that a computer solution producing any meaningful statistics would require 10^{22} numerical operations at a $Re = 10^{7}$. Working at a typical computer speed of 10 microseconds per operation, the complete calculation would take 10^{17} seconds or approximately 10^{10} years which is about the age of the universe. It is true that the operating speeds of computers is increasing by about an order of magnitude every three years, yet even a computer working at the speed of light (presumably the limiting speed) would still require 32 000 years, according to White [53], to complete its computation. It is possible that in the future low Reynolds number turbulent flows may be within the range of investigation, but it remains highly unlikely that we shall ever be able to simulate turbulence mathematically.

The conclusion is that approximate solutions of the Navier Stokes solutions can only be obtained for turbulent flows where some mechanical assumption is made. Identification of, and data for, these assumptions must come from the laboratory.

6.2 The Mean Flow Equations and their Application to Circular Pipes and Annuli

The equations of motion for the conservation of mass and momentum have been established for incompressible constant viscosity flow as

$$\nabla \cdot \underline{u} = 0 \qquad \text{(Eq. 47)}$$

and

$$\frac{D\underline{u}}{Dt} = -\frac{1}{\rho}\nabla p + \nu \nabla^2 \underline{u}$$

These equations written in the above vector notation are coordinate free and providing the proper form of the operators is adhered to, the equations may be expanded using any coordinate system.

The instantaneous velocity vector $\underline{u}$ can be expressed as the sum of the mean and fluctuating components. Thus

$$\underline{u} = \underline{U} + \underline{u}' \qquad \text{(Eq. 48)}$$

where $$\underline{U} = \lim_{T\to\infty} \frac{1}{T} \int_{t_0}^{t_0+T} \underline{u}\, dt$$

Now in order for $\partial \underline{U}/\partial t$ to be equal to zero, $\underline{U}$ must be defined as the steady velocity. In practice the time interval T is chosen to be larger than any significant period of the fluctuation $\underline{u}'$. The period obviously depends upon the nature of the problem and would range from a few secondsin channel flow to 30 minutes or more for ocean wave measurements.

Substituting Eq. 48 into Eq. 47 yields

$$\nabla \cdot (\underline{U} + \underline{u}') = 0$$

and taking the average of this yields

$$\nabla \cdot \underline{U} = 0$$

and $$\nabla \cdot \underline{u}' = 0$$

The above are merely mathematical equations expressing the physically obvious fact: that if the total flow field is incompressible, then so are the mean flow and the fluctuating flow fields Now substitution of Eq. 48 into the Navier Stokes equation yields after taking the average:

$$\overline{\frac{\partial}{\partial t}(\underline{U} + \underline{u}')} + \overline{(\underline{U} + \underline{u}') \cdot \nabla (\underline{U} + \underline{u}')} = \overline{-\frac{1}{\rho}\nabla(P + p')} + \overline{\nu \nabla^2 (\underline{U} + \underline{u}')}.$$

Now since the advective term is the only non-linear term:

$$\frac{\partial \underline{U}}{\partial t} + \underline{U} \cdot \nabla \underline{U} = -\frac{1}{\rho}\nabla P + \nu \nabla^2 \underline{U} - \overline{\underline{u}' \cdot \nabla \underline{u}'} \qquad \text{(Eq. 49)}$$

6.2.1 Expansion of the Mean Flow Equations in Cylindrical Coordinates

The expansion and translation of Eq. 49 into cyclindrical coordinates is not straightforward. This is because the direction of the radial and angular unit vectors at a point vary with a change in the angular coordinate of that point. Thus with the expansion of Eq. 49 in the $\hat{\theta}$ direction, we should expect extra terms to occur in the $\hat{r}$ direction and vice-versa. This in fact does happen.

Now expanding Eq. 49 into cylindrical coordinates being careful to use the correct form of the operators appropriate to cylindrical coordinates, as well as bearing in mind the inclusion of additional terms due to a moving coordinate system and using the continuity equation for fluctuating velocity components to transform the average product of a fluctuating component and a derivative into the derivative of the average product of two fluctuating components, the mean flow equations in cylindrical coordinates are determined:

$$\frac{\partial U_x}{\partial t} + U_x \frac{\partial U_x}{\partial x} + U_r \frac{\partial U_x}{\partial r} + \frac{U_\theta}{r} \frac{\partial U_x}{\partial \theta} = - \frac{1}{\rho} \frac{\partial P}{\partial x} + \nu \nabla^2 U_x$$

$$- \frac{\partial}{\partial x} \overline{u_x'^2} - \frac{1}{r} \frac{\partial}{\partial r} \overline{r u_x' u_r'} - \frac{1}{r} \frac{\partial}{\partial \theta} \overline{u_x' u_\theta'} \qquad \text{(Eq. 50a)}$$

$$\frac{\partial U_r}{\partial t} + U_x \frac{\partial U_r}{\partial x} + U_r \frac{\partial U_r}{\partial r} + \frac{U_\theta}{r} \frac{\partial U_r}{\partial \theta} - \frac{U_\theta^2}{r} = - \frac{1}{\rho} \frac{\partial P}{\partial r}$$

$$+ \nu \nabla^2 U_r - \frac{2\nu}{r^2} \frac{\partial U_\theta}{\partial \theta} - \frac{\nu U_r}{r^2} - \frac{\partial}{\partial x} \overline{u_x' u_r'} - \frac{1}{r} \frac{\partial}{\partial r} \overline{r u_r'^2}$$

$$- \frac{1}{r} \frac{\partial}{\partial \theta} \overline{u_r' u_\theta'} + \frac{\overline{u_\theta'^2}}{r} \qquad \text{(Eq. 50b)}$$

$$\frac{\partial U_\theta}{\partial t} + U_x \frac{\partial U_\theta}{\partial x} + U_r \frac{\partial U_\theta}{\partial r} + \frac{U_\theta}{r} \frac{\partial U_\theta}{\partial \theta} + \frac{U_\theta U_r}{r} = - \frac{1}{\rho r} \frac{\partial P}{\partial \theta}$$

$$+ \nu \nabla^2 U_\theta + \frac{2\nu}{r^2} \frac{\partial U_r}{\partial \theta} - \frac{\nu U_\theta}{r^2} - \frac{\partial}{\partial x} \overline{u_x' u_\theta'}$$

$$- \frac{\partial}{\partial r} \overline{u_r' u_\theta'} - \frac{1}{r} \frac{\partial}{\partial \theta} \overline{u_\theta'^2} - \frac{2 u_r' u_\theta'}{r} \qquad \text{(Eq. 50c)}$$

6.2.2 Simplification for Pipe and Annular Flow

Certain flow conditions and boundary conditions pertinent to pipe flow may now be inserted to simplify the mean flow equations. Only those conditions common to both annular and pipe flow will be applied in this section. Thus the equations derived will be equally suitable for further investigation in both types of conduit. The conditions for mean unidirectional axial flow are:

(i) All average quantities are constant in an axial direction except for pressure.

(ii) All average quantities are constant in a circumferential direction.

(iii) All average quantities are independent of time.

(iv) There is no slip at the boundary walls.

(v) The continuity equation applies.

The mathematical results of these conditions are:

(i) $\frac{\partial}{\partial x} = 0$, all mean quantities except pressure

(ii) $\frac{\partial}{\partial \theta} = 0$, all mean quantities.

(iii) $U_r = U_\theta = 0$

(iv) $U_x = u'_x = u'_r = u'_\theta = 0$ at the conduit walls.

Substituting the results of these conditions into Eq. 50 the following simplifications result:

$$\frac{1}{r}\frac{\partial}{\partial r}\left(\nu r \frac{\partial U_x}{\partial r} - \overline{r u'_x u'_r}\right) = \frac{1}{\rho}\frac{\partial P}{\partial x} \qquad \text{(Eq. 51a)}$$

$$-\frac{1}{r}\frac{\partial}{\partial r}\left(\overline{r u'^2_r}\right) + \frac{\overline{u'^2_\theta}}{r} = \frac{1}{\rho}\frac{\partial P}{\partial r} \qquad \text{(Eq. 51b)}$$

$$\frac{\partial}{\partial r}\overline{u'_r u'_\theta} + \frac{\overline{2u'_r u'_\theta}}{r} = 0 \quad . \qquad \text{(Eq. 51c)}$$

These simplified equations still remain insoluble. Nevertheless, they do yield important insights into the turbulence mechanism. For laminar flows, the equations will obviously reduce to soluble expressions. Certain results for pipe and annular flows will now be examined.

6.2.3 Results for Pipe Flow

Pressure gradient

Differentiation of Eq. 51b with respect to x yields

$$\frac{\partial}{\partial x}\left(\frac{\partial P}{\partial r}\right) = 0 \qquad \text{(Eq. 52)}$$

$$\therefore \quad \frac{\partial}{\partial r}\left(\frac{\partial P}{\partial x}\right) = 0$$

Thus $\frac{\partial P}{\partial x}$ the axial pressure gradient is independent of r. This is an extremely important result since it enables the measurement of the axial pressure gradient by means of pressure tappings in the conduit walls. However, the pressure itself does depend on the radial position. Integrating equation Eq. 51b with respect to r from r to r_2 to obtain

$$\frac{1}{\rho}(P_2 - P_r) = -\int_r^{r_2} \frac{\overline{u_r'^2 - u_\theta'^2}}{r}\,dr + \overline{u_r'^2}$$

Very little information about this radial variation in pressure is available. Measurements of the r.m.s. values of the fluctuating components give an estimate of the pressure variation across a pipe as being about 0,3% of the mean dynamic pressure in the pipe.

Shear stress gradient

It is evident that

$$\tau_{xr} = \mu \frac{\partial U_x}{\partial r} - \rho \overline{u_x' u_r'} \quad . \qquad \text{(Eq. 53)}$$

Now Eq. 51a becomes

$$\frac{\partial}{\partial r}(r\,\tau_{xr}) = r \frac{\partial P}{\partial x} \qquad \text{(Eq. 54)}$$

and integrating from r to zero

$$\tau_{xr} = \tfrac{1}{2} r \frac{\partial P}{\partial x}$$

and $\frac{\partial P}{\partial x}$ has been seen to be constant.

Now because τ must reduce to τ_2 at $r = r_2$ and to zero at $r = 0$

$$\tau_{xr} = \mu \frac{\partial U_x}{\partial r} - \rho \overline{u'_x u'_r} = \frac{\tau_2 r}{r_2} \qquad \text{(Eq. 55)}$$

Thus it can be seen that even in turbulent flow the shear stress varies linearly with the radius. Realising that the velocity fluctuations are absent in laminar flow, Eq. 55 reduces to the well-known expression

$$\tau_{xr} = \mu \frac{\partial U_x}{\partial r} \qquad \text{(Eq. 56)}$$

It is well to note that Eq. 56 is not as is often supposed, the original concept embodied in the modern definition of Newtonian fluids, but is rather a consequence of the definition, which, as a form of a transport process is intended to apply to the general flow field.

Although it is useful to know that the shear stress varies linearly in turbulent flow, Eq. 55 unfortunately cannot be integrated in order to ascertain the nature of the velocity profile $U_x(r)$ since we have no theoretical knowledge of the not insignificant contribution of $\overline{u'_x u'_r}$.

Velocity gradient

Integrating Eq. 51a with respect to r yields:

$$\nu r \frac{\partial U_x}{\partial r} - \overline{r u'_x u'_r} = \frac{r^2}{2\rho} \frac{\partial P}{\partial x} + C \qquad \text{(Eq. 57)}$$

At $r = 0$, $C = 0$ and Eq. 57 becomes

$$\nu \frac{\partial U_x}{\partial r} - \overline{u'_x u'_r} = \frac{r}{2\rho} \frac{\partial P}{\partial x} \qquad \text{(Eq. 58)}$$

Integrating Eq. 58 from $r = 0$ to $r = r_2$ and realising that at $r = 0$, $U_x = U_x$ max and that at $r = r_2$, $U_x = 0$.

$$\mu \int_{U_x max}^{0} \partial U_x - \rho \int_0^{r_2} \overline{u'_x u'_r}\, \partial r - \tfrac{1}{2} \frac{\partial P}{\partial x} \int_0^{r_2} r \partial r = 0$$

$$\therefore \quad -\mu U_x max - \rho \int_0^{r_2} \overline{u'_x u'_r}\, \partial r - \frac{1}{4} \frac{\partial P}{\partial x} r_2^2 = 0$$

$$\therefore \quad U_x max = -\frac{1}{4\mu} \left[\frac{\partial P}{\partial x} r_2^2 + 4\rho \int_0^{r_2} \overline{u'_x u'_r}\, \partial r \right]$$

Since P falls in the direction of flow, $U_x max$ is positive. If Eq. 58 had been integrated for $r = r$ to $r = r_2$ then the general velocity profile would have been obtained:

$$U\Big|_r = -\frac{1}{4\mu} \left[\frac{\partial P}{\partial x} (r_2^2 - r^2) - 4\rho \int_r^{r_2} \overline{u'_x u'_r}\, \partial r \right]$$

For laminar flow the above equation would reduce to

$$U_{max} = -\frac{1}{4\mu} \left(\frac{\partial P}{\partial x} r_2^2 \right)$$

6.2.4 Results for Annular Flow

Pressure gradient

Differentiation of Eq. 51b with respect to x still yields

$$\frac{\partial}{\partial x}\left(\frac{\partial P}{\partial r}\right) = 0$$

$$\therefore \quad \frac{\partial}{\partial r}\left(\frac{\partial P}{\partial x}\right) = 0$$

Thus $\partial P/\partial x$ is still independent of r and is constant, and the results for pipe flow apply to annular flow.

Shear stress gradient and the position of zero shear

From Eq. 51a

$$\frac{\partial}{\partial r}(r\,\tau_{xr}) = \frac{\partial P}{\partial x}\,r \qquad \text{(Eq. 59)}$$

and $$\tau_{xr} = \mu\frac{\partial U_x}{\partial r} - \rho\overline{u'_x\,u'_r}$$

Thus for the position of maximum velocity to coincide with the position of zero shear stress, $\overline{u'_x\,u'_r} = 0$ at the position where $\partial U_x/\partial r = 0$. This is possibly the most important result achieved so far. It should be noted that there is no theoretical evidence to suggest that $\overline{u'_x\,u'_r} = 0$ at $\partial U_x/\partial r = 0$ except for cases where symmetry is present.

The widely made assumption that these two positions are coincident appears to be groundless.

Integrating Eq. 59 between $r = r_2$ and $r = r$ gives:

$$r_2\,\tau_2 - r\tau_{xr} = \left(\frac{r_2^2 - r^2}{2}\right)\frac{\partial P}{\partial x}$$

and between $r = r$ and $r = r_1$ gives:

$$r_1\,\tau_1 - r\tau_{xr} = \left(\frac{r_1^2 - r^2}{2}\right)\frac{\partial P}{\partial x}$$

Adding

$$r_1 \tau_1 + r_2 \tau_2 - 2r\tau_{xr} = \left(\frac{r_1^2 + r_2^2 - 2r^2}{2}\right) \frac{\partial P}{\partial x}$$

$$\therefore \quad \tau_{xr} = -\frac{1}{r}\frac{\partial P}{\partial x}\left[\frac{r_2^2 + r_1^2 - 2r^2}{4}\right] + \left[\frac{r_1\tau_1 + r_2\tau_2}{2r}\right]$$

$$= Ar - \frac{B}{r} \quad \text{where A and B are constants}$$

Thus it can be seen that the shear stress no longer varies linearly in the radial direction as was the case for pipe flow. The value of the radius of zero shear cannot be solved analytically for turbulent shear, but the integration of Eq. 51a forms one basis for the determination of the zero shear position by hot wire anemometry:

$$\int_{r_1}^{r_2}\int_{r_0}^{r} \frac{\partial r\tau}{\partial r} = \int_{r_1}^{r_2}\int_{r_0}^{r} r\frac{\partial P}{\partial x} \qquad \text{(Eq. 60)}$$

$$\therefore \quad \int_{r_1}^{r_2} \left(\mu r \frac{\partial U_x}{\partial r} - r\rho\,\overline{u_x' u_r'}\right) - \int_{r_1}^{r_2} \frac{r^2}{2}\frac{\partial P}{\partial x} - \frac{r_0^2}{2}\frac{\partial P}{\partial x} = 0$$

Now dividing through by r and noting the change of limits for U_x:

$$\mu\int_{U_1}^{U_2} \partial U_x - \rho\int_{r_1}^{r_2} \overline{u_x' u_r'}\,\partial r - \frac{1}{2}\frac{\partial P}{\partial x}\int_{r_1}^{r_2} r\partial r + \frac{r_0^2}{2}\frac{\partial P}{\partial x}\int_{r_1}^{r_2}\frac{1}{r}\partial r = 0$$

$$\therefore \quad \frac{r_0^2}{2}\frac{\partial P}{\partial x}(\ell n\, r_2 - \ell n\, r_1) = \frac{1}{4}\frac{\partial P}{\partial x}(r_2^2 - r_1^2) + \frac{1}{\rho}\int_{r_1}^{r_2} \overline{u_x' u_r'}\,\partial r$$

$$\therefore \quad r_0 = \sqrt{\frac{r_2^2 - r_1^2 + k\int_{r_1}^{r_2} \overline{u_x' u_r'}\,\partial r}{2(\ell n\, r_2/r_1)}}$$

where $k = 4\rho / \frac{\partial P}{\partial x}$

For laminar flow this result simplifies to the identical expression obtained by a simple force balance. It can also be seen that earlier suppositions that $r_{0t} = r_{0\ell}$ are completely unfounded since they neglect the integral of the mean fluctuating u'_x and u'_r components.

Velocity gradient

Integrating Eq. 60 from r = r instead of from r = r_1 yields:

$$\mu \int_U^0 \partial U_x - \rho \int_r^{r_2} \overline{u'_x u'_r}\, \partial r - \frac{1}{2}\frac{\partial P}{\partial x} \int_r^{r_2} r\partial r + \frac{r_0^2}{2}\frac{\partial P}{\partial x} \int_r^{r_2} \frac{1}{r}\partial r = 0$$

$$\therefore \quad -\mu U_x - \rho \int_r^{r_2} \overline{u'_x u'_r}\, \partial r - \frac{1}{4}\frac{\partial P}{\partial x}[r_2^2 - r^2] + \frac{r_0^2}{2}\frac{\partial P}{\partial x}[\ell n\, r_2 - \ell n r] = 0$$

$$\therefore \quad U_{xr} = -\frac{1}{\nu}\int_r^{r_2} \overline{u'_x u'_r}\, \partial r - \frac{1}{4\mu}\frac{\partial P}{\partial x}[r_2^2 - r^2] - \frac{r_0^2}{2\mu}\frac{\partial P}{\partial x}\left[\ell n \frac{r}{r_2}\right]$$

$$\therefore \quad U_{xr} = -\frac{1}{4\mu}\frac{\partial P}{\partial x}\left(r_2^2 - r^2 + \frac{r_2^2 - r_1^2}{\ell n\, r_2/r_1}\ell n \frac{r}{r_2}\right)$$

$$-\frac{1}{\nu}\left(\int_r^{r_2} \overline{u'_x u'_r}\, \partial r - \frac{\ell n\, r_2/r}{\ell n\, r_2/r_1}\int_{r_1}^{r_2} \overline{u'_x u'_r}\, \partial r\right) \quad \text{(Eq. 61)}$$

For laminar flow an alternative expression for τ_{xr} may be obtained from Eq. 60.

$$\tau_{xr} = \mu \frac{\partial U_x}{\partial r}$$

$$\therefore \quad \tau_{xr} = -\frac{1}{4} \frac{\partial P}{\partial x} \left(-2r + \frac{1}{r} \frac{r_2 - r_1}{\ell n\, r_2/r_1} \right)$$

$$= Ar - \frac{B}{r} \quad \text{as before.}$$

SECTION 7

ANALYSIS OF RESULTS

The program of experimental work may be divided into the following sections:

(i) Determination of the sensitivity of the floating sleeve.

(ii) Calibration of the floating sleeve for end effects due to the bottom leakage gap.

(The above were proving tests designed to determine the accuracy and sensitivity of the floating sleeve.

(iii) The smooth annular tests.

(iv) The rough annular tests.

(These produced the individual annular wall shear stresses, the position of zero shear stress and friction factor - Reynolds number curves).

7.1 The Sensitivity of the Floating Sleeve

Preliminary tests were conducted to determine the sensitivity of the floating sleeve to factors which might influence its accuracy.

7.1.1 Density of Flotation Liquid

Changes in temperature of the water in the float channel would cause density changes resulting in varying upthrusts on the floating sleeve. Should these changes be significant, inaccuracies in the weight readings of the floating sleeve would occur. A thermostatically controlled heater was placed in the float channel and a record kept of the effective weights of the sleeve (as shown on the scale) with various temperature settings. The results showed a negligible change in density for temperature differences corresponding to those experienced during a normal day. Seasonal temperature variations may be significant but these are discounted since a new zero scale reading is taken daily.

The floating sleeve was thus insensitive to flotation liquid density changes caused by differences in room temperature.

7.1.2 Changes in Float Size

The float is defined as any part of the floating sleeve apparatus which is fully immersed in the flotation liquid. Thus the main part of the float consisted of the square P.V.C. float. Screw rods were used to connect the floating sleeve cross arm supports to the P.V.C. float. Since a portion of these rods were immersed in the flotation liquid, those portions formed part of the float and thus suffered an upthrust equal to the weight of water that they displaced. Now because the scale worked on a deflection principle, differing effective weights of the floating sleeve as read on the scale, would cause differing amounts of these screw rods to be immersed in the liquid. The screw rods had been chosen for their small displacements, in order to minimise errors caused by changes in the float size.

The maximum scale pan deflection was 16 mm. Thus the maximum error to the weight readings caused by the four 10 mm diameter screw rods would be approximately 5 gf.

Although this error is fairly small, it was circumvented to a large extent during the weight tests, by adjusting the initial no flow readings to the centre of the scale. For flow conditions, the scale was brought to within 100 grams of the initial reading by the judicious choice of added brass weights. The float size was thus kept fairly constant and the error minimised to less than 1 gf.

7.1.3 Roller Bearing Friction

The accuracy of the weight readings obtained by the floating sleeve is dependent upon the friction in the roller bearing assemblies. The minimum number of roller bearings necessary to fully constrain the sleeve were used in the design in order to minimise this friction.

Estimates of the roller bearing friction were made with the

dry sleeve. Various brass weights were added to the floating sleeve and their effects registered on the sleeve scale. The tests were performed for various overlap distances of the bottom inlet nozzle and sleeve.

Nowhere was the discrepancy between added weights and corresponding scale readings greater than 8 gf. The mean for 58 tests for varying weights and overlap distances was 2,3 gf with a standard deviation of 3,8 gf. The bottom overlap distance had no effect on the ball race friction as detected by the sleeve scale. Full results are shown in Table 3.

Range of errors	= -7 to +8 gf
Mod Error	= observed weight - added weight
Mean of mod error	= x* = 3,9 gf
Standard deviation of x*	= 1,9 gf

Table 3.

The mean of the mod error gives a measure of the average amount of friction encountered by the roller assemblies. The results of the roller friction appeared encouraging. The floating sleeve having a dead weight of about 200 kgf was now able to register changes in weight with a sensitivity of only a few grams force (or approximately 0,002 per cent of its own weight).

7.1.4 Pressure Tapping Gradient

Whenever wall piezometers are used in turbulent flow, pressure fluctuations occur in the manometer tubes. In order to read a constant mean pressure, the tubes were throttled down using adjustable clamps. This and other factors, such as wall tappings not being normal to the

velocity stream, could cause non-linearities in the axial pressure gradient. It was necessary to check that this gradient was in fact linear.

A typical set of readings is shown in Table 4. They have been randomly selected from data obtained from tests in a smooth annulus. Table 5 shows typical data from a rough annulus.

Pressure tapping	Distance of Pressure tapping above top of inlet nozzle (mm)	Reading on common scale manometer (mm) water			
		Series 11 Test 1	Series 11 Test 23	Series 12 Test 9	Series 12 Test 26
P_1	240	927	312	1080	567
P_2	1769	705	280	799	531
P_3	3289	476	250	523	495
P_4	4808	253	220	258	455
P_5	6318	24	192	0	425
Gradient		-0,0419	-0,0197	-0,0178	-0,0237
Regression coefficient		1,0000	0,9996	0,9998	0,9986

Table 4. Pressure gradient for smooth annuli

The best fit straight line through the points has been determined in each case by regression analysis. As can be seen from these two tables, the coefficient of regression, which gives a measure of the dispersion of points about the best fit straight line, is almost exactly unity. This indicates a negligible amount of deviation and the pressure tappings were regarded as producing a linear pressure gradient.

Pressure tapping	Distance of Pressure tapping above top of inlet nozzle (mm)	Reading on common scale manometer (mm) water			
		Series 30 Test 2	Series 30 Test 17	Series 33 Test 1	Series 33 Test 6
P_1	240	1218	505	3099	476
P_2	1769	932	428	2334	400
P_3	3289	669	356	1586	322
P_4	4808	404	277	845	247
P_5	6318	139	198	112	171
Gradient		-0,1768	-0,0503	-0,4912	-0,0502
Regression coefficient		0,9998	0,9997	1,0000	1,0000

Table 5. Pressure gradient for rough annuli

7.1.5 Prolonged Flow through the Leakage Gap

Before the filter had been installed in the test rig, prolonged flow through the floating sleeve had caused particles and waste matter to gradually become lodged in the leakage gap. This caused 'sticking' of the floating sleeve and rendered operation inaccurate.

After the filter had been installed, no further matter of a nature sufficient to cause clogging passed through the sleeve and the sensitivity of the sleeve was no longer affected by prolonged flows.

7.2 Calibration of the Floating Sleeve for the Bottom Leakage Gap Effects

The two methods of determining the end correction as well as the nature of the correction have already been examined (refer back to Section 4). The numerical results achieved will be dealt with here.

7.2.1 Static Head Methods

Whenever the floating sleeve contains water, a downward shear force will be caused by the leakage of water through the bottom leakage gap. In order to measure the correct upward shear force when there is an upward flow through the sleeve, the magnitude of this leakage shear force must be known.

The fundamental postulate in this method of correction is that the nature of the end correction is unaltered by flow conditions.

In order to determine the value of this correction, the floating sleeve was filled with various static heads of water and the downward leakage shear force was registered on the scale (of course this method could only be applied to a smooth sleeve for reasons outlined in Section 5).

There were two methods of achieving this static head.

(i) The sleeve was completely filled with water which was then allowed to drain out through the leakage gap. The dropping head was noted at certain positions together with the respective scale reading. Because of the small area of the leakage gap the head in the sleeve dropped very slowly (approximately 0,01 m/s). This slowly dropping head was regarded as producing a series of different static heads.

(ii) The sleeve was filled to specific heights and the head held constant by careful adjustment of the inlet control valve ((d) in Fig. 15), the inflow through the valve could be made to balance the outflow through the leakage gap. Here of course although the level of the water head was static, water was continually fed into the rig. The flow through the leakage gap was so low that the upward shear of inflowing water on the floating sleeve, was considered negligible.

Although the graphs of the two methods are of the same order, there is a slight difference in trend. It was decided to use the results based on the second method as being appropriate. The trend difference is so small (of the order of 7 gf for a static head of 7 m) as to make no appreciable difference to the main results except perhaps for very low flows. Both the abovementioned methods were carried out for varying overlap lengths. Figs 30a and 30b show the results. As can be seen from the graphs, the overlap length has very little appreciable effect on the downward shear force. A possible explanation for this could be that for a large overlap length (see Fig. 25), the flow through the leakage gap is reduced whilst the area for the shear force to act on is increased; whereas for a small overlap length, the flow is increased and the area is reduced. A least squares straight line through the origin gives the equation used for the extrapolation of static heads to moving heads. Thus if the initial effective weight reading of the sleeve is taken for the empty sleeve:

$$F_L = 17{,}33 \times (\text{head on leakage gap}) \qquad \text{(Eq. 62)}$$

where F_L = leakage force in grams force

and the head on the leakage gap is in metres.

or if the initial effective weight of the sleeve is taken for a sleeve filled with a maximum static head (as would be necessary if the sleeve ~~was~~ were rough) then:

$$F_L = 17{,}33 \text{ (head on leakage gap - length of sleeve).}$$

In general then

$$F_L = 17{,}33 \, (z + h) \qquad \text{(Eq. 63)}$$

where the terminology is that used in Section 4.

Using the above correction Eq. 63, the friction factor vs Reynolds number curves for $\alpha = 0$ (plain pipe) should coincide if determined

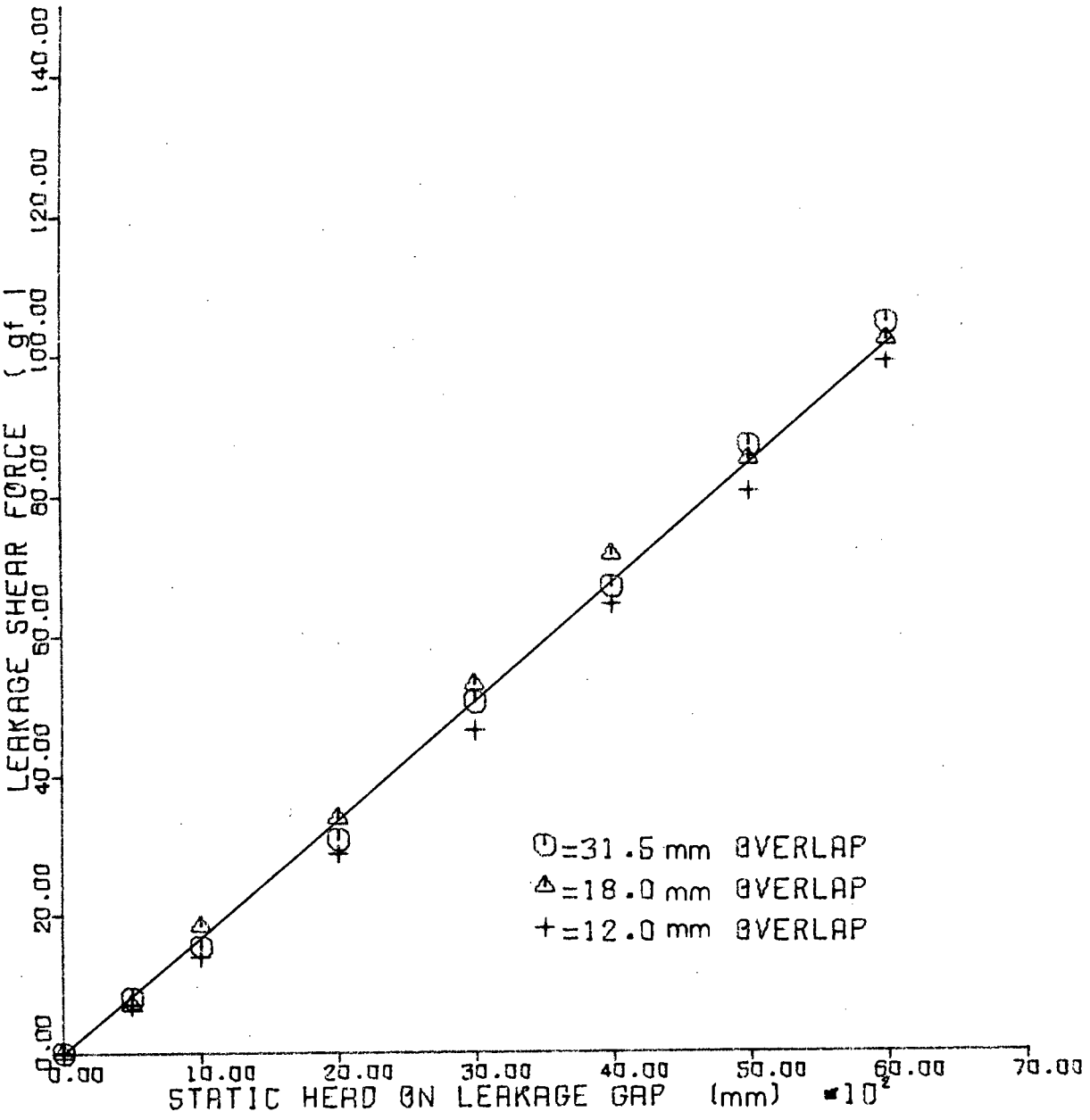

Fig. 30a Constant head method of determining leakage correction

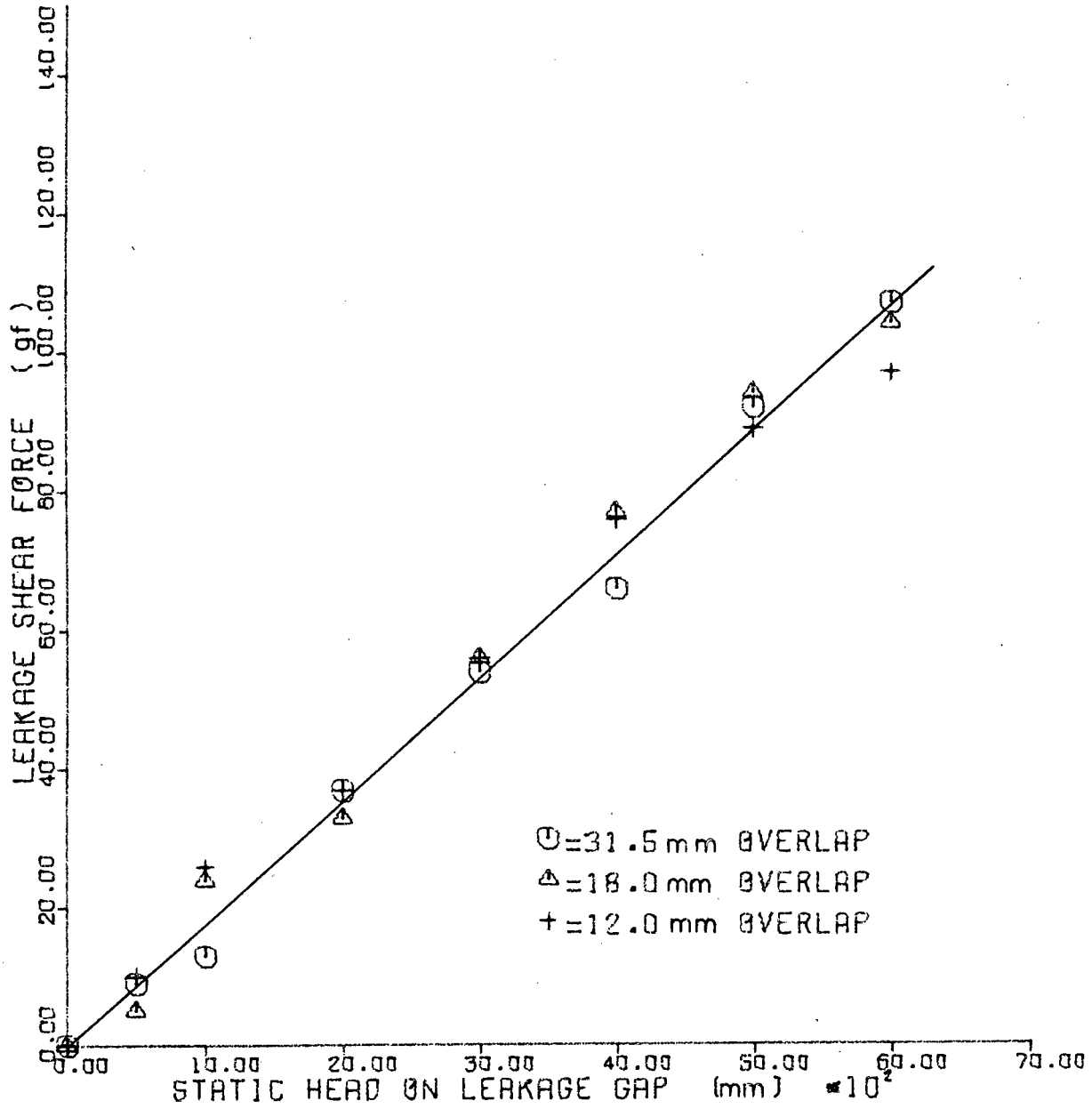

Fig. 30b Down drain method of determining leakage correction

independently by pressure readings and weight readings. This was very nearly the case; however it was found that a very slight modification to Eq. 63 resulted in an even better coincidence of the curves. Thus Eq. 63 was modified to

$$F_L = 17{,}80\ (z + h) \qquad \text{(Eq. 64)}$$

Using Eq. 64 it was found that the best fit curves for pressure and weight readings coincided almost exactly (for $\alpha = 0$). Equation 64 was used as the equation for the correction of the bottom leakage shear force.

7.2.2 Theoretical Method

A crude estimate of the downward shear force was made using the theoretical equation for laminar flow through the annular leakage gap.

Radius of sleeve = 70,0 mm

Clearance of gap = 0,15 mm in diameter

Flow through gap = 31,7 cm^3/s for a head of 6 m

Overlap distance = 31,5 mm

$$\tau_2 = 4\mu\, \hat{U}_x \frac{r_2^2 - r_0^2}{r_2(r_2^2 + r_1^2 - 2r_0^2)}$$

and $r_0 \doteq (r_1 + r_2)/2$ for the small clearance gap.

$\tau_2 = 199\ N/m^2$

$F_2 = 141 \times 10^{-3}$ Kgf

= 141 gf under a head of 6 m, compared with the value of 107 gf obtained from Eq. 64.

It must be emphasised that this last check is only a crude estimate of the order of magnitude of the correction. Probable errors such as eccentricity could markedly affect the result.

For a typical low flow through the sleeve (Re ≑ 35000) the downward leakage force would be about 110 gf whilst the upward shear force of the main flow would be about 120 gf. For a typical high flow (Re ≑ 200 000) the downward leakage force would be about 120gf whilst the upward shear force would be about 3400 gf. For low flows the leakage force correction was of the same order of magnitude as the upward shear force, for this reason it was very advantageous to have available a check on the accuracy of the correction, (viz coincidence of f vs Re curves for $\alpha = 0$ and established smooth pipe data).

7.3 Smooth Annular Tests

After the sensitivity tests and calibration of the floating sleeve were completed, tests were performed on smooth annuli of four radius ratios $\alpha = 0$; 0,091; 0,226 and 0,363. (The smooth pipe ($\alpha = 0$) was regarded as a special geometric case of annular flow). The equations used for calculating the friction factor - Reynolds number curves are presented below.

7.3.1 Equations for Evaluation of Data

f_2 vs Re:

The total upward force on the floating sleeve due to wall friction is

$$F_2 = (F_i - F_f) + F_L \qquad \text{(Eq. 65)}$$

where F_i = initial zero flow scale reading

F_f = final scale reading for steady flow

F_L = appropriate force correction due to leakage effects.

The shear force on the outer (sleeve) wall is given by

$$\tau_2 = F_2/A_2 \qquad \text{(Eq. 66)}$$

where $A_2 = 2\pi r_2$ (length of floating sleeve),

and the friction factor for the sleeve is given by

$$f_2 = \frac{2 F_2}{\ell \hat{U}_x^2 A_2} \qquad \text{(Eq. 67)}$$

The Reynolds number is based on the equivalent diameter $D_e = 2(r_2 - r_1)$ and is defined for all friction factors as $R_e = \frac{\hat{U}_x D_e}{\nu}$

f_T vs Re

Across any longitudinal annular section of length ℓ

$$\Delta P A_x = \tau_T A_T$$

Now $$\frac{\Delta P}{\ell} = \theta w$$

where $\theta = h_f/\ell$ = slope of the hydraulic grade line

In order to determine θ, the best fit straight line through the points (h_{f_i}, ℓ_i), where i is the position of the pressure tapping, was calculated each time θ was altered.

$$\therefore \quad \tau_T = \frac{w\theta\ell A_x}{A_T}$$

$$= \frac{w\theta D_e}{4} \qquad \text{(Eq. 68)}$$

and $$f_T = \frac{g\theta D_e}{2\hat{U}_x^2} \qquad \text{(Eq. 69)}$$

f_1 vs Re

We now have two curves f_2 vs Re and f_T vs Re. From these curves f_1 vs Re can be deduced (and hence if desired τ, and F_1)

$$F_1 = \tau_1 A_1$$

$$F_2 = \tau_2 A_2$$

$$F_T = \tau_T A_T$$

$$F_1 = F_T - F_2$$

and $$f_1 = \frac{2F_1}{\rho \hat{U}_x^2 A_1}$$

$$\therefore \quad f_1 = f_T(1 + 1/\alpha) - f_2(1/\alpha) \qquad \text{(Eq. 70)}$$

From Eq.67 and Eq. 69 it can be seen that the calculation of f_2 is less sensitive to changes in the value of r_2 than f_T is. The relevance of this will become apparent when dealing with roughened annuli.

From the above equations, all the information about forces, shears and friction factors on the annular walls may be deduced. Furthermore a force balance enables the radius of zero shear as well as the shear stress profile to be calculated.

Thus

$$r_0 = \sqrt{r_2 r_2 \; \frac{\tau_1 r_2 + \tau_2 r_1}{\tau_2 r_2 + \tau_1 r}} \qquad \text{(Eq. 71)}$$

and the shear stress at any radius is given by

$$\tau_r = \frac{\partial P}{\partial x} \left| \frac{r^2 - r_0^2}{2r} \right|$$

$$= \frac{r_2\tau_2 + r_1\tau_1}{r_2^2 - r_1^2} \left| \frac{r^2 - r_0^2}{r} \right| \qquad \text{(Eq. 72)}$$

Removing the modulus sign in Eq. 72 satisfies the sign convention for τ_r.

7.3.2 Discussion

Figs 32 to 40 show the various friction factor-Reynolds number results. For $\alpha = 0$, the coincidence of the friction factor-Reynolds number diagrams, obtained from weight measurements and pressure measurements, is clearly established. From the best fit curve it can be seen that the f_2 vs Re curve is parallel to and only slightly above the Nikuradse smooth pipe plot. Fig. 31 shows a trace of the actual sleeve and core roughnesses. The confidence limit for these and all other f vs Re curves appears to be ± 2 per cent.

From dimensional analysis

$$\frac{\partial P}{\partial x} = \frac{\rho \hat{U}_x^2}{D_e} \text{fn}(\text{Re}, \alpha, k/D_e)$$

and as might be expected (from dimensional analysis) a radius ratio effect is noticeably present in all f vs Re curves. This effect is most marked for f_1 vs Re, less significant for f_T vs Re and f_2 vs Re, appearing in the last case to alter slightly the slope of the curves. It appears that the overall friction factor for $\alpha > 0$ is 4 per cent to 9 per cent greater than that for a smooth pipe, at least for the range of α investigated here. There is evidence, from the friction factor and other graphs, to show that the floating sleeve and pressure manometers become too insensitive at Re < 40 000. Little confidence can be placed in results for a Re less than this figure.

Fig. 41 shows the relationship used to determine the kinematic viscosity ν from temperature measurements.

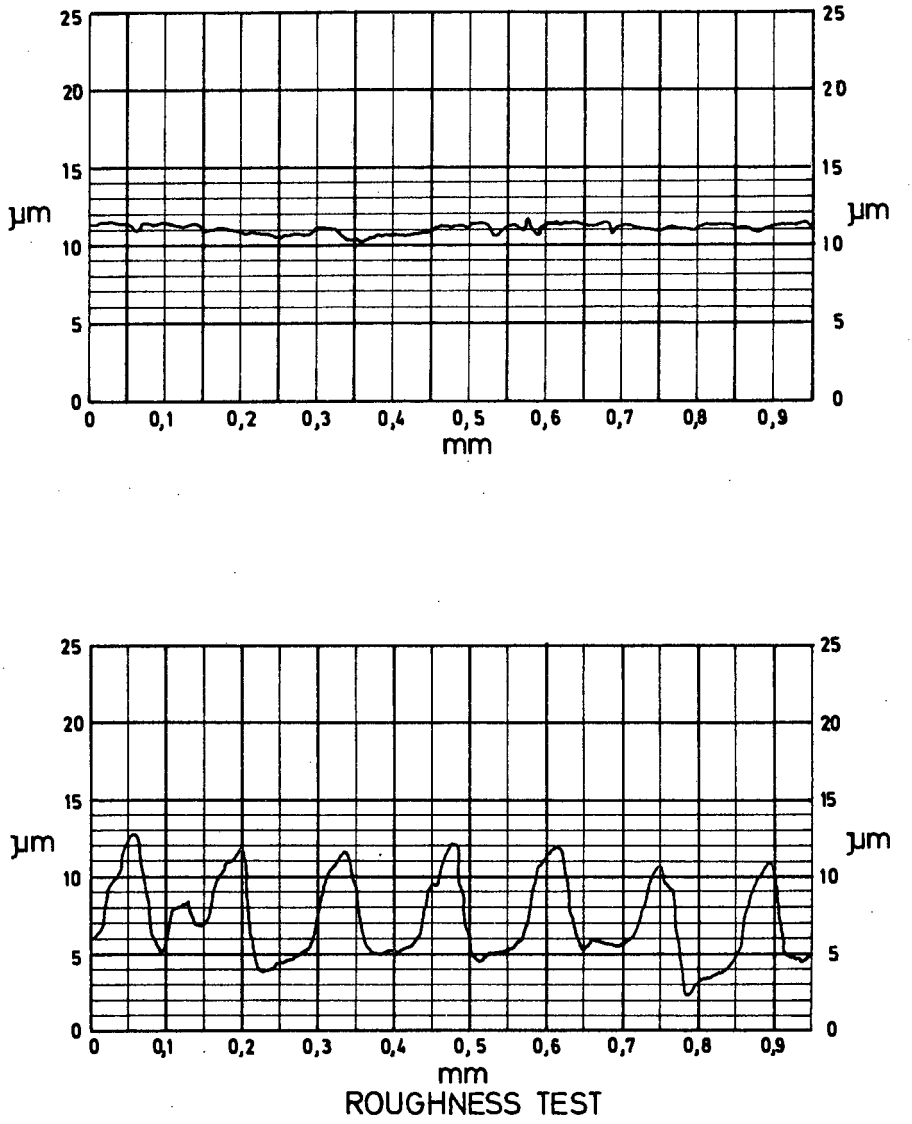

Fig. 31 Typical roughness traces for the 'smooth' drawn cores (above) and the 'smooth' machined sleeve (below). The uniform machine cuts on the sleeve can clearly be seen. The relative roughness for the sleeve (= $k/2r_2$) obtained from the above trace is 0,00011 which is slightly above the smooth pipe curve obtained by Nikuradse. This compares favourably with the result obtained in Fig. 32.

Fig. 42 shows the variation of the inner to outer wall shear stresses for the three radius ratios for varying Reynolds number. As can be seen the ratio τ_1/τ_2 depends upon Re and α. As α approaches zero, τ_1/τ_2 approaches infinity for laminar flow. This can be seen in Fig. 43 where a plot of τ_2/τ_1 vs α, for laminar flow, is given. This graph was obtained from the theoretical equations governing laminar flow in annuli viz:

$$\beta = \sqrt{\frac{\alpha^2 - 1}{2 \ln \alpha}} \qquad \text{(Eq. 73)}$$

and

$$\tau_1/\tau_2 = \frac{\beta^2 - \alpha^2}{\alpha(1 - \beta^2)} \qquad \text{(Eq. 74)}$$

Thus it can be seen that the ratio τ_1/τ_2 is entirely dependent upon the radius ratio α, for laminar flow. The dependence of τ_1/τ_2 upon Re as found in Fig. 42 (i.e. turbulent flow) deviates from the laminar flow situation where there is no Re dependence. Fig. 42 is also in disagreement with Lawn and Elliot [13], who found that τ_1/τ_2 was independent of Re for turbulent flow in the range $3 \times 10^4 < Re < 2{,}4 \times 10^5$. The fact that as α tends to zero, the flow situation does <u>not</u> tend to that of a circular pipe, is well illustrated by the above graphs.* (Figs 42 and 43) It appears that the ratio τ_1/τ_2 increases with decreasing Re (for a particular α) for turbulent flow and then becomes constant for laminar flow. If Lawn and Elliot's results are correct, it would be interesting to know where their value of the ratio τ_1/τ_2 in turbulent flow changed to that obtained for laminar flow. The ratio τ_1/τ_2 appears to be larger at all times for laminar flow than for turbulent flow.

A force balance enabled the shear stress distribution for a particular Reynolds number and radius ratio to be calculated if the wall shear stresses and the position of zero shear are known. Such

* It is a popular misconception that as $\alpha \to 0$, the annulus yields a circular pipe. However it is true that as $\alpha \to 1$, the annulus approaches a parallel plate.

distributions are shown in Figs 44 and 45 for a Reynolds number of 50 000 and 100 000 respectively. It is interesting to note how the outer shear stress profile becomes more linear as α decreases and approaches the plain pipe. The rapid curvature of the inner profile for low α, decreases as α increases, and for α very large one would expect a linear profile.

The graph showing the position of zero shear stress as a function of Reynolds number and radius ratio (Fig. 46), indicates that this position exhibits a slight Reynolds number dependency varying approximately 7 per cent for a Reynolds number range of 40 000 to 220 000 (i.e. an increase in Re of 450 per cent). Also r_0 appears to remain at almost a constant distance expressed by the ratio $(r_0 - r_1)/r_2$ for varying radius ratios. This ratio varies linearly with Reynolds number. This is in agreement with the results of Rehme [35]. Lawn and Elliot's results however, do not show this trend and their conclusion was that r_0/r_2 is independent of Reynolds number. The floating sleeve results disagree with this conclusion. Fig. 47 shows results for the position of zero shear stress obtained by previous investigators (for Re $\doteqdot$ 100 000). The Kays and Leung method of plotting the results has been used. Thus the ordinate chosen is

$$s^* = \frac{r_0 - r_1}{r_2 - r_0}$$

Also shown in Fig. 47 is the relationship for laminar flow which is independent of Re. This is a straight line relationship (on a double logarithmic plot) expressed by

$$s^* = \alpha^{0,16}$$

This equation describes a far easier method of obtaining the position of zero shear stress in laminar flow than the usual exact method given by Eq. 73, and is very nearly as accurate. The floating sleeve results shown in Fig. 47 are fairly centrally placed between previous investigations. The value of s^* generally agrees well with that obtained by hot wire anemometry and Preston tubes. There is a definite difference in trend between the results of Rehme [35] and

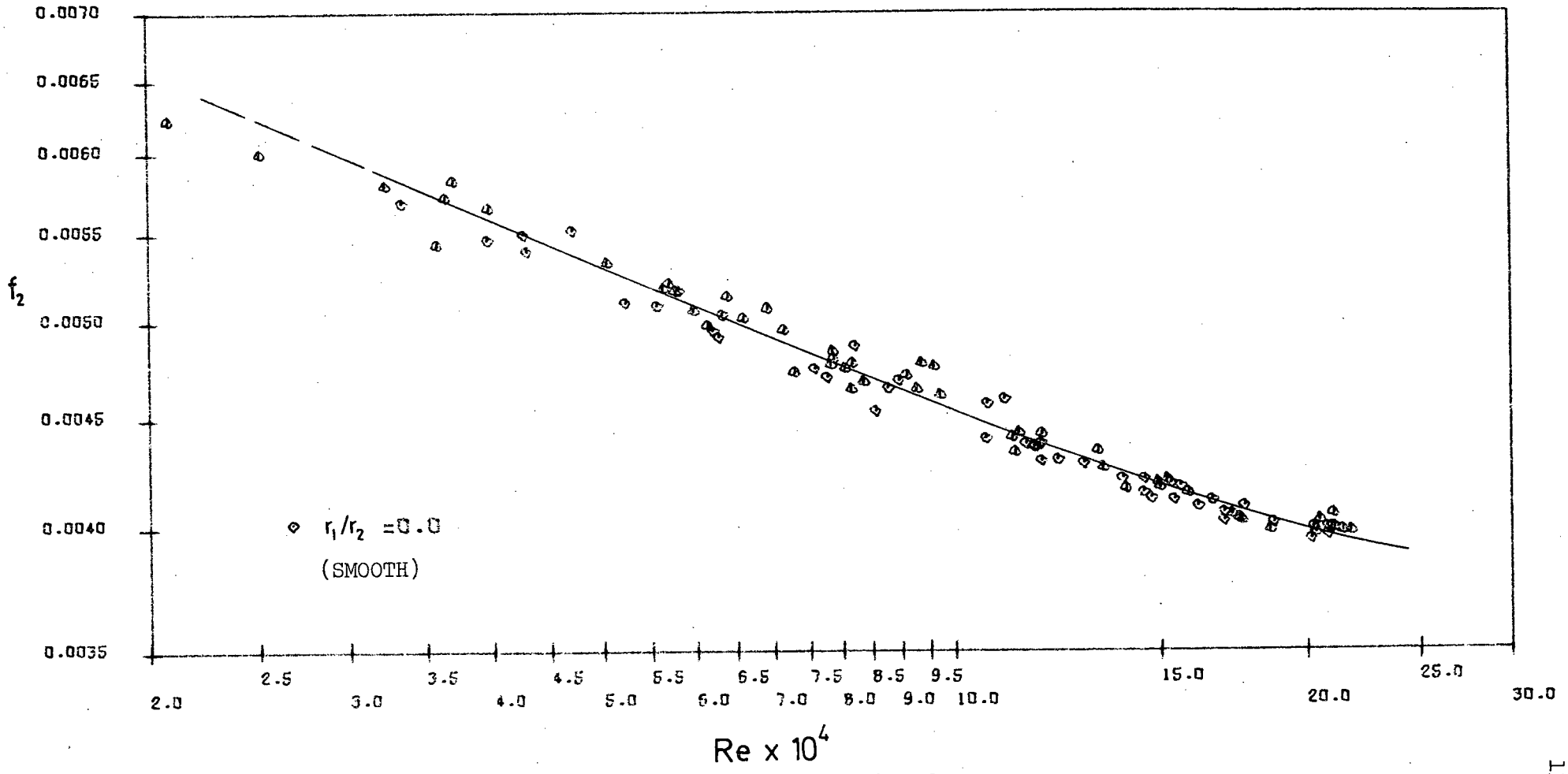

Fig. 32 Outer wall friction factor

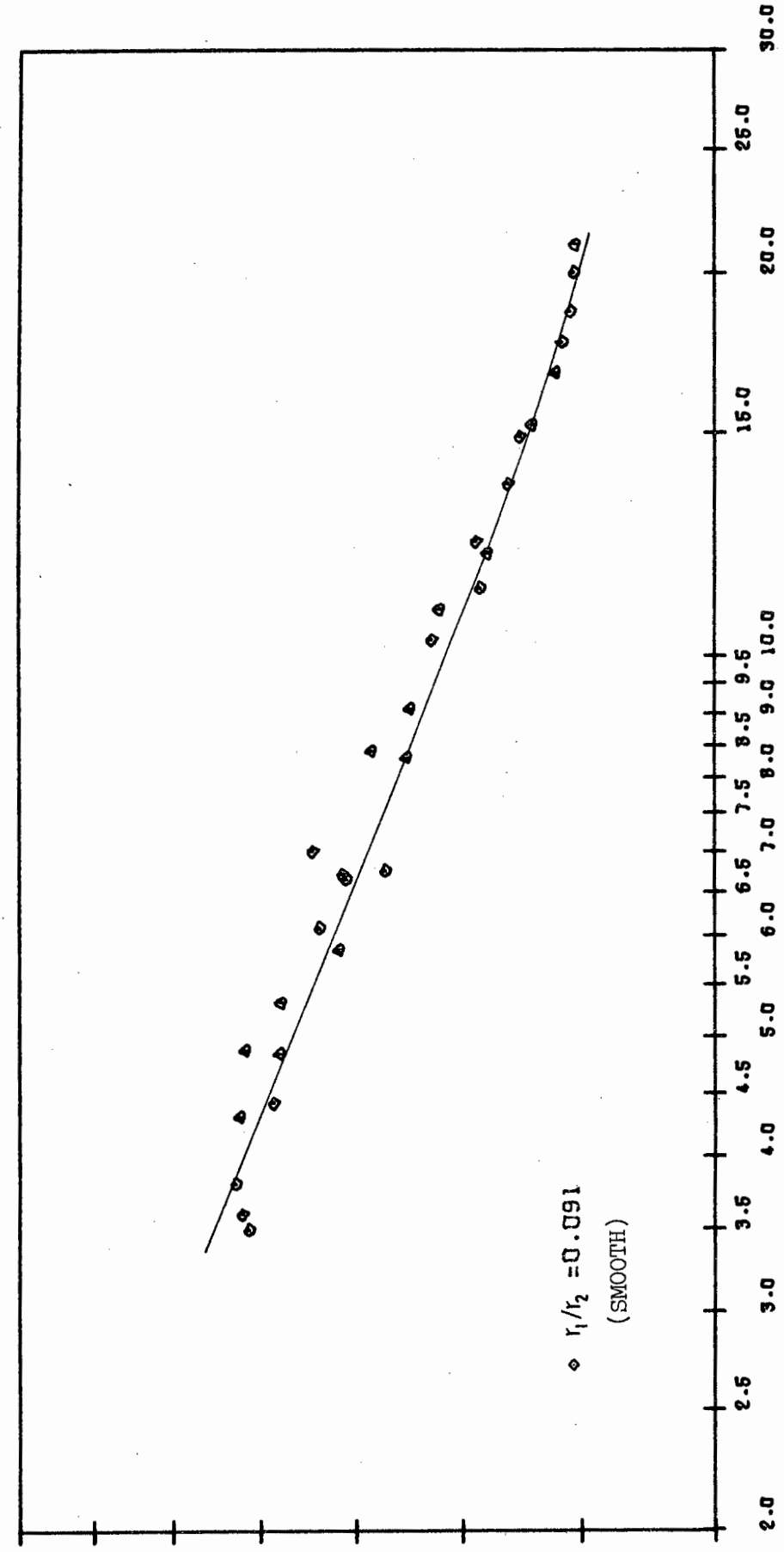

Fig. 33 Outer wall friction factor

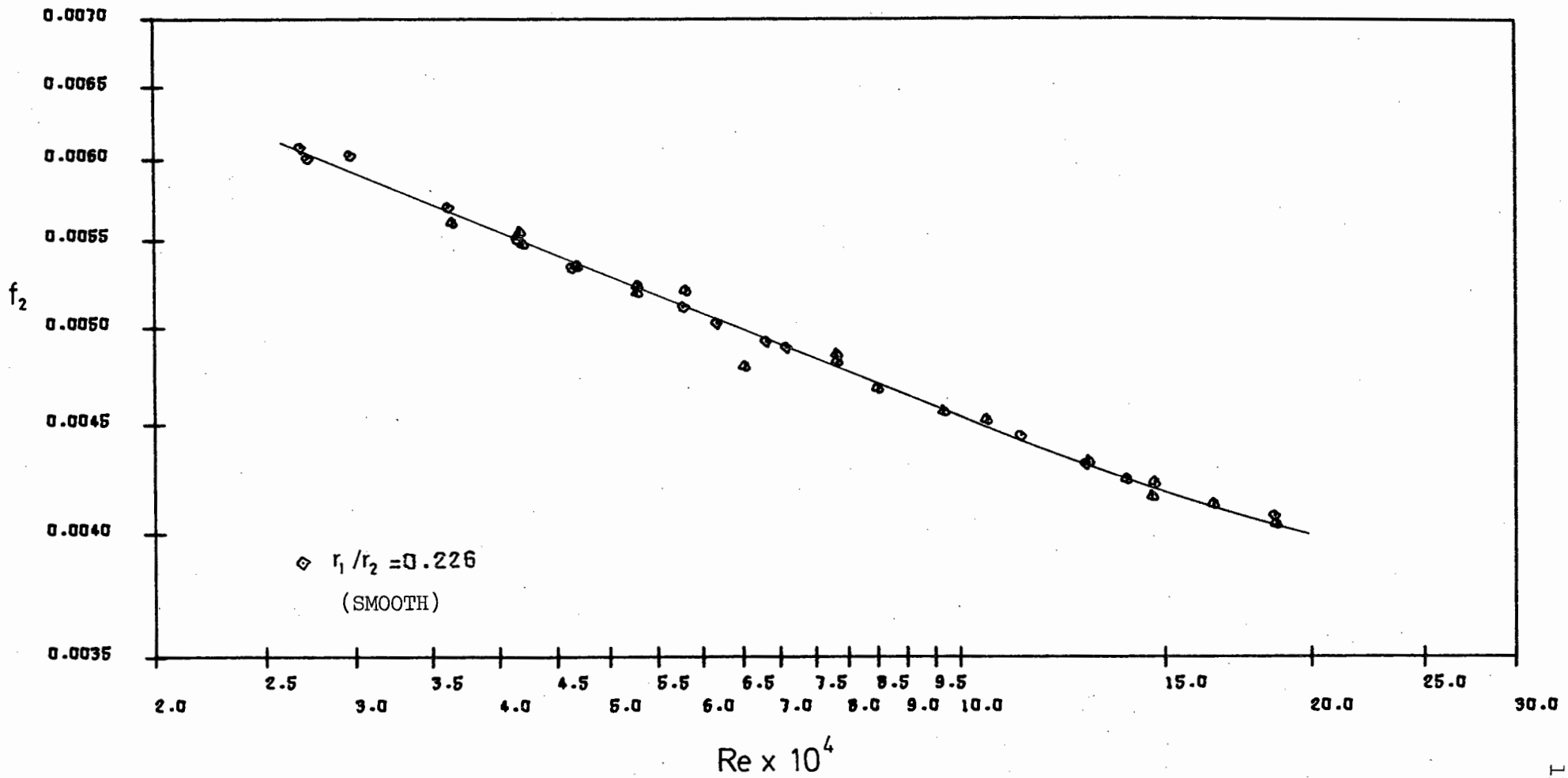

Fig. 34 Outer wall friction factor

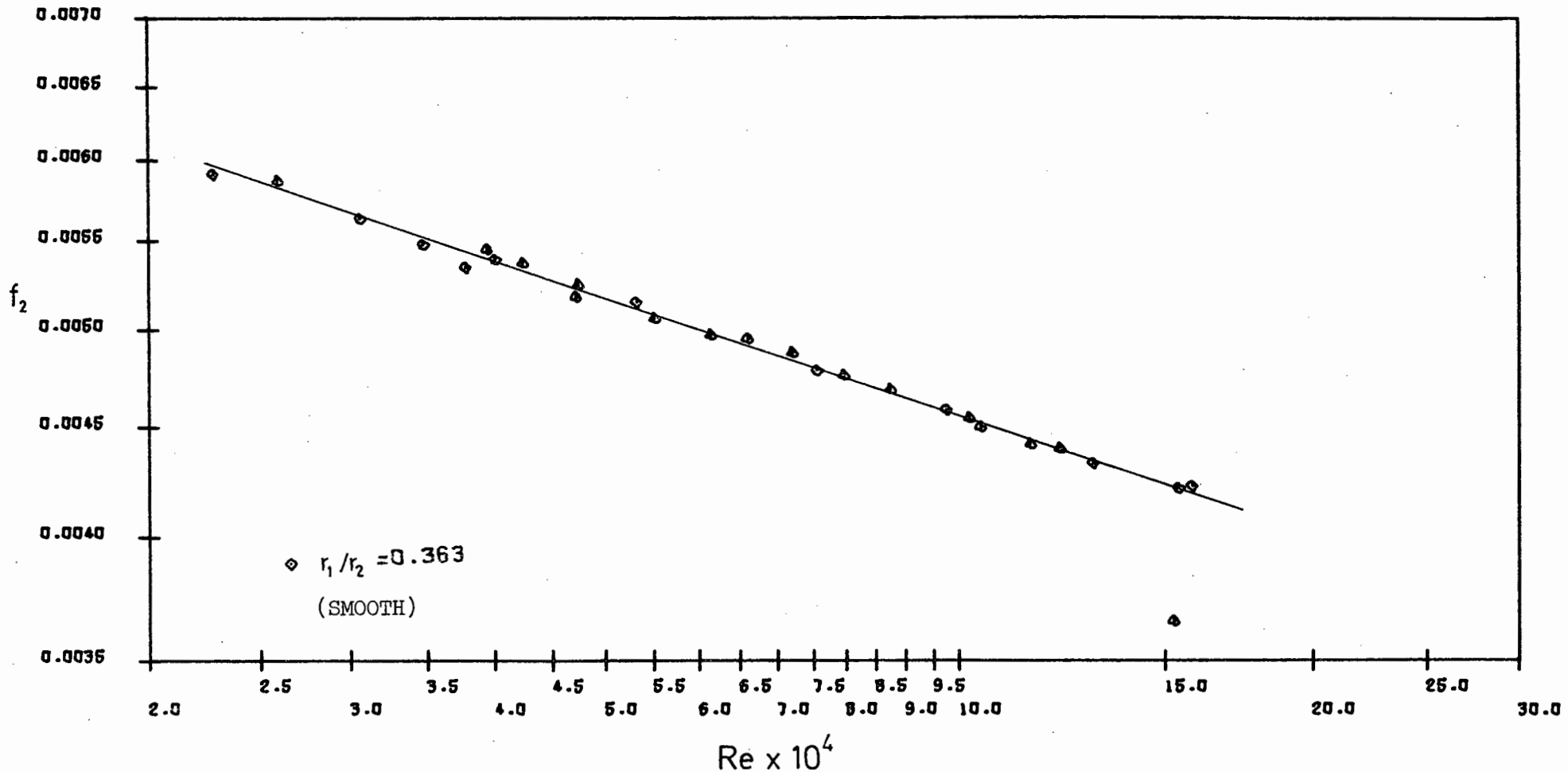

Fig. 35 Outer wall friction factor

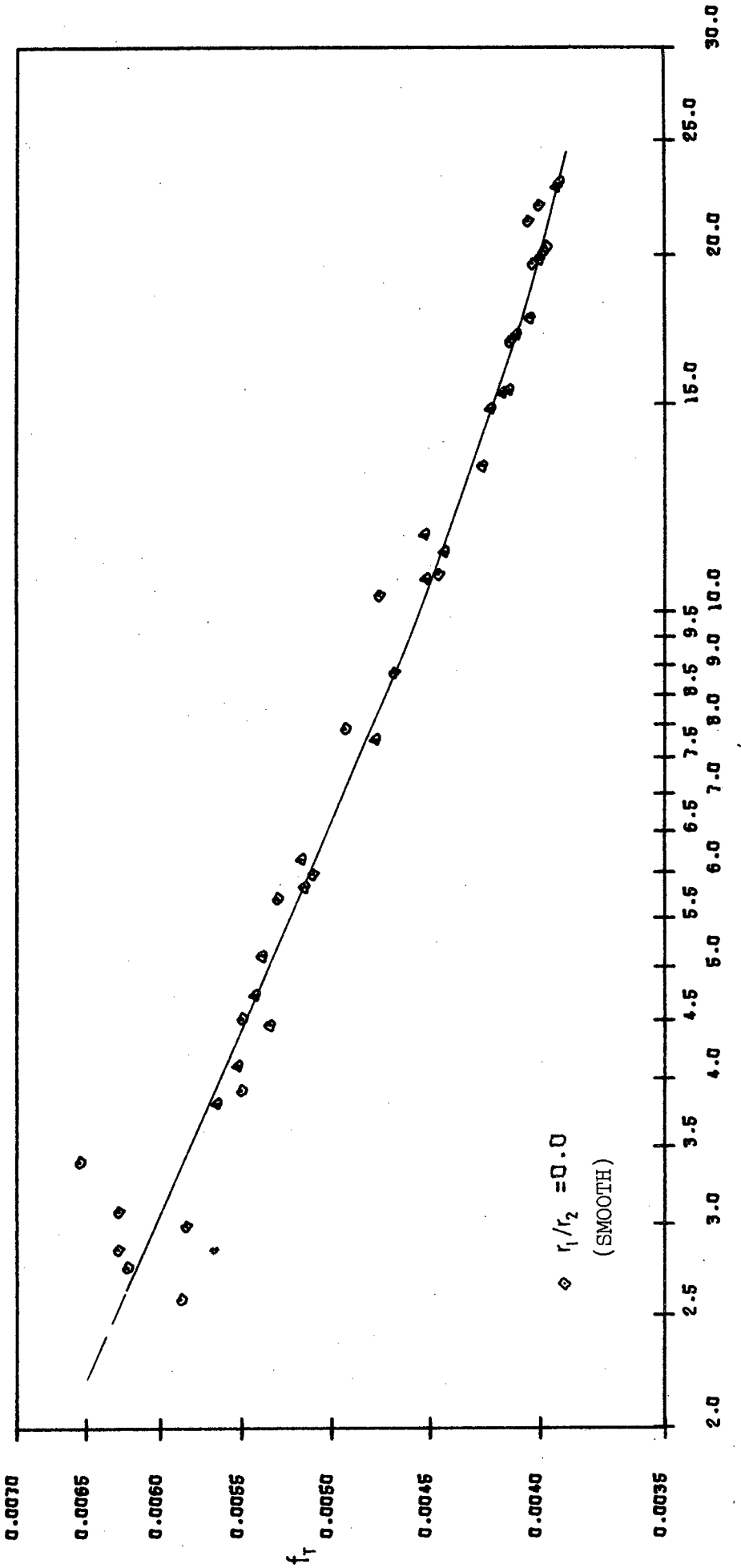

Fig. 36 Total friction factor

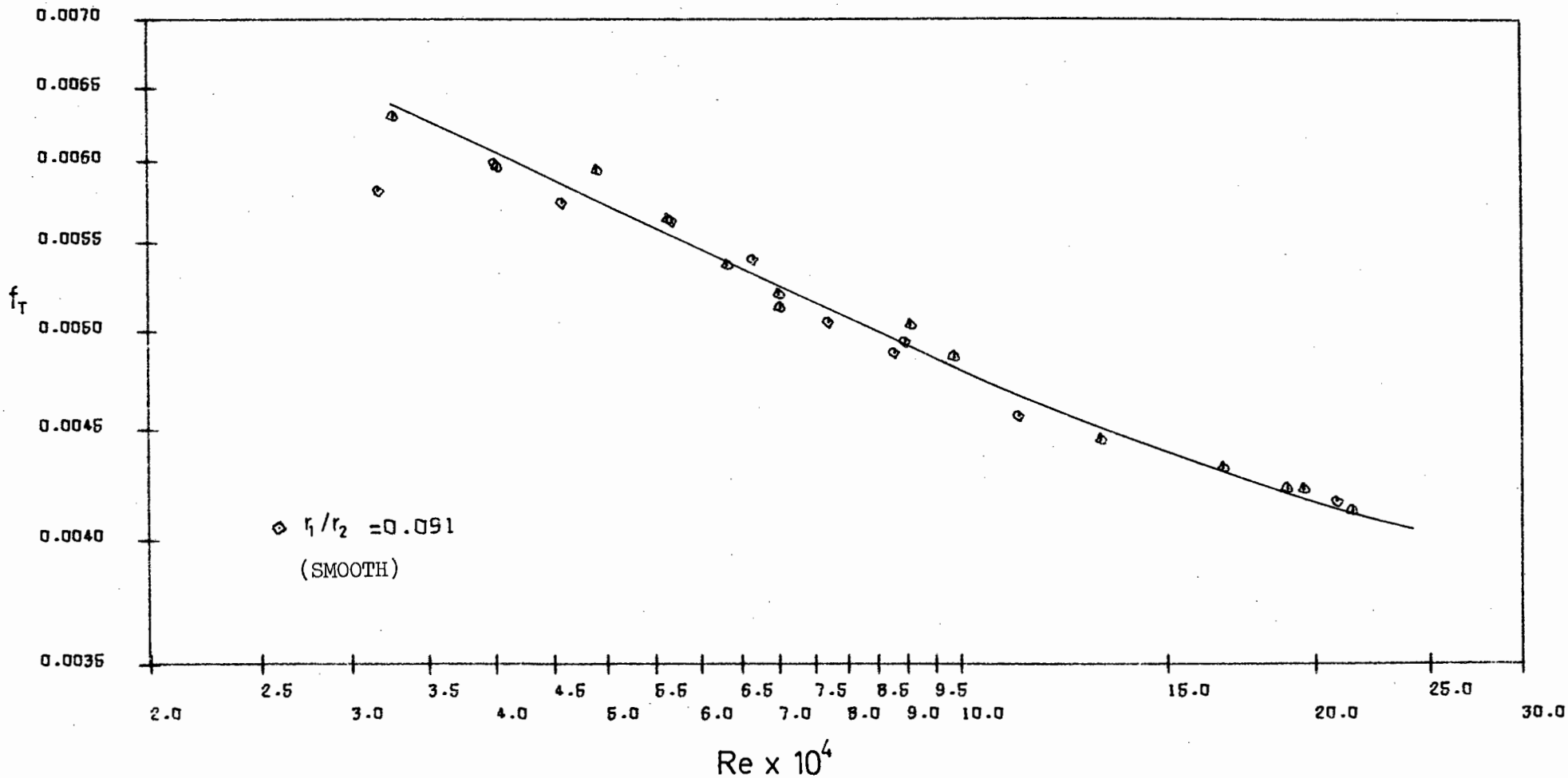

Fig. 37 Total friction factor

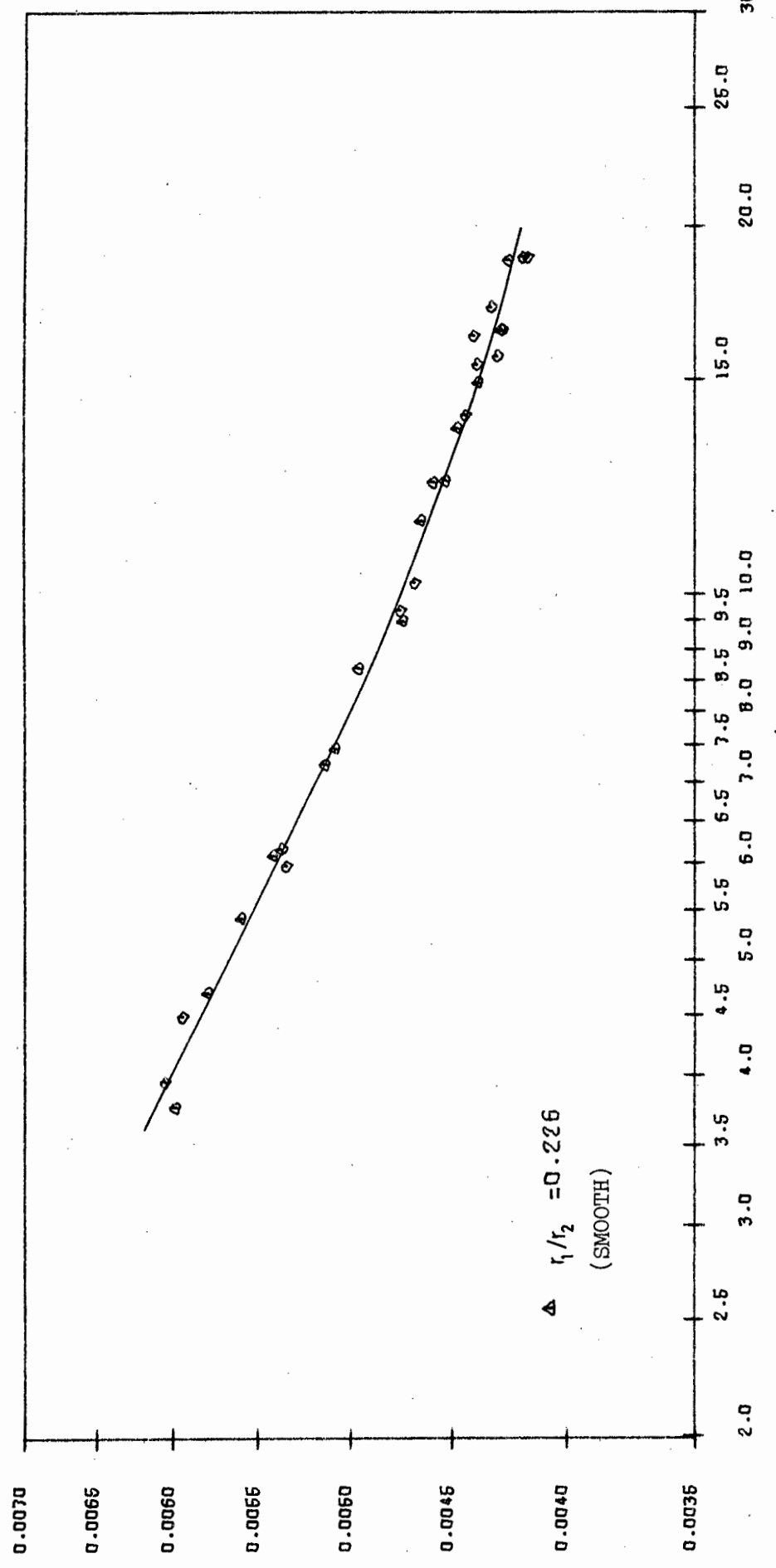

Fig. 38 Total friction factor

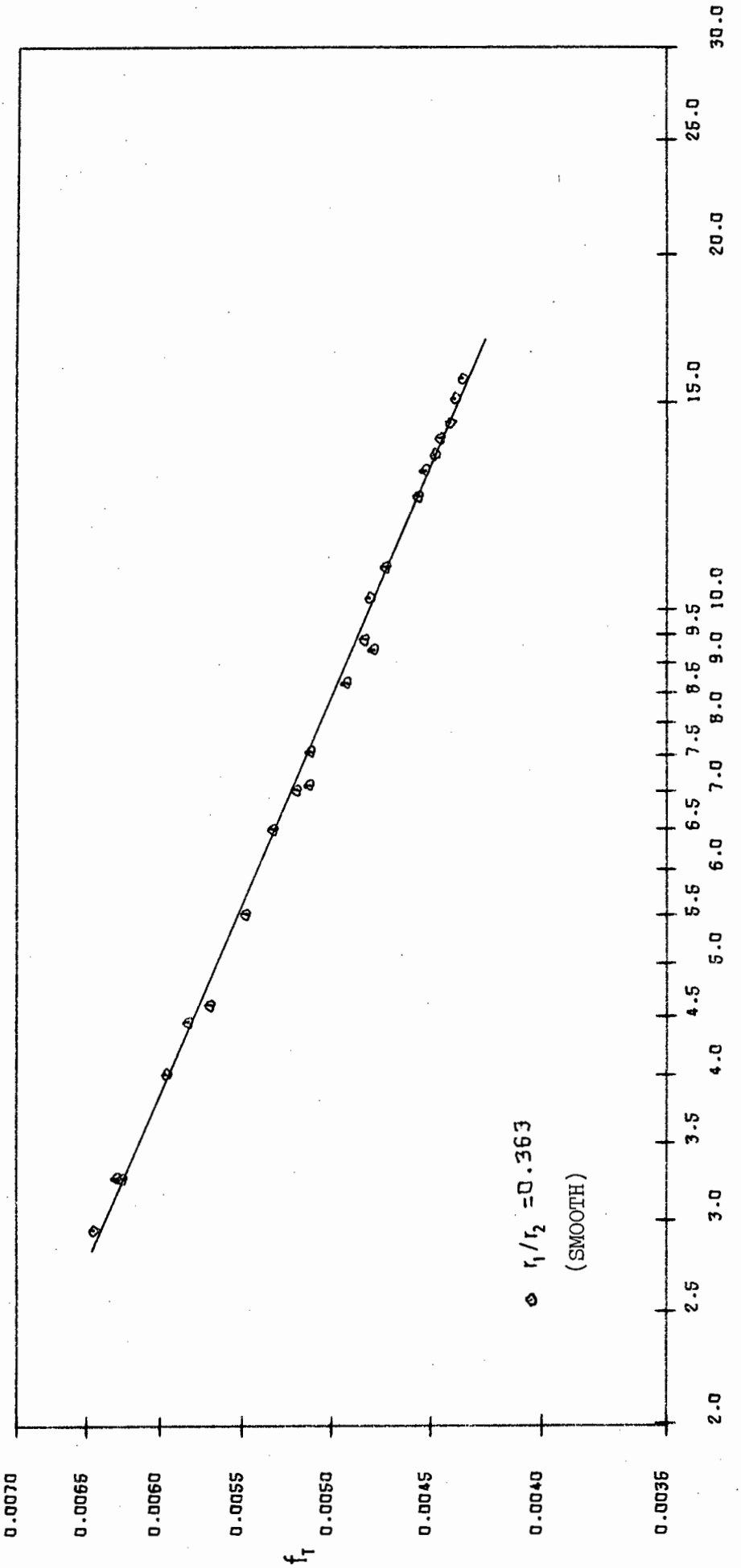

Fig. 39 Total friction factor

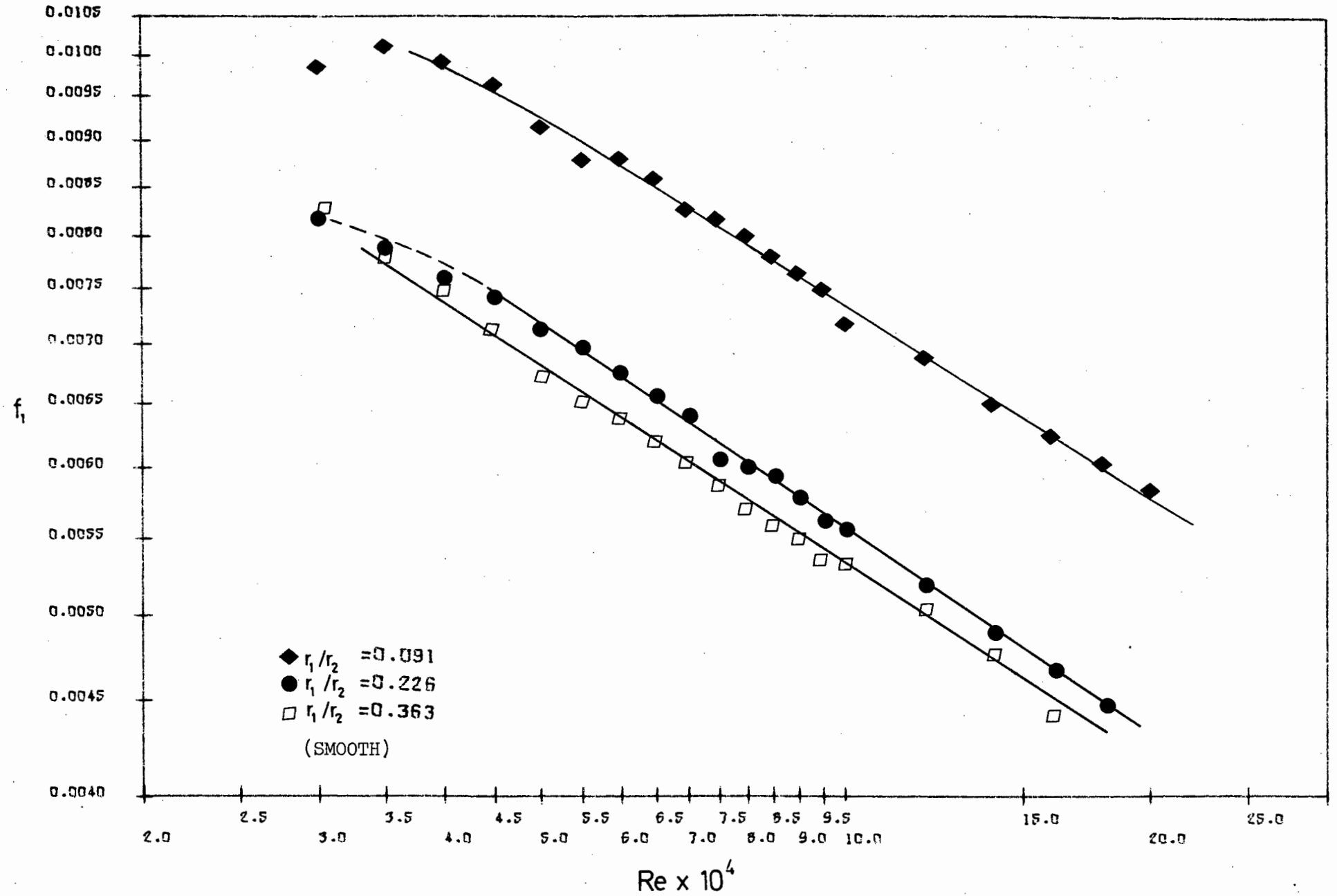

Fig. 40 Inner wall friction factors

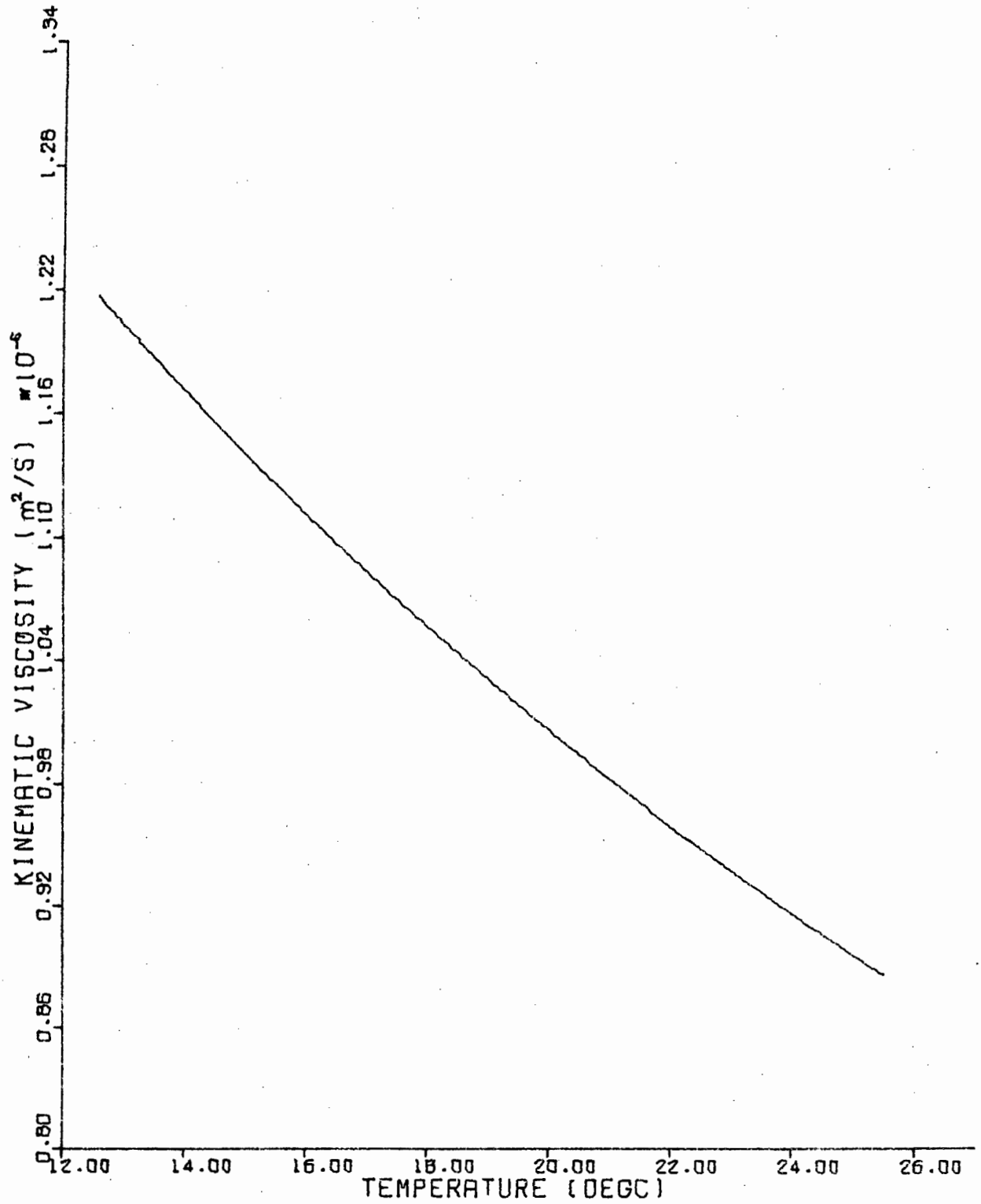

Fig. 41 Dependence of viscosity of water upon temperature

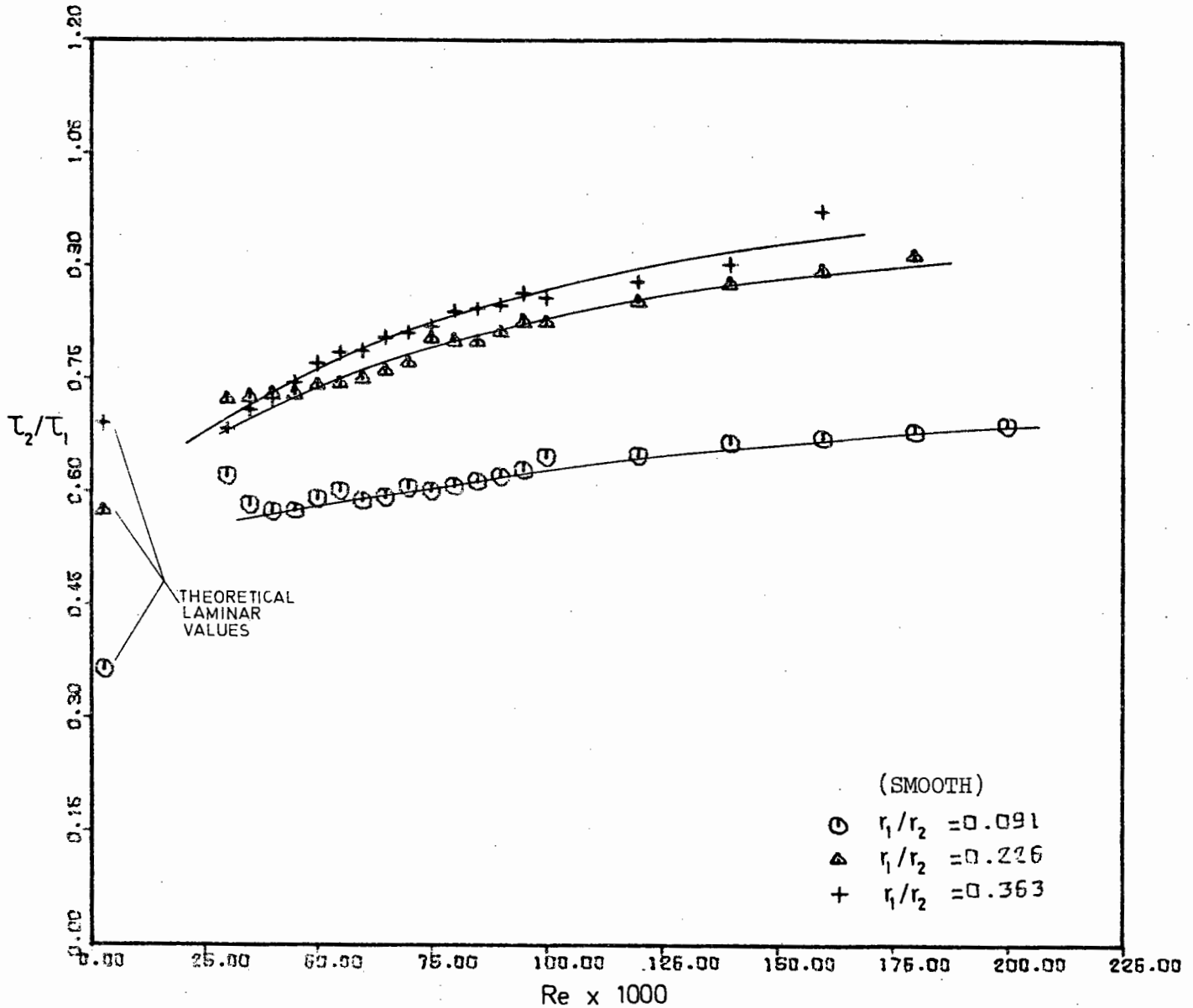

Fig. 42 The ratio of the wall shear stresses

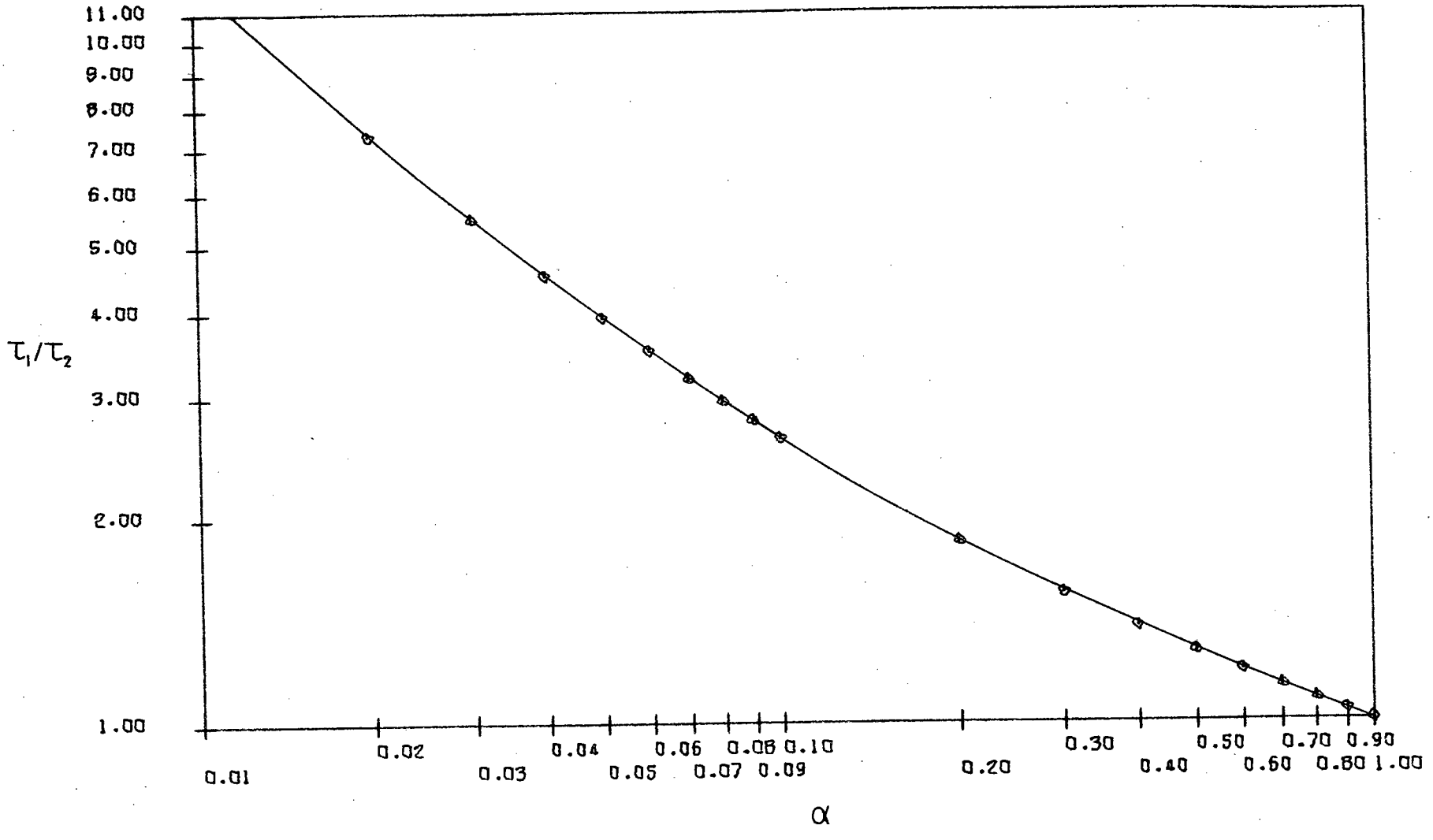

Fig. 43 The ratio of the wall shear stresses in laminar flow

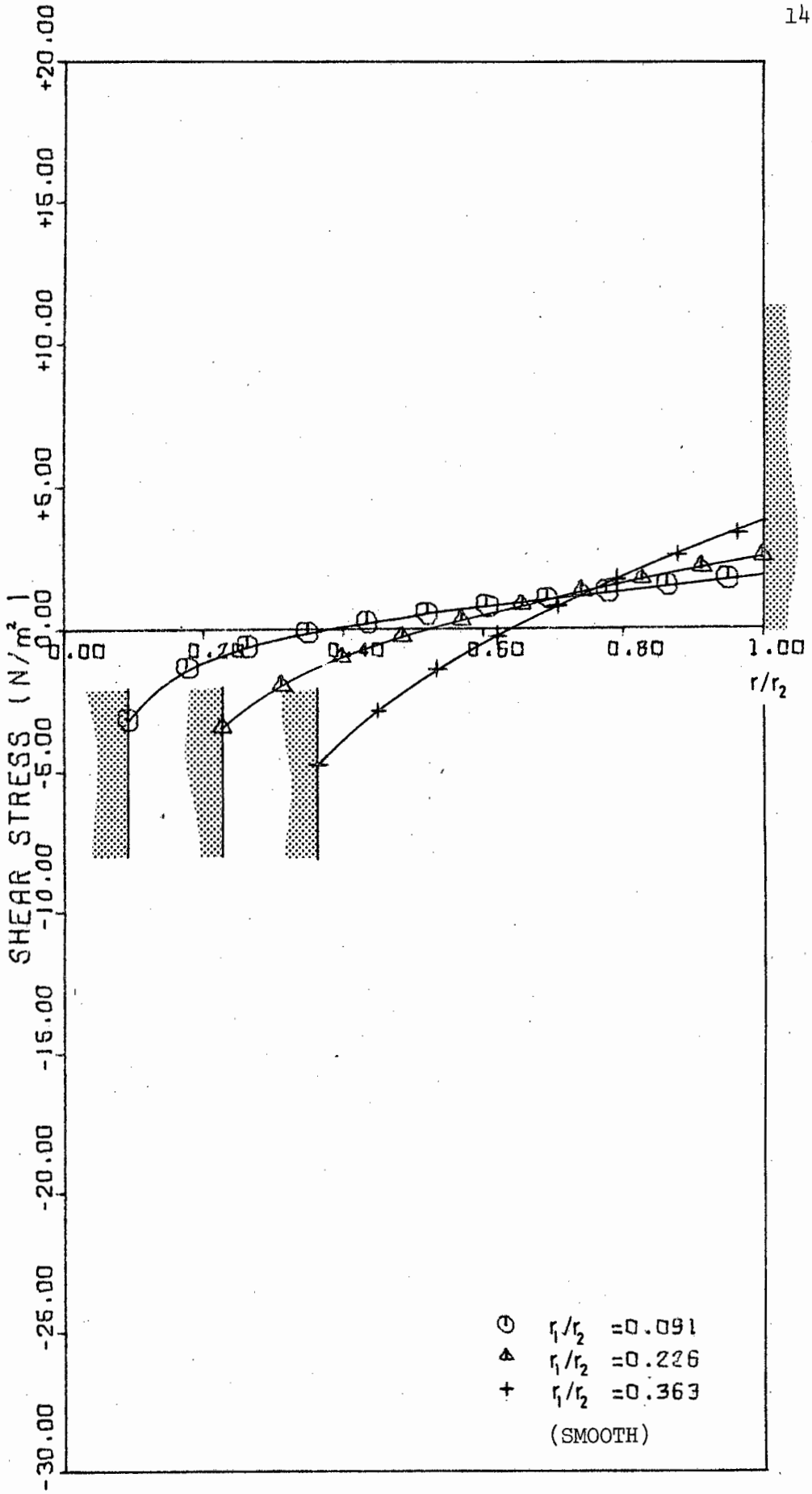

Fig. 44 Shear stress distributions in smooth annuli for Re = 50 000

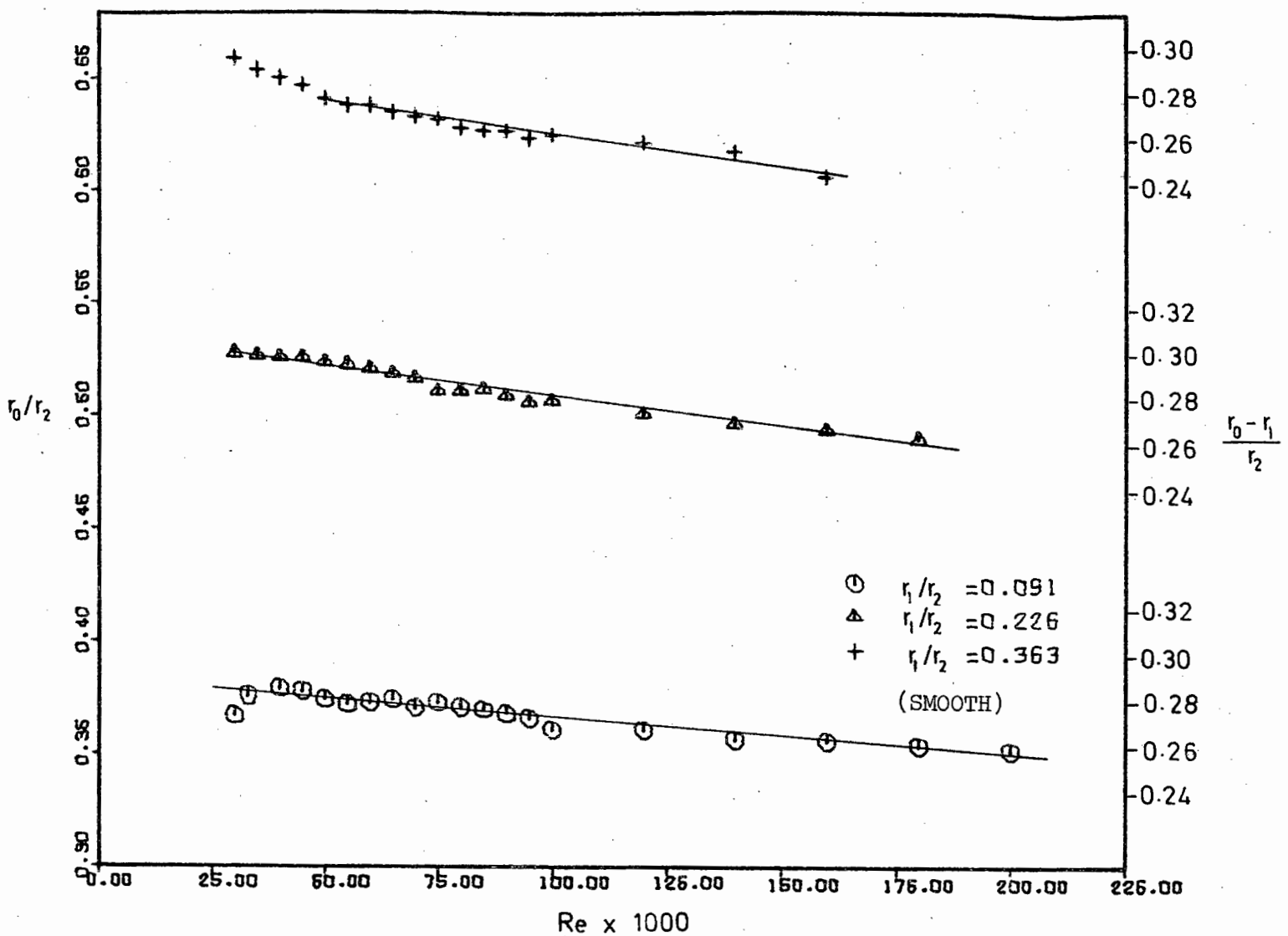

Fig. 46 The position of zero shear stress in smooth annuli

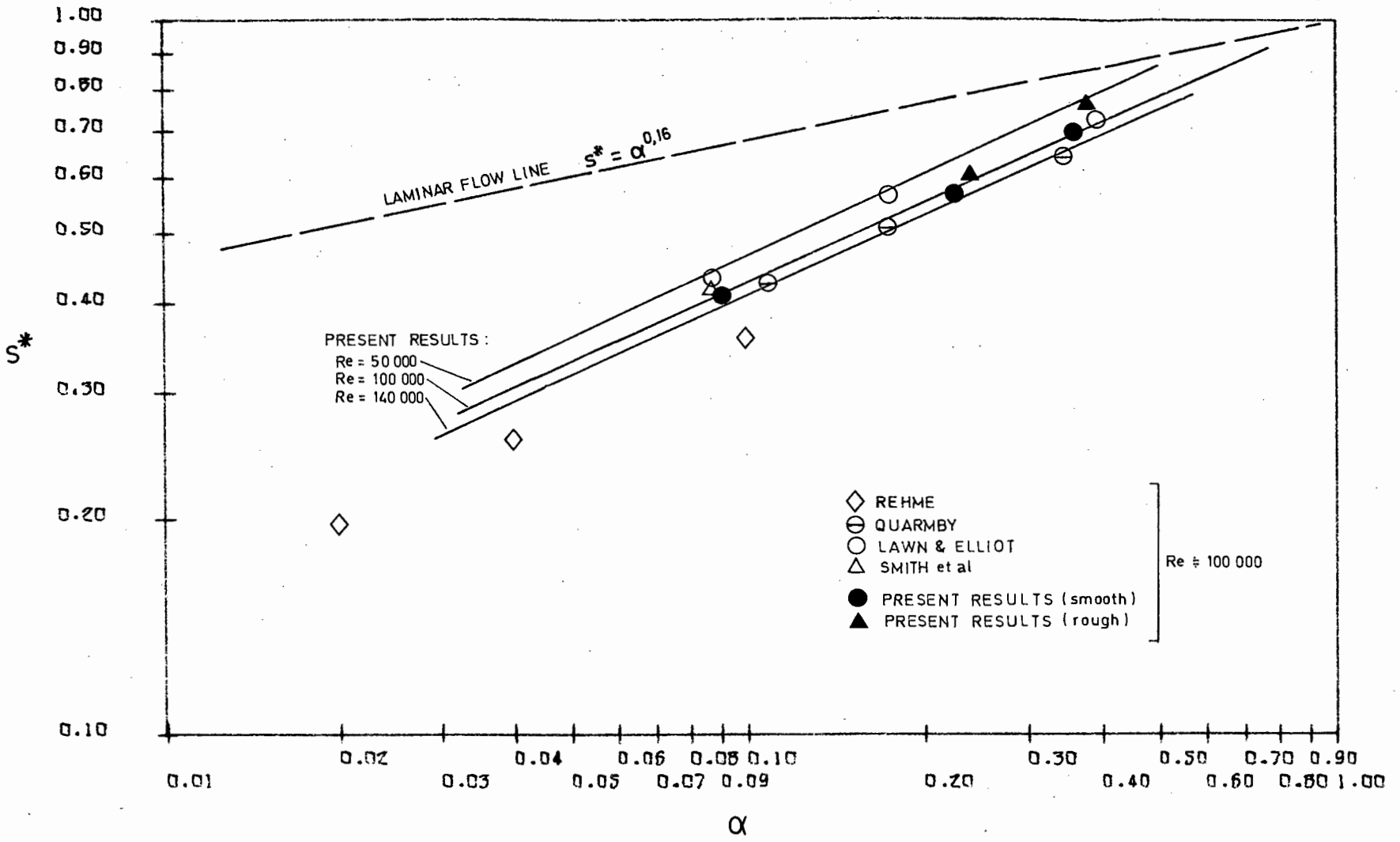

Fig. 47 The Kays and Leung plot of the position of zero shear stress for Re ≒ 100 000

those obtained by the floating sleeve, exemplified by the difference in s^* at $\alpha \doteqdot 0,1$. It might be said that the central position of the present results amongst previous results, inspires confidence in the floating sleeve method. For a particular radius ratio, the position of zero shear stress lies further from the inner wall for laminar flow than for turbulent flow, the difference between $r_{m\ell}$ and r_{mt} increasing with decreasing radius ratio.

7.4 Rough Annular Tests

Once the smooth annular tests had been completed, the rough annular tests were begun. These tests were performed on a sand roughened annulus of radius ratio $\alpha = 0$ and on mesh roughened annuli of radius ratio $\alpha = 0$; 0,238 and 0,376. In computing the radius ratio and all other relevant results the diameter of cores and sleeve need to be accurately known.

7.4.1 Determination of Rough Sleeve Diameters

Before a suitable method of measuring the diameter of the sleeve can be found the required diameter must be defined. In this respect most tests are unclear as to this definition. Yet the definition and determination of rough pipe diameters are necessary for research purposes, if units involving wall shear force are to be determined from static tap results. This is due to the fact that shear force results obtained in this way are dependent on the square of the diameter of the rough sleeve. In his paper, Nikuradse [26] defined the diameter found from the equivalent water volume of the rough pipe. This measurement obviously cannot be represented clearly on sketches and has led to some confusion in the past.

For the floating sleeve system, three ways of determining the equivalent diameter can be used:

(i) For a radius ratio of $\alpha = 0$ the f vs Re results for pressure tappings and corrected weight readings should coincide for equal roughness. Since a change in diameter will effect a

greater change in the f_T results than the f_2 result, a diameter could be selected such that the results of the two methods coincide. A 1 per cent change in diameter will cause a 5 per cent change in f_T and a 3 per cent change in f_2. (This is analogous to the argument used for checking the leakage gap correction.)

(ii) Obtain the equivalent water volume diameter (D_w) as defined by Nikuradse.

(iii) Select some equivalent diameter between the limits imposed by the thickness of the wire mesh. That is, a diameter based on the direct physical measurement of the smooth pipe diameter and the roughness thickness.

Of these methods, the last is by far the easiest. In order to carry out the second method some means of blocking the leakage gap must be found. In order to compare the results of the three methods, this was in fact done. A piece of strong vellum was inserted in the joint between the lowest two sleeve sections.

The results for D_w obtained by the three different methods indicated that for

Method (i) $D_w = 69{,}0 \pm 0{,}3$ mm

Method (ii) $D_w = 69{,}4 \pm 0{,}2$ mm

Method (iii) D_w must lie somewhere between the limits of $2r_2$ and $2r_2 - 2 \times$ (max. roughness projection = k)

i.e. $68{,}3 < D_w < 70{,}0$ mm

An arbitrary choice might be the average between these two limits which would give $D_w = 69{,}15$. Nikuradse's definition suggests that the value of D_w should depend to some extent on the ratio

$$K_m = \frac{\text{density of wire in mesh}}{\text{density of mesh (wire and holes)}}$$

Since for the mesh used, this ratio was less than 1,0; D_w would be larger than that obtained by our arbitrary choice and would be more in line with that obtained in methods (i) and (ii).
For the mesh used $K_m \doteqdot \frac{1}{3}$.

$$\therefore \quad D_w = 2(r_2 - K_m k) \qquad \text{(Eq. 75)}$$

Eq. 75 yielded a D_w = 69,4 mm. Since all three methods yielded similar results, and owing to the fact that method (i) cannot be used to determine D_w for $\alpha > 0$, and that method (ii) is laborious and time consuming, method (iii) was used for all future radius ratios to calculate D_w.

7.4.2 Equations for the Evaluation of Data

The equations developed in 7.3.1 are again used for the evaluation of the rough annuli data, D_e now being equal to $(D_w - 2r_1)$.

7.4.3 Discussion

Fig. 48 shows the one f vs Re curve obtained for the sand roughened sleeve. As can be seen the curves obtained from weight measurements and pressure measurements again coincide. This is also the case for the mesh roughened sleeve ($\alpha = 0$) as shown in Fig. 49 and 50. Figs 49 to 51 show the various f vs Re curves for the mesh roughened annuli. (For $\alpha > 0$ only mesh roughness was used). Here a very distinct radius ratio effect can be observed for f_T and f_2. For these cases it also appears as though the friction factor becomes constant for Re > 90 000. Comparing the results for $\alpha = 0$ with those of Nikuradse for rough pipes, it can be seen that the mesh roughness has a $k/D_w \doteqdot 0{,}028$ and thus that the equivalent k for the mesh $\doteqdot$ 1,9 mm which is similar for example to that obtained in concrete conduits. (The actual value of k for the mesh was 0,85 mm). The beginning of the dependency of the friction factor on Reynolds number also occurs at about the same point (namely Re = 90 000), as that obtained by Nikuradse for a similar k/d for artificially sand roughened pipes. However, this dependency increases more rapidly for the mesh roughness with decreasing Re.

As expected the wall shear stresses are greatly increased by the addition of roughness. For example for an Re = 100 000 the wall shear stresses were increased by about 350 per cent over the smooth annuli, by the addition of the mesh. Examples of the shear stress distribution for Re = 50 000 and Re = 100 000 are given in Figs 53 and 54 respectively. Fig. 52 shows the ratio τ_1/τ_2 as a function of α and Re. It appears that the ratio of the wall stresses is altered by the addition of identical roughess to each wall. The downward trend of τ_1/τ_2 with increasing Re as exhibited in smooth annuli is not present in the rough annuli. For α = 0,238 the ratio τ_1/τ_2 is fairly constant, whilst for α = 0,376 the previous downward trend is reversed.

The position of zero shear stress (as shown in Fig. 55) exhibits little Reynolds number dependency although there is a curious upward trend for α = 0,376 which is probably related to the upward trend in τ_1/τ_2 in Fig. 52. For α = 0,238 the position of zero shear stress remains essentially unchanged with varying Reynolds number.

A comparison of the position of zero shear stress for rough annuli with that in smooth annuli at a Re = 100 000 is made in Fig. 47. This position seems to be slightly further from the inner wall for rough annuli than is the case for smooth annuli.

Owing to the scarcity of previous investigations into rough annuli there is unfortunately no data available for direct comparison with the floating sleeve results. A graph (Fig. 56) shows all the friction factor-Reynolds number curves obtained in the present investigation for both rough and smooth annuli.

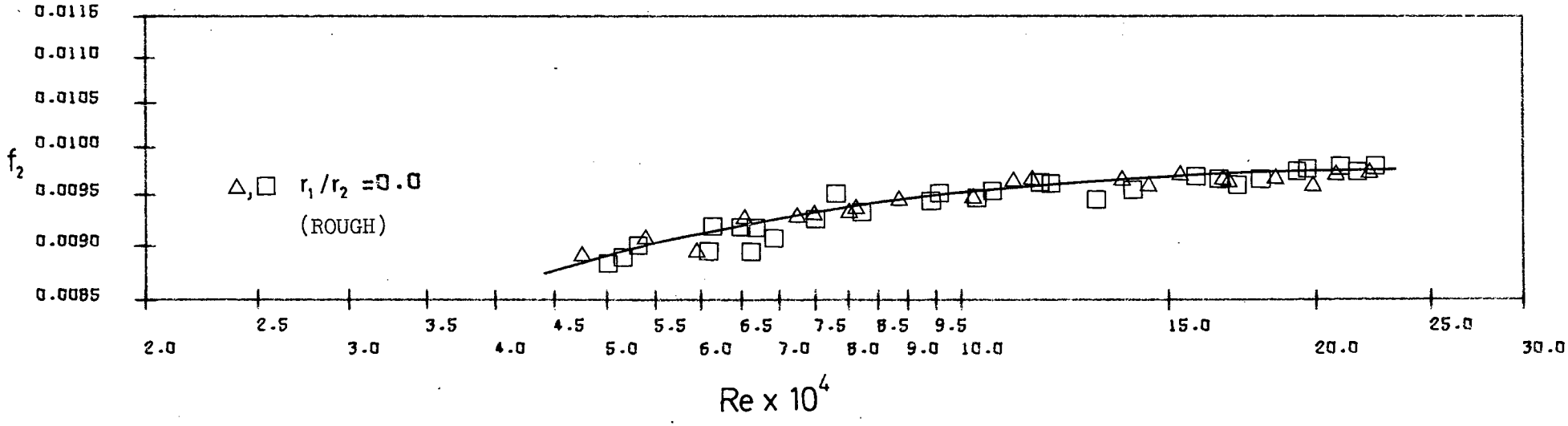

Fig. 48 Outer wall friction factors for the sand roughened sleeve

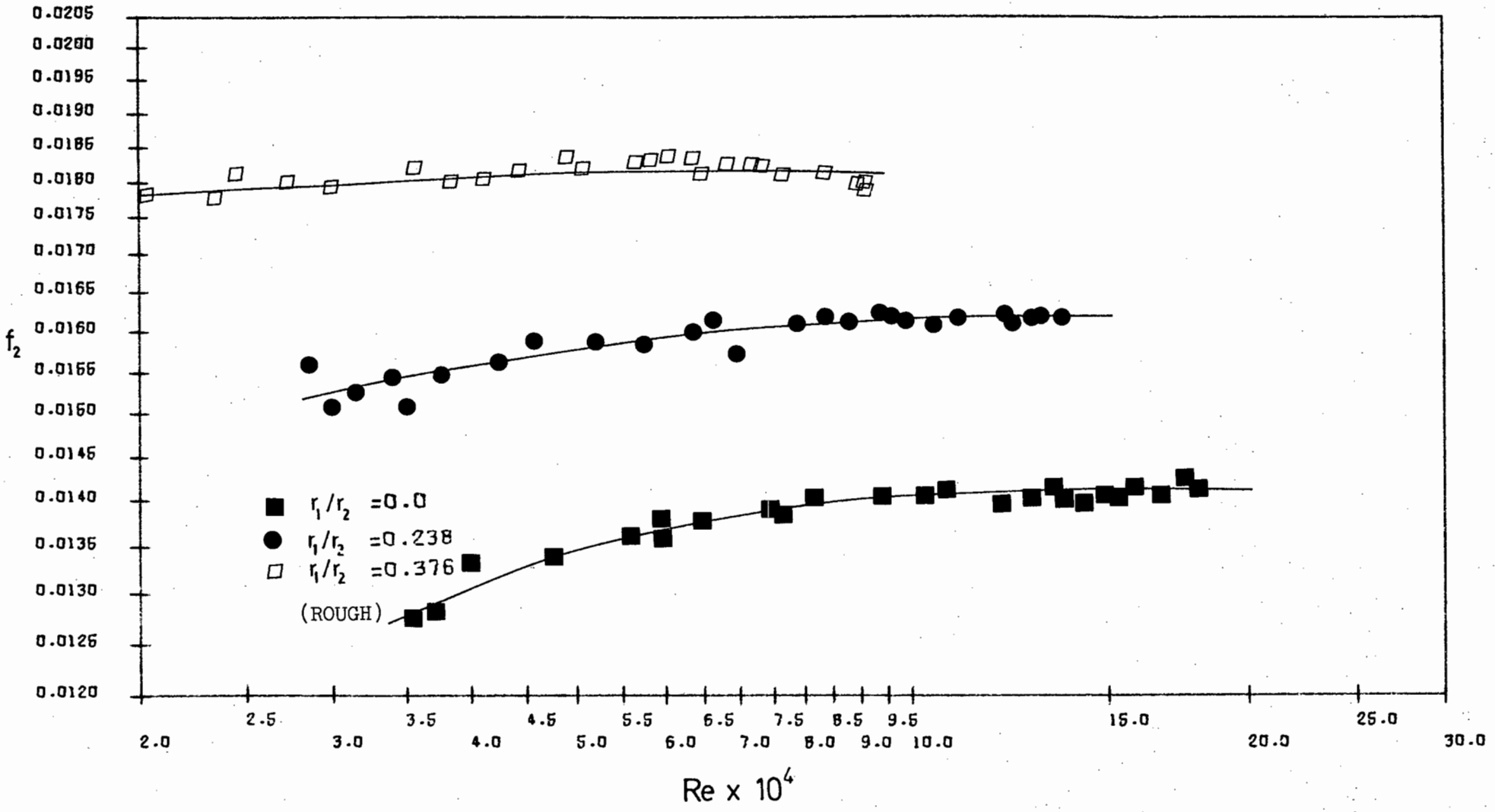

Fig. 49 Outer wall friction factors for mesh roughened annuli

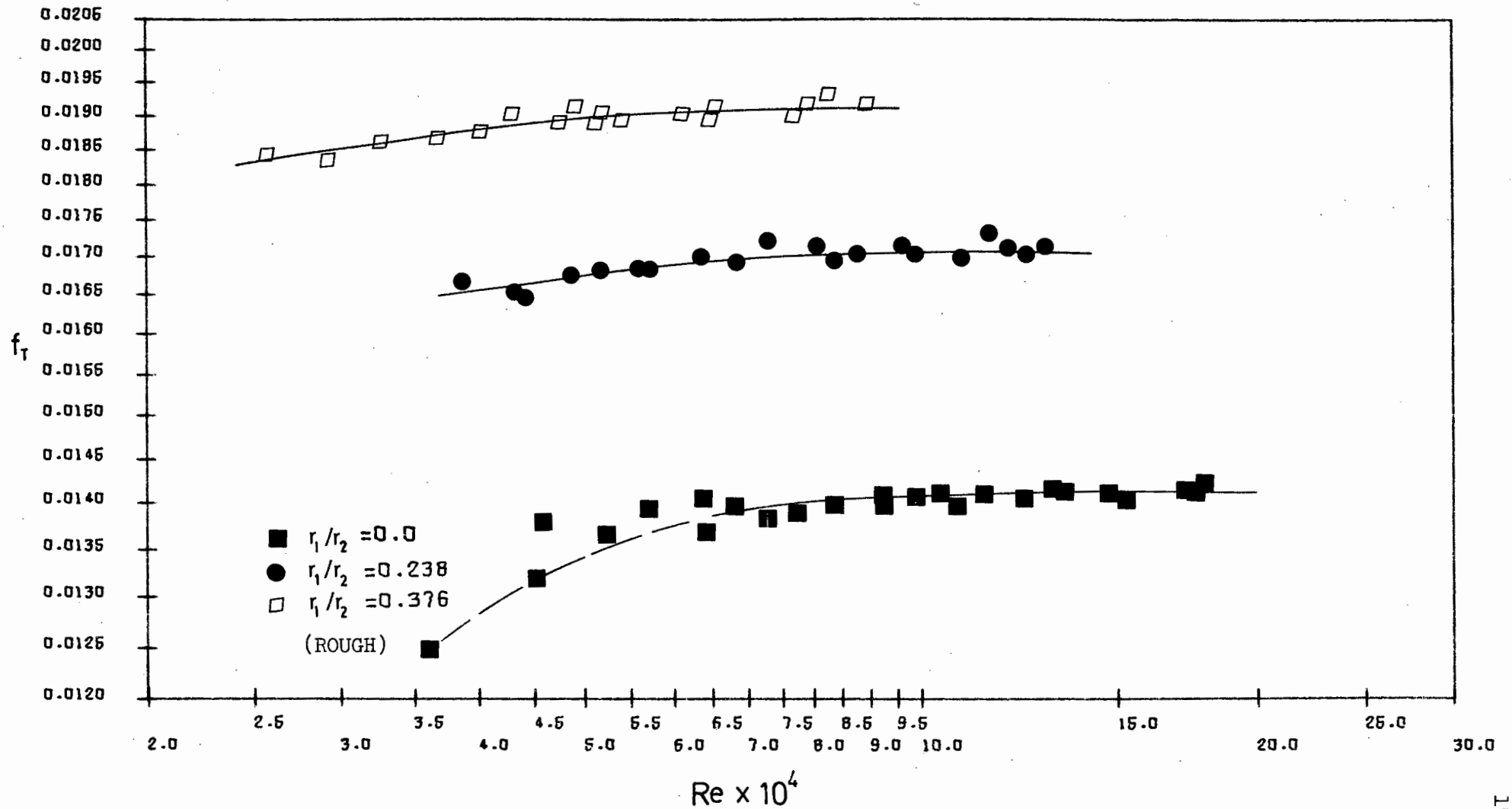

Fig. 50 Total friction factors for mesh roughened annuli

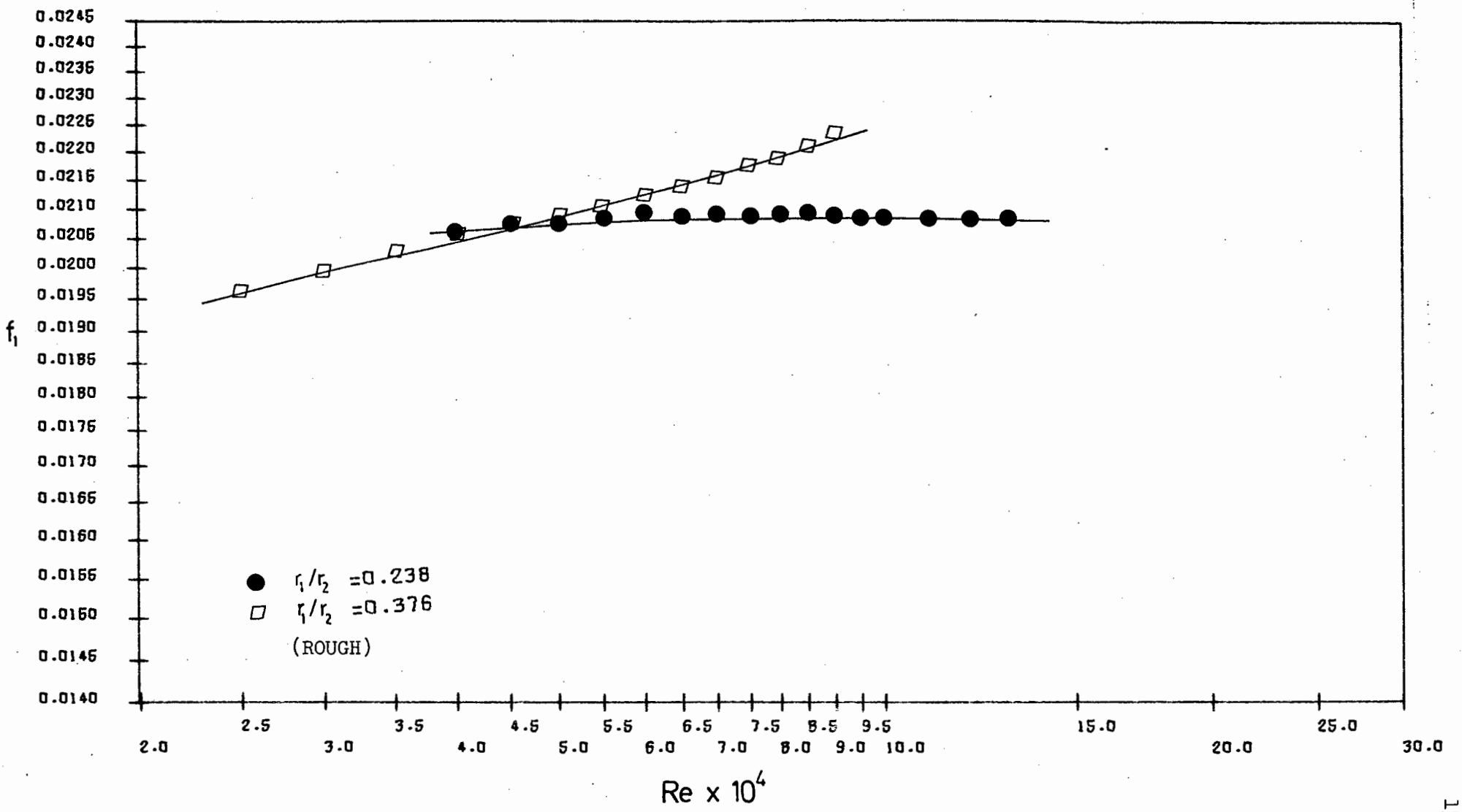

Fig. 51 Inner wall friction factors for mesh roughened annuli

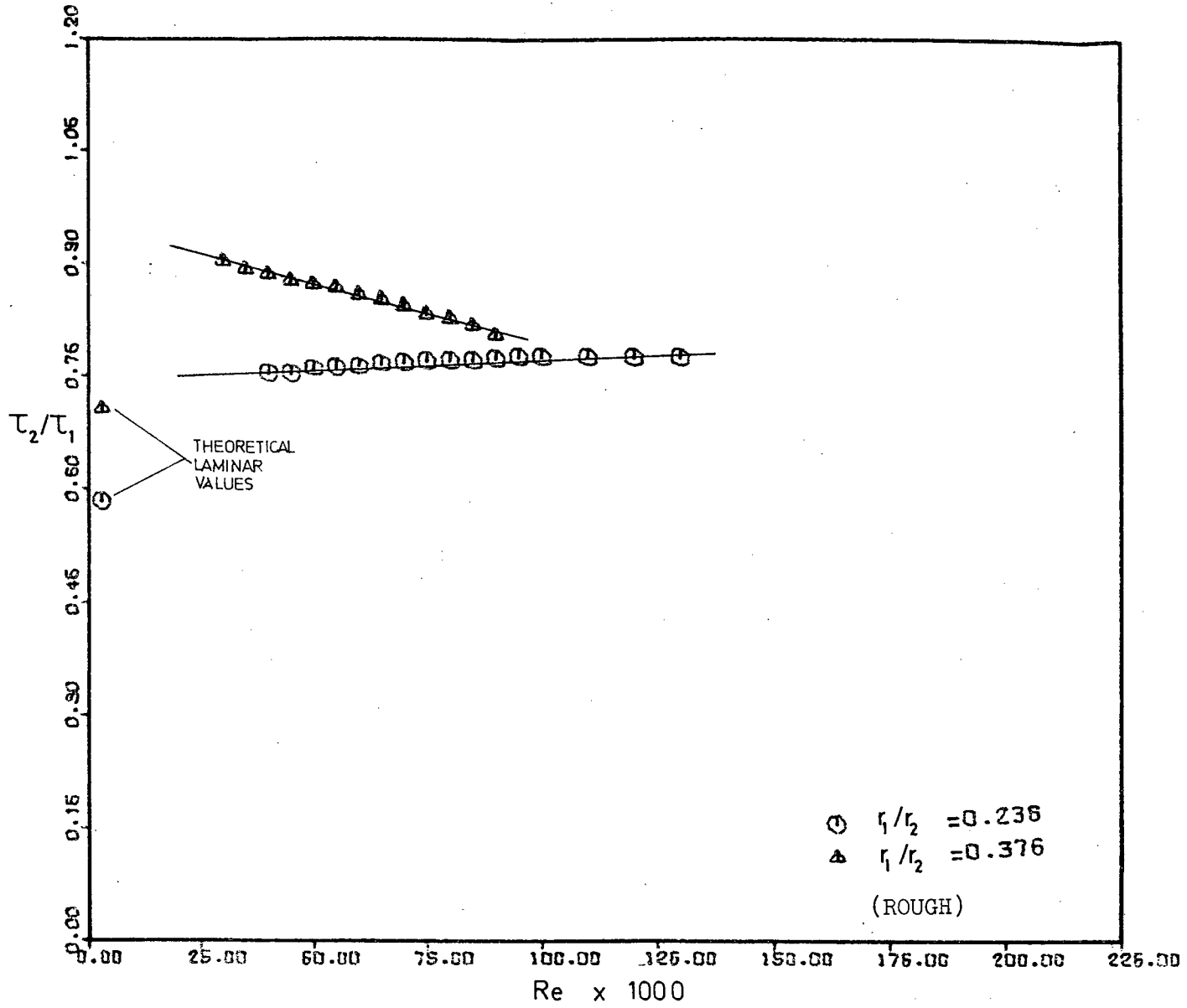

Fig. 52 The ratio of the wall shear stresses for mesh roughened annuli

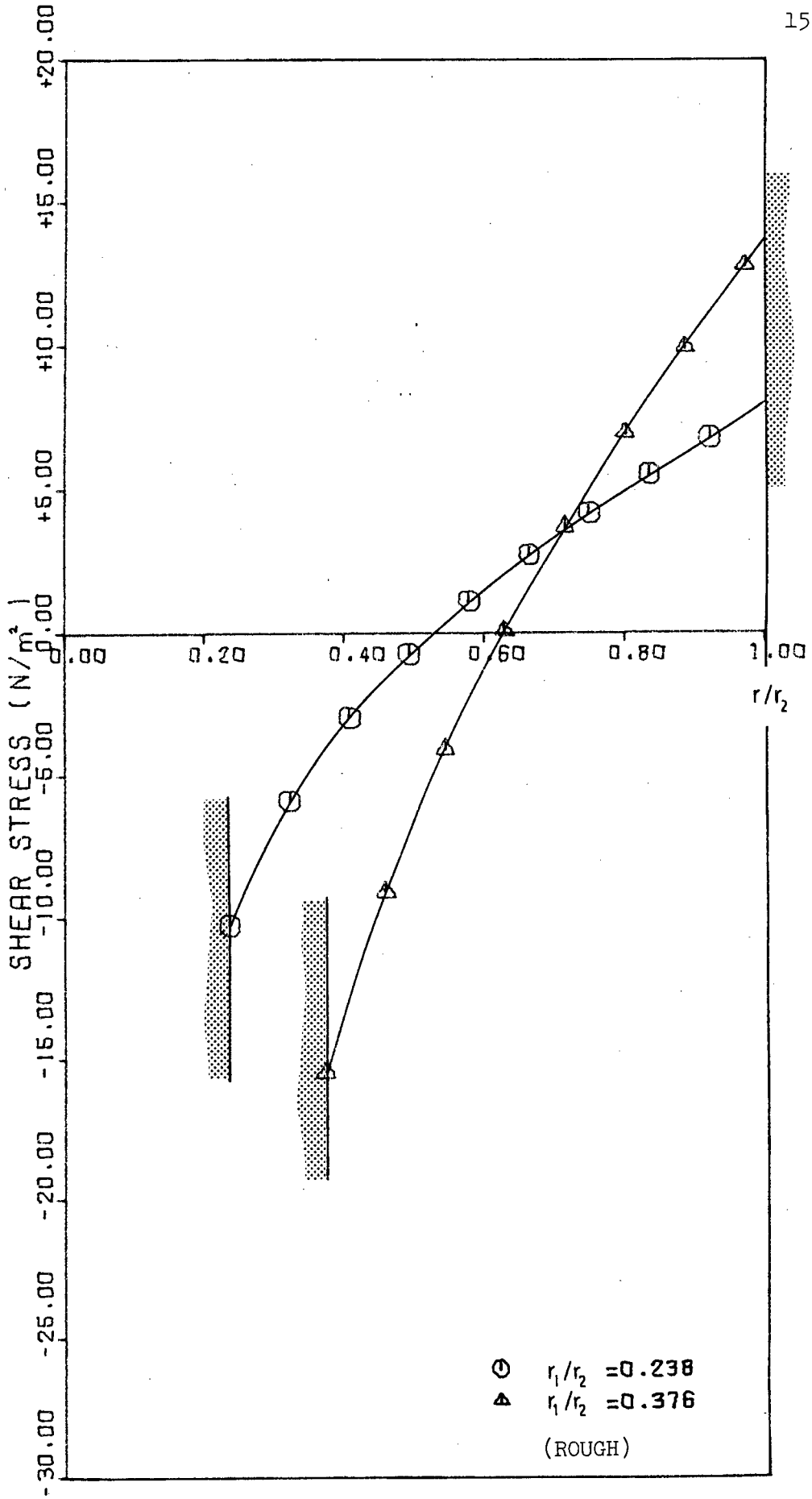

Fig. 53 Shear stress distributions in mesh roughened annuli for Re = 50 000

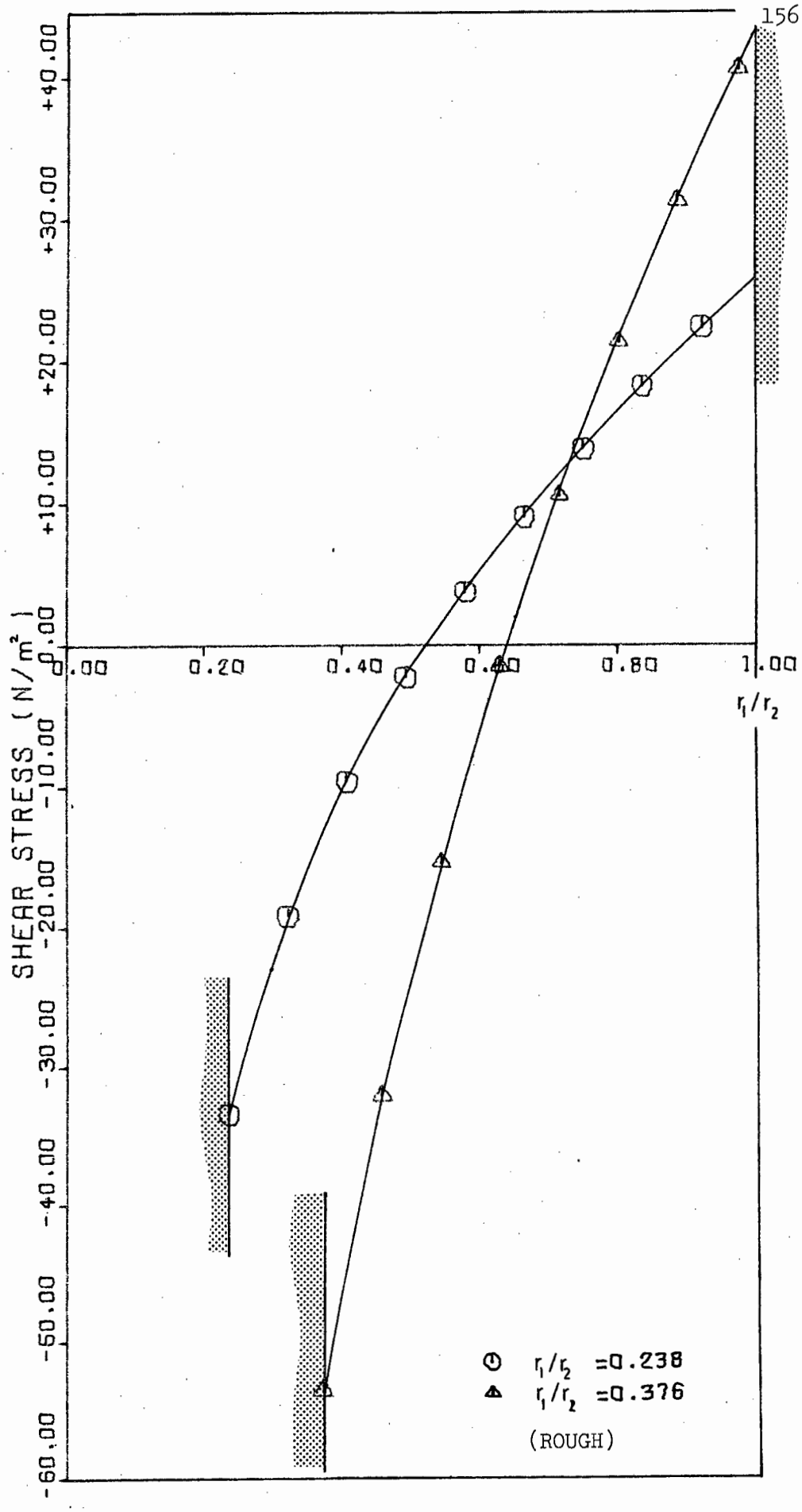

Fig. 54 Shear stress distributions in mesh roughened annuli for Re = 100 000

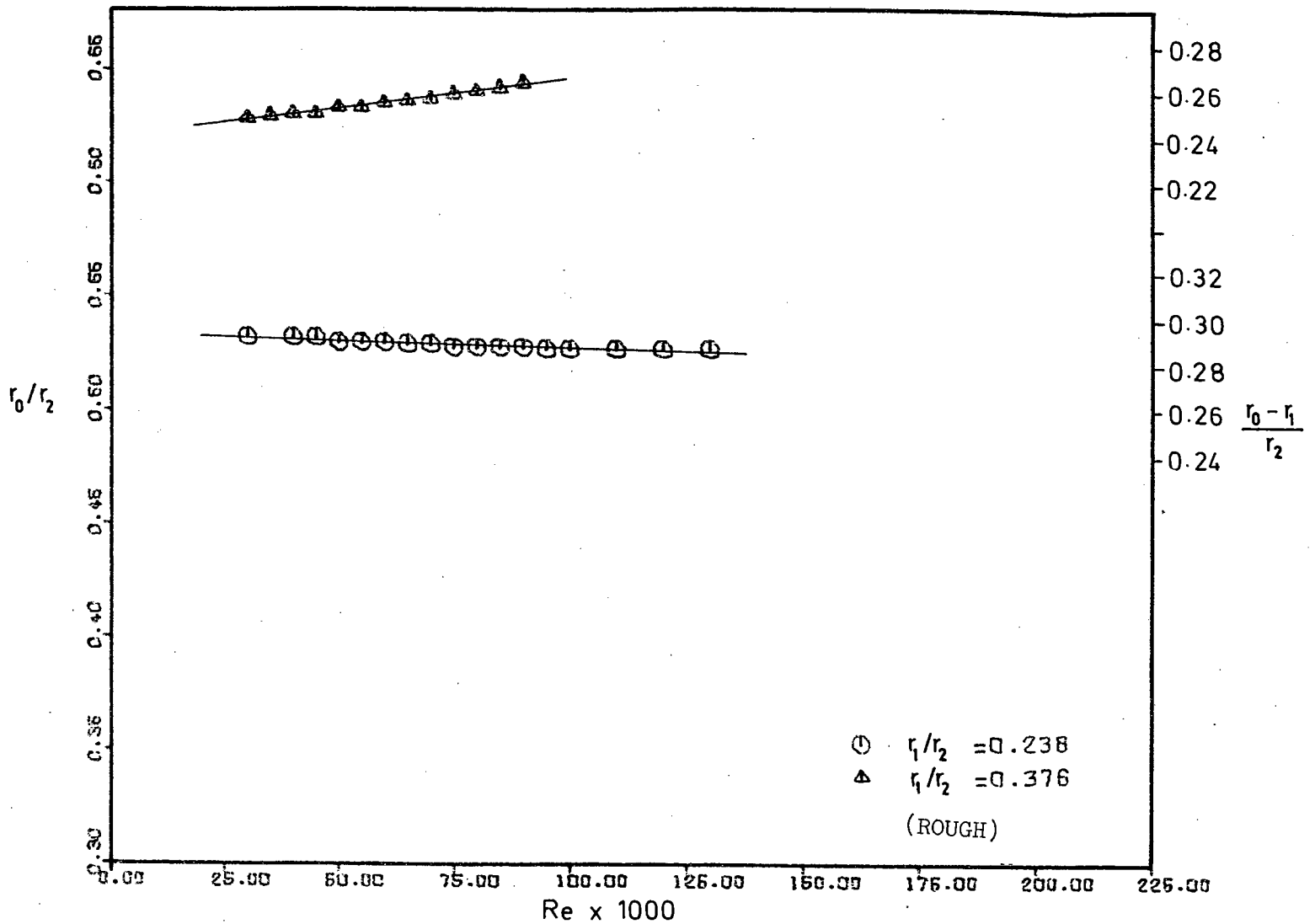

Fig. 55 The position of zero shear stress in mesh roughened annuli

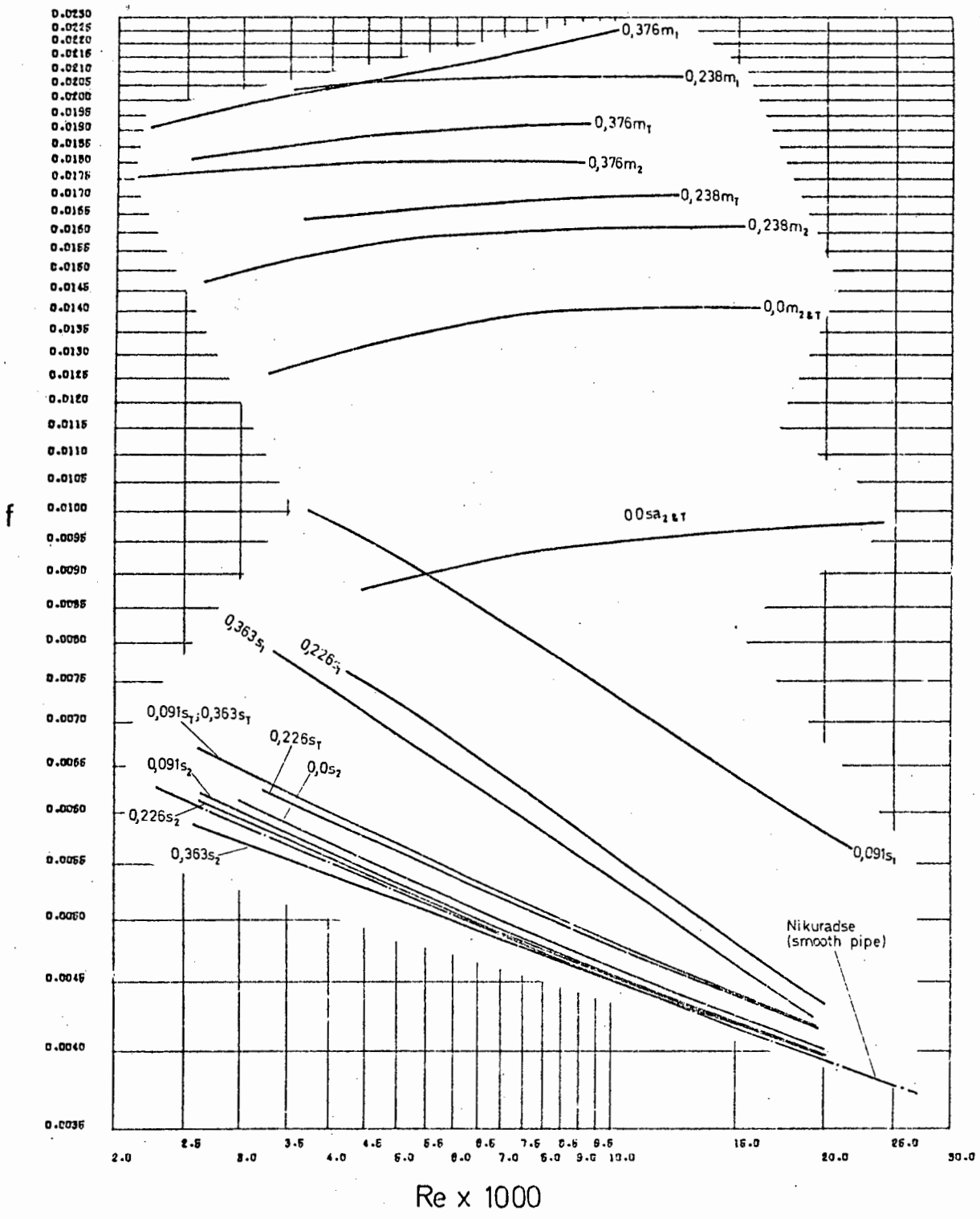

Fig. 56 Summary of friction factor curves

Key: First number (e.g. 0,226) gives radius ratio
S = Smooth surface Sa = Sand roughened surface M = mesh roughened surface 1 = core 2 = sleeve wall T = overall or total
e.g. $0{,}363S_1$ is the inner or core wall friction factor curve for a smooth annulus of radius ratio 0,363

SECTION 8

CONCLUSION

The main results of this investigation into concentric annular flow may be summarised as follows:

1. There have in the past been discrepancies in the results of the main parameters in annular flow. These discrepancies have usually arisen through a false assumption, (or the inaccurate measurement,) of the position of zero shear stress.

2. It has been proved in Section 6 that the position of zero shear stress for laminar flow does not coincide with that for turbulent flow, and it has also been shown that the position of maximum velocity and zero shear stress in turbulent flow, are not necessarily coincident.

3. To determine the individual wall shear stresses, friction factors and shear stress distributions without determining in any way the position of zero shear stress, required a novel method of measuring at least one of the wall shear stresses directly.

4. The floating sleeve was constructed for this purpose, and succeeded in measuring accurately the outer wall shear stress directly and the axial pressure gradient, thus allowing the inner wall shear stress to be obtained from a simple force balance.

5. The floating sleeve method was not accurate for a Reynolds number less than about 40 000. However, it is conceivable that rigs of greater sensitivity could be constructed, enabling accurate measurements at lower flows.

6. The position of the radius of zero shear stress is closer to the inner wall than the outer wall. This position is slightly dependent upon Reynolds number for smooth annuli.

7. The ratio τ_1/τ_2 is always greater than unity and increases with decreasing radius ratio and Reynolds number for smooth annuli. The ratio is constant for laminar flow (determined theoretically) for a particular radius ratio.

8. The total friction factor for a smooth annulus is between 4 and 9% above that of a pipe and is dependent upon radius ratio. The inner wall friction factor exhibits a marked dependence upon the radius ratio and is 10 to 55% greater than the friction factor for the outer sleeve (depending upon α and Re).

9. The positions of zero shear stress obtained by the floating sleeve are centrally placed amongst the results of previous investigations when expressed in the form proposed by Kays and Leung.

10. The floating sleeve worked equally well for rough and smooth annuli, providing always that no granular material clogged the leakage gap.

11. There is a curious upward trend in the graph of r_0/r_2 vs Re for α = 0,376 (rough annulus). The friction factors for rough annuli are more dependent upon the radius ratio than is the case for smooth annuli, the exception being the inner friction factors.

12. The floating sleeve / Concept has proved a reliable method of determining the individual wall shear stresses in smooth or rough annuli and is easily adaptable for similar studies with eccentric cores.

BIBLIOGRAPHY*

1. BATCHELOR, G.K.
An Introduction to Fluid Dynamics
Cambridge University Press (1967)

2. BRADSHAW, P.
Experimental Fluid Mechanics
Pergamon Press (1964)

3. BRADSHAW, P.
An Introduction to Turbulence and its Measurement
Pergaman Press (1971)

4. BRIGHTON, J.A. and JONES, J.B.
Fully Developed Turbulent Flow in Annuli
J. Basic Engng. (1964) 86, 835-844

5. BROWN, K.C. and JOUBERT, P.N.
The Measurement of Skin Friction in Turbulent Boundary Layers with Adverse Pressure Gradients
J. Fluid Mech. (1969) 35 (pt 4), 737-757

6. CHAMPAGNE, F.H., SLEICHER, C.A. and WEHRMANN, O.H.
Turbulence Measurements with Inclined Hot-wires
J. Fluid Mech. (1967) 28 (pt 1), 153-182

7. CLUMP, C.W. and KWASNOSKI, D.
Turbulent Flow in Concentric Annuli
A.I.Ch.E. Jnl. (1968) 14 (pt 1), 164-168

8. EMMONS, H.W.
Critique of Numerical Modeling of Fluid Mechanics Phenomena
Annual Review of Fluid Mechanics (1970) 2, 15-36

9. FOLSOM, R.G.
Review of the Pitot Tube
Trans. A.S.M.E. (1956) 78, 1447

10. HEAD, M.R. and RECHENBERG, I.
The Preston Tube as a Means of Measuring Skin Friction
J. Fluid Mech. (1962) 14 (pt 1), 1-17

11. HINZE, J.O.
Turbulence: An Introduction to its Mechanism and Theory
McGraw-Hill (1959)

12. KNUDSEN, J.G. and KATZ, D.L.
Fluid Dynamics and Heat Transfer
McGraw-Hill (1958)

* The format for journal references is: Name of Journal (Year), Volume, Pages

13. LAWN, C.J. and ELLIOT, C.J.
Fully Developed Turbulent Flow through Concentric Annuli
Central Electricity Generating Board (C.E.G.B.) (1971)
Report RD/B/N 1878

14. LAWN, C.J. and ELLIOT, C.J.
Fully Developed Turbulent Flow through Concentric Annuli
J. Mech. Eng. Sci (1972) 14 (pt 3), 195-204

15. LEVY, S.
Turbulent Flow in an Annulus
J. Heat Transfer (1967) 89, 25-31

16. LONGWELL, P.A.
Mechanics of Fluid Flow
McGraw-Hill (1966)

17. LYALL, H.G.
On the Use of the Preston Tube in Concentric Annuli
J. Roy. Aero. Soc. (1967) 71, 865-866

18. MACAGNO, E.O. and McDOUGAL, D.W.
Turbulent Flow in Annular Pipes
A.I.Ch.E. Jnl. (1966) 12 (pt 3), 437-444

19. MAUBACH, K. and REHME, K.
Negative Eddy Diffusivities for Asymmetric Turbulent Velocity Profiles ?
J. Heat Mass Transfer (1972) 15, 425-432

20. MICHIYOSHI, I. and NAKAJIMA, T.
Fully Developed Flow in a Concentric Annulus
J. Nuc. Sci. Tech. (1968) 5 (pt 7), 354-359

21. MILLER, B.
The Laminar Film Hypothesis
Trans. A.S.M.E. (1949) 71, 357-367

22. MOODY, L.F. and PRINCETON, N.J.
Friction Factors for Pipe Flow
Trans. A.S.M.E. (1944) 66, 671-684

23. MORRIS, H.M.
Flow in Rough Conduits
Trans. A.S.C.E. (1955) 120, 373-410

24. NELSON, A.R. and ROBERTSON, J.M.
Analytical Studies of Turbulent Friction in Annular Conduits
Univ. of Illinois T. & A.M. Report No. 321 (1968)

25. NICOL, A.A. and MEDWELL, J.O.
Velocity Profiles and Roughness Effects in Annular Pipes
J. Mech. Eng. Sci. (1964) 6 (pt 2), 110-115

26. NIKURADSE, J.
Strömungsgeseltze in Rauhen Rohren
VDI - Forschungsheft 361 (1933)
Translated as:
NACA Technical Memorandum 1292 (1950)

27. OLSEN, R.M. and SPARROW, E.M.
Measurement of Turbulent Flow in Tubes and Annuli with Square or Rounded Entrances
A.I.Ch.E. Jnl. (1963) 9 (pt 6), 766-770

28. OWEN, W.M.
Experimental Study of Water Flow in Annular Pipes
Proc. A.S.C.E. Separate No. 88 (1951) 77

29. PATEL, V.C.
Calibration of the Preston Tube and Limitations on its use in Pressure Gradients
J. Fluid Mech. (1965) 23 (pt 1), 185-208

30. PRESTON, J.H.
The Determination of Turbulent Skin Friction by Means of Pitot Tubes
J. Roy. Aero. Soc. (1954) 58, 109-121

31. QUARMBY, A.
On the Use of the Preston Tube in Concentric Annuli
J. Roy. Aero. Soc. (1967) 71, 47-49

32. QUARMBY, A.
An Experimental Study of Turbulent Flow through Concentric Annuli
Int. J. Mech. Sci. (1967) 9, 205-221

33. QUARMBY, A.
The Ratio of the Wall Shear Stresses in Concentric Annuli
J. Roy. Aero. Soc. (1968) 72, 345-346

34. RATKOWSKY, D.A.
Fluid Friction and Heat Transfer in Plain Concentric Annuli
Canadian J. Ch. Eng. (1966) 44, 8-12

35. REHME, K.
Turbulent Flow in Smooth Concentric Annuli with Small Radius Ratios
J. Fluid Mech. (1974) 64 (pt 2), 263-287

36. ROBERTSON, J.M., BURKHART, T.H. and MARTIN, J.D.
A Study of Turbulent Flow in Rough Pipes
Univ. of Illinois T. & A.M. Report No. 279 (1965)

37. ROTHFUS, R.R., MONRAD, C.E., SIKCHI, K.G. and HEIDEGER, W.J.
Isothermal Skin Friction in Flow through Annular Sections
Ind. and Eng. Chem. (1955) 47 (pt 5), 913-918

38. ROTHFUS, R.R., SARTORY, W.K. and KERMODE, R.I.
Flow in Concentric Annuli at High Reynolds Numbers
A.I.Ch.E. Jnl. (1966) 12 (pt 6), 1086 - 1091

39 ROUSE, H.
Fluid Mechanics for Hydraulic Engineers
McGraw-Hill (1938)

40. SMITH, S.L., LAWN, C.J. and HAMLIN, M.J.
The Direct Measurement of Wall Shear Stress in an Annulus
C.E.G.B. Report RD/B/N 1232 (1968)

41. WHITE, F.M.
Viscous Fluid Flow
McGraw-Hill (1974)

42. KJELLSTROM, B. and HEDBERG, S.
Aktiebolaget Atomenergie
Rep. 243, (1966)

APPENDIX A

This appendix contains the main data obtained from this investigation. The format consists of a separate section for the total wall shear results (obtained from pressure measurements), the sleeve wall shear results (obtained from weight measurements), the core wall data (obtained from the respective f vs Re curves), and an analysis sheet; for each radius ratio.

The nature of each page of results may thus be ascertained from the heading and the series number. A guide to the series number is given:

	Radius Ratio	Wall Surfaces
SERIES 10	0	Smooth
SERIES 11	0,091	Smooth
SERIES 12	0,226	Smooth
SERIES 13	0,363	Smooth
SERIES 20	0	Sand Roughened
SERIES 30	0	Mesh Roughened
SERIES 32	0,238	Mesh Roughened
SERIES 33	0,376	Mesh Roughened

Thus for example a page headed

RESULTS FOR : SLEEVE WALL SHEAR
SERIES 32

would be the results obtained from weight measurements on the floating sleeve for a mesh roughened annulus with a radius ratio of 0,238.

Note: Owing to the 'upper case only' facility of the computer printer, certain symbols used in this appendix do not correspond exactly with those found elsewhere in the text. For example N/m^2 is written N/M2.

DATA SHEET

DATA FOR :SLEEVE WALL SHEAR
SERIES 10 ALPHA = .000
SLEEVE INTERNAL DIAMETER = .07000M RELATIVE ROUGHNESS = .0001140
CORE OUTER DIAMETER = .06990M RELATIVE ROUGHNESS = .0001000

TEST UNITS	SW0 GF	+WT GF	SW1 GF	P0 CM	FW1 KG	TIME SEC	TEMP DEGC
1	157.	200.	130.	24.6	676.	180.0	15.0
2	157.	300.	113.	27.8	783.	180.0	15.0
3	157.	1250.	85.	44.8	756.	90.0	15.0
4	157.	1700.	62.	54.2	881.	90.0	15.0
5	157.	3200.	112.	81.6	797.	60.0	15.0
6	155.	0.	123.	20.0	415.	180.0	14.7
7	155.	0.	77.	21.3	486.	180.0	14.7
8	155.	300.	170.	25.6	726.	180.0	14.8
9	155.	500.	88.	34.2	665.	120.0	14.8
10	155.	1000.	144.	40.6	882.	120.0	14.9
11	155.	1400.	128.	46.5	788.	90.0	14.9
12	155.	1700.	114.	52.1	578.	60.0	14.9
13	155.	2200.	187.	58.5	652.	60.0	14.9
14	155.	3200.	133.	82.3	794.	60.0	14.9
15	159.	0.	104.	19.5	761.	300.0	14.3
16	159.	100.	109.	22.5	772.	240.0	14.4
17	159.	200.	102.	25.1	713.	180.0	14.4
18	159.	400.	107.	29.7	748.	150.0	14.5
19	159.	680.	111.	35.2	742.	120.0	14.5
20	159.	950.	106.	39.2	878.	120.0	14.5
21	159.	1550.	101.	51.3	842.	90.0	14.5
22	159.	2070.	106.	61.2	648.	60.0	14.5
23	159.	3150.	92.	80.1	965.	73.0	14.6
24	152.	1000.	113.	39.7	900.	120.0	14.7
25	152.	1500.	100.	50.4	734.	80.0	14.7
26	160.	200.	156.	21.8	542.	150.0	13.7
27	160.	300.	72.	29.7	566.	120.0	13.9
28	160.	1000.	176.	45.4	802.	110.0	13.8
29	160.	500.	107.	30.'	666.	120.0	13.8
30	190.	200.	122.	26.4	484.	120.0	14.1
31	190.	500.	193.	30.0	630.	120.0	14.1
32	190.	700.	260.	33.2	692.	120.0	14.1
33	190.	1200.	134.	41.2	900.	120.0	14.2
34	190.	1300.	210.	45.9	826.	100.0	14.2
35	190.	1800.	192.	53.5	888.	90.0	14.2
36	190.	2300.	173.	64.3	900.	80.0	14.3
37	190.	3000.	95.	81.0	976.	75.0	14.3
38	190.	2700.	258.	72.3	898.	75.0	14.3
39	190.	2200.	210.	60.7	816.	75.0	14.3
40	190.	1200.	248.	43.4	704.	90.0	14.3
41	190.	300.	210.	24.6	364.	90.0	14.3
42	167.	2000.	236.	58.0	915.	90.0	14.1
43	167.	1800.	330.	54.0	747.	80.0	14.1
44	167.	1000.	194.	38.7	647.	90.0	14.1
45	167.	500.	195.	28.9	455.	90.0	14.2
46	167.	200.	138.	25.7	447.	120.0	14.2
47	167.	50.	174.	17.7	284.	120.0	14.3
48	167.	0.	162.	20.0	248.	120.0	14.3
49	167.	0.	227.	16.5	160.	120.0	14.3
50	167.	500.	233.	28.8	494.	100.0	14.6
51	167.	0.	90.	22.8	272.	100.0	14.6
52	167.	0.	158.	19.1	212.	100.0	14.6
53	167.	0.	208.	20.2	159.	100.0	14.7
54	124.	1000.	252.	38.5	950.	140.3	16.6
55	134.	800.	314.	33.5	964.	169.8	16.4
56	134.	1100.	267.	41.5	911.	127.3	16.5
57	125.	3000.	287.	76.2	955.	77.3	17.6
58	125.	2800.	255.	72.5	938.	77.9	17.6
59	125.	1300.	306.	41.0	931.	120.7	17.9
60	125.	1000.	332.	36.0	961.	149.4	17.9
61	125.	800.	334.	34.6	977.	175.4	18.1
62	117.	700.	304.	30.0	992.	186.5	18.6
63	117.	600.	318.	28.0	967.	205.8	18.7
64	117.	500.	306.	25.5	977.	225.8	18.8
65	117.	400.	292.	24.5	954.	253.7	18.8
66	117.	300.	277.	22.2	991.	309.8	18.9
67	100.	530.	292.	25.0	964.	218.0	19.4
68	100.	1500.	264.	46.7	977.	115.0	19.5
69	100.	2000.	365.	53.5	983.	100.3	19.5
70	134.	1000.	299.	35.7	960.	142.4	18.8
71	134.	500.	252.	28.0	956.	205.1	18.8
72	134.	400.	256.	26.5	1003.	246.4	18.8
73	134.	300.	281.	22.9	964.	293.3	18.8
74	134.	200.	257.	22.4	913.	339.6	18.7
75	134.	150.	258.	20.4	996.	438.5	18.7
76	132.	1500.	259.	45.5	961.	111.5	18.2
77	132.	1800.	234.	50.5	947.	97.9	18.2
78	132.	850.	265.	31.5	965.	156.5	18.2
79	132.	650.	270.	27.0	977.	185.3	18.2

80	132.	500.	252.	26.5	926.	198.5	18.2
81	132.	300.	276.	23.4	954.	289.9	18.2
82	183.	3000.	405.	75.3	901.	73.0	18.4
83	183.	2000.	374.	69.6	905.	75.4	18.4
84	183.	2500.	261.	67.1	872.	75.1	18.4
85	183.	2200.	330.	59.0	854.	80.0	18.5
86	183.	1700.	322.	52.5	836.	90.2	18.5
87	183.	1200.	212.	42.1	836.	104.3	18.5
88	183.	700.	217.	34.3	758.	124.4	18.6
89	222.	3000.	321.	74.1	906.	72.5	18.6
90	222.	2500.	278.	65.7	846.	72.9	18.6
91	222.	2000.	337.	54.4	748.	73.9	18.6
92	222.	1500.	377.	44.7	791.	92.4	18.7
93	222.	1000.	380.	34.9	816.	120.7	18.7
94	222.	500.	325.	25.5	697.	144.4	18.7
95	222.	200.	242.	20.7	543.	154.6	18.7
96	222.	100.	218.	19.5	534.	179.0	18.7
97	222.	100.	326.	16.4	314.	153.5	18.7

RESULT SHEET

RESULTS FOR:SLEEVE WALL SHEAR
SERIES 10 ALPHA = .000
SLEEVE INTERNAL DIAMETER = .07000M RELATIVE ROUGHNESS = .0001143
CORE OUTER DIAMETER = .00000M RELATIVE ROUGHNESS = .0000000

TEST UNITS	SLEEVE FORCE GF	SLEEVE SHEAR N/M2	BULK FLOW M3/S	BULK VEL M/S	RE	F2	KINEMATIC VISCOSITY M2/S
1	341.4	2.410	.00376	.976	59847.	.005060	.1141-05
2	458.9	3.239	.00435	1.130	69320.	.005071	.1141-05
3	1440.0	10.164	.00840	2.183	133860.	.004267	.1141-05
4	1914.6	13.514	.00979	2.544	155993.	.004178	.1141-05
5	3369.5	23.783	.01328	3.452	211679.	.003993	.1141-05
6	145.6	1.027	.00231	.599	36453.	.005725	.1150-05
7	191.8	1.354	.00270	.702	42689.	.005500	.1150-05
8	399.6	2.820	.00403	1.048	63938.	.005135	.1147-05
9	683.1	4.821	.00554	1.440	87849.	.004650	.1147-05
10	1128.2	7.963	.00735	1.910	116821.	.004366	.1144-05
11	1545.3	10.907	.00876	2.275	139161.	.004214	.1144-05
12	1860.3	13.130	.00963	2.503	153113.	.004191	.1144-05
13	2288.4	16.152	.01087	2.824	172715.	.004052	.1144-05
14	3346.6	23.622	.01323	3.439	210331.	.003996	.1144-05
15	168.5	1.189	.00254	.659	39686.	.005474	.1163-05
16	264.0	1.863	.00322	.836	50458.	.005335	.1160-05
17	371.5	2.622	.00396	1.029	62135.	.004950	.1160-05
18	567.3	4.004	.00499	1.296	78429.	.004770	.1156-05
19	844.3	5.959	.00618	1.607	97250.	.004617	.1156-05
20	1120.0	7.905	.00732	1.901	115075.	.004374	.1156-05
21	1727.1	12.191	.00936	2.431	147143.	.004126	.1156-05
22	2243.9	15.838	.01080	2.806	169861.	.004022	.1156-05
23	3341.3	23.584	.01322	3.435	208458.	.003998	.1153-05
24	1156.1	8.160	.00750	1.949	118581.	.004297	.1150-05
25	1671.0	11.794	.00917	2.384	145065.	.004150	.1150-05
26	317.9	2.244	.00361	.939	55635.	.005090	.1181-05
27	503.3	3.552	.00472	1.226	73012.	.004730	.1175-05
28	1102.1	7.779	.00729	1.895	112560.	.004335	.1178-05
29	668.4	4.717	.00555	1.442	85683.	.004537	.1178-05
30	382.7	2.701	.00403	1.048	62768.	.004918	.1169-05
31	612.3	4.322	.00525	1.364	81702.	.004645	.1169-05
32	745.9	5.265	.00577	1.498	89742.	.004690	.1169-05
33	1173.3	8.282	.00750	1.949	117827.	.004361	.1166-05
34	1398.2	9.869	.00826	2.146	128886.	.004285	.1166-05
35	1917.5	13.535	.00987	2.564	153955.	.004119	.1166-05
36	2438.4	17.211	.01125	2.923	176006.	.004028	.1163-05
37	3219.4	22.724	.01301	3.381	203593.	.003975	.1163-05
38	2754.9	19.445	.01197	3.111	187322.	.004018	.1163-05
39	2300.8	16.240	.01088	2.827	170217.	.004064	.1163-05
40	1259.7	8.892	.00782	2.033	122378.	.004304	.1163-05
41	394.4	2.784	.00404	1.051	63275.	.005041	.1163-05
42	2051.3	14.479	.01017	2.642	158216.	.004149	.1169-05
43	1756.6	12.399	.00934	2.426	145312.	.004212	.1169-05
44	1089.9	7.693	.00719	1.868	111875.	.004409	.1169-05
45	587.1	4.144	.00506	1.314	78885.	.004803	.1166-05
46	343.6	2.425	.00372	.968	58123.	.005177	.1166-05
47	156.1	1.102	.00237	.615	37026.	.005828	.1163-05
48	118.6	.837	.00207	.537	32333.	.005803	.1163-05
49	52.9	.374	.00133	.346	20860.	.006225	.1163-05
50	549.1	3.876	.00494	1.284	77900.	.004705	.1153-05
51	191.1	1.349	.00272	.707	42893.	.005399	.1153-05
52	122.4	.864	.00212	.551	33431.	.005694	.1153-05
53	72.6	.512	.00159	.413	25139.	.006003	.1150-05
54	988.8	6.980	.00683	1.775	113457.	.004430	.1095-05
55	736.0	5.195	.00567	1.475	93765.	.004778	.1101-05
56	1084.4	7.654	.00716	1.860	118584.	.004424	.1098-05

57	2961.6	20.904	.01236	3.212	210530.	.004053	.1068-05
58	2792.9	19.713	.01164	3.129	205126.	.004026	.1068-05
59	1236.3	8.726	.00771	2.005	132390.	.004343	.1068-05
60	909.4	6.419	.00643	1.671	110346.	.004598	.1068-05
61	707.2	4.991	.00557	1.448	96080.	.004763	.1055-05
62	628.3	4.435	.00532	1.382	92844.	.004646	.1042-05
63	514.0	3.628	.00470	1.221	82235.	.004868	.1039-05
64	425.5	3.004	.00433	1.125	75944.	.004749	.1037-05
65	339.4	2.395	.00376	.977	65967.	.005020	.1037-05
66	253.9	1.792	.00320	.831	56283.	.005186	.1034-05
67	452.4	3.194	.00442	1.149	78721.	.004840	.1022-05
68	1454.3	10.265	.00858	2.209	151717.	.004208	.1019-05
69	1854.5	13.090	.00981	2.548	175021.	.004033	.1019-05
70	951.3	6.715	.00674	1.752	118291.	.004376	.1037-05
71	497.0	3.508	.00466	1.212	81829.	.004778	.1037-05
72	392.7	2.772	.00407	1.058	71425.	.004955	.1037-05
73	267.1	1.885	.00329	.854	57659.	.005171	.1037-05
74	191.0	1.348	.00269	.699	47057.	.005524	.1039-05
75	139.6	.986	.00227	.590	39749.	.005661	.1039-05
76	1491.1	10.525	.00862	2.240	149807.	.004197	.1052-05
77	1817.0	12.825	.00961	2.496	166086.	.004116	.1052-05
78	832.6	5.877	.00617	1.603	106658.	.004574	.1052-05
79	626.8	4.424	.00527	1.370	91135.	.004716	.1052-05
80	494.7	3.492	.00466	1.212	80651.	.004753	.1052-05
81	270.2	1.907	.00329	.855	56911.	.005213	.1052-05
82	2901.4	20.479	.01234	3.207	214442.	.003982	.1047-05
83	2731.4	19.279	.01200	3.119	208538.	.003964	.1047-05
84	2543.9	17.956	.01161	3.017	201737.	.003945	.1047-05
85	2173.5	15.341	.01067	2.774	185930.	.003988	.1044-05
86	1680.3	11.860	.00927	2.408	161429.	.004090	.1044-05
87	1288.5	9.095	.00804	2.089	140008.	.004169	.1044-05
88	782.1	5.520	.00609	1.583	106390.	.004404	.1042-05
89	2974.2	20.993	.01250	3.247	218194.	.003982	.1042-05
90	2573.7	18.166	.01160	3.015	202626.	.003996	.1042-05
91	2004.7	14.150	.01012	2.630	176730.	.004091	.1042-05
92	1463.0	10.326	.00856	2.224	149839.	.004174	.1039-05
93	958.2	6.763	.00676	1.757	118333.	.004383	.1039-05
94	511.5	3.611	.00478	1.242	83638.	.004684	.1039-05
95	293.7	2.073	.00351	.913	61477.	.004977	.1039-05
96	217.5	1.535	.00298	.775	52217.	.005109	.1039-05
97	108.9	.769	.00205	.532	35805.	.005442	.1039-05

DATA SHEET

DATA FOR :TOTAL WALL SHEAR
SERIES 10 ALPHA = .000
SLEEVE INTERNAL DIAMETER = .07000M RELATIVE ROUGHNESS = .0001140
CORE OUTER DIAMETER = .00000M RELATIVE ROUGHNESS = .0000000

TEST UNITS	P0 CM	P1 CM	P2 CM	P3 CM	P4 CM	P5 CM	FW1 KG	TIME SEC	TEMP DEGC
1	16.4	30.7	30.2	30.0	29.2	29.0	429.	271.0	16.0
2	16.7	31.5	31.0	30.3	29.9	29.4	403.	238.8	16.0
3	21.0	32.7	31.6	30.6	29.8	29.0	478.	202.0	16.5
4	20.8	31.8	30.7	29.6	28.7	27.7	431.	173.2	16.5
5	21.5	33.1	31.8	30.5	29.8	28.3	473.	175.3	16.5
6	23.2	34.2	32.7	31.2	29.6	28.1	439.	142.3	16.5
7	17.3	32.2	31.5	31.0	30.4	29.8	429.	241.8	15.5
8	15.7	30.5	29.8	29.2	28.6	28.1	443.	238.7	15.5
9	18.3	33.3	32.5	31.5	30.7	29.9	478.	227.8	15.7
10	79.4	94.4	75.2	56.6	39.0	21.4	804.	65.0	15.8
11	25.7	40.5	38.2	35.9	33.8	31.6	668.	176.0	15.8
12	32.9	47.8	43.5	39.3	35.3	31.2	819.	150.5	15.9
13	42.2	57.7	51.0	44.5	38.4	32.7	857.	124.6	16.0
14	48.7	63.6	55.3	46.6	38.4	30.2	899.	110.7	16.0
15	56.4	71.8	60.6	49.6	38.9	28.4	941.	100.8	16.1
16	65.4	80.9	66.5	52.0	38.1	24.5	951.	87.9	16.1
17	82.0	95.8	78.1	59.0	41.2	23.6	978.	79.1	16.2
18	.0	44.1	40.8	37.4	34.5	31.3	888.	187.8	16.3
19	25.0	39.8	37.6	35.7	33.7	32.1	854.	241.0	16.4
20	.0	33.7	32.4	30.9	29.7	28.4	632.	220.7	16.5
21	18.1	33.1	31.9	31.1	30.3	29.4	896.	380.0	16.5
22	17.0	32.0	31.3	30.7	30.0	29.4	862.	462.7	16.6
23	18.5	33.3	32.6	32.0	31.0	31.2	890.	541.7	16.6
24	39.5	54.2	49.7	43.3	37.8	32.4	947.	146.7	16.7
25	78.4	83.2	61.7	40.8	21.3	2.0	920.	70.0	18.4
26	72.8	77.6	58.8	39.9	21.2	4.6	766.	62.2	18.4
27	54.8	58.9	47.7	35.0	23.3	12.5	804.	82.5	18.4
28	45.3	49.3	40.4	31.0	21.8	12.7	798.	93.5	18.5
29	33.1	37.3	32.6	28.0	22.4	17.4	715.	120.5	18.5
30	88.1	84.5	62.9	42.1	22.5	2.8	924.	70.0	18.6
31	74.6	78.7	58.7	39.2	20.3	2.6	847.	67.1	18.6
32	62.5	67.0	51.5	36.1	20.2	5.4	864.	76.0	18.6
33	53.8	57.7	45.9	34.1	21.9	10.5	812.	82.6	18.6
34	35.0	39.3	33.5	29.1	21.0	15.6	732.	110.0	18.6

35	27.2	30.5	27.8	25.0	21.2	18.5	705.	154.6	18.6
36	21.6	25.1	23.5	21.7	19.9	18.4	592.	180.6	18.6
37	61.5	65.1	49.6	33.9	18.6	4.2	792.	70.3	18.6
38	43.9	47.3	37.7	27.9	18.0	9.0	618.	70.0	18.6
39	31.0	34.1	29.1	23.5	19.0	14.1	427.	70.1	18.7
40	19.1	22.1	20.2	18.5	16.5	15.0	279.	81.4	18.7
41	16.8	19.9	18.9	17.8	16.5	15.6	312.	120.6	18.7

RESULT SHEET

RESULTS FOR:TOTAL WALL SHEAR
SERIES 10 ALPHA = .000
SLEEVE INTERNAL DIAMETER = .07100M RELATIVE ROUGHNESS = .0001140
CORE OUTER DIAMETER = .00000M RELATIVE ROUGHNESS = .0000000

TEST UNITS	TOTAL FORCE GF	TOTAL SHEAR N/M2	BULK FLOW M3/S	BULK VEL M/S	RE	FT	KINEMATIC VISCOSITY M2/S
1	70.4	.497	.00158	.412	25919.	.005863	.1112-05
2	84.8	.599	.00169	.439	27634.	.006213	.1112-05
3	147.3	1.040	.00237	.615	39198.	.005499	.1098-05
4	163.3	1.152	.00249	.646	41183.	.005523	.1098-05
5	185.7	1.311	.00270	.701	44677.	.005337	.1098-05
6	244.9	1.729	.00309	.802	51115.	.005377	.1098-05
7	94.4	.667	.00177	.461	28644.	.006273	.1127-05
8	96.1	.678	.00186	.482	29949.	.005836	.1127-05
9	137.7	.972	.00210	.545	34052.	.006537	.1121-05
10	2916.5	20.586	.01237	3.215	201301.	.003984	.1118-05
11	355.4	2.508	.00379	.986	61716.	.005164	.1118-05
12	662.7	4.678	.00545	1.415	88823.	.004673	.1115-05
13	1002.1	7.073	.00688	1.787	112459.	.004431	.1112-05
14	1339.8	9.457	.00812	2.110	132770.	.004250	.1112-05
15	1736.8	12.259	.00934	2.427	153130.	.004163	.1109-05
16	2260.2	15.953	.01082	2.810	177338.	.004040	.1109-05
17	2902.0	20.484	.01235	3.212	203205.	.003971	.1106-05
18	510.6	3.604	.00473	1.229	77954.	.004772	.1104-05
19	309.0	2.181	.00354	.921	58550.	.005144	.1101-05
20	212.9	1.503	.00286	.744	47458.	.005423	.1098-05
21	144.1	1.017	.00231	.600	38240.	.005653	.1098-05
22	104.0	.734	.00186	.484	30928.	.006272	.1095-05
23	92.9	.656	.00164	.427	27295.	.007189	.1095-05
24	888.3	6.270	.00646	1.678	107513.	.004454	.1092-05
25	3246.3	22.914	.01314	3.415	228348.	.003929	.1047-05
26	2939.0	20.744	.01232	3.200	213967.	.004052	.1047-05
27	1876.0	13.242	.00975	2.532	169321.	.004130	.1047-05
28	1469.4	10.372	.00853	2.218	148652.	.004218	.1044-05
29	800.3	5.649	.00593	1.542	103347.	.004752	.1044-05
30	3262.3	23.026	.01320	3.430	230476.	.003915	.1042-05
31	3051.0	21.535	.01262	3.280	220401.	.004003	.1042-05
32	2473.1	17.456	.01137	2.954	198496.	.004001	.1042-05
33	1895.2	13.377	.00983	2.554	171644.	.004100	.1042-05
34	958.7	6.767	.00665	1.729	116190.	.004527	.1042-05
35	489.8	3.457	.00456	1.185	79622.	.004924	.1042-05
36	272.1	1.921	.00328	.852	57234.	.005295	.1042-05
37	2445.9	17.264	.01127	2.927	196708.	.004029	.1042-05
38	1541.5	10.880	.00883	2.294	154150.	.004135	.1042-05
39	862.0	5.661	.00609	1.583	106618.	.004519	.1039-05
40	286.5	2.022	.00343	.891	59993.	.005099	.1039-05
41	176.1	1.243	.00259	.672	45282.	.005500	.1039-05

DATA SHEET

DATA FOR :SLEEVE WALL SHEAR
SERIES 11 ALPHA = .091
SLEEVE INTERNAL DIAMETER = .07000M RELATIVE ROUGHNESS = .0001140
CORE OUTER DIAMETER = .00635M RELATIVE ROUGHNESS = .0000200

TEST UNITS	SW0 GF	+WT GF	SW1 GF	P0 CM	FW1 KG	TIME SEC	TEMP DEGC
1	283.	3000.	200.	86.5	842.	66.9	20.4
2	283.	1500.	155.	54.5	839.	94.3	20.4
3	283.	500.	110.	36.5	817.	150.7	20.5
4	270.	200.	170.	25.2	840.	240.4	20.5
5	270.	100.	230.	21.2	682.	300.4	20.6
6	270.	2400.	285.	83.2	766.	69.3	20.8
7	270.	1900.	233.	76.2	694.	70.2	20.8
8	270.	1500.	123.	55.3	687.	76.3	20.8
9	270.	1200.	111.	50.7	582.	72.0	20.8
10	270.	1000.	189.	44.0	643.	90.1	20.8
11	270.	900.	211.	43.6	605.	90.3	20.8
12	270.	800.	236.	40.8	685.	112.3	20.8
13	270.	500.	212.	35.1	592.	120.1	20.8

14	270.	300.	189.	27.3	594.	150.3	20.8
15	270.	250.	195.	25.8	730.	200.6	20.9
16	270.	100.	112.	20.3	710.	225.8	20.9
17	270.	100.	194.	20.1	765.	300.3	20.9
18	220.	50.	156.	18.2	747.	362.7	21.1
19	220.	100.	199.	20.6	810.	382.4	21.1
20	220.	200.	209.	24.4	712.	250.0	21.1
21	220.	300.	138.	28.9	992.	251.0	21.1
22	220.	500.	293.	37.5	496.	120.3	21.1
23	220.	500.	141.	39.7	605.	122.5	21.2
24	220.	1200.	303.	50.0	657.	91.0	21.2
25	220.	2200.	309.	76.5	731.	70.6	21.2
26	220.	2600.	130.	81.0	765.	65.1	21.2
27	220.	800.	113.	43.6	592.	92.7	21.2
28	229.	200.	220.	24.8	768.	275.6	22.3
29	229.	200.	262.	26.7	709.	280.0	22.3
30	229.	300.	178.	29.5	582.	150.3	22.3

RESULT SHEET

RESULTS FOR:SLEEVE WALL SHEAR
SERIES 11 ALPHA = .091
SLEEVE INTERNAL DIAMETER = .07000M RELATIVE ROUGHNESS = .0001140
CORE OUTER DIAMETER = .00635M RELATIVE ROUGHNESS = .0000200

TEST UNITS	SLEEVE FORCE GF	SLEEVE SHEAR N/M2	BULK FLOW M3/S	BULK VEL M/S	RE	F2	KINEMATIC VISCOSITY M2/S
1	3095.9	21.852	.01259	3.298	210486.	.004019	.9972-06
2	1635.2	11.542	.00890	2.331	148795.	.004248	.9972-06
3	677.0	4.779	.00542	1.420	90884.	.004737	.9948-06
4	302.0	2.132	.00349	.915	58576.	.005087	.9948-06
5	141.3	.997	.00227	.595	38150.	.005637	.9924-06
6	2397.3	16.921	.01105	2.896	186631.	.004035	.9877-06
7	1948.1	13.750	.00980	2.590	166920.	.004099	.9877-06
8	1654.4	11.677	.00900	2.359	152027.	.004197	.9877-06
9	1365.5	9.638	.00808	2.118	136483.	.004298	.9877-06
10	1086.3	7.668	.00714	1.878	120496.	.004387	.9877-06
11	964.3	6.806	.00670	1.755	113124.	.004418	.9877-06
12	838.8	5.920	.00610	1.598	102991.	.004636	.9877-06
13	561.8	3.965	.00493	1.291	83227.	.004755	.9877-06
14	383.4	2.706	.00395	1.035	66729.	.005048	.9877-06
15	327.1	2.309	.00360	.944	60982.	.005181	.9853-06
16	259.1	1.829	.00314	.824	53218.	.005390	.9853-06
17	177.1	1.250	.00255	.667	43115.	.005612	.9853-06
18	114.7	.810	.00206	.540	35023.	.005563	.9807-06
19	122.2	.862	.00212	.555	36021.	.005600	.9807-06
20	212.9	1.502	.00285	.746	48431.	.005397	.9807-06
21	384.7	2.715	.00395	1.035	67208.	.005064	.9807-06
22	431.2	3.043	.00412	1.080	70113.	.005216	.9807-06
23	583.6	4.119	.00494	1.294	84184.	.004920	.9783-06
24	1123.4	7.929	.00722	1.892	123065.	.004432	.9783-06
25	2122.1	14.979	.01035	2.713	176492.	.004071	.9783-06
26	2701.9	19.071	.01175	3.079	200305.	.004024	.9783-06
27	912.3	6.439	.00639	1.673	108856.	.004600	.9783-06
28	210.9	1.489	.00279	.730	48743.	.005586	.9534-06
29	169.3	1.195	.00253	.663	44291.	.005429	.9534-06
30	353.8	2.497	.00387	1.015	67732.	.004852	.9534-06

DATA SHEET

DATA FOR :TOTAL WALL SHEAR
SERIES 11 ALPHA = .091
SLEEVE INTERNAL DIAMETER = .07000M RELATIVE ROUGHNESS = .0001140
CORE OUTER DIAMETER = .00635M RELATIVE ROUGHNESS = .0000220

TEST UNITS	P0 CM	P1 CM	P2 CM	P3 CM	P4 CM	P5 CM	FW1 KG	TIME SEC	TEMP DEGC
1	88.1	92.7	70.5	47.6	25.3	2.4	833.	65.1	20.6
2	77.6	80.3	61.3	42.0	22.9	3.7	761.	65.3	20.6
3	60.8	63.4	49.2	35.0	20.4	6.0	703.	70.5	20.6
4	48.9	43.3	36.7	29.7	23.0	16.1	606.	90.7	20.6
5	36.1	39.0	33.3	27.8	22.1	16.4	708.	128.2	20.6
6	33.0	37.2	32.4	27.5	22.8	17.4	821.	151.8	20.6
7	32.9	36.2	31.9	27.0	22.9	18.3	789.	150.6	20.6
8	30.1	33.8	30.2	26.5	23.0	19.6	828.	160.2	20.7
9	29.6	32.5	29.4	26.4	23.3	20.4	791.	189.5	20.7
10	27.7	31.9	29.3	26.2	23.3	20.7	836.	210.7	20.7
11	26.8	30.8	28.2	25.7	23.1	20.6	796.	211.1	20.7
12	26.2	30.0	27.8	25.7	23.5	21.4	728.	215.3	20.7
13	26.0	30.1	28.0	25.8	23.6	21.7	840.	250.5	20.7
14	25.9	29.6	27.7	26.2	24.4	22.8	739.	253.4	20.8

15	24.8	28.5	27.3	26.2	25.1	23.9	719.	300.6	20.8
16	23.1	27.1	26.4	25.7	24.9	24.4	567.	300.9	20.8
17	23.5	28.5	27.4	26.3	25.1	24.8	713.	300.1	20.8
18	82.2	89.5	66.5	44.3	22.9	2.7	776.	62.1	20.4
19	73.2	76.9	58.0	39.5	21.4	4.3	799.	70.4	20.4
20	45.8	50.4	41.0	31.6	22.3	13.6	873.	110.8	20.4
21	33.0	37.0	32.0	26.9	22.3	18.0	808.	150.3	20.4
22	25.0	29.8	27.8	26.6	25.2	23.9	659.	240.5	20.5
23	28.0	31.2	28.0	25.6	22.0	19.2	755.	180.4	20.6
24	23.0	27.1	26.3	25.5	24.7	23.9	410.	210.3	20.6

RESULT SHEET

RESULTS FOR:TOTAL WALL SHEAR
SERIES 11 ALPHA = .091
SLEEVE INTERNAL DIAMETER = .07000M RELATIVE ROUGHNESS = .0001140
CORE OUTER DIAMETER = .06350M RELATIVE ROUGHNESS = .0000200

TEST UNITS	TOTAL FORCE GF	TOTAL SHEAR N/M2	BULK FLOW M3/S	BULK VEL M/S	RE	FT	KINEMATIC VISCOSITY M2/S
1	3584.5	23.197	.01280	3.352	215020.	.004128	.9924-06
2	3041.6	19.683	.01165	3.053	195833.	.004223	.9924-06
3	2279.6	14.752	.00997	2.613	167564.	.004323	.9924-06
4	1081.1	6.996	.00668	1.751	112274.	.004566	.9924-06
5	895.3	5.794	.00589	1.543	98979.	.004866	.9924-06
6	781.0	5.054	.00541	1.417	90884.	.005034	.9924-06
7	711.2	4.602	.00524	1.373	88037.	.004885	.9924-06
8	565.2	3.657	.00459	1.204	77398.	.005047	.9900-06
9	481.0	3.113	.00417	1.094	70310.	.005205	.9900-06
10	450.9	2.918	.00397	1.040	66833.	.005400	.9900-06
11	404.8	2.620	.00377	.988	63515.	.005368	.9900-06
12	341.3	2.209	.00338	.886	56956.	.005629	.9900-06
13	336.6	2.178	.00335	.879	56484.	.005643	.9900-06
14	268.3	1.736	.00292	.764	49241.	.005948	.9877-06
15	181.0	1.171	.00239	.627	40386.	.005964	.9877-06
16	109.5	.709	.00188	.494	31816.	.005817	.9877-06
17	179.4	1.161	.00238	.622	40115.	.005992	.9877-06
18	3448.2	22.315	.01253	3.274	208981.	.004164	.9972-06
19	2886.2	18.677	.01135	2.974	189866.	.004225	.9972-06
20	1465.3	9.482	.00788	2.064	131768.	.004450	.9972-06
21	757.3	4.901	.00538	1.408	89906.	.004941	.9972-06
22	228.6	1.480	.00274	.718	45935.	.005741	.9948-06
23	476.3	3.082	.00419	1.097	70328.	.005127	.9924-06
24	127.0	.822	.00195	.511	32761.	.006300	.9924-06

DATA SHEET

DATA FOR :CORE WALL SHEAR
SERIES 11 ALPHA = .091
SLEEVE INTERNAL DIAMETER = .07000M RELATIVE ROUGHNESS = .0001140
CORE OUTER DIAMETER = .06350M RELATIVE ROUGHNESS = .0000200

TEST	RE	FT	F2
1	30000.	.006450	.006140
2	35000.	.006240	.005890
3	40000.	.006040	.005690
4	45000.	.005880	.005540
5	50000.	.005720	.005410
6	55000.	.005570	.005280
7	60000.	.005470	.005170
8	65000.	.005380	.005090
9	70000.	.005280	.005010
10	75000.	.005180	.004910
11	80000.	.005110	.004850
12	85000.	.005040	.004790
13	90000.	.004980	.004740
14	95000.	.004930	.004700
15	100000.	.004850	.004640
16	120000.	.004660	.004460
17	140000.	.004500	.004320
18	160000.	.004360	.004190
19	180000.	.004270	.004110
20	200000.	.004180	.004030

RESULT SHEET

RESULTS FOR:CORE WALL SHEAR
SERIES 11 ALPHA = .091
SLEEVE INTERNAL DIAMETER = .07000M RELATIVE ROUGHNESS = .0001140
CORE OUTER DIAMETER = .06635M RELATIVE ROUGHNESS = .0000200

TEST UNITS	TOTAL FORCE N	SLEEVE FORCE N	CORE FORCE N	CORE SHEAR N/M2	RE	F1
1	1.213	1.059	.154	1.225	30000.	.009867
2	1.598	1.383	.215	1.706	35000.	.010098
3	2.020	1.745	.275	2.184	40000.	.009808
4	2.489	2.150	.339	2.688	45000.	.009628
5	2.989	2.592	.397	3.150	50000.	.009137
6	3.522	3.061	.461	3.657	55000.	.008767
7	4.116	3.567	.549	4.357	60000.	.008777
8	4.751	4.121	.630	4.997	65000.	.008577
9	5.408	4.705	.703	5.578	70000.	.008256
10	6.090	5.293	.798	6.326	75000.	.008156
11	6.836	5.949	.887	7.039	80000.	.007976
12	7.611	6.632	.979	7.767	85000.	.007796
13	8.432	7.358	1.074	8.517	90000.	.007626
14	9.300	8.129	1.171	9.290	95000.	.007465
15	10.138	8.892	1.246	9.880	100000.	.007165
16	14.026	12.308	1.718	13.630	120000.	.006865
17	18.436	16.227	2.209	17.524	140000.	.006484
18	23.331	20.556	2.774	22.005	160000.	.006234
19	28.918	25.520	3.399	26.956	180000.	.006034
20	34.949	30.892	4.057	32.175	200000.	.005834

ANALYSIS SHEET

SERIES 11 ALPHA = .091
SLEEVE INTERNAL DIAMETER = .07000M RELATIVE ROUGHNESS = .0001140
CORE OUTER DIAMETER = .06635M RELATIVE ROUGHNESS = .0000200

TEST	TOR1 / TORT	TOR2 / TORT	TOR2 / TOR1	TOR1 N/M2	TOR2 N/M2	TORT N/M2	R0 / R2	RE
1	1.530	.952	.622	1.225	.762	.800	.367	30000.
2	1.618	.944	.583	1.706	.995	1.054	.376	35000.
3	1.639	.942	.575	2.184	1.255	1.333	.379	40000.
4	1.637	.942	.575	2.688	1.547	1.642	.379	45000.
5	1.597	.946	.592	3.150	1.865	1.972	.374	50000.
6	1.574	.948	.602	3.657	2.202	2.323	.372	55000.
7	1.605	.945	.589	4.357	2.566	2.715	.375	60000.
8	1.594	.946	.593	4.997	2.965	3.134	.374	65000.
9	1.564	.949	.607	5.578	3.385	3.567	.370	70000.
10	1.575	.948	.602	6.326	3.808	4.018	.372	75000.
11	1.561	.949	.608	7.039	4.280	4.509	.370	80000.
12	1.547	.950	.614	7.767	4.772	5.021	.369	85000.
13	1.531	.952	.622	8.517	5.294	5.562	.367	90000.
14	1.514	.953	.630	9.290	5.849	6.135	.365	95000.
15	1.477	.957	.648	9.880	6.398	6.688	.361	100000.
16	1.473	.957	.650	13.630	8.856	9.253	.360	120000.
17	1.441	.960	.666	17.524	11.675	12.162	.356	140000.
18	1.430	.961	.672	22.005	14.790	15.390	.355	160000.
19	1.413	.963	.681	26.956	18.362	19.076	.353	180000.
20	1.396	.964	.691	32.175	22.227	23.055	.351	200000.

DATA SHEET

DATA FOR :SLEEVE WALL SHEAR
SERIES 12 ALPHA = .226
SLEEVE INTERNAL DIAMETER = .07000M RELATIVE ROUGHNESS = .0001140
CORE OUTER DIAMETER = .01585M RELATIVE ROUGHNESS = .0000160

TEST UNITS	SW0 GF	+WT GF	SW1 GF	P0 CM	FW1 KG	TIME SEC	TEMP DEGC
1	148.	3200.	200.	107.9	834.	67.5	21.1
2	159.	3200.	215.	107.8	832.	67.7	21.2
3	159.	2500.	179.	86.2	811.	74.4	21.2
4	159.	1500.	136.	61.1	826.	97.5	21.2
5	159.	500.	85.	37.7	733.	141.7	21.2
6	159.	200.	77.	25.8	516.	135.1	21.2
7	159.	2000.	267.	69.1	731.	76.6	21.7
8	159.	300.	112.	27.1	778.	182.7	21.7
9	186.	300.	207.	28.5	641.	169.8	21.9
10	186.	150.	124.	20.7	398.	116.0	21.9
11	186.	50.	137.	21.4	299.	110.9	21.9
12	186.	0.	84.	20.6	542.	199.1	22.0
13	169.	2000.	250.	69.3	744.	78.0	21.9

14	169.	500.	233.	31.2	624.	135.5	21.9
15	169.	300.	259.	24.1	593.	173.0	21.9
16	169.	200.	226.	24.7	490.	162.7	21.9
17	169.	100.	216.	21.1	390.	164.8	21.9
18	169.	150.	216.	23.7	450.	165.8	21.9
19	169.	50.	232.	18.0	342.	193.1	21.9
20	169.	80.	264.	19.8	346.	198.1	21.9
21	175.	200.	226.	21.9	391.	128.5	21.9
22	175.	100.	222.	22.2	438.	186.6	21.9
23	175.	50.	219.	18.3	465.	241.0	21.9
24	230.	1050.	119.	80.2	777.	105.3	21.6
25	230.	900.	111.	76.3	825.	119.6	21.6
26	230.	750.	129.	70.2	825.	138.2	21.6
27	230.	600.	183.	65.9	833.	149.8	21.6
28	230.	500.	174.	50.6	869.	169.2	21.6
29	230.	300.	128.	45.3	759.	170.3	21.6
30	230.	1500.	227.	99.8	760.	90.2	21.6
31	230.	1750.	250.	110.2	787.	86.6	21.6
32	220.	300.	205.	29.8	804.	200.3	21.9

RESULT SHEET

RESULTS FOR:SLEEVE WALL SHEAR
SERIES 12 ALPHA = .226
SLEEVE INTERNAL DIAMETER = .07000M RELATIVE ROUGHNESS = .0001140
CORE OUTER DIAMETER = .01585M RELATIVE ROUGHNESS = .0000160

TEST	SLEEVE FORCE	SLEEVE SHEAR	BULK FLOW	BULK VEL	RE	F2	KINEMATIC VISCOSITY
UNITS	GF	N/M2	M3/S	M/S			M2/S
1	3277.2	23.132	.01236	3.384	186859.	.004040	.9807-06
2	3273.2	23.103	.01229	3.366	186301.	.004078	.9783-06
3	2605.7	18.392	.01090	2.986	165245.	.004127	.9783-06
4	1643.9	11.603	.00847	2.320	128427.	.004310	.9783-06
5	690.7	4.875	.00517	1.417	78418.	.004858	.9783-06
6	396.6	2.799	.00382	1.046	57900.	.005116	.9783-06
7	2014.3	14.218	.00954	2.614	146383.	.004162	.9669-06
8	461.8	3.260	.00426	1.166	65320.	.004793	.9669-06
9	394.1	2.781	.00378	1.034	58178.	.005204	.9623-06
10	327.1	2.309	.00343	.940	52877.	.005229	.9623-06
11	212.8	1.502	.00270	.738	41551.	.005509	.9623-06
12	215.7	1.522	.00272	.746	42052.	.005477	.9601-06
13	2041.3	14.408	.00954	2.612	147001.	.004222	.9623-06
14	551.5	3.893	.00461	1.261	70972.	.004894	.9623-06
15	324.3	2.289	.00343	.939	52826.	.005194	.9623-06
16	257.4	1.817	.00301	.825	46414.	.005340	.9623-06
17	166.7	1.177	.00237	.648	36471.	.005603	.9623-06
18	217.2	1.533	.00271	.743	41820.	.005549	.9623-06
19	100.2	.707	.00177	.485	27295.	.006011	.9623-06
20	98.5	.695	.00175	.478	26917.	.006077	.9623-06
21	262.9	1.856	.00304	.833	46894.	.005343	.9623-06
22	166.9	1.178	.00235	.643	36175.	.005702	.9623-06
23	119.3	.842	.00193	.528	29736.	.006028	.9623-06
24	1285.3	9.072	.00738	2.021	112921.	.004442	.9691-06
25	1142.6	8.065	.00690	1.889	105561.	.004519	.9691-06
26	973.5	6.871	.00634	1.735	96967.	.004563	.9691-06
27	768.7	5.426	.00556	1.523	85097.	.004678	.9691-06
28	675.0	4.764	.00514	1.407	78596.	.004816	.9691-06
29	520.1	3.671	.00446	1.221	68204.	.004927	.9691-06
30	1630.8	11.511	.00843	2.308	128940.	.004323	.9691-06
31	1859.6	13.126	.00909	2.489	139072.	.004237	.9691-06
32	430.3	3.037	.00401	1.099	61861.	.005026	.9623-06

DATA SHEET

DATA FOR :TOTAL WALL SHEAR
SERIES 12 ALPHA = .226
SLEEVE INTERNAL DIAMETER = .07000M RELATIVE ROUGHNESS = .0001140
CORE OUTER DIAMETER = .01585M RELATIVE ROUGHNESS = .0000160

TEST	P0	P1	P2	P3	P4	P5	FW1	TIME	TEMP
UNITS	CM	CM	CM	CM	CM	CM	KG	SEC	DEGC
1	125.8	109.1	80.9	53.6	26.5	.1	746.	61.0	21.8
2	86.4	89.5	67.9	46.7	25.6	4.8	657.	61.2	21.8
3	34.4	37.8	32.6	27.3	22.0	17.2	585.	120.0	21.8
4	22.4	25.6	24.1	22.3	20.8	18.6	548.	212.3	21.9
5	43.2	46.4	38.5	30.6	23.3	15.4	773.	125.1	21.9
6	65.5	68.5	53.8	37.5	22.3	7.2	816.	90.9	22.5
7	28.0	31.2	27.5	24.0	20.5	16.9	707.	197.6	22.5
8	41.9	44.9	36.9	29.8	21.2	13.4	975.	156.8	22.5
9	104.1	108.8	79.9	52.3	25.8	.8	816.	66.5	21.9
10	27.0	30.4	26.8	23.3	19.9	16.5	707.	181.7	21.9
11	44.3	47.6	38.5	29.8	21.0	12.1	811.	122.1	21.9

12	77.2	80.0	61.0	41.4	22.2	3.7	985.	92.7	21.9
13	108.5	111.1	82.2	55.1	29.3	3.3	829.	67.5	21.9
14	28.6	31.9	28.2	24.6	20.5	16.9	724.	178.9	21.6
15	142.7	149.6	119.9	90.7	62.6	34.9	921.	74.1	17.5
16	137.8	140.9	114.7	88.8	62.8	37.8	933.	79.8	17.8
17	132.5	132.9	109.8	85.6	62.6	39.9	928.	83.3	17.6
18	130.5	131.2	108.2	86.8	65.3	43.9	928.	86.3	17.6
19	109.5	108.8	93.0	77.3	61.9	46.5	957.	107.6	17.7
20	101.4	101.0	87.6	73.5	60.0	46.8	954.	115.5	17.8
21	82.9	81.8	73.5	64.9	56.8	48.6	960.	153.5	17.8
22	106.7	107.2	91.7	75.7	60.7	45.4	970.	108.7	17.7
23	117.3	117.8	99.0	79.3	61.9	43.6	963.	98.0	17.8
24	48.1	47.6	45.9	44.2	42.0	40.2	325.	120.3	18.0
25	54.0	53.1	50.6	47.1	44.3	42.2	401.	119.3	18.0
26	57.4	56.7	53.1	49.5	45.5	42.5	418.	107.9	18.0
27	63.3	62.4	57.4	52.5	47.8	42.8	519.	110.2	21.9
28	51.0	50.3	47.8	45.2	43.0	41.8	702.	240.1	21.9
29	137.6	134.7	113.1	92.0	71.6	50.6	879.	82.2	21.9

RESULT SHEET

RESULTS FOR:TOTAL WALL SHEAR
SERIES 12 ALPHA = .226
SLEEVE INTERNAL DIAMETER = .07000M RELATIVE ROUGHNESS = .0001140
CORE OUTER DIAMETER = .01585M RELATIVE ROUGHNESS = .0000160

TEST UNITS	TOTAL FORCE GF	TOTAL SHEAR N/M2	BULK FLOW M3/S	BULK VEL M/S	RE	FT	KINEMATIC VISCOSITY M2/S
1	4136.8	23.808	.01223	3.350	180032.	.004244	.9646-06
2	3214.9	18.503	.01074	2.940	165058.	.004280	.9646-06
3	786.7	4.527	.00487	1.335	74954.	.005079	.9646-06
4	262.7	1.512	.00258	.707	39781.	.006050	.9623-06
5	1176.9	6.774	.00618	1.692	95228.	.004730	.9623-06
6	2328.0	13.398	.00898	2.459	140296.	.004433	.9490-06
7	540.6	3.111	.00391	1.072	61182.	.005413	.9490-06
8	1195.1	6.878	.00622	1.703	97180.	.004743	.9490-06
9	4101.9	23.607	.01227	3.361	189108.	.004180	.9623-06
10	527.0	3.033	.00389	1.066	59966.	.005341	.9623-06
11	1344.0	7.735	.00664	1.819	102364.	.004674	.9623-06
12	2906.6	16.728	.01019	2.792	157106.	.004292	.9623-06
13	4077.6	23.468	.01227	3.360	189046.	.004158	.9623-06
14	572.5	3.295	.00405	1.108	61931.	.005364	.9691-06
15	4354.0	25.058	.01244	3.406	172270.	.004320	.1071-05
16	3919.6	22.558	.01169	3.203	163199.	.004399	.1063-05
17	3541.4	20.382	.01114	3.050	154645.	.004382	.1068-05
18	3303.0	19.010	.01076	2.947	149414.	.004378	.1068-05
19	2364.5	13.608	.00889	2.436	123838.	.004596	.1065-05
20	2065.3	11.886	.00826	2.262	115245.	.004648	.1063-05
21	1262.0	7.263	.00625	1.712	87252.	.004955	.1063-05
22	2347.8	13.512	.00892	2.444	124224.	.004525	.1065-05
23	2817.1	16.213	.00983	2.692	137206.	.004473	.1063-05
24	284.0	1.634	.00270	.739	37948.	.005985	.1057-05
25	426.8	2.456	.00336	.921	47171.	.005790	.1057-05
26	546.7	3.147	.00387	1.061	54313.	.005595	.1057-05
27	741.1	4.265	.00471	1.290	72582.	.005127	.9623-06
28	331.1	1.906	.00292	.801	45072.	.005940	.9623-06
29	3184.5	18.328	.01076	2.930	164857.	.004270	.9623-06

DATA SHEET

DATA FOR :CORE WALL SHEAR
SERIES 12 ALPHA = .226
SLEEVE INTERNAL DIAMETER = .07000M RELATIVE ROUGHNESS = .0001140
CORE OUTER DIAMETER = .01585M RELATIVE ROUGHNESS = .0000160

TEST	RE	FT	F2
1	30000.	.006350	.005930
2	35000.	.006130	.005730
3	40000.	.005950	.005570
4	45000.	.005800	.005430
5	50000.	.005640	.005300
6	55000.	.005530	.005200
7	60000.	.005400	.005090
8	65000.	.005300	.005010
9	70000.	.005210	.004940
10	75000.	.005100	.004800
11	80000.	.005030	.004810
12	85000.	.004920	.004750
13	90000.	.004900	.004700
14	95000.	.004820	.004640
15	100000.	.004770	.004590

16	120000.	.004570	.004430
17	140000.	.004400	.004290
18	160000.	.004270	.004180
19	180000.	.004150	.004080

RESULT SHEET

RESULTS FOR:CORE WALL SHEAR
SERIES 12 ALPHA = .226
SLEEVE INTERNAL DIAMETER = .07000M RELATIVE ROUGHNESS = .0001140
CORE OUTER DIAMETER = .01585M RELATIVE ROUGHNESS = .0000160

TEST UNITS	TOTAL FORCE N	SLEEVE FORCE N	CORE FORCE N	CORE SHEAR N/M2	RE	F1
1	1.856	1.413	.443	1.407	30000.	.008205
2	2.439	1.859	.580	1.843	35000.	.007897
3	3.091	2.360	.732	2.325	40000.	.007628
4	3.814	2.911	.903	2.868	45000.	.007434
5	4.579	3.508	1.070	3.401	50000.	.007142
6	5.432	4.165	1.267	4.027	55000.	.006987
7	6.313	4.852	1.461	4.643	60000.	.006769
8	7.272	5.605	1.667	5.297	65000.	.006581
9	8.290	6.409	1.881	5.977	70000.	.006402
10	9.316	7.268	2.048	6.507	75000.	.006072
11	10.454	8.151	2.303	7.318	80000.	.006002
12	11.661	9.087	2.574	8.178	85000.	.005942
13	12.889	10.080	2.809	8.924	90000.	.005783
14	14.126	11.088	3.038	9.654	95000	.005615
15	15.490	12.153	3.336	10.602	100000.	.005565
16	21.370	16.891	4.479	14.233	120000.	.005188
17	28.005	22.264	5.741	18.244	140000.	.004886
18	35.497	28.334	7.164	22.764	160000.	.004667
19	43.664	35.002	8.662	27.525	180000.	.004459

ANALYSIS SHEET

SERIES 12 ALPHA = .226
SLEEVE INTERNAL DIAMETER = .07000M RELATIVE ROUGHNESS = .0001140
CORE OUTER DIAMETER = .01585M RELATIVE ROUGHNESS = .0000160

TEST	TOR1 / TORT	TOR2 / TORT	TOR2 / TOR1	TOR1 N/M2	TOR2 N/M2	TORT N/M2	B0 / B2	RE
1	1.292	.934	.723	1.407	1.017	1.089	.527	30000.
2	1.288	.935	.726	1.843	1.337	1.431	.526	35000.
3	1.282	.936	.730	2.325	1.698	1.814	.525	40000.
4	1.282	.936	.730	2.868	2.095	2.238	.525	45000.
5	1.266	.940	.742	3.401	2.524	2.686	.523	50000.
6	1.264	.940	.744	4.027	2.997	3.187	.522	55000.
7	1.254	.943	.752	4.643	3.491	3.704	.520	60000.
8	1.242	.945	.761	5.297	4.033	4.266	.518	65000.
9	1.229	.948	.772	5.977	4.612	4.864	.516	70000.
10	1.191	.957	.804	6.507	5.230	5.465	.510	75000.
11	1.193	.956	.801	7.318	5.865	6.133	.510	80000.
12	1.195	.956	.799	8.178	6.538	6.841	.511	85000.
13	1.180	.959	.813	8.924	7.253	7.561	.508	90000.
14	1.165	.963	.826	9.654	7.978	8.287	.505	95000.
15	1.167	.962	.825	10.602	8.745	9.087	.506	100000.
16	1.135	.969	.854	14.233	12.153	12.537	.500	120000.
17	1.110	.975	.878	18.244	16.019	16.430	.496	140000.
18	1.093	.979	.896	22.764	20.386	20.825	.493	160000.
19	1.074	.983	.915	27.525	25.184	25.616	.489	180000.

DATA SHEET

DATA FOR :SLEEVE WALL SHEAR
SERIES 13 ALPHA = .363
SLEEVE INTERNAL DIAMETER = .07000M RELATIVE ROUGHNESS = .0001140
CORE OUTER DIAMETER = .02540M RELATIVE ROUGHNESS = .0000100

TEST UNITS	SW0 GF	+WT GF	SW1 GF	P0 CM	FW1 KG	TIME SEC	TEMP DEGC
1	235.	50.	270.	19.1	745.	401.2	22.3
2	235.	150.	186.	26.7	912.	300.5	22.3
3	235.	200.	260.	24.4	650.	226.6	22.3
4	235.	500.	151.	41.3	564.	119.3	22.3
5	235.	700.	230.	44.4	634.	122.9	22.3
6	235.	900.	271.	52.9	627.	109.8	22.3
7	235.	1300.	242.	69.7	737.	105.6	22.3

8	235.	1400.	225.	72.1	769.	105.4	22.3
9	235.	1900.	151.	88.1	916.	105.3	22.4
10	235.	2600.	232.	112.3	963.	88.6	22.4
11	235.	3100.	241.	131.5	935.	85.1	22.4
12	235.	300.	182.	35.6	859.	226.6	22.4
13	235.	800.	266.	45.2	949.	175.5	22.4
14	235.	1500.	273.	76.6	868.	116.4	22.4
15	228.	3330.	275.	135.9	818.	72.4	22.3
16	228.	2300.	260.	99.2	842.	90.1	22.2
17	228.	1000.	177.	58.8	864.	137.6	22.2
18	228.	500.	234.	36.6	896.	203.6	22.3
19	228.	250.	221.	29.6	870.	258.5	22.4
20	228.	150.	246.	26.8	816.	302.5	22.4
21	206.	2900.	300.	88.3	770.	90.4	20.8
22	206.	400.	188.	36.5	512.	125.5	20.8
23	206.	300.	211.	29.6	844.	240.4	20.8
24	206.	200.	225.	25.5	879.	300.6	20.8
25	206.	150.	240.	23.6	928.	360.6	20.8
26	206.	100.	237.	22.4	693.	306.3	20.9
27	206.	50.	264.	18.4	814.	485.8	21.1

RESULT SHEET

RESULTS FOR:SLEEVE WALL SHEAR
SERIES 13 ALPHA = .363
SLEEVE INTERNAL DIAMETER = .07000M RELATIVE ROUGHNESS = .0001140
CORE OUTER DIAMETER = .02540M RELATIVE ROUGHNESS = .0000100

TEST	SLEEVE FORCE	SLEEVE SHEAR	BULK FLOW	BULK VEL	RE	F2	KINEMATIC VISCOSITY
UNITS	GF	N/M2	M3/S	M/S			M2/S
1	128.4	.906	.00196	.556	25995.	.005870	.9534-06
2	313.7	2.215	.00303	.908	42486.	.005370	.9534-06
3	281.3	1.986	.00287	.858	40155.	.005390	.9534-06
4	701.3	4.950	.00473	1.415	66180.	.004947	.9534-06
5	822.9	5.808	.00516	1.544	72215.	.004875	.9534-06
6	983.4	6.941	.00571	1.709	79939.	.004754	.9534-06
7	1415.4	9.990	.00698	2.088	97700.	.004581	.9534-06
8	1532.8	10.819	.00730	2.183	102136.	.004539	.9534-06
9	2189.7	14.891	.00870	2.603	122059.	.004395	.9512-06
10	2733.0	19.290	.01087	3.253	152509.	.003647	.9512-06
11	3227.4	22.780	.01029	3.288	154164.	.004215	.9512-06
12	469.3	3.313	.00379	1.134	53191.	.005149	.9512-06
13	887.0	6.261	.00541	1.618	75874.	.004782	.9512-06
14	1585.6	11.192	.00746	2.231	104633.	.004495	.9512-06
15	3417.2	24.120	.01130	3.381	158163.	.004220	.9534-06
16	2395.7	16.909	.00935	2.796	130517.	.004324	.9556-06
17	1171.3	8.268	.00628	1.879	87695.	.004683	.9556-06
18	610.5	4.309	.00440	1.317	61606.	.004969	.9534-06
19	372.3	2.628	.00337	1.007	47224.	.005181	.9512-06
20	246.8	1.742	.00270	.807	37850.	.005346	.9512-06
21	2031.7	14.341	.00852	2.549	115099.	.004415	.9877-06
22	534.5	3.773	.00408	1.221	55128.	.005063	.9877-06
23	410.3	2.896	.00351	1.051	47441.	.005247	.9877-06
24	295.5	2.086	.00292	.875	39514.	.005449	.9877-06
25	230.2	1.625	.00257	.770	34775.	.005479	.9877-06
26	183.8	1.292	.00226	.677	30646.	.005635	.9853-06
27	105.3	.743	.00168	.501	22804.	.005911	.9807-06

DATA SHEET

DATA FOR :TOTAL WALL SHEAR
SERIES 13 ALPHA = .363
SLEEVE INTERNAL DIAMETER = .07000M RELATIVE ROUGHNESS = .0001140
CORE OUTER DIAMETER = .02540M RELATIVE ROUGHNESS = .0000100

TEST	P0	P1	P2	P3	P4	P5	FW1	TIME	TEMP
UNITS	CM	CM	CM	CM	CM	CM	KG	SEC	DEGC
1	46.0	47.7	40.0	31.4	23.3	15.3	668.	132.9	22.3
2	32.2	35.3	31.4	27.5	23.6	19.9	400.	121.1	22.3
3	118.0	121.0	91.6	61.7	31.9	2.7	832.	80.0	21.9
4	127.1	129.2	96.8	64.7	33.0	1.9	761.	70.4	22.3
5	26.3	27.9	26.0	24.3	22.5	20.7	685.	324.0	22.3
6	26.4	27.9	25.7	23.6	21.4	19.3	704.	300.3	22.3
7	25.2	27.4	25.3	23.1	21.0	18.9	664.	283.6	22.3
8	30.0	31.3	28.2	25.1	22.1	19.0	813.	282.5	22.3
9	30.2	33.6	29.8	26.2	22.5	18.8	798.	250.0	22.3
10	44.5	46.4	39.3	32.0	24.8	17.8	750.	161.1	22.3
11	37.7	39.5	34.2	28.8	23.4	18.4	632.	160.2	22.3
12	58.3	59.5	43.3	33.7	24.4	15.3	668.	123.3	22.3
13	62.1	64.6	51.7	38.5	25.4	12.6	668.	100.9	22.3
14	71.8	74.1	58.3	42.1	26.1	10.2	711.	97.1	22.3
15	78.5	81.0	63.5	45.4	27.7	10.2	707.	90.9	22.3

16	93.8	96.4	74.8	52.2	30.2	8.4	796.	98.2	22.8
17	107.2	110.9	84.5	57.5	31.0	4.7	815.	83.4	21.9
18	130.1	140.3	105.8	70.6	35.8	1.3	743.	65.5	21.9
19	112.2	115.3	87.4	59.8	30.6	2.9	707.	70.1	21.9
20	103.2	106.6	81.7	56.6	30.6	5.6	716.	75.5	21.9
21	66.1	67.7	54.8	39.8	25.9	12.2	689.	101.2	21.9
22	58.8	61.2	49.5	37.1	25.1	13.3	787.	125.6	21.9
23	45.9	48.8	39.8	31.2	22.9	14.6	685.	133.6	21.9

RESULT SHEET

RESULTS FOR:TOTAL WALL SHEAR
SERIES 13 ALPHA = .363
SLEEVE INTERNAL DIAMETER = .07000M RELATIVE ROUGHNESS = .0001140
CORE OUTER DIAMETER = .02540M RELATIVE ROUGHNESS = .0000100

TEST	TOTAL FORCE	TOTAL SHEAR	BULK FLOW	BULK VEL	RE	FT	KINEMATIC VISCOSITY
UNITS	GF	N/M2	M3/S	M/S			M2/S
1	1132.8	5.867	.00503	1.504	70363.	.005186	.9534-06
2	536.5	2.779	.00330	.988	46239.	.005688	.9534-06
3	4118.3	21.329	.01040	3.112	144234.	.004404	.9623-06
4	4425.6	22.920	.01081	3.235	151322.	.004381	.9534-06
5	248.8	1.289	.00211	.633	29596.	.006438	.9534-06
6	298.8	1.548	.00234	.702	32818.	.006290	.9534-06
7	296.1	1.533	.00234	.701	32776.	.006247	.9534-06
8	426.7	2.210	.00288	.861	40287.	.005960	.9534-06
9	512.9	2.656	.00319	.955	44684.	.005823	.9534-06
10	996.6	5.161	.00466	1.393	65171.	.005319	.9534-06
11	736.7	3.815	.00395	1.181	55226.	.005475	.9534-06
12	1296.8	6.716	.00542	1.621	75841.	.005111	.9534-06
13	1811.1	9.380	.00662	1.981	92678.	.004780	.9534-06
14	2223.9	11.518	.00732	2.191	102504.	.004798	.9534-06
15	2465.7	12.770	.00778	2.327	108880.	.004715	.9534-06
16	3066.1	15.880	.00882	2.641	124979.	.004554	.9424-06
17	3695.8	19.141	.00977	2.924	135527.	.004477	.9623-06
18	4836.9	25.051	.01134	3.394	157319.	.004348	.9623-06
19	3914.0	20.271	.01009	3.018	139873.	.004451	.9623-06
20	3517.9	18.219	.00948	2.838	131522.	.004525	.9623-06
21	1933.4	10.013	.00681	2.037	94422.	.004825	.9623-06
22	1670.7	8.653	.00627	1.875	86900.	.004922	.9623-06
23	1163.4	6.025	.00513	1.534	71108.	.005119	.9623-06

DATA SHEET

DATA FOR :CORE WALL SHEAR
SERIES 13 ALPHA = .363
SLEEVE INTERNAL DIAMETER = .07000M RELATIVE ROUGHNESS = .0001140
CORE OUTER DIAMETER = .02540M RELATIVE ROUGHNESS = .0000100

TEST	RE	FT	F2
1	30000.	.006400	.005700
2	35000.	.006170	.005560
3	40000.	.005980	.005430
4	45000.	.005810	.005320
5	50000.	.005630	.005220
6	55000.	.005500	.005130
7	60000.	.005400	.005040
8	65000.	.005300	.004980
9	70000.	.005200	.004900
10	75000.	.005100	.004820
11	80000.	.005020	.004780
12	85000.	.004950	.004720
13	90000.	.004900	.004680
14	95000.	.004820	.004630
15	100000.	.004780	.004580
16	120000.	.004580	.004420
17	140000.	.004430	.004310
18	160000.	.004320	.004290

RESULT SHEET

RESULTS FOR:CORE WALL SHEAR
SERIES 13 ALPHA = .363
SLEEVE INTERNAL DIAMETER = .07000M RELATIVE ROUGHNESS = .0001140
CORE OUTER DIAMETER = .02540M RELATIVE ROUGHNESS = .0000100

TEST	TOTAL FORCE	SLEEVE FORCE	CORE FORCE	CORE SHEAR	RE	F1
UNITS	N	N	N	N/M2		
1	3.864	2.002	1.962	2.105	30000.	.008329

2	4.021	2.658	1.362	2.701	35000.	.003051
3	5.090	3.391	1.699	3.368	40000.	.002496
4	6.258	4.205	2.054	4.072	45000.	.002160
5	7.487	5.094	2.393	4.746	50000.	.001960
6	8.850	6.057	2.793	5.539	55000.	.001820
7	10.341	7.082	3.259	6.462	60000.	.001692
8	11.912	8.212	3.699	7.335	65000.	.001582
9	13.554	9.371	4.182	8.293	70000.	.001427
10	15.260	10.582	4.678	9.275	75000.	.001272
11	17.090	11.941	5.150	10.211	80000.	.001081
12	19.024	13.311	5.714	11.330	85000.	.000984
13	21.113	14.796	6.317	12.525	90000.	.000906
14	23.140	16.310	6.830	13.544	95000.	.000844
15	25.427	17.876	7.550	14.972	100000.	.000831
16	35.083	24.843	10.240	20.305	125000.	.000821
17	46.188	32.972	13.215	26.205	140000.	.000761
18	58.829	42.866	15.963	31.652	160000.	.000603

ANALYSIS SHEET

SERIES 13 ALPHA = .363
SLEEVE INTERNAL DIAMETER = .07000M RELATIVE ROUGHNESS = .0001140
CORE OUTER DIAMETER = .02540M RELATIVE ROUGHNESS = .0000100

TEST	TOR1/TORT	TOR2/TORT	TOR2/TOR1	TOR1 N/M2	TOR2 N/M2	TORT N/M2	R0/R2	RE
1	1.301	.891	.684	2.105	1.441	1.618	.658	30000.
2	1.272	.901	.708	2.701	1.913	2.123	.653	35000.
3	1.253	.908	.724	3.368	2.440	2.687	.649	40000.
4	1.232	.916	.743	4.072	3.025	3.304	.645	45000.
5	1.201	.927	.772	4.746	3.665	3.953	.640	50000.
6	1.185	.933	.787	5.539	4.358	4.672	.637	55000.
7	1.184	.933	.788	6.462	5.095	5.459	.637	60000.
8	1.166	.940	.806	7.335	5.909	6.289	.634	65000.
9	1.159	.942	.813	8.293	6.743	7.156	.632	70000.
10	1.151	.945	.821	9.275	7.614	8.056	.631	75000.
11	1.132	.952	.841	10.211	8.591	9.023	.627	80000.
12	1.128	.954	.845	11.330	9.577	10.044	.626	85000.
13	1.124	.955	.850	12.525	10.646	11.146	.626	90000.
14	1.109	.961	.866	13.544	11.735	12.216	.623	95000.
15	1.115	.958	.859	14.972	12.862	13.424	.624	100000.
16	1.096	.965	.880	20.305	17.875	18.522	.621	120000.
17	1.075	.973	.905	26.205	23.724	24.384	.617	140000.
18	1.019	.993	.974	31.652	30.842	31.058	.606	160000.

DATA SHEET

DATA FOR :SLEEVE WALL SHEAR
SERIES 20 ALPHA = .000
SLEEVE INTERNAL DIAMETER = .06900M RELATIVE ROUGHNESS = .0064100
CORE OUTER DIAMETER = .00000M RELATIVE ROUGHNESS = .0000000

TEST UNITS	SW0 GF	+WT GF	SW1 GF	P0 CM	FW1 KG	TIME SEC	TEMP DEGC
1	224.	6350.	224.	171.6	864.	75.9	22.1
2	224.	5650.	280.	150.7	812.	75.9	22.1
3	249.	3630.	251.	106.6	908.	104.6	22.1
4	249.	2130.	324.	66.7	886.	134.4	22.2
5	249.	1130.	100.	51.6	708.	136.0	22.2
6	215.	5000.	195.	135.5	916.	90.4	22.0
7	215.	3000.	90.	92.0	923.	115.0	22.0
8	215.	1000.	135.	43.5	863.	180.6	22.0
9	215.	400.	114.	30.6	706.	210.5	22.2
10	230.	600.	87.	37.5	833.	210.5	22.2
11	230.	400.	108.	29.5	710.	210.5	22.2
12	230.	300.	108.	27.2	476.	155.0	22.2
13	230.	200.	148.	25.4	458.	180.6	22.2
14	230.	200.	117.	30.2	426.	161.1	22.2
15	230.	300.	88.	29.3	560.	180.2	22.2
16	230.	300.	42.	29.6	590.	180.6	22.2
17	230.	400.	79.	32.2	630.	180.4	22.2
18	230.	600.	163.	37.6	689.	181.2	22.2
19	230.	1000.	125.	44.2	876.	181.9	22.2
20	230.	1200.	66.	52.3	963.	180.3	22.2
21	230.	1600.	155.	59.0	708.	120.1	22.1
22	217.	150.	65.	27.3	569.	217.7	22.0
23	217.	800.	207.	42.2	760.	182.2	22.0
24	217.	1800.	252.	60.5	727.	120.2	22.0
25	217.	2400.	200.	65.8	859.	120.3	22.0
26	217.	3420.	197.	90.3	759.	90.0	22.0
27	217.	4020.	222.	144.9	835.	91.6	22.0

28	217.	4620.	151.	151.1	751.	76.6	22.0
29	217.	5820.	60.	169.9	790.	71.3	22.0

RESULT SHEET

RESULTS FOR:SLEEVE WALL SHEAR
SERIES 20 ALPHA = .000
SLEEVE INTERNAL DIAMETER = .06900M RELATIVE ROUGHNESS = .0064100
CORE OUTER DIAMETER = .00000M RELATIVE ROUGHNESS = .0000000

TEST UNITS	SLEEVE FORCE GF	SLEEVE SHEAR N/M2	BULK FLOW M3/S	BULK VEL M/S	RE	F2	KINEMATIC VISCOSITY M2/S
1	6378.1	45.671	.01138	3.044	219299.	.009856	.9578-06
2	5618.3	40.231	.01070	2.861	206100.	.009830	.9578-06
3	3644.5	26.097	.00868	2.321	167232.	.009685	.9578-06
4	2064.4	14.782	.00659	1.763	127295.	.009512	.9556-06
5	1285.7	9.206	.00521	1.392	100525.	.009500	.9556-06
6	5041.6	36.101	.01013	2.710	194749.	.009833	.9601-06
7	3138.9	22.477	.00803	2.146	154260.	.009757	.9601-06
8	1885.3	7.771	.00478	1.278	91842.	.009517	.9601-06
9	504.0	3.609	.00335	.897	64764.	.008971	.9556-06
10	747.2	5.350	.00396	1.058	76414.	.009554	.9556-06
11	524.8	3.758	.00337	.902	65130.	.009236	.9556-06
12	424.4	3.039	.00307	.821	59302.	.009010	.9556-06
13	284.0	2.034	.00254	.678	48970.	.008844	.9556-06
14	315.9	2.262	.00264	.707	51061.	.009046	.9556-06
15	444.7	3.185	.00311	.831	60008.	.009221	.9556-06
16	490.8	3.514	.00327	.874	63083.	.009208	.9556-06
17	554.2	3.969	.00349	.934	67434.	.009100	.9556-06
18	671.2	4.806	.00380	1.017	73424.	.009296	.9556-06
19	1110.4	7.951	.00482	1.288	92993.	.009587	.9556-06
20	1370.8	9.816	.00534	1.428	103136.	.009622	.9556-06
21	1683.0	12.052	.00590	1.577	113568.	.009698	.9578-06
22	304.4	2.179	.00261	.699	50235.	.008922	.9601-06
23	815.0	5.836	.00417	1.116	80170.	.009380	.9601-06
24	1773.3	12.698	.00605	1.617	116246.	.009707	.9601-06
25	2426.8	17.377	.00711	1.901	136600.	.009620	.9601-06
26	3455.0	24.740	.00843	2.255	162087.	.009728	.9601-06
27	4038.3	28.917	.00912	2.438	175202.	.009731	.9601-06
28	4710.4	33.730	.00980	2.622	188434.	.009813	.9601-06
29	6004.8	42.998	.01108	2.963	212954.	.009794	.9601-06

DATA SHEET

DATA FOR :TOTAL WALL SHEAR
SERIES 20 ALPHA = .000
SLEEVE INTERNAL DIAMETER = .06900M RELATIVE ROUGHNESS = .0064100
CORE OUTER DIAMETER = .00000M RELATIVE ROUGHNESS = .0000000

TEST UNITS	P0 CM	P1 CM	P2 CM	P3 CM	P4 CM	P5 CM	FW1 KG	TIME SEC	TEMP DEGC
1	171.1	170.3	126.2	86.5	45.8	9.1	874.	77.3	22.0
2	95.6	97.0	75.4	54.6	31.3	11.8	986.	119.0	22.0
3	70.8	72.6	57.7	43.0	27.0	13.7	978.	141.5	22.1
4	30.2	32.8	27.8	23.6	19.4	15.5	695.	183.5	22.1
5	23.8	26.8	25.0	23.4	21.6	20.2	674.	280.0	22.2
6	39.3	42.1	36.7	32.0	26.6	22.4	748.	184.2	22.2
7	56.1	57.6	47.5	37.9	27.5	18.8	797.	142.2	22.2
8	78.2	80.2	63.1	47.2	30.1	15.2	807.	111.1	22.3
9	95.5	96.5	74.4	53.4	30.5	12.3	987.	118.4	22.3
10	118.4	119.5	91.0	64.5	36.0	12.8	843.	98.4	22.4
11	133.5	133.8	101.2	71.1	38.1	9.1	772.	77.1	22.4
12	28.2	30.9	28.5	26.7	24.3	22.0	796.	291.3	22.0
13	29.2	31.7	29.0	26.6	23.7	21.7	833.	275.0	22.0
14	32.1	34.1	30.7	27.5	24.2	20.9	874.	262.8	22.0
15	33.1	35.3	31.2	27.0	23.2	19.1	829.	225.7	22.0
16	35.4	38.9	33.8	28.7	23.5	18.3	748.	181.3	22.1
17	38.1	40.0	33.7	27.9	21.9	15.6	804.	180.1	22.1
18	47.6	51.0	42.7	34.0	26.4	18.2	781.	154.5	22.1
19	58.3	61.5	50.8	40.4	29.9	19.3	875.	150.3	22.2
20	82.1	90.0	71.0	52.7	34.2	15.7	935.	121.4	22.2
21	142.3	146.9	112.1	78.1	43.2	9.0	743.	71.0	22.2

RESULT SHEET

RESULTS FOR:TOTAL WALL SHEAR
SERIES 20 ALPHA = .000
SLEEVE INTERNAL DIAMETER = .06900M RELATIVE ROUGHNESS = .0064100
CORE OUTER DIAMETER = .00000M RELATIVE ROUGHNESS = .0000000

TEST UNITS	TOTAL FORCE GF	TOTAL SHEAR N/M2	BULK FLOW M3/S	BULK VEL M/S	RE	FT	KINEMATIC VISCOSITY M2/S
1	6265.0	44.861	.01131	3.024	217311.	.009813	.9601-06
2	3336.1	23.889	.00829	2.216	159250.	.009731	.9601-06
3	2309.6	16.538	.00691	1.848	133152.	.009681	.9578-06
4	658.8	4.789	.00379	1.013	72965.	.009336	.9578-06
5	258.2	1.849	.00241	.644	46481.	.009923	.9556-06
6	769.9	5.513	.00406	1.086	78413.	.009349	.9556-06
7	1518.0	10.870	.00560	1.499	108227.	.009676	.9556-06
8	2535.2	18.154	.00726	1.943	140589.	.009622	.9534-06
9	3364.1	24.089	.00834	2.229	161345.	.009694	.9534-06
10	4236.7	30.337	.00933	2.494	180009.	.009756	.9512-06
11	4860.3	34.803	.01001	2.678	194251.	.009707	.9512-06
12	338.7	2.425	.00273	.731	52520.	.009084	.9601-06
13	412.1	2.951	.00303	.810	58219.	.008994	.9601-06
14	511.7	3.664	.00333	.889	63920.	.009264	.9601-06
15	628.3	4.499	.00367	.982	70595.	.009326	.9601-06
16	800.9	5.735	.00413	1.103	79482.	.009422	.9578-06
17	942.5	6.749	.00446	1.194	86002.	.009470	.9578-06
18	1273.7	9.121	.00519	1.388	99972.	.009471	.9578-06
19	1637.7	11.727	.00582	1.557	112416.	.009676	.9556-06
20	2883.5	20.648	.00770	2.060	148721.	.009734	.9556-06
21	5361.0	38.388	.01046	2.799	202073.	.009803	.9556-06

DATA SHEET

DATA FOR :SLEEVE WALL SHEAR
SERIES 30 ALPHA = .000
SLEEVE INTERNAL DIAMETER = .06940M RELATIVE ROUGHNESS = .0122500
CORE OUTER DIAMETER = .00000M RELATIVE ROUGHNESS = .0000000

TEST UNITS	SW0 GF	+WT GF	SW1 GF	P0 CM	FW1 KG	TIME SEC	TEMP DEGC
1	155.	7420.	210.	198.0	931.	90.5	17.3
2	155.	6000.	265.	160.0	835.	90.4	17.4
3	155.	4500.	212.	126.0	838.	104.0	17.4
4	155.	2500.	186.	77.0	738.	123.1	17.5
5	155.	1500.	97.	55.0	860.	180.5	17.5
6	155.	800.	145.	38.0	729.	210.3	17.5
7	155.	300.	190.	22.0	378.	183.3	17.5
8	155.	800.	150.	36.0	732.	210.3	17.5
9	177.	5000.	177.	139.0	882.	103.3	18.3
10	177.	7420.	289.	199.0	883.	85.8	18.3
11	177.	6320.	197.	176.0	887.	92.6	18.3
12	177.	5200.	121.	162.0	852.	97.4	18.3
13	177.	4500.	183.	128.0	811.	100.0	18.4
14	177.	4000.	138.	136.0	769.	100.5	18.4
15	177.	3700.	217.	109.0	932.	127.7	18.4
16	177.	3200.	174.	94.0	830.	121.2	18.5
17	177.	2500.	127.	76.0	730.	120.1	18.5
18	177.	2000.	188.	65.0	663.	123.2	18.5
19	177.	1200.	97.	49.0	676.	155.5	18.5
20	189.	1200.	84.	47.0	792.	180.7	17.5
21	189.	1000.	220.	43.0	710.	187.1	17.5
22	189.	600.	82.	39.0	604.	185.1	17.5
23	189.	400.	83.	27.0	609.	219.0	17.5
24	189.	300.	136.	24.0	654.	280.6	17.5
25	189.	300.	196.	20.0	709.	328.2	17.5

RESULT SHEET

RESULTS FOR:SLEEVE WALL SHEAR
SERIES 30 ALPHA = .000
SLEEVE INTERNAL DIAMETER = .06940M RELATIVE ROUGHNESS = .0122500
CORE OUTER DIAMETER = .00000M RELATIVE ROUGHNESS = .0000000

TEST UNITS	SLEEVE FORCE GF	SLEEVE SHEAR N/M2	BULK FLOW M3/S	BULK VEL M/S	RE	F2	KINEMATIC VISCOSITY M2/S
1	7397.8	52.668	.01029	2.720	175401.	.014243	.1076-05
2	5916.0	42.118	.00924	2.442	157885.	.014128	.1073-05
3	4462.9	31.773	.00806	2.130	137232.	.014005	.1073-05
4	2480.2	17.658	.00600	1.585	102233.	.014060	.1071-05
5	1565.3	11.144	.00476	1.260	81646.	.014049	.1071-05

6	814.3	5.297	.00347	.916	59402.	.013087	.1071-05
7	266.4	1.697	.00106	.545	35338.	.012765	.1071-05
8	868.9	5.759	.00340	.920	59647.	.013694	.1071-05
9	5022.3	35.755	.00854	2.257	149259.	.014036	.1049-05
10	7340.9	52.263	.01029	2.721	179986.	.014122	.1049-05
11	6320.9	45.058	.00950	2.532	167450.	.014054	.1049-05
12	5282.4	37.687	.00875	2.312	152916.	.014066	.1049-05
13	4514.3	32.139	.00811	2.144	142124.	.013984	.1047-05
14	4068.7	28.910	.00765	2.023	134093.	.014131	.1047-05
15	3676.9	26.177	.00730	1.929	127988.	.014064	.1047-05
16	3217.2	22.905	.00685	1.810	120308.	.013977	.1044-05
17	2561.8	18.233	.00600	1.607	106782.	.014124	.1044-05
18	1998.1	14.225	.00530	1.423	94541.	.014057	.1044-05
19	1286.2	9.157	.00435	1.149	76372.	.013867	.1044-05
20	1314.9	9.333	.00438	1.159	75107.	.013903	.1071-05
21	974.2	6.935	.00379	1.003	65028.	.013783	.1071-05
22	711.5	5.065	.00326	.863	55917.	.013614	.1071-05
23	508.3	3.619	.00278	.735	47653.	.013393	.1071-05
24	354.8	2.526	.00233	.616	39940.	.013307	.1071-05
25	294.1	2.094	.00216	.571	37019.	.012839	.1071-05

DATA SHEET

DATA FOR :TOTAL WALL SHEAR
SERIES 30 ALPHA = .000
SLEEVE INTERNAL DIAMETER = .06940M RELATIVE ROUGHNESS = .0122500
CORE OUTER DIAMETER = .00000M RELATIVE ROUGHNESS = .0000000

TEST UNITS	P0 CM	P1 CM	P2 CM	P3 CM	P4 CM	P5 CM	FW1 KG	TIME SEC	TEMP DEGC
1	195.0	191.6	143.2	97.0	51.2	5.1	872.	84.9	17.7
2	120.7	121.8	93.2	66.9	40.4	13.9	784.	100.5	17.7
3	81.5	83.0	65.4	48.4	31.6	15.0	774.	124.0	17.7
4	66.2	68.2	54.6	42.4	30.1	18.0	821.	153.8	17.8
5	146.8	145.6	109.8	75.6	41.3	7.0	820.	92.3	17.5
6	32.0	34.0	29.9	26.0	22.2	18.4	551.	182.4	17.9
7	24.2	26.7	25.0	23.3	21.6	20.0	561.	269.9	18.0
8	28.0	31.0	27.8	25.4	23.0	19.4	549.	210.5	18.0
9	41.5	44.1	37.5	32.0	26.1	20.5	668.	180.4	18.0
10	194.3	193.0	150.5	101.8	53.5	5.3	854.	81.9	17.7
11	90.1	90.6	71.9	52.8	34.2	14.8	661.	100.9	17.9
12	81.3	78.3	62.6	46.7	31.4	15.1	727.	121.5	17.9
13	75.8	73.5	59.4	44.7	30.4	16.4	688.	120.4	17.9
14	71.7	68.4	56.7	43.7	31.5	18.7	647.	121.1	17.9
15	61.0	59.7	49.8	39.4	29.2	19.4	669.	138.9	18.0
16	55.6	53.7	45.4	36.3	27.7	19.5	672.	150.8	18.0
17	53.2	50.5	42.8	35.6	27.7	19.8	792.	188.1	18.0
18	48.5	46.9	40.2	33.3	26.9	20.0	745.	189.8	18.1
19	45.5	43.4	37.2	31.5	26.0	20.2	785.	216.4	18.4
20	39.6	37.9	33.6	28.8	24.1	19.7	689.	212.0	18.4
21	34.0	32.1	29.4	26.2	23.5	20.4	631.	241.7	18.4
22	132.0	135.9	103.8	70.4	39.4	7.1	782.	91.4	17.7
23	182.2	184.4	140.8	95.8	51.4	6.9	909.	90.5	17.7
24	112.7	115.2	89.3	63.9	38.3	12.2	729.	95.6	17.7
25	103.1	105.0	82.4	59.8	37.3	14.6	724.	100.9	17.7
26	117.1	115.0	89.6	63.9	38.3	12.6	728.	95.6	17.8

RESULT SHEET

RESULTS FOR:TOTAL WALL SHEAR
SERIES 30 ALPHA = .000
SLEEVE INTERNAL DIAMETER = .06940M RELATIVE ROUGHNESS = .0122500
CORE OUTER DIAMETER = .00000M RELATIVE ROUGHNESS = .0000000

TEST UNITS	TOTAL FORCE GF	TOTAL SHEAR N/M2	BULK FLOW M3/S	BULK VEL M/S	RE	FT	KINEMATIC VISCOSITY M2/S
1	7316.2	52.087	.01027	2.715	176808.	.014130	.1065-05
2	4226.1	30.087	.00780	2.062	134358.	.014149	.1065-05
3	2668.4	18.998	.00624	1.650	107500.	.013954	.1065-05
4	1965.2	13.991	.00534	1.411	92164.	.014051	.1063-05
5	5439.1	38.723	.00888	2.349	152239.	.014141	.1071-05
6	612.0	4.357	.00302	.799	52286.	.013665	.1060-05
7	264.3	1.882	.00208	.549	36066.	.012466	.1057-05
8	440.5	3.136	.00261	.689	45254.	.013195	.1057-05
9	922.0	6.564	.00370	.979	64251.	.013701	.1057-05
10	7589.8	54.034	.01043	2.757	179582.	.014222	.1065-05
11	2978.3	21.204	.00656	1.734	113500.	.014112	.1060-05
12	2479.6	17.653	.00590	1.562	103565.	.014111	.1060-05
13	2253.0	16.040	.00571	1.511	98905.	.014058	.1060-05
14	1960.3	13.956	.00534	1.412	92473.	.013903	.1060-05
15	1592.2	11.336	.00482	1.273	83522.	.013985	.1057-05

16	1354.7	9.644	.00446	1.178	72323.	.013899	.1057-05
17	1203.6	8.569	.00421	1.113	73059.	.013832	.1057-05
18	1055.7	7.516	.00393	1.038	68278.	.013961	.1055-05
19	906.3	6.452	.00363	.959	63571.	.014032	.1047-05
20	722.2	5.141	.00325	.859	56955.	.013930	.1047-05
21	461.0	3.282	.00261	.690	45751.	.013780	.1047-05
22	5066.2	36.068	.00956	2.262	147350.	.014101	.1065-05
23	6991.9	49.778	.01004	2.655	172983.	.014121	.1065-05
24	4043.5	28.787	.00763	2.016	131328.	.014168	.1065-05
25	3554.2	25.304	.00718	1.897	123576.	.014065	.1065-05
26	4029.3	28.686	.00762	2.013	131476.	.014157	.1063-05

DATA SHEET

DATA FOR :SLEEVE WALL SHEAR
SERIES 32 ALPHA = .238
SLEEVE INTERNAL DIAMETER = .06940M RELATIVE ROUGHNESS = .0122500
CORE OUTER DIAMETER = .01655M RELATIVE ROUGHNESS = .0535400

TEST UNITS	SW0 GF	+WT GF	SW1 GF	P0 CM	FW1 KG	TIME SEC	TEMP DEGC
1	187.	7200.	225.	266.0	812.	90.4	19.5
2	96.	4000.	95.	156.0	769.	114.4	19.9
3	96.	3700.	151.	119.0	868.	150.5	19.5
4	96.	2000.	162.	91.0	857.	180.6	20.2
5	132.	1000.	56.	56.0	638.	181.1	20.2
6	132.	500.	85.	40.0	630.	247.0	20.2
7	132.	400.	80.	35.0	829.	361.2	20.2
8	132.	300.	54.	29.0	768.	360.7	20.2
9	132.	7500.	86.	282.0	808.	87.6	20.2
10	132.	6800.	277.	222.0	807.	93.1	20.3
11	132.	6000.	186.	219.0	747.	91.3	20.3
12	132.	6000.	43.	230.0	817.	98.3	20.3
13	132.	5000.	259.	198.0	707.	95.4	20.4
14	132.	4500.	250.	173.0	649.	92.1	20.4
15	132.	4000.	402.	161.0	676.	104.1	20.4
16	132.	3500.	78.	138.0	795.	125.6	20.4
17	132.	3000.	62.	109.0	851.	144.2	20.5
18	132.	2500.	163.	107.7	796.	150.2	20.5
19	132.	1800.	201.	88.0	803.	181.6	20.5
20	132.	1500.	30.	75.0	816.	190.5	20.5
21	132.	1200.	28.	64.0	821.	211.6	20.5
22	132.	1000.	306.	54.0	853.	276.6	20.5
23	132.	700.	144.	48.0	760.	267.5	20.5
24	132.	500.	170.	39.0	707.	300.9	20.4
25	132.	300.	115.	22.0	579.	301.1	20.4
26	132.	300.	94.	27.0	662.	327.0	20.4

RESULT SHEET

RESULTS FOR:SLEEVE WALL SHEAR
SERIES 32 ALPHA = .238
SLEEVE INTERNAL DIAMETER = .06940M RELATIVE ROUGHNESS = .0122500
CORE OUTER DIAMETER = .01655M RELATIVE ROUGHNESS = .0535400

TEST UNITS	SLEEVE FORCE GF	SLEEVE SHEAR N/M2	BULK FLOW M3/S	BULK VEL M/S	RE	F2	KINEMATIC VISCOSITY M2/S
1	7206.9	51.309	.00898	2.518	130574	.016188	.1019-05
2	4026.3	28.665	.00672	1.884	98668.	.016149	.1009-05
3	2963.7	21.100	.00577	1.617	83840.	.016147	.1019-05
4	1947.7	13.867	.00475	1.330	70158.	.015676	.1002-05
5	1083.5	7.714	.00352	.987	52086.	.015822	.1002-05
6	551.6	3.927	.00254	.713	37588.	.015467	.1002-05
7	447.7	3.188	.00230	.643	33933.	.015404	.1002-05
8	380.7	2.710	.00213	.597	31480.	.015218	.1002-05
9	7593.7	54.063	.00922	2.585	136371.	.016176	.1002-05
10	6692.0	47.643	.00867	2.430	128464.	.016142	.9996-06
11	5982.5	42.592	.00818	2.293	121257.	.016196	.9996-06
12	6127.5	43.624	.00831	2.330	123176.	.016076	.9996-06
13	4985.8	34.926	.00741	2.077	110896.	.016188	.9972-06
14	4410.3	31.399	.00705	1.975	104685.	.016097	.9972-06
15	3756.2	26.742	.00649	1.820	96471.	.016143	.9972-06
16	3576.1	25.460	.00633	1.774	94032.	.016177	.9972-06
17	3086.9	21.977	.00590	1.654	87883.	.016063	.9948-06
18	2485.6	17.696	.00530	1.485	78919.	.016039	.9948-06
19	1744.2	12.417	.00442	1.239	65848.	.016167	.9968-06
20	1612.9	11.483	.00428	1.201	63787.	.015931	.9948-06
21	1312.9	9.347	.00388	1.088	57779.	.015806	.9948-06
22	833.1	5.931	.00308	.864	45924.	.015876	.9948-06
23	694.1	4.941	.00284	.796	42309.	.015583	.9948-06
24	458.5	3.264	.00235	.659	34906.	.015750	.9972-06

25	318.4	2.267	.00192	.539	28567.	.015696	.9972-06
26	340.3	2.423	.00202	.567	30075.	.015049	.9972-06

DATA SHEET

DATA FOR :TOTAL WALL SHEAR
SERIES 32 ALPHA = .238
SLEEVE INTERNAL DIAMETER = .06940M RELATIVE ROUGHNESS = .0122500
CORE OUTER DIAMETER = .01655M RELATIVE ROUGHNESS = .0535400

TEST UNITS	P? CM	P1 CM	P2 CM	P3 CM	P4 CM	P5 CM	FW1 KG	TIME SEC	TEMP DEGC
1	250.5	250.2	190.5	132.0	71.3	13.0	800.	92.0	18.9
2	263.0	261.2	200.1	135.0	71.2	9.0	830.	92.3	18.9
3	184.8	186.5	140.9	96.2	52.2	8.5	774.	93.1	19.0
4	184.8	187.0	140.7	96.2	52.9	8.6	704.	93.1	19.0
5	128.5	131.0	100.9	71.5	42.5	13.3	926.	151.0	18.9
6	128.5	131.8	101.0	71.5	43.6	14.0	926.	151.0	18.9
7	86.2	88.8	70.3	52.7	35.1	17.2	876.	182.6	18.9
8	86.2	89.0	70.3	52.7	35.2	17.1	876.	182.6	18.9
9	.0	48.3	40.8	33.4	26.9	19.2	748.	242.9	18.9
10	.0	55.9	47.8	38.1	29.3	20.8	830.	245.1	18.9
11	.0	43.6	37.6	31.8	26.6	21.1	811.	300.9	18.9
12	.0	48.5	41.3	34.4	27.7	21.0	781.	260.3	18.9
13	.0	67.4	54.3	41.8	29.6	17.3	715.	178.2	18.8
14	.0	57.8	47.5	37.6	27.1	17.2	869.	240.2	18.8
15	121.3	118.6	92.8	67.1	42.0	16.5	704.	123.6	18.9
16	123.0	123.3	96.6	69.7	43.2	16.8	733.	125.2	18.9
17	153.0	155.4	118.5	82.5	46.7	10.6	677.	99.8	18.9
18	228.0	227.8	174.1	119.5	63.9	9.3	737.	88.0	18.9
19	265.0	263.9	197.9	131.6	72.8	9.8	813.	90.7	19.0
20	.0	80.4	64.4	49.0	33.8	18.4	693.	155.7	19.0
21	.0	66.1	53.7	42.1	30.6	18.9	985.	252.8	19.0
22	163.0	160.0	122.1	85.5	48.8	11.9	689.	100.1	19.1
23	218.0	214.7	160.0	110.3	60.5	10.0	822.	102.5	19.1
24	.0	68.0	55.0	42.9	31.0	18.9	636.	160.4	19.1
25	98.0	99.0	77.5	57.1	37.2	16.9	682.	134.0	19.1

RESULT SHEET

RESULTS FOR:TOTAL WALL SHEAR
SERIES 32 ALPHA = .238
SLEEVE INTERNAL DIAMETER = .06940M RELATIVE ROUGHNESS = .0122500
CORE OUTER DIAMETER = .01655M RELATIVE ROUGHNESS = .0535400

TEST UNITS	TOTAL FORCE GF	TOTAL SHEAR N/M2	BULK FLOW M3/S	BULK VEL M/S	RE	FT	KINEMATIC VISCOSITY M2/S
1	8808.3	50.635	.00870	2.437	124569.	.017046	.1034-05
2	9486.1	54.531	.00899	2.521	128820.	.017167	.1034-05
3	6598.9	37.934	.00756	2.120	108591.	.016888	.1032-05
4	6597.4	37.925	.00756	2.120	108591.	.016884	.1032-05
5	4359.7	25.062	.00613	1.719	87850.	.016964	.1034-05
6	4347.8	24.994	.00613	1.719	87850.	.016918	.1034-05
7	2647.3	15.218	.00480	1.345	68724.	.016832	.1034-05
8	2654.7	15.260	.00480	1.345	68724.	.016879	.1034-05
9	1069.9	6.150	.00308	.863	44115.	.016509	.1034-05
10	1316.2	7.566	.00339	.949	48511.	.016796	.1034-05
11	831.0	4.777	.00270	.755	38611.	.016740	.1034-05
12	1018.0	5.852	.00301	.841	42982.	.016547	.1034-05
13	1853.4	10.654	.00401	1.125	57338.	.016847	.1034-05
14	1507.6	8.667	.00362	1.014	51700.	.016856	.1037-05
15	3783.9	21.752	.00570	1.597	81595.	.017068	.1034-05
16	3953.0	22.724	.00585	1.641	83870.	.016976	.1034-05
17	5362.7	30.828	.00670	1.901	97177.	.017054	.1034-05
18	8119.6	46.676	.00837	2.347	119975.	.016940	.1034-05
19	9397.6	54.023	.00896	2.512	128723.	.017116	.1032-05
20	2294.1	13.188	.00445	1.248	63917.	.016946	.1032-05
21	1743.6	10.023	.00390	1.092	55954.	.016806	.1032-05
22	5482.9	31.519	.00698	1.929	99788.	.016935	.1029-05
23	7551.6	43.411	.00802	2.248	115447.	.017103	.1029-05
24	1813.3	10.424	.00397	1.111	57080.	.016878	.1029-05
25	3034.6	17.444	.00509	1.427	73268.	.017143	.1029-05

DATA SHEET

DATA FOR :CORE WALL SHEAR
SERIES 32 ALPHA = .238
SLEEVE INTERNAL DIAMETER = .06940M RELATIVE ROUGHNESS = .0122500
CORE OUTER DIAMETER = .01650M RELATIVE ROUGHNESS = .0535400

TEST	RE	F1	F2
1	40000.	.016520	.015550
2	45000.	.016680	.015700
3	50000.	.016750	.015800
4	55000.	.016850	.015900
5	60000.	.016930	.015980
6	65000.	.016950	.016020
7	70000.	.017000	.016070
8	75000.	.017020	.016100
9	80000.	.017030	.016110
10	85000.	.017030	.016110
11	90000.	.017040	.016130
12	95000.	.017050	.016150
13	100000.	.017050	.016150
14	110000.	.017050	.016150
15	120000.	.017050	.016150
16	130000.	.017050	.016150

RESULT SHEET

RESULTS FOR:CORE WALL SHEAR
SERIES 32 ALPHA = .238
SLEEVE INTERNAL DIAMETER = .06940M RELATIVE ROUGHNESS = .0122500
CORE OUTER DIAMETER = .01650M RELATIVE ROUGHNESS = .0535400

TEST	TOTAL FORCE	SLEEVE FORCE	CORE FORCE	CORE SHEAR	RE	F1
UNITS	N	N	N	N/M2		
1	8.999	6.844	2.155	6.580	40000.	.020600
2	11.500	8.745	2.755	8.409	45000.	.020802
3	14.257	10.865	3.392	10.353	50000.	.020746
4	17.354	13.230	4.124	12.588	55000.	.020846
5	20.750	15.824	4.927	15.038	60000.	.020926
6	24.382	18.618	5.764	17.595	65000.	.020862
7	28.360	21.659	6.701	20.455	70000.	.020912
8	32.595	24.911	7.684	23.456	75000.	.020890
9	37.108	28.360	8.747	26.701	80000.	.020900
10	41.891	32.016	9.875	30.143	85000.	.020900
11	46.992	35.938	11.054	33.741	90000.	.020868
12	52.389	40.092	12.297	37.537	95000.	.020835
13	58.049	44.423	13.626	41.592	100000.	.020835
14	70.239	53.752	16.487	50.327	110000.	.020835
15	83.599	63.969	19.621	59.893	120000.	.020835
16	98.102	75.075	23.028	70.291	130000.	.020835

ANALYSIS SHEET

SERIES 32 ALPHA = .238
SLEEVE INTERNAL DIAMETER = .06940M RELATIVE ROUGHNESS = .0122500
CORE OUTER DIAMETER = .01650M RELATIVE ROUGHNESS = .0535400

TEST	TOR1 / TORT	TOR2 / TORT	TOR2 / TOR1	TOR1 N/M2	TOR2 N/M2	TORT N/M2	R1 / R2	RE
1	1.247	.941	.755	6.580	4.967	5.276	.532	40000.
2	1.247	.941	.755	8.409	6.346	6.743	.532	45000.
3	1.239	.943	.762	10.353	7.865	8.359	.530	50000.
4	1.237	.944	.763	12.588	9.601	10.175	.530	55000.
5	1.236	.944	.764	15.038	11.484	12.167	.530	60000.
6	1.231	.945	.768	17.595	13.511	14.296	.529	65000.
7	1.230	.945	.768	20.455	15.719	16.629	.529	70000.
8	1.227	.946	.771	23.456	18.078	19.111	.528	75000.
9	1.227	.946	.771	26.701	20.582	21.757	.528	80000.
10	1.227	.946	.771	30.143	23.235	24.562	.528	85000.
11	1.225	.947	.773	33.741	26.081	27.553	.528	90000.
12	1.222	.947	.775	37.537	29.096	30.717	.527	95000.
13	1.222	.947	.775	41.592	32.239	34.036	.527	100000.
14	1.222	.947	.775	50.327	39.009	41.183	.527	110000.
15	1.222	.947	.775	59.893	46.424	49.011	.527	120000.
16	1.222	.947	.775	70.291	54.484	57.520	.527	130000.

DATA SHEET

DATA FOR :SLEEVE WALL SHEAR
SERIES 33 ALPHA = .376
SLEEVE INTERNAL DIAMETER = .06940M RELATIVE ROUGHNESS = .0122500
CORE OUTER DIAMETER = .02610M RELATIVE ROUGHNESS = .0334600

TEST UNITS	SW0 GF	+WT GF	SW1 GF	P0 CM	FW1 KG	TIME SEC	TEMP DEGC
1	293.	7000.	380.	303.0	757.	99.2	15.3
2	293.	4500.	270.	286.0	754.	123.0	15.4
3	293.	3500.	235.	156.0	761.	141.4	15.5
4	293.	2000.	186.	113.0	752.	180.3	15.5
5	293.	1000.	196.	66.0	800.	264.6	15.5
6	293.	500.	30.	56.0	700.	278.4	15.6
7	293.	500.	279.	43.0	962.	277.7	15.6
8	293.	7000.	365.	304.0	800.	104.4	15.6
9	293.	3500.	325.	165.0	805.	157.4	15.6
10	293.	7000.	365.	304.0	921.	120.6	15.6
11	295.	6000.	313.	306.0	717.	101.3	15.4
12	295.	5000.	240.	225.0	777.	119.4	15.4
13	295.	4500.	149.	212.0	761.	122.5	15.4
14	295.	4000.	262.	172.0	684.	118.3	15.4
15	295.	3000.	123.	148.0	679.	132.7	15.5
16	295.	3500.	189.	160.0	617.	112.4	15.5
17	295.	3000.	377.	131.0	780.	158.8	15.5
18	295.	2500.	14.	126.0	744.	155.0	15.6
19	295.	2000.	102.	112.0	797.	186.4	15.6
20	295.	1500.	94.	86.0	795.	211.0	15.6
21	295.	1200.	44.	74.0	753.	215.8	15.6
22	295.	1000.	39.	65.0	960.	295.4	15.6
23	295.	500.	162.	47.0	743.	321.5	15.6
24	295.	200.	152.	38.0	724.	423.0	15.6
25	295.	300.	131.	42.0	800.	401.4	15.5

RESULT SHEET

RESULTS FOR:SLEEVE WALL SHEAR
SERIES 33 ALPHA = .376
SLEEVE INTERNAL DIAMETER = .06940M RELATIVE ROUGHNESS = .0122500
CORE OUTER DIAMETER = .02610M RELATIVE ROUGHNESS = .0334600

TEST UNITS	SLEEVE FORCE GF	SLEEVE SHEAR N/M2	BULK FLOW M3/S	BULK VEL M/S	RE	F2	KINEMATIC VISCOSITY M2/S
1	6964.5	49.583	.00763	2.350	89836.	.017962	.1133-05
2	4557.2	32.444	.00613	1.887	72353.	.018214	.1130-05
3	3533.3	25.155	.00538	1.657	63688.	.018321	.1127-05
4	2124.6	15.126	.00417	1.284	49356.	.018343	.1127-05
5	1106.3	7.876	.00302	.931	35778.	.018176	.1127-05
6	770.5	5.485	.00254	.783	30172.	.017892	.1124-05
7	519.2	3.696	.00208	.639	24632.	.018090	.1124-05
8	6979.6	49.691	.00766	2.359	90915.	.017852	.1124-05
9	3494.9	24.882	.00535	1.648	63573.	.018322	.1124-05
10	6979.6	49.691	.00764	2.351	90606.	.017974	.1124-05
11	6034.0	42.958	.00708	2.179	83542.	.018080	.1130-05
12	5092.6	36.256	.00651	2.004	76889.	.018061	.1130-05
13	4681.3	33.328	.00621	1.913	73323.	.018218	.1130-05
14	4061.1	28.913	.00578	1.780	68244.	.018245	.1132-05
15	3195.9	22.753	.00512	1.575	60551.	.018333	.1127-05
16	3632.8	25.858	.00549	1.690	64959.	.018173	.1127-05
17	2938.8	20.923	.00491	1.512	58125.	.018295	.1127-05
18	2800.9	19.941	.00480	1.478	56949.	.018258	.1124-05
19	2218.5	15.737	.00428	1.317	50729.	.018159	.1124-05
20	1715.8	12.281	.00377	1.162	44702.	.018131	.1124-05
21	1461.7	10.426	.00349	1.074	41399.	.018030	.1124-05
22	1265.1	9.007	.00325	1.001	38557.	.017990	.1124-05
23	638.9	4.548	.00231	.712	27419.	.017965	.1124-05
24	347.3	2.472	.00171	.527	20307.	.017804	.1124-05
25	469.0	3.339	.00199	.614	23585.	.017732	.1127-05

DATA SHEET

DATA FOR :TOTAL WALL SHEAR
SERIES 33 ALPHA = .376
SLEEVE INTERNAL DIAMETER = .06940M RELATIVE ROUGHNESS = .0122500
CORE OUTER DIAMETER = .02610M RELATIVE ROUGHNESS = .0334600

TEST UNITS	P0 CM	P1 CM	P2 CM	P3 CM	P4 CM	P5 CM	FW1 KG	TIME SEC	TEMP DEGC
1	.0	309.9	233.4	150.6	84.5	11.2	914.	120.5	15.4
2	.0	171.6	131.6	92.5	53.9	14.9	829.	150.3	15.4

3	.0 45.9	39.6	33.6	27.9	21.9	600.	274.2	15.4
4	.0 113.2	88.2	63.6	40.8	16.2	785.	180.6	15.3
5	.0 78.5	63.5	48.6	33.7	19.3	718.	210.4	15.4
6	.0 47.6	40.0	32.2	24.7	17.1	807.	325.9	15.4
7	.0 118.0	92.7	67.7	43.2	19.0	791.	180.5	15.5
8	.0 174.0	134.0	94.0	55.4	16.8	776.	141.0	15.6
9	.0 271.1	203.7	139.2	74.9	11.5	833.	118.3	15.4
10	.0 246.2	186.6	128.1	68.4	12.2	841.	125.2	15.4
11	.0 236.3	180.4	122.9	68.6	12.7	799.	121.5	15.4
12	.0 172.3	132.6	91.8	53.6	14.1	688.	124.7	15.4
13	.0 155.8	120.7	84.8	50.7	15.8	815.	156.6	15.5
14	.0 124.5	97.5	68.3	43.3	16.3	789.	172.1	15.5
15	.0 112.2	88.1	63.5	39.6	16.4	812.	187.6	15.6
16	.0 106.2	82.9	60.7	38.6	16.6	779.	188.0	15.6
17	.0 99.3	78.1	57.3	37.1	17.3	781.	195.4	15.6
18	.0 87.0	70.3	53.0	35.8	18.3	840.	230.2	15.4
19	.0 68.8	56.8	44.2	32.0	20.1	950.	305.7	15.6
20	.0 59.2	49.9	40.1	30.5	20.8	949.	343.8	15.5

RESULT SHEET

RESULTS FOR:TOTAL WALL SHEAR
SERIES 33 ALPHA = .376
SLEEVE INTERNAL DIAMETER = .06940M RELATIVE ROUGHNESS = .0122500
CORE OUTER DIAMETER = .02610M RELATIVE ROUGHNESS = .0334600

TEST	TOTAL FORCE	TOTAL SHEAR	BULK FLOW	BULK VEL	RE	FT	KINEMATIC VISCOSITY
UNITS	GF	N/M2	M3/S	M/S			M2/S
1	10081.3	52.157	.00759	2.335	89527.	.019124	.1130-05
2	5299.3	27.417	.00552	1.698	65101.	.019012	.1130-05
3	806.5	4.172	.00219	.674	25827.	.018382	.1130-05
4	3271.7	16.927	.00435	1.338	51170.	.018900	.1133-05
5	2001.9	10.357	.00341	1.051	40278.	.018762	.1130-05
6	1030.7	5.332	.00248	.762	29227.	.018346	.1130-05
7	3343.3	17.297	.00435	1.349	51858.	.019001	.1127-05
8	5308.8	27.466	.00550	1.695	65296.	.019129	.1124-05
9	8753.5	45.288	.00704	2.168	83112.	.019269	.1130-05
10	7918.6	40.968	.00672	2.068	79284.	.019154	.1130-05
11	7551.1	39.067	.00658	2.025	77618.	.019057	.1130-05
12	5341.2	27.633	.00552	1.699	65120.	.019151	.1130-05
13	4727.9	24.461	.00520	1.602	61587.	.019051	.1127-05
14	3655.4	18.912	.00458	1.412	54252.	.018981	.1127-05
15	3243.4	16.780	.00433	1.333	51353.	.018695	.1124-05
16	3019.1	15.620	.00414	1.276	49161.	.019192	.1124-05
17	2769.2	14.327	.00490	1.231	47421.	.018919	.1124-05
18	2322.0	12.013	.00365	1.124	43069.	.019033	.1130-05
19	1650.7	8.540	.00311	.957	36870.	.018655	.1124-05
20	1299.5	6.723	.00276	.850	32665.	.018614	.1127-05

DATA SHEET

DATA FOR :CORE WALL SHEAR
SERIES 33 ALPHA = .376
SLEEVE INTERNAL DIAMETER = .06940M RELATIVE ROUGHNESS = .0122500
CORE OUTER DIAMETER = .02610M RELATIVE ROUGHNESS = .0334600

TEST	RE	FT	F2
1	25000.	.018330	.017850
2	30000.	.018530	.018000
3	35000.	.018680	.018080
4	40000.	.018810	.018170
5	45000.	.018920	.018220
6	50000.	.019010	.018260
7	55000.	.019090	.018290
8	60000.	.019160	.018240
9	65000.	.019220	.018220
10	70000.	.019110	.018190
11	75000.	.019140	.018150
12	80000.	.019160	.018100
13	85000.	.019140	.018030
14	90000.	.019170	.017970

RESULT SHEET

RESULTS FOR:CORE WALL SHEAR
SERIES 33 ALPHA = .376
SLEEVE INTERNAL DIAMETER = .0694ØM RELATIVE ROUGHNESS = .ØØ122ØØ
CORE OUTER DIAMETER = .Ø261ØM RELATIVE ROUGHNESS = .ØØ334ØØ

TEST UNITS	TOTAL FORCE N	SLEEVE FORCE N	CORE FORCE N	CORE SHEAR N/M2	RE	F1
1	6.472	4.580	1.892	3.651	25000.	.019606
2	8.422	6.651	2.771	5.347	30000.	.019939
3	12.928	9.093	3.835	7.400	35000.	.020275
4	17.003	11.936	5.067	9.778	40000.	.020512
5	21.645	15.148	6.498	12.538	45000.	.020781
6	26.793	18.721	8.072	15.576	50000.	.020911
7	32.488	22.665	9.823	18.955	55000.	.021031
8	38.765	26.959	11.806	22.783	60000.	.021240
9	45.543	31.604	13.939	26.897	65000.	.021367
10	52.902	36.593	16.309	31.471	70000.	.021556
11	60.825	41.915	18.910	36.490	75000.	.021772
12	69.205	47.559	21.646	41.771	80000.	.021905
13	78.126	53.482	24.644	47.556	85000.	.022091
14	87.725	59.759	27.966	53.966	90000.	.022361

ANALYSIS SHEET

SERIES 33 ALPHA = .376
SLEEVE INTERNAL DIAMETER = .0694ØM RELATIVE ROUGHNESS = .ØØ122ØØ
CORE OUTER DIAMETER = .Ø261ØM RELATIVE ROUGHNESS = .ØØ334ØØ

TEST	TOR1 / TORT	TOR2 / TORT	TOR2 / TOR1	TOR1 N/M2	TOR2 N/M2	TORT N/M2	R0 / R2	RE
1	1.070	.974	.910	3.651	3.324	3.413	.626	25000.
2	1.076	.971	.903	5.347	4.827	4.969	.628	30000.
3	1.085	.968	.892	7.400	6.599	6.818	.629	35000.
4	1.090	.966	.886	9.778	8.662	8.967	.630	40000.
5	1.098	.963	.877	12.538	10.993	11.415	.632	45000.
6	1.102	.962	.872	15.576	13.587	14.130	.633	50000.
7	1.106	.960	.868	18.955	16.449	17.134	.633	55000.
8	1.114	.957	.859	22.783	19.565	20.444	.635	60000.
9	1.120	.955	.853	26.897	22.936	24.019	.636	65000.
10	1.128	.952	.844	31.471	26.557	27.900	.637	70000.
11	1.138	.948	.834	36.490	30.419	32.078	.639	75000.
12	1.144	.946	.826	41.771	34.515	36.498	.640	80000.
13	1.154	.942	.816	47.556	38.813	41.203	.642	85000.
14	1.166	.937	.804	53.966	43.369	46.265	.644	90000.

APPENDIX B

Details of the expansion of the terms in the mean flow equations in cylindrical coordinates are not available in any standard texts, for convenience they are given here:

B.1 Derivatives of the unit vectors $\hat{r}$, $\hat{\theta}$ and $\hat{x}$

$$\frac{\partial \hat{r}}{\partial r} = 0 \qquad \frac{\partial \hat{\theta}}{\partial r} = 0 \qquad \frac{\partial \hat{x}}{\partial r} = 0$$

$$\frac{\partial \hat{r}}{\partial \theta} = \hat{\theta} \qquad \frac{\partial \hat{\theta}}{\partial \theta} = -\hat{r} \qquad \frac{\partial x}{\partial \theta} = 0$$

$$\frac{\partial \hat{r}}{\partial x} = 0 \qquad \frac{\partial \hat{\theta}}{\partial x} = 0 \qquad \frac{\partial \hat{x}}{\partial x} = 0$$

B.2 Expanding $\underline{u}\cdot\nabla\underline{u}$ into cylindrical coordinates

$$\underline{u}\cdot\nabla = \left(u_r\hat{r} + u_\theta\hat{\theta} + u_x\hat{x}\right)\cdot\left(\frac{\partial}{\partial r}\hat{r} + \frac{1}{r}\frac{\partial}{\partial\theta}\hat{\theta} + \frac{\partial}{\partial x}\hat{x}\right)$$

$$= u_r\frac{\partial}{\partial r} + \frac{u_\theta}{r}\frac{\partial}{\partial\theta} + u_x\frac{\partial}{\partial x}$$

$$\underline{u}\cdot\nabla\underline{u} = u_r\frac{\partial u_r}{\partial r}\hat{r} + u_r\frac{\partial u_\theta}{\partial r}\hat{\theta} + u_r\frac{\partial u_x}{\partial r}\hat{x}$$

$$+ \frac{u_\theta}{r}\frac{\partial u_r}{\partial\theta}\hat{r} + \frac{u_\theta}{r}\frac{\partial u_\theta}{\partial\theta}\hat{\theta} + \frac{u_\theta}{r}\frac{\partial u_x}{\partial\theta}\hat{x}$$

$$+ u_x\frac{\partial u_r}{\partial x}\hat{r} + u_x\frac{\partial u_\theta}{\partial x}\hat{\theta} + u_x\frac{\partial u_x}{\partial x}\hat{x}$$

$$= \left[u_r\frac{\partial u_r}{\partial r} + \frac{u_\theta}{r}\frac{\partial u_r}{\partial\theta} - \frac{u_\theta^2}{r} + u_x\frac{\partial u_r}{\partial x}\right]\hat{r}$$

$$+ \left[u_r\frac{\partial u_\theta}{\partial r} + \frac{u_\theta}{r}\frac{\partial u_\theta}{\partial\theta} + \frac{u_\theta}{r}u_r + u_x\frac{\partial u_\theta}{\partial x}\right]\hat{\theta}$$

$$+ \left[u_r\frac{\partial u_x}{\partial r} + \frac{u_\theta}{r}\frac{\partial u_x}{\partial\theta} + u_x\frac{\partial u_x}{\partial x}\right]\hat{x}$$

B.3 Expanding $\nabla^2 \underline{u}$ into cylindrical coordinates

$$\nabla^2 \underline{u} = \frac{1}{r}\frac{\partial}{\partial r}\left(r\frac{\partial \underline{u}}{\partial r}\right) + \frac{1}{r^2}\frac{\partial^2 \underline{u}}{\partial \theta^2} + \frac{\partial^2 \underline{u}}{\partial x^2}$$

$$\frac{1}{r}\frac{\partial}{\partial r}\left(r\frac{\partial \underline{u}}{\partial r}\right) = \frac{1}{r}\frac{\partial}{\partial r}\left(r\frac{\partial u_r}{\partial r}\hat{r} + r\frac{\partial u_\theta}{\partial r}\hat{\theta} + r\frac{\partial u_x}{\partial r}\hat{x}\right)$$

$$= \frac{1}{r}\frac{\partial}{\partial r} r\left(\hat{r}\frac{\partial u_r}{\partial r} + \hat{\theta}\frac{\partial u_\theta}{\partial r} + \hat{x}\frac{\partial u_x}{\partial r}\right)$$

$$\frac{1}{r^2}\frac{\partial^2 \underline{u}}{\partial \theta^2} = \frac{1}{r^2}\left(\frac{\partial^2 u_r}{\partial \theta^2}\hat{r} + \frac{\partial^2 u_\theta}{\partial \theta^2}\hat{\theta} + \frac{\partial^2 u_x}{\partial \theta^2}\hat{x}\right)$$

$$= \frac{1}{r^2}\left(\hat{r}\frac{\partial^2 u_r}{\partial \theta^2} + \hat{\theta}\frac{\partial u_r}{\partial \theta} - \hat{r}u_r + \hat{\theta}\frac{\partial u_r}{\partial \theta}\right.$$

$$\left. + \hat{\theta}\frac{\partial^2 u_\theta}{\partial \theta^2} - \hat{r}\frac{\partial u_\theta}{\partial \theta} - \hat{\theta}u_\theta - \hat{r}\frac{\partial u_\theta}{\partial \theta} + \hat{x}\frac{\partial^2 u_x}{\partial \theta^2}\right)$$

$$\frac{\partial^2 \underline{u}}{\partial x^2} = \hat{r}\frac{\partial^2 u_r}{\partial x^2} + \hat{\theta}\frac{\partial^2 u_\theta}{\partial x^2} + \hat{x}\frac{\partial^2 u_x}{\partial x^2}$$

$\therefore$

$$\nabla^2 \underline{u} = \left[\frac{1}{r}\frac{\partial}{\partial r}\left(r\frac{\partial u_r}{\partial r}\right) + \frac{1}{r^2}\frac{\partial^2 u_r}{\partial \theta^2} - \frac{u_r}{r^2} - \frac{2}{r^2}\frac{\partial u_\theta}{\partial \theta} + \frac{\partial^2 u_r}{\partial x^2}\right]\hat{r}$$

$$+ \left[\frac{1}{r}\frac{\partial}{\partial r}\left(r\frac{\partial u_\theta}{\partial r}\right) + \frac{1}{r^2}\frac{\partial^2 u_\theta}{\partial \theta^2} - \frac{u_\theta}{r} + \frac{2}{r^2}\frac{\partial u_r}{\partial \theta} + \frac{\partial^2 u_\theta}{\partial x^2}\right]\hat{\theta}$$

$$+ \left[\frac{1}{r}\frac{\partial}{\partial r}\left(r\frac{\partial u_x}{\partial r}\right) + \frac{1}{r^2}\frac{\partial^2 u_x}{\partial \theta^2} + \frac{\partial^2 u_x}{\partial x^2}\right]\hat{x}$$

$$= \left[\nabla^2 u_r - \frac{u_r}{r^2} - \frac{2}{r^2}\frac{\partial u_\theta}{\partial \theta}\right]\hat{r}$$

$$+ \left[\nabla^2 u_\theta - \frac{u_\theta}{r^2} + \frac{2}{r^2}\frac{\partial u_r}{\partial \theta}\right]\hat{\theta} + \left[\nabla^2 u_x\right]\hat{x}$$

B.4 Expanding $\underline{u}\cdot\nabla\underline{u} + \underline{u}(\nabla\cdot\underline{u})$ into cylindrical coordinates

From continuity $\underline{u}\cdot\nabla\underline{u} + \underline{u}(\nabla\cdot\underline{u}) = \underline{u}\cdot\nabla\underline{u}$

$$\underline{u}\nabla\cdot\underline{u} = \left(u_r \hat{r} + u_\theta \hat{\theta} + u_x \hat{x}\right)\left(\frac{\partial u_x}{\partial x} + \frac{1}{r}\frac{\partial r u_r}{\partial r} + \frac{1}{r}\frac{\partial u_\theta}{\partial \theta}\right)$$

$$= \left[u_r \frac{\partial u_x}{\partial x} + \frac{u_r}{r}\frac{\partial r u_r}{\partial r} + \frac{u_r}{r}\frac{\partial u_\theta}{\partial \theta}\right]\hat{r}$$

$$+ \left[u_\theta \frac{\partial u_x}{\partial x} + \frac{u_\theta}{r}\frac{\partial r u_r}{\partial r} + \frac{u_\theta}{r}\frac{\partial u_\theta}{\partial \theta}\right]\hat{\theta}$$

$$+ \left[u_x \frac{\partial u_x}{\partial x} + \frac{u_x}{r}\frac{\partial r u_x}{\partial r} + \frac{u_x}{r}\frac{\partial u_x}{\partial \theta}\right]\hat{x}$$

$$\underline{u}\cdot\nabla\underline{u} + \underline{u}\nabla\cdot\underline{u} = \left[u_r \frac{\partial u_r}{\partial r} + \frac{u_r}{r}\frac{\partial r u_r}{\partial r} + \frac{u_\theta}{r}\frac{\partial u_r}{\partial \theta} + \frac{u_r}{r}\frac{\partial u_\theta}{\partial \theta} + u_x \frac{\partial u_r}{\partial x}\right.$$

$$\left. + u_r \frac{\partial u_x}{\partial x} - \frac{u_\theta}{r}\right]\hat{r}$$

$$+ \left[u_r \frac{\partial u_\theta}{\partial r} + \frac{u_\theta}{r}\frac{\partial r u_r}{\partial r} + \frac{u_\theta}{r}\frac{\partial u_\theta}{\partial \theta} + \frac{u_\theta}{r}\frac{\partial u_\theta}{\partial \theta} + u_x \frac{\partial u_\theta}{\partial x}\right.$$

$$\left. + u_\theta \frac{\partial u_x}{\partial x} + \frac{\partial u_\theta u_r}{\partial r}\right]\hat{\theta}$$

$$+ \left[u_r \frac{\partial u_x}{\partial r} + \frac{u_x}{r}\frac{\partial r u_r}{\partial r} + \frac{u_\theta}{r}\frac{\partial u_x}{\partial \theta} + \frac{u_x}{r}\frac{\partial u_\theta}{\partial \theta}\right.$$

$$\left. + u_x \frac{\partial u_x}{\partial x} + u_x \frac{\partial u_x}{\partial x}\right]\hat{x}$$

$$\therefore \quad \underline{u}\cdot\nabla\underline{u} = \left[\frac{1}{r}\frac{\partial}{\partial r}(r u_r^2) + \frac{1}{r}\frac{\partial}{\partial \theta}(u_r u_\theta) + \frac{\partial}{\partial x}(u_x u_r) - \frac{u_\theta^2}{r}\right]\hat{r}$$

$$+ \left[\frac{1}{r}\frac{\partial}{\partial r}(r u_\theta u_r) + \frac{1}{r}\frac{\partial}{\partial \theta}(u_\theta^2) + \frac{\partial}{\partial x}(u_x u_\theta) + \frac{u_\theta u_r}{r}\right]\hat{\theta}$$

$$+ \left[\frac{1}{r}\frac{\partial}{\partial r}(r u_x u_r) + \frac{1}{r}\frac{\partial}{\partial \theta}(u_x u_\theta) + \frac{\partial}{\partial x}(u_x^2)\right]\hat{x}$$

Substituting the appropriate results obtained in B.2, B.3 and B.4 into Eq. 49, yields Eq. 50 - the mean flow equations in cylindrical coordinates.